

**A Study of the Piezocone Penetrometer  
in Normally Consolidated Clay**

Thesis submitted for the degree  
of Doctor of Philosophy

R. E. May.  
Exeter College

**A Study of the Piezocone Penetrometer  
in Normally Consolidated Clay**

**R.E. May, Exeter College**

**Submitted for the degree Doctor of Philosophy,  
Hilary 1987**

**Abstract**

The research was intended to enhance the understanding of penetrometer behaviour in normally consolidated clay. The effects of varying penetration rate and clay shear strength were studied and the distribution of pore pressures determined.

To meet these objectives laboratory testing was undertaken. Penetration tests were to be performed in tanks of clay consolidated from slurry and maintained under known stresses. An initial series of tests examined the effect of stiff tank walls. These showed unexpectedly high radial boundary stresses were generated with tank to probe diameter ratios of 50:1. This finding dictated laboratory tests with small scale penetrometers in the largest practical size of tank. Field tests with small scale and full size penetrometers demonstrated an absence of scale effect in the penetrometer pore pressures and total stress data.

Two consolidation tanks of 580mm diameter and one of 1000mm diameter were built with the facility for maintaining constant stresses on the top of the sample during penetration. Piezocone penetrometers of 5cm<sup>2</sup> and 1cm<sup>2</sup> cross-section were built. Penetration tests were performed from 2cm/s to 3m/s with hydraulic insertion equipment.

At lower rates the total cone resistance factor  $N_{kt}$  was shown to be  $10.3 \pm 0.9$  in normally consolidated kaolin. The corresponding pore pressure factor  $N_{\Delta u}$  was  $8.25 \pm 1.0$  at the cone shoulder. A hundredfold increase in the penetration rate increased the  $N_{kt}$  factor by 40% but the  $N_{\Delta u}$  factor was unchanged.

Various subsidiary points emerged. The type of strength test used for comparison with penetrometer data is significant. Major strength reductions occur on sample depressurization. These were demonstrated with vane and triaxial tests.

Baligh and Levadoux's method for determining  $c_h$  from pore pressure dissipation around penetrometers matched experimental data.

Ratios of excess pore pressures on the cone face and shoulder show some promise in the evaluation of OCR.

## Acknowledgements

I would like to express my sincere thanks to everyone who has enabled this project to be completed.

First and foremost may I thank Julie my wife for her tremendous support and encouragement.

My thanks to Dr. Gilliane Sills who brought the project to life and guided its development so astutely. My thanks are due to all who provided funds, the SERC, Thorburn Associates and Fugro Limited. I am particularly grateful to Mr. Sam Thorburn, Mr. David Biddle and Mr. Eugene Toolan for their generosity.

My thanks goes to all my colleagues at Oxford; Tom Henderson, Stuart Oldham, Steve Hoare, Bob Sawala and Chris Waddup all played invaluable roles. My fellow students provided much help in the exchange of ideas. Professor Peter Wroth and Dr. Guy Houlsby provided challenging insights.

Finally my thanks go to the typists who have worked so hard and especially Pamela Fairley.

"If the building of a bridge does not enrich the awareness of those who work on it, then that bridge ought not to be built" - Frantz Fanon.

## C O N T E N T S

	Page
<b>ACKNOWLEDGEMENTS</b>	i
<b>ABSTRACT</b>	ii
<b>1. INTRODUCTION</b>	1
1.1 The historical development of the cone penetrometer	1
1.2 The analysis of the cone penetration test in clays during penetration	7
1.3 Comparison of field and laboratory tests against analytical solutions	23
1.4 The analysis of pore pressure dissipation following penetration	35
1.5 Aims of the present research work	40
<b>2. INVESTIGATIONS INTO THE EFFECT OF TANK CONFINEMENT</b>	42
2.1 Introduction	42
2.2 Small scale equipment	46
2.3 Small scale testing procedures	49
2.4 Results of experimental study on confinement effects	53
2.5 Calculations of confinement effect	57
<b>3. LARGE SCALE EQUIPMENT AND TESTING PROCEDURE</b>	67
3.1 Introduction	67
3.2 Consolidation tanks	68
3.3 Penetrometers	75
3.4 Hydraulic driving system	78
3.5 Logging system and instrumentation	80
3.6 Tank preparation	85
3.7 Slurry mixing procedure	88

## CONTENTS (continued)

	Page
<b>3. LARGE SCALE EQUIPMENT AND TESTING PROCEDURE PROCEDURE (continued)</b>	
3.8 Top plate preparation and fitting	90
3.9 Sample consolidation	91
3.10 Pore pressure transducer installation	93
3.11 Penetrometer saturation	94
3.12 Penetration testing	96
3.13 Post penetration soil testing	99
<b>4. LARGE SCALE LABORATORY TESTING RESULTS</b>	<b>102</b>
4.1 Large scale test series	102
4.2 Data quality	105
4.3 Shear strength measurements	110
4.4 Cone resistance at slower penetration rates	117
4.5 Pore pressures during penetration at lower penetration rates	120
4.6 Dissipation of pore pressures	123
4.7 Rate effects	129
<b>5. FIELDWORK</b>	<b>132</b>
5.1 Introduction	132
5.2 Site description and geology	133
5.3 Site investigation equipment	135
5.4 Borehole and Piezocone data	137
5.5 Analysis of field data	138
<b>6. CONCLUSIONS AND RECOMMENDATIONS</b>	<b>142</b>
6.1 Introduction	142
6.2 Fundamental aspects of piezocone behaviour	142
6.3 Practical conclusions and recommendations	146
6.4 Recommendations for further analytical and practical work	148

## 1.0 INTRODUCTION

### 1.1 The Historical Development of the Cone Penetrometer

The cone penetration test (CPT) can be traced back to the early years of this century. The Swedish State Railways had developed a static sounding probe around 1917 (Terzaghi and Peck 1967) followed by the Danish Railways in about 1927 (Godskesen 1936). In the early 1930's penetrometers of the now internationally recognised standard shape had been produced by the Delft Soil Mechanics Laboratory (Delft 1936) and the Dutch Department of Public Works (Barentsen 1936). These mechanical penetrometers were equipped with a  $60^\circ$  conical tip having a  $10\text{cm}^2$  base area. The tip was connected to a small diameter inner rod which was sleeved within hollow "sounding tubes". The method of operation of this device is shown in Fig. 1.1.

During soil testing first the conical tip was pushed into the soil using the inner rods. Then the sounding tubes were advanced into the soil to reclose the penetrometer. The resistance to penetration during both stages was measured with a Bourdon Gauge.

This simple design of penetrometer was prone to jamming as soil was forced into the annulus between the inner rods and the sounding tubes. A number of modified penetrometers were developed and of these the Delft mechanical penetrometer (Vermeiden 1948) became a widely used standard instrument. In this instrument the outside diameter of the leading sounding tube was reduced for a length immediately above the tip. The tip itself was fitted with a tapered sleeve or mantle into which the waisted section of sounding tube was fitted. Although this design largely overcame the problems of jamming it may be noted that problems associated with the joint between the tip and shaft of the penetrometer persist even in modern electric penetrometers.

The early mechanical penetrometers enabled good predictions to be made for the end-bearing resistance of driven piles (Boonstra 1936). However, the skin friction of such piles proved to be considerably greater than that scaled from the total friction on the sounding tubes (Huizinga 1951). It also proved impossible to use the instrument to determine the localized skin friction of a given layer (Begemann 1953 and 1965). This shortcoming led to the next major development of the cone penetrometer with the inclusion of a "friction sleeve". The design was

developed by Begemann in the early 1950s (Begemann 1963) and incorporated a sleeve of the same diameter as the tip, with a surface area of  $150\text{cm}^2$  and located between the tip and the sounding rods (Fig. 1.2). With this penetrometer the inner push rods first pushed the conical tip down 40mm. The sleeve was then engaged and pushed down with the tip, the combined load being measured for a further 40mm. Finally the outer sounding rods were pushed down telescoping the sleeve back into its original position behind the tip in preparation for the next cycle.

The advent of the electric cone penetrometer heralded the next significant advance. The early electric cones measured only tip resistance by means of vibrating wire or resistance strain gauges (Begemann 1963). By 1970 Fugro B.V. had produced a commercial electric cone penetrometer capable of measuring both tip resistance and sleeve friction continuously during penetration (De Ruiter 1971). The external geometry of the electric cone penetrometer was standardized (ASTM 1977 and ISSMFE 1977) as shown in Fig. 1.3. Although the tip resistances of the mechanical and electric cones were very similar in the same conditions, the electric penetrometer recorded friction values of about half those measured by the Begemann mechanical penetrometer (De Ruiter 1971). The major reason for this difference was the



complex shape of the mechanical penetrometer which resulted in the generation of large forces on the bevelled leading edge of its sleeve during penetration.

Once the electric friction cone penetrometer had become established it was logical to consider the incorporation of additional sensors into the instrument. Among these were inclinometers for measuring penetrometer verticality (De Ruiter 1971), thermocouples for detecting soil temperature (Marr 1981), geophones for assessing shear modulus (Campanella et al 1985) and radio-active backscatter devices for evaluating soil density (e.g. Nieuwenhuis & Smits 1982). The most important sensor to be added from the stand-point of assessing fundamental geotechnical parameters from the CPT was the soil pore pressure transducer.

The development of the cone penetrometer with pore pressure measuring facilities (the "piezo-cone penetrometer") proceeded along two separate lines. Firstly, probes were developed which had the capability of measuring only pore pressures during and after penetration. In Sweden during the early 1970s Torstenssen produced a probe of rather complex geometry (Fig. 1.4) whilst in the U.S.A. Wissa and his colleagues produced a similar instrument

(Torstensson 1975 & Wissa et al 1975). The use of these instruments on clay sites showed considerable promise for the evaluation of undrained shear strength, and the co-efficient of horizontal consolidation  $c_h$  (Battaglio et al 1981). The Norwegian Geotechnical Institute (N.G.I.) developed a pore pressure probe with the same shape as the standard cone penetrometer in 1973. The results from this device were combined with those from standard CPTs (Janbu & Senneset 1974).

In a separate line of development, piezometric elements were fitted to early electric cones to measure excess static pore pressures in sand strata beneath the Dutch polders (Zuidberg et al 1982). By 1973 the usefulness of measuring pore pressures during cone penetration (dynamic pore pressures) was being realized (Schmertmann 1974 a & b) and a research penetrometer without friction sleeve was developed to measure these values (Zuidberg et al 1982). In the late 1970s and early 1980s a large number of piezocone penetrometers appeared. The majority of these devices conformed approximately to the standard cone penetrometer dimensions (Fig. 1.3) with the addition of a single pore pressure transducer and attendant filter.

Three main choices for the location of pore pressure measurement emerged (Fig. 1.5) with commercial and research penetrometers of each variety. Several designs have been built with the filter at the apex of the cone tip (Baligh et al 1981, Franklin & Cooper 1981, Rocha Filho 1982). A number of groups have placed the filter at approximately mid-height on the face of the cone (Jones and van Zyl 1981, Tumay et al 1981 and Zuidberg et al 1982). The third common location for the filter is on the cone shoulder, above the conical tip and below the friction sleeve (Campanella et al 1981, Jones & Rust 1982, Muromachi et al 1982, Smits 1982 and Torstensson 1982).

Some research has also been conducted with filters mounted higher up the penetrometer shaft (Levadoux & Baligh 1980, Roy 1981, Smits 1982, Sugawara & Chikaraishi 1982, Torstensson 1975). The pore pressures measured at these different locations show substantial differences in magnitude and dissipation rate for CPTs in clay soils. Despite the clear need for standardization of the position(s) at which pore pressure is measured no consensus of opinion has yet emerged. Comment on this subject is given in Section 6.3.2.

## 1.2 The Analysis of the Cone Penetration Test in Clays during Penetration

The analysis of the CPT has been tackled using four principal methods. The first two approaches are quasi-closed form analytical methods using slip-surface or cavity expansion theories. More recently two numerical techniques have been employed, these being the finite element and strain field methods.

The original work on bearing capacity in soil mechanics was based on the slip line approach. Terzaghi (1943) developed general bearing capacity equations based on work by Prandtl and Reissner in the 1920s. Considering the soil behaviour as rigid-perfectly plastic the following solution was produced for a surface strip footing on clay ( $\theta = 0$ )

$$q_c = N_c c_u$$

where:

- $q_u$  = ultimate bearing pressure
- $N_c$  = bearing capacity factor
- $c_u$  = undrained shear strength

Terzaghi calculated the following values for the bearing capacity factor:

$$N_c = 1 + 3(\pi/2) = 5.71 \quad (\text{Rough base})$$

$$N_c = 2 + \pi = 5.14 \quad (\text{Smooth base})$$

(The rough base calculation was incorrect)

For shallow circular footings Terzaghi introduced an empirical shape factor and a surcharge term neglecting any shear contribution from the clay above the base thus:

$$q_u = 1.3 N_c c_u + \gamma D$$

where  $\gamma$  = unit weight of soil above base

$D$  = depth of base below surface

The slip line approach was extended to deep foundations by Meyerhof (1951). For a strip footing he calculated that the value of  $N_c$  rose from 5.14 at the surface to limiting values of 8.28 to 8.85 for smooth and rough shafts respectively. In order to obtain these values the slip surface was brought back to the surface of the shaft although this is kinematically inadmissible. For circular footings Meyerhof performed an approximate calculation which gave values of  $N_c$  increasing from 6.18 at the surface to limiting values of 9.34 to 9.74. These values incorporate the

shape factor. Meyerhof's approach predicted that the limiting values of  $N_c$  would be reached at a depth of two shaft diameters although he noted that experimental data showed penetrations of 4 to 5 diameters were required to reach peak values.

This form of analysis was further developed by Brinch-Hansen (1961) in a semi-empirical fashion. He suggested:

$$q_u = (\pi + 2) c_u (1 + S_c + d_c)$$

where  $S_c$  = shape factor  
           = 0.2 for a circular base  
 $d_c$  = depth factor  
           =  $0.4 \tan^{-1} (D/B)$   
 $B$  = footing diameter

This formula produces a limiting ultimate base resistance of  $9.4 c_u$ .

More rigorous solutions of the axi-symmetric bearing capacity problem on rigid-plastic soils have been produced by the numerical technique of the method of characteristics. Cox (1962) produced solutions for a flat surface footing and Houlsby (1982) extended this work for conical footings.

However, attempts to use this solution technique for deep bases have not been successful. The soil model forces the zone of plastic behaviour to extend from beneath the footing back to the soil surface with an increasing radius of plastic behaviour with height above the tip. Bearing capacity factors calculated with this model increase indefinitely with tip penetration and rapidly exceed observed values, as demonstrated by Houlsby and Wroth (1982).

An important alternative to the above plasticity analyses was provided by the emergence of cavity expansion solutions applicable to clays. In general the advantage of the cavity expansion formulation is that the shear modulus ( $G$ ) of a clay is considered together with its shear strength ( $c_u$ ). However, the only cavity expansion cases to be solved are those of spherical and cylindrical cavity expansion, neither of which model very closely the case of cone penetration.

The original work on the expansion of spherical and cylindrical cavities in materials with a von Mises yield surface was performed by Bishop et al (1945). The formulae were applied to the deep penetration of copper blocks by a pointed indenter. Bishop considered the cases of cylindrical and spherical expansion to bound the pressure required for deep indentation and demonstrated the importance of adding the frictional forces acting on the tip onto the normal

expansion pressure to obtain the penetration resistance. Their experimental work showed that a penetration of four to five probe diameters was required before peak resistances were obtained.

Gibson (1950) suggested the application of this work to pile tip resistances in clay. From the consideration of spherical cavity expansion he derived:

$$N_k = \frac{4}{3} \left( \ln \frac{E_o}{3c_u} + 1 \right) + 1$$

Note:  $\frac{E}{3c_u} = \frac{G}{c_u} = I_r$  for undrained conditions

where:  $E_o$  = Undrained initial tangent modulus of elasticity

$I_r$  = Rigidity index

Skempton (1951) suggested a different formula for  $N_k$  but attributed it to Gibson (1950).

$$N_k = \frac{4}{3} \left( \ln \frac{E_s}{c_u} + 1 \right) + 1$$

where:  $E_s$  = Undrained secant modulus at half the peak deviator stress.



Skempton suggested values of  $E_s/c_u$  of between 50 and 200 resulting in  $N_k$  values from 7.5 to 9.4. It must be noted however that Skempton provided no derivation of the above formula and that it appears to lack rigour. While it is appropriate to consider whether  $E_o$  or  $E_s$  is better suited to this analysis the Gibson form of the equation is correct.

Vesic (1972) produced a full solution for a Mohr-Coulomb soil with or without internal friction and volumetric strain for conditions of both spherical and cylindrical cavity expansion. Vesic's solution for the spherical expansion under conditions of zero average volumetric strain and zero internal friction was:

$$p_u = \frac{4}{3} (\ln I_r + 1) c_u + p_o'$$

where:  $p_u$  = ultimate cavity expansion pressure  
 $p_o'$  = initial isotropic effective stress

This result is equivalent to those of Bishop et al (1945) and Gibson (1950) if a shear stress equal to  $c_u$  is added to the cavity expansion pressure to model a rough footing surface. The equivalent

result of cylindrical expansion under the same conditions was given as:

$$p_u = (\ln I_r + 1) c_u + p_o'$$

which is identical to analysis of undrained pressure-meter expansion in clay given by Gibson and Anderson (1961). Vesic also produced solutions for the excess pore pressures ( $\Delta u$ ) generated by spherical or cylindrical expansion. At the cavity wall these expressions become:

$$\Delta u_{\max} = (0.943 a_f + \frac{4}{3} \ln I_r) c_u \quad (\text{spherical cavity})$$

$$\Delta u_{\max} = (0.817 a_f + \ln I_r) c_u \quad (\text{cylindrical cavity})$$

where:  $a_f$  is the Henkel pore pressure parameter at failure.

This approach is semi-empirical as the pore pressures generated due to pure shear are accounted for by the empirical factor  $a_f$ . Strictly, the linear elastic perfectly plastic soil model would predict pore pressures solely due to the change in mean stress, i.e:

$$\Delta u_{\max} = \frac{4}{3} c_u \ln I_r \quad (\text{spherical cavity})$$

$$\Delta u_{\max} = c_u \ln I_r \quad (\text{cylindrical cavity})$$

as described by Randolph and Wroth (1978). For values of  $G/c_u$  between 100 and 250 the above expressions produce the values of pore pressure shown in Table 1.1.

The range of ( $\alpha_f = 0.8 - 2.0$ ) chosen corresponds to normally consolidated clays.

G/c <sub>u</sub>	$\Delta u_{\max}/c_u$ Randolph & Wroth (1978)		$\Delta u_{\max}/c_u$ ( $\alpha_f=0.8-2.0$ ) Vesic (1972)	
	Spherical	Cylindrical	Spherical	Cylindrical
100	6.1	4.6	6.9-8.0	5.3-6.2
150	6.7	5.0	7.5-8.6	5.7-6.6
200	7.1	5.3	7.9-9.0	6.0-6.9
250	7.4	5.5	8.2-9.3	6.2-7.1

**TABLE 1.1 PREDICTED EXCESS PORE PRESSURES FOR SPHERICAL AND CYLINDRICAL CAVITY EXPANSION IN CLAY**

In addition to the simple linear elastic-perfectly plastic soil models considered above, more complex soil models have been analysed for spherical and cylindrical expansion. Ladanyi and Eden (1969) produced a closed form solution for a sensitive clay.

The stress vs. strain curve was simplified into 3 straight lines as shown in Figure 1.6. For Canadian Leda clay with a sensitivity of 2.2 an  $N_k$  in the range of 5.9 to 6.7 was calculated while an equivalent insensitive clay would have had an  $N_k$  value of between 8.2 and 9.2. Laboratory and field tests with an enlarged tip Borros penetrometer were analysed against vane test data in these clays. Good agreement with the theoretical  $N_k$  was obtained. However it should be noted that the laboratory penetration rate was 0.059mm/s and the field rate was 3.3mm/s. Rate effect measurements on these clays are discussed below.

Ladanyi (1963) proposed a more elaborate solution to the cavity expansion problem using the actual stress vs strain curves measured in undrained triaxial compression. The solution applied to deep circular footings consisted of four steps:

- a) obtain the unique strain field around a spherical cavity:

$$\gamma = 2 \tan^{-1} \left( 2 \left( \frac{r}{a} \right)^3 - 1 \right)^{-1}$$

Where  $\gamma$  = shear strain

$r$  = radius considered

$a$  = cavity radius

- b) From the shear strain distribution and the triaxial tests determine the radial distribution of deviatoric and mean normal effective stresses ( $q$  and  $p'$ ).
- c) Calculate the radial distribution of principal total stresses by numerical integration of the equilibrium equation.
- d) Calculate the pore pressure distribution by calculation of the mean normal total stress ( $p$ ) and subtraction of the corresponding mean normal effective stress ( $p'$ ).

$$\text{i.e. } \Delta u = p - p'$$

This method bears considerable similarity to the more recent strain field solutions mentioned below. The results of the study produced  $N_k$  values lower than those obtained by Gibson (1950) or Skempton (1951). Using six normally consolidated stress vs strain curves from three different clays a mean  $N_k$  of 8.8 was calculated. Recent developments in triaxial testing have demonstrated that soil stiffness increases dramatically at very low strains. Such data were not available to Ladanyi but would have increased his calculated values of  $N_k$ . Ladanyi also

concluded that for normally consolidated clays the pore water pressure reached approximately 75% of the internal cavity pressure. On the basis of one triaxial test he calculated a fall in  $N_k$  for a high value of OCR.

Recently the Modified Cam Clay soil model has been applied to cylindrical cavity expansion by finite element techniques (e.g. Carter et al 1979, Randolph, Carter and Wroth 1979). Details are given in the second of these papers of the principal effective stress and pore pressure changes for cylindrical cavity expansion and subsequent consolidation using Boston Blue Clay (BBC) soil parameters at OCRs ranging from 1 to 32. For normally consolidated BBC a value for the increase in mean total stress of  $3.6 c_u$  was calculated corresponding to a secant  $G/c_u$  of just over 30. The corresponding value of  $(\Delta u_{\max}/c_u)$  was 4.2. The low value for secant  $G/c_u$  was justified because, unlike the overconsolidated cases, the normally consolidated clay lies on the yield surface prior to cavity expansion and thus plastic yield occurs even at very small strains. The idealised stress paths predicted are shown in Figure 1.7. Randolph et al considered that the rigidity index would gradually rise with increasing OCR arguing that  $G$  should be related to the maximum past value of the

bulk modulus ( $K_{\max}$ ). A result of this relationship is that ( $\Delta u_{\max}/c_u$ ) only falls gradually with increasing OCR (Figure 1.8). However the normalised total cavity expansion pressure ( $\Delta p/c_u$ ) rises with increasing OCR. Opinion on the trend of  $G/c_u$  with OCR is divided with many authors suggesting the opposite trend to Randolph et al. (e.g. Battaglio et al 1981, Jamiolkowski et al 1979). If in fact the rigidity index decreases with increasing OCR then ( $\Delta u_{\max}/c_u$ ) will decrease more rapidly with OCR than shown on Figure 1.8 and ( $\Delta p/c_u$ ) will tend to decrease rather than increase with higher OCR.

As a development from the relatively simple case of cylindrical or spherical cavity expansion Levadoux and Baligh (1980) presented their strain field solution. The approach used by these authors considered the soil flowing around an approximately penetrometer shaped object as if it were a non-viscous incompressible fluid. Their method consisted of four principal steps:-

1. The first step was to determine the strain paths followed in the soil. This was done by estimating a velocity field and from this the deformation field by integration along the streamlines

(Figure 1.9). The strain rates along the streamlines were then calculated and by integration of these rates the strain paths were obtained.

2. Having obtained the strain field which, as noted by Ladanyi (1963) is independent of basic soil properties (excepting bulk modulus), the deviatoric stresses were calculated. Levadoux and Baligh used a complex deviatoric stress soil model for this purpose noting that the model had to be capable of handling a stress reversal.
3. The shear induced pore pressures were then calculated in a similar manner to the deviatoric stresses using a separate model.
4. The final step was to use equilibrium considerations to calculate the total, effective and mean normal stresses. The excess pore pressure was calculated by adding the shear induced pore pressure to the change in mean normal stress.

Although the implementation of this method by Levadoux and Baligh contains a number of serious shortcomings (including failure to meet the stress equilibrium requirement and use of a penetrator shape with a "smoothed off" shoulder) their work



represented a major advance in the understanding of the penetration process. The absolute magnitude of the pore pressures was not particularly well predicted by this method but the normalised distribution of these pressures (Figure 1.10) is still the only analytical solution available for a quasi-penetrometer shaped object. In order to predict values of total cone resistance ( $q_t$ ) account had to be taken of the frictional forces developed on the cone surface. The  $q_t$  values obtained from the smooth case were modified as follows:-

$$q_t(\text{rough}) = q_t(\text{smooth}) + \tau_r / \tan \delta$$

Where:  $\tau_r$  = average shear stress acting on the face of the cone  
 $\tau_r$   $\approx$  residual shear stress  
 $2\delta$  = cone tip angle

Using this method and making further allowance for OCR, cone resistances within 10% of those measured were predicted in Boston Blue Clay.

Considerable further work is required on this promising form of calculation in order to produce reliable stress and pore pressure predictions for the

cone penetrometer in clays with a range of significant properties (e.g.  $I_r$ ,  $S_t$ ,  $a_f$  or equivalent etc). Current work at Oxford including principally the research of C.I. Teh is directed at this object.

Recent attempts have been made to use the finite element method to obtain values for  $N_k$  in an elastic-perfectly plastic soil. De Borst (1982) compared the results of calculations performed with 15 noded triangular elements with those produced by 8 noded quadrilaterals (De Borst and Vermeer 1982). In both sets of calculations the usual small strain formulation was used and the rigid penetrometer was taken to be initially embedded in the soil without disturbance. The penetrometer was then advanced axially in finite displacement steps until the tip loads reached an arbitrary failure criterion. Although the 8 noded quadrilateral elements produced values of  $N_k=18$  for  $G/c_u = 125$  and  $v=0.49$ , serious stress instabilities were found when the rough shaft case was examined. The more sophisticated 15 noded triangular formulation gave stable stresses and produced a value of  $N_k=10.2$ . Values of  $(c_a/c_u)^*$  of 0.8 and 0.5 were used for the cone and shaft respectively. An important conclusion from this study was that the 8 noded quadrilateral elements with their associated reduced integration technique were unsuitable for the analysis of this type of heavily constrained problem.

\* where  $c_a$  is the adhesion between the soil and the cone face.

Sloan and Randolph (1982) had earlier argued the same point demonstrating the superiority of the higher order element with its possibilities of full integration in axi-symmetric problems.

A summary of the analytically predicted  $N_k$  factors for undrained clays from the different approaches discussed above is given in Table 1.2. It may be noted that the different techniques show considerable agreement with predictions of  $N_k$  from 7.4 to 10.2 for insensitive clays.

Author	Type of Analysis	$N_k$ (inclusive of shape factor)	Significant Soil Parameters
Meyerhof (1951)	Slip Surface	9.3	Rigid-Perfectly Plastic
De Beer (1977)	Slip Surface	9.9	Rigid-Perfectly Plastic
Gibson (1950) & Meyerhof (1951)	Spherical Cavity Expansion	8.5 - 9.7	$E_o/c_u = 300-750$
Skempton (1951)	Spherical Cavity Expansion	7.5 - 9.4	$E_s/c_u = 50-200$
Ladanyi (1963)	Spherical Cavity Expansion	7.4 - 9.3	Use of triaxial stress vs strain curves
Ladanyi & Eden (1969)	{ Spherical	8.2 - 9.2	$S_t=1, E_s/c_u=200-500$
	{ Cavity Expansion	5.9 - 6.7	$S_t=16, E_s/c_u=250-500$
De Borst (1982)	Finite Element	10.2	$G/c_u=125$

**TABLE 1.2 SUMMARY OF ANALYTICAL  $N_k$  FACTORS FOR DEEP CIRCULAR FOUNDATIONS**

### 1.3 Comparison of Field and Laboratory Tests against Analytical Solutions

#### 1.3.1 Tip Resistance

In Skempton's formative paper on bearing capacity (Skempton 1951) he reported the experimental results of Meigh and Yassin concerning the increase of bearing capacity with depth of penetration. Using circular plates they obtained limiting  $N_k$  factors at a penetration equal to approximately 4 plate diameters. The different clays tested gave slightly different maximum  $N_k$  factors with a value of 9.8 for remoulded London Clay and approximately 8 in remoulded Horton Clay and undisturbed Shellhaven Clay. Using a penetrometer with an enlarged tip Koumoto and Kaku (1982) obtained reasonable agreement between experimental results and their predicted combined bearing capacity factor ( $N_k$ ) of 9.8 (assuming  $\sigma_2 = \sigma_3$ ).

Bearing the above remarks in mind it would be of considerable interest to compare the bearing capacity of buried plates with the tip resistance of flush sided penetrometers or piles. The 100mm diameter self boring plate tests of Kay and Parry (1982) provided such a comparison. These tests, on a thoroughly investigated site in Cambridgeshire, were conducted adjacent to conventional CPTs. The  $N_k$  value from the CPTs averaged 20 while the bearing

capacity factor for the plates averaged 9 when derived from the mean undrained shear strength from triaxial extension and compression tests. It may be noted that the rate of penetration for the plate tests was 0.3mm/min compared with a rate of 1200mm/min for the CPTs. In addition the cone resistance ( $q_c$ ) data given was uncorrected for the effects of water pressure acting in the groove above the tip, although this correction is probably small for the overconsolidated Gault Clay. It may be concluded that the failure mechanisms in the soil around a vertically loaded buried plate and a penetrometer are substantially different and while limit analysis using plasticity provides a reasonable method for the analysis of the plate it is inadequate for the analysis of the CPT.

Despite this conclusion a plasticity derived formula is almost universally used for the practical analysis of the CPT. The equation is written:

$$q_c = N_k c_u + \gamma D$$

where  $q_c$  = cone resistance

$N_k$  = empirical bearing capacity factor

A number of recently published values for the empirical  $N_k$  are shown in Table 1.3.

Author(s)	Location/Soil	Empirical $N_k$	Correlating Test for Undrained Shear Strength
De Beer (1977)	Boom clay: "very soft" "soft" "firm (overconsolidated)"	20 15 9-10	Field Vane
Kjekstad et al (1978)	North Sea clays	15-20	Consolidated undrained triaxial
Nash and Duffin (1982)	Northern England: Glacial till Laminated clays	19 12.5	Unconsolidated undrained triaxial
Lacasse and Lunne (1982)	Onsøy Norway Drammen Norway	12.4-19.4 12.6-17.3	Corrected field vane
Toolan and Fox (1977)	Highly sensitive normally consolidated clay: Insensitive normally and lightly over-consolidated clay: Heavily overconsolidated clay:	6-8  10-15  15-30	Mainly quick unconsolidated undrained (QUU) triaxial tests
Thorburn et al (1981)	Scottish clays: Normally consolidated to moderately over-consolidated	12-20 (increasing with OCR)	"High quality sampling and testing" (thin walled plus sampling and QUU triaxial tests)

TABLE 1.3 EMPIRICAL  $N_k$  FACTORS FROM FIELD TESTING

It may be noted that Thorburn et al (1981) plot  $N_k$  against the projected cone resistance intercept at ground level ( $q_{CO}$ ). The value of  $q_{CO}$  may be related to the maximum past overconsolidation stress at ground level. Although from a theoretical standpoint it would be preferable to plot  $N_k$  against OCR or even the rigidity index ( $I_r = G/c_u$ ), the plot of  $q_{CO}$  against  $N_k$  has proved to be of considerable practical use.

When considering the empirical  $N_k$  values shown in Table 1.3 various points should be borne in mind.

1. Potentially the most serious short-coming of this data is that the measured cone resistance ( $q_c$ ) rather than the total cone resistance ( $q_t$ ) has been used to derive  $N_k$ . The difference between  $q_c$  and  $q_t$  arises from pore pressure acting in the joint between the tip and shaft of the penetrometer (Fig. 1.11). The value of  $q_t$  corresponds to the total end bearing capacity and is independent of internal penetrometer design. This effect is most severe in normally consolidated clays in which the highest excess pore pressures are generated at the cone shoulder (see Schaap and Hoogenboom 1983).

2. The values of undrained shear strength used to calculate  $N_k$  are of variable quality and fundamental nature. Concerning the quality of results, different sampling techniques will have produced differing degrees of sample disturbance for the triaxial tests. The field vane produces results that are rate sensitive and may in any case be best interpreted as a drained test due to the thin zone of soil sheared (Wroth 1984) or as a strength index test. Different vane designs introduce varying degrees of soil disturbance. Even if the different tests were conducted without disturbance differences between the undrained shear strengths would be obtained due to strength anisotropy and the differing stress paths followed by different tests (Wroth 1984).
3. Some variation in  $N_k$  factors may be expected due to variations in soil properties not considered by plasticity theory. Such properties include the shear modulus ( $G$ ) the sensitivity ( $S_t$ ) and the soil response to the rate of shearing ( $\dot{\gamma}$ ).



The effect of failure to apply water pressure corrections to  $q_c$  in order to produce  $q_t$  is that empirical  $N_k$  factors in normally and lightly over-consolidated clays will have been underestimated. However, sampling disturbance will tend to have produced underestimates of the clay's shear strength  $c_u$ . If  $c_u$  is underestimated then  $N_k$  is over-estimated. Thus these errors are to some extent compensating. When the field correlations presented in Table 1.3 are compared to the theoretical  $N_k$  values of Table 1.2 a considerable discrepancy is apparent.  $N_k$  values from high quality field testing are frequently twice the maximum theoretical values. It is not credible that this magnitude of difference is due to errors in assessing insitu elastic parameters. The rigidity index would have been increased by three orders of magnitude from its maximum likely value to obtain an  $N_k$  of 20 from Gibson's analysis for example.

A fundamental reason for cone resistances exceeding the theoretical values may be the effect of the rate of shearing on the undrained shear strength. Levadoux and Baligh (1980) and Tumay et al (1985) have predicted the distribution of shear strain rate around a perfectly smooth penetrometer advancing at 20mm/sec. (Fig. 1.12). This analysis suggests an octahedral shear strain rate ( $\dot{\gamma}_{oct}$ )

of between  $100 \text{ hr}^{-1}$  and  $500 \text{ hr}^{-1}$  around the tip within 2 shaft radii of the cone centre line. Unconsolidated undrained triaxial tests are usually conducted at an axial strain rate of  $2\% \text{ min}^{-1}$  which is equivalent to a  $\dot{\gamma}_{\text{oct}}$  of approximately  $1.5 \text{ hr}^{-1}$ . Higher quality consolidated undrained triaxial tests may be conducted with a  $\dot{\gamma}_{\text{oct}}$  of around  $0.02 \text{ hr}^{-1}$ . The field vane however imposes a high rate of shear strain on the soil which is difficult to assess accurately due to uncertainty over the width of the shear zone. From a consideration of the above range of shear rates it seems probable that some correction of the shear strengths produced by triaxial testing will be required for comparison with the standard CPT.

Mitchell (1964) demonstrated that the rate dependence of the shearing resistance of clay soils could be expressed as:

$$q_f = a + b \ln \dot{\epsilon}$$

where:                    a and b are constants  
 $\dot{\epsilon}$  is the strain rate

Marayama and Shibata (1964) showed that this relationship was a special case of the more general sinh relationship:

$$q_f = a + d \sinh^{-1} \dot{\epsilon}$$

where:  $d$  is a constant

Triaxial test data from Mitchell (1964) and others indicate that the logarithmic form of the relationship adequately models the behaviour of most clays at axial strain rates of  $0.002\% \text{ min}^{-1}$  and above.

---

Applying the logarithmic approximation to the CPT problem each tenfold increase in rate of shearing could be expected to produce a fixed percentage increase in shearing resistance. Limited data suggests that the magnitude of shear strength increase is commonly between 5% and 10% for each tenfold increase in shear rate. Such a rate effect suggests that QUU triaxial shear strengths might need to be increased by around 10% and CU triaxials by up to 40% for use in CPT correlations. Such increases would lead to proportional decreases in the value of  $N_k$ .

The evidence for a rate effect of Mitchell's form from cone penetration tests run at varying rates is somewhat ambiguous. Lacasse and Lunne (1982) report increases in cone resistance of between 5% and 10% for an increase in CPT rate from 2mm/sec to 20mm/sec

at Onsøy and Drammen. No change in the measured pore pressures was observed. Campanella et al (1981) show an approximate 4% increase in  $q_t$  for the same increase in rate when testing a very silty clay. As the penetration rate was reduced below 1mm/sec noticeable reductions in measured pore pressure began to be recorded, Figure 1.13. Laboratory studies on sensitive Canadian clays performed by Ladanyi and Eden (1969) showed an average 7.5% increase in tip resistance for tenfold rate increases. Test rates of between 0.059 and 2.1mm/sec were used for a 15.5mm diameter flat ended probe.

Set against this evidence are the field tests of De Beer (1977), Kerisel (1967) and the laboratory tests Luger et al (1982). All of these authors failed to find any change in  $q_c$  for tests conducted at less than about 20mm/sec. Bemben and Myers (1974) and Roy et al (1982b) reported variable cone resistances at rates of less than 20mm/sec (Figure 1.14). Neither set of authors were able to offer satisfactory explanations for the observed behaviour.

Bruzzi and Cestari (1982) published data from two CPT's in Port Tolle clay that suggested a 30% increase in  $q_c$  for a decrease in rate from 20mm/s to 3mm/s. If this data is reliable it may fit into the pattern of Roy et al and Bemben and Myers.

The most reliable data on cone resistances at rates substantially in excess of 20mm/sec was provided by Luger et al (1982). Using a small scale penetrometer with an undersized shaft they investigated penetration rates of up to 2m/s. Their results showed a 17% increase in  $q_c$  for each tenfold increase in penetration rate above a rate of 10mm/sec.

The above evidence from field and laboratory CPT's does suggest the presence of a rate effect on the cone resistance and hence presumably also on the shear strength of the different clays. However the scatter in the data indicates that the effect of rate varies in different deposits from quite low values perhaps in very silty or overconsolidated clays to higher values in normally consolidated or sensitive clays.

### 1.3.2 Pore Pressure Response

Theoretical predictions of normalised excess pore pressure ( $\Delta u/c_u$ ) range between 6.1 and 7.4 for spherical expansion and 4.6 to 5.5 for cylindrical expansion with  $I_r$  varying between 100 and 250. (Table 1.1). Vesic's semi-empirical formulae produce rather higher values of  $\Delta u/c_u$  for normally consolidated clays. For spherical expansion a  $\Delta u/c_u$  of up to 9.3 is calculated with a corresponding maximum of 7.1 for cylindrical expansion. As the Henkel pore

pressure parameter at failure ( $a_f$ ) increases for sensitive clays even higher values of  $\Delta u/c_u$  may be produced here. However overconsolidated clays would generate lower pore pressures due to reduced  $a_f$  values. For the linear elastic perfectly plastic soil model only the variation of  $G/c_u$  alters the generated pore pressure as  $a$  is zero for true elastic behaviour.

It has commonly been assumed that the spherical expansion solution is appropriate for the tip behaviour and the cylindrical expansion can be applied to the pore pressures generated on the shaft.

Empirical correlations between excess pore pressure and undrained shear strength are usually expressed in the following form derived from the cavity expansion model for a linear elastic-plastic soil:

$$\Delta u = N_{\Delta u} c_u$$

where:  $N_{\Delta u}$  = the excess pore pressure factor.

The  $N_{\Delta u}$  factor is also a function of the location of pore pressure measurement on the penetrometer (Figure 1.15) and of OCR (or a related parameter). Table 1.4 shows values for this factor at various clays sites. Comparison of this data with the theoretical values presented in Table 1.1 indicates that high values of  $I_r$  (i.e.  $I_r > 250$ ) are required to

match elasto-plastic theory to field data. Rigidity indices of 100 to 250 may account for the field data if the semi-empirical Vesic approach is adopted with the incorporation of  $\alpha_f$ . However, the problem of selecting a single value of  $I_r$  for each soil remains.

Author	Location of pore pressure measurement	$N_{\Delta u}$	Soil	Correlating test for $c_u$
Baligh & Vivatrat (1979).	All on cone apex	8.2	Boston Blue Clay OCR=6-7	Triaxial and Field vane
Baligh et al (1981)		11.1 16.9-17.9	OCR=3-4 OCR=1.1-1.3	
Lacasse & Lunne (1982).	All on cone shoulder	6.6-9.3	Onsøy OCR=1.3 $S_t=5-7$ Drammen	CAU triaxial
Lacasse et al (1981)		5.9-6.2 5.4-5.9	OCR=1.5 $S_t=7$ OCR=1.15 $S_t=3$	CAU triaxial
Roy et al (1982 a)	Cone face Cone shoulder 1Ø above shoulder	7.4-9.5 6.3-8.0 4.4-5.6	Champlain Clay OCR=2.1-2.3 "Sensitive"	Field vane

NOTE: CAU = anisotropically consolidated undrained triaxial compression

TABLE 1.4 FIELD CORRELATIONS FOR EXCESS PORE PRESSURE

FACTOR  $N_{\Delta U}$

#### 1.4 The Analysis of Pore Pressure Dissipation Following Penetration.

The hydraulic characteristics of primary interest to the geotechnical engineer are the permeability of a soil ( $k_h$  and  $k_v$ ) and the coefficient of consolidation ( $c_h$  and  $c_v$ ). It has been suggested by several authors that one or both of these parameters may be determined from records of the dissipation of excess pore pressures during a stop in penetration.

Two basic methods of analysis have been employed:

1. One dimensional radial consolidation (cylindrical or spherical) usually with a logarithmic initial pore water pressure distribution derived from cavity expansion.
2. Two dimensional consolidation incorporating the actual probe geometry and a more complex initial pore water pressure distribution.

1) The earliest analysis of this problem was aimed at the determination of set-up times for piles. Soderberg (1962) and Ladanyi (1963) produced solutions for the dissipation of pore pressure in a homogenous soil after spherical or cylindrical cavity expansion. The cylindrical solution was seen as applicable to the pile shaft while the spherical



solution was suggested for the behaviour around a pile (or penetrometer) tip. The use of this one dimensional analysis for predicting the behaviour of pile shafts has been advanced recently by a number of teams working on the ESACC project (Kraft, 1982). The most successful of these methods (Randolph, Carter and Wroth, 1979) appears capable of predicting shaft capacities to the same sort of accuracy as more traditional empirical methods.

Torstensson (1978 and 1982) suggested that the cylindrical and spherical analyses of Soderberg and Ladanyi should be applicable to dissipation around a pore pressure probe. Results of this analysis are given in Fig. 1.16. Calculation of the coefficient of consolidation was recommended at 50% dissipation. Several authors have used these results. Roy et al (1982b) applied them to their Canadian piezocone field tests taking  $E/c_u = 400$ . Assuming the spherical solution to be applicable to the penetrometer tip and the cylindrical solution to the shaft, Torstensson's values for the time factor  $T$  were 0.7 and 3.5 respectively. The measured ratio ( $t_{50}$  shaft/ $t_{50}$  tip) was 4 for the field tests which agrees reasonably well with Torstensson's (or Baligh

and Levadoux's) analysis. However since independent measurements of the hydraulic characteristics of the deposit were not available the absolute accuracy of the predicted values was not assessed.

Lacasse and Lunne (1982) have compared the results of field and laboratory tests with Torstensson's dissipation curves and Baligh and Levadoux's analysis (see below). For a  $60^\circ$  probe they report that Torstensson under predicts  $c_h$  by a factor of between 4 and 6 while Baligh and Levadoux's values "agree amazingly well" with laboratory values from the reconsolidation stage of loading. However Campanella et al (1982) claim that predicted values of  $c_h$  in the overconsolidated range "compare favourably" with Torstensson's cylindrical solution at 50% dissipation for a clay with an OCR of 2.

Battaglio et al (1981) have presented an analysis similar to that of Torstensson but incorporating the empirical pore pressure coefficient  $A_f$ . These authors report that the dissipation curves were unsatisfactory, yielding different values for the coefficient of consolidation ( $c_h$  or  $c_{average}$ ) depending on the degree of dissipation at which the theoretical and measured curves were matched.

2) Results of two dimensional finite element analyses of consolidation around penetrometers have been presented by Baligh and Levadoux (1980) and Acar et al (1982) (Fig. 1.16). These analyses have produced several interesting results:

i) The initial distribution of excess pore pressures strongly affects the shape of the dissipation curves. Baligh and Levadoux used a normalised initial excess pore pressure distribution derived from their strain path approach which, they suggest, should be valid for any clay. Acar et al used a different distribution without indicating how it was derived. This results in rather different dissipation curves (Fig. 1.16).

ii) The rate of dissipation is primarily controlled by the horizontal permeability. Parametric studies by both groups conducted by reducing the vertical permeability to 1/8th or 1/10th of the horizontal permeability showed little change in the dissipation curves. Acar et al found that the variation was rather greater than Baligh and Levadoux however.

iii) As can be seen in Fig. 1.16, the location of the porous filter significantly affects the predicted dissipation curve. Both groups agree that filters

located at the tip or at mid-height on the face of a  $60^\circ$  cone will give essentially identical dissipation curves. Filters located on the shaft of the penetrometer will give longer dissipation times.

Baligh and Levadoux emphasise that the values of  $c_h$  (probe) obtained from the dissipation record apply to the recompression value of  $c_h$  i.e. overconsolidated behaviour. They suggest the following steps (requiring oedometer data) to evaluate  $c_v$  in virgin compression from  $c_h$  (probe):

$$i) \quad c_v(\text{probe}) = c_h(\text{probe}) \, k_v/k_h$$

The ratio  $k_v/k_h$  is difficult to measure with any accuracy but Ladd (1976) gives estimates of its value for various soil types.

$$ii) \quad c_v(N/C) = c_v(\text{probe}) \, [RR/CR]$$

where CR = compression ratio =  $C_c/(1 + e_o)$

RR = recompression ratio =  $C_s/(1 + e_o)$

For dissipation around penetrometers it is suggested that  $RR = 0.5 \times 10^{-2}$  to  $2 \times 10^{-2}$  for many clays.

This method was used with some success to determine normally consolidated values for  $c_v$  in Boston Blue Clay.

Baligh and Levadoux also emphasise the requirement for the theoretical dissipation curve to produce the same value for  $c_h$  (probe) regardless of the degree of dissipation at which the measured curve is analysed. If matching is only attempted at 50% consolidation any "theoretical" dissipation curve (even one drawn randomly) could produce some value for  $c_h$ . In practice a consistent match over the range of 20% to 80% dissipation would suggest a reliable theoretical model as errors in measurement of the hydrostatic pore pressure ( $u_o$ ) or the initial penetration pore pressure ( $u_i$ ) tend to introduce uncertainties into the beginning and end of field records.

#### 1.5 Aims of the Present Research Work

The objectives of this research programme were as follows:

1. The effect of variation in fundamental clay properties on piezocone data was to be evaluated. The following properties were to be considered for normally consolidated clays:

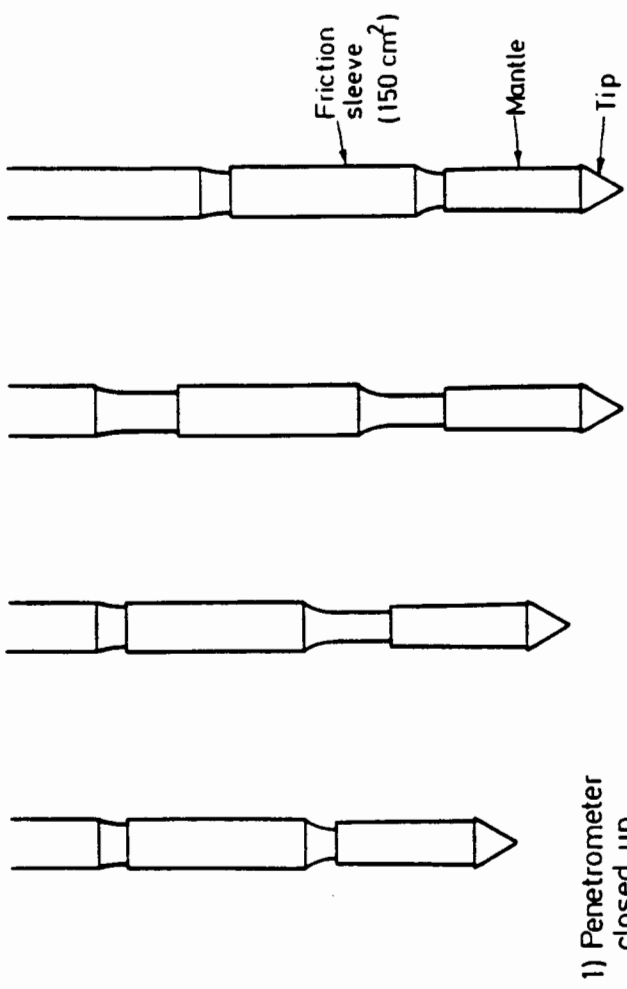
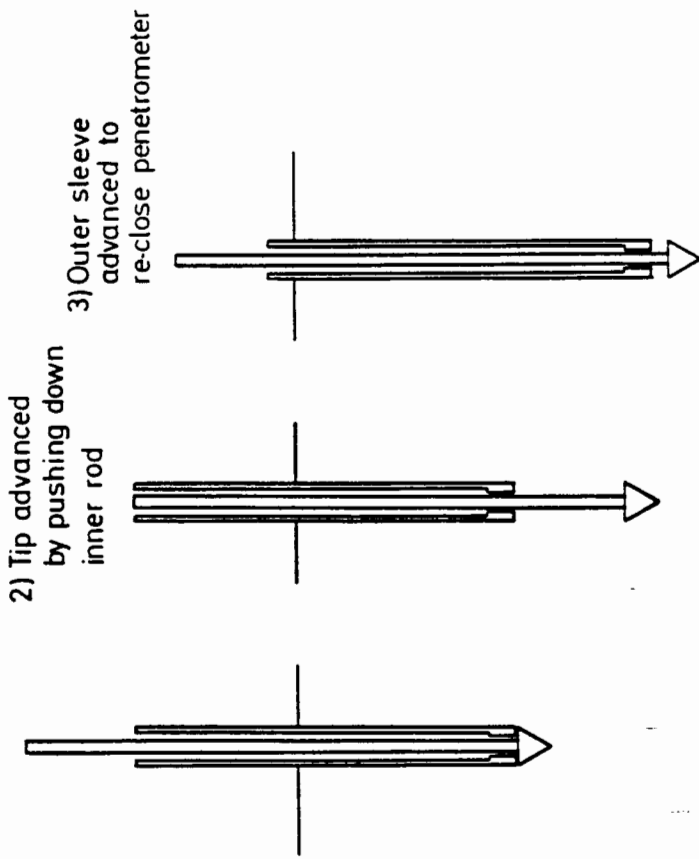
- a) Undrained shear strength  $c_u$
- b) Hydraulic characteristics  $c_h$  and  $k_h$
- c) Soil stiffness  $G$ .

2. The effect of variation in penetration rate on piezocone behaviour was to be determined experimentally. The range of rates to be studied was 20mm/s to 2m/s.
  
3. The experimental results were to be compared with existing theories. They were also to provide a sound experimental data set against which to evaluate new penetration theories.

As the majority of the experimental work was to be conducted in the laboratory it became necessary to evaluate the effects of radial confinement on the CPT. This became a secondary aim and an experimental programme was conducted to evaluate this effect before the main experimental apparatus was constructed.

In conjunction with the work presented in this thesis a number of separate projects have been undertaken at Oxford University by others. A series of studies have been performed to obtain an improved theoretical model for cone penetration. A current DPhil study on this subject is being conducted by C.I. Teh. Laboratory research into piezocone behaviour in overconsolidated clay is also being performed.

1) Penetrometer closed up



Note: Tip and sleeve forces measured independently with Bourdon gauge.

FIGURE 1.1 MECHANICAL PENETROMETER OPERATION

FIGURE 1.2 BEGEMANN MECHANICAL PENETROMETER

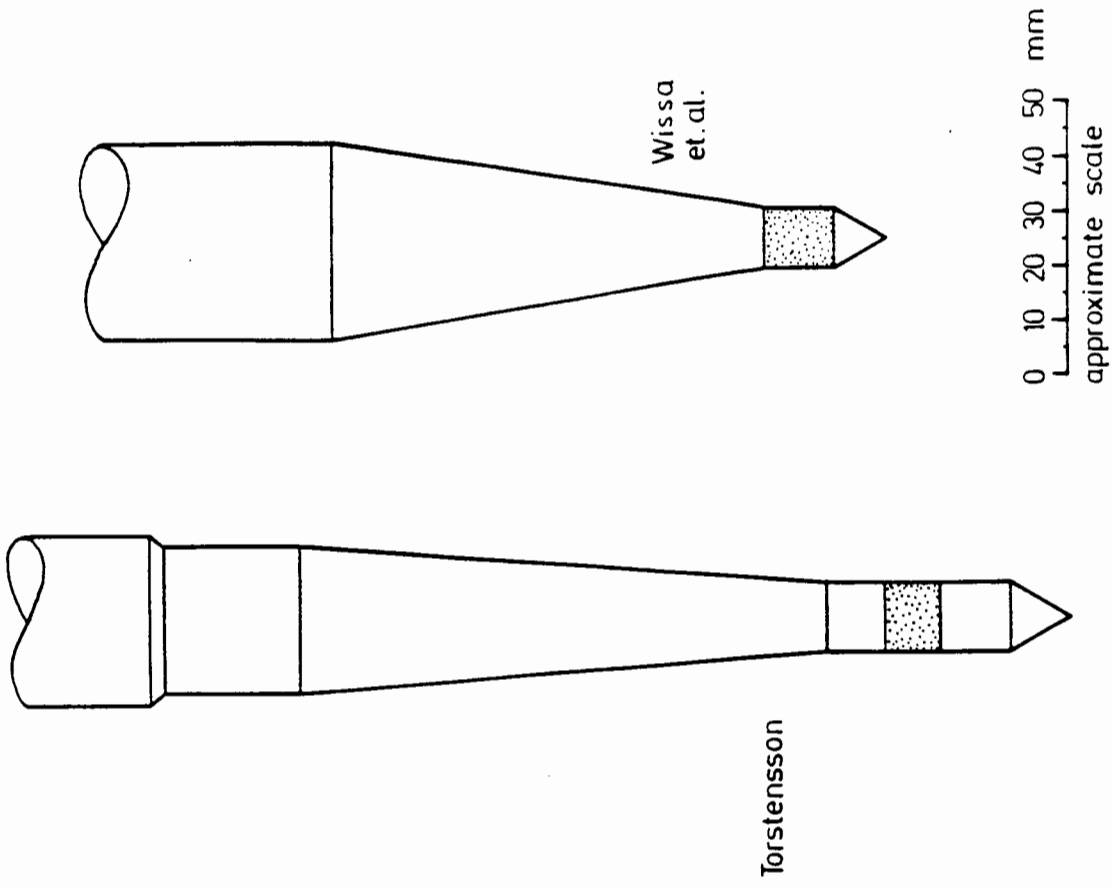
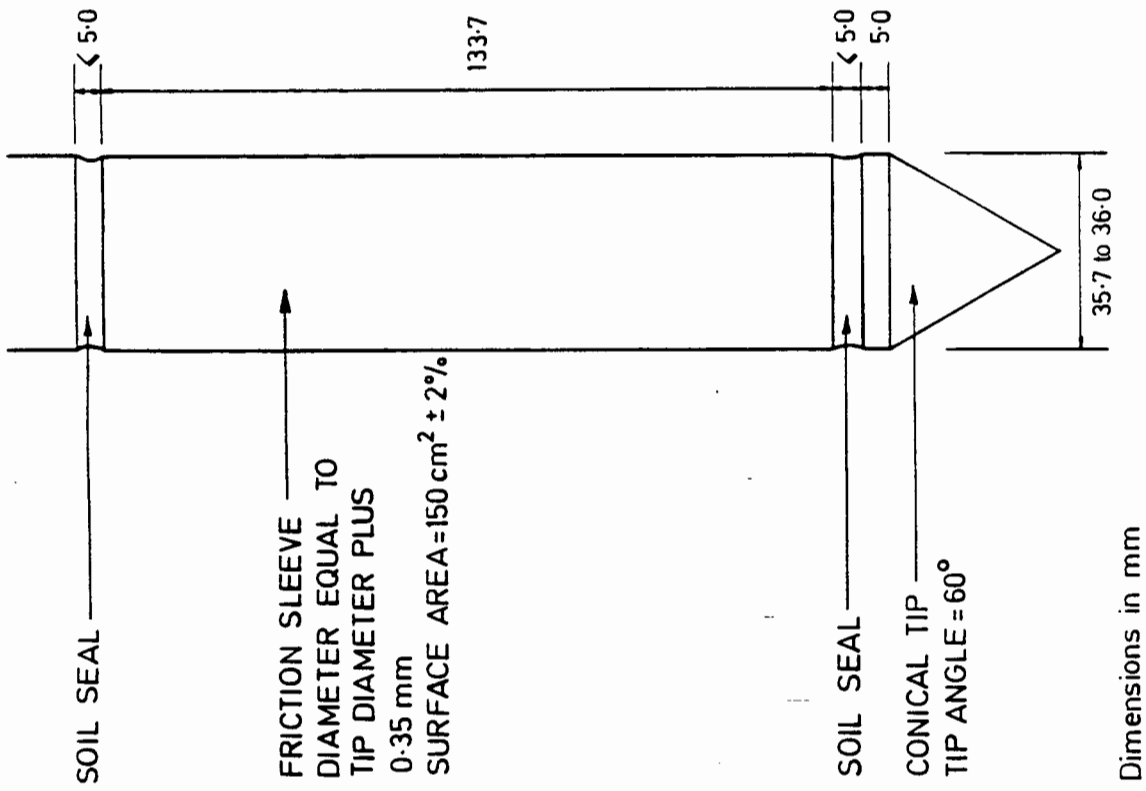


FIGURE 1.3 STANDARD DIMENSIONS OF ELECTRIC CONE PENETROMETER

FIGURE 1.4 TORSTENSSON AND WISSA PIEZOMETER PROBES



- a) Tip filter  
e.g. Baligh et al. (1981)  
Franklin and Cooper (1981)
- b) Face mounted filter  
eg. Tumay et al. (1981)  
Zuidberg et al. (1982)
- c) Filter between Tip and sleeve  
eg. Campanella et al. (1981)  
Smits (1982)

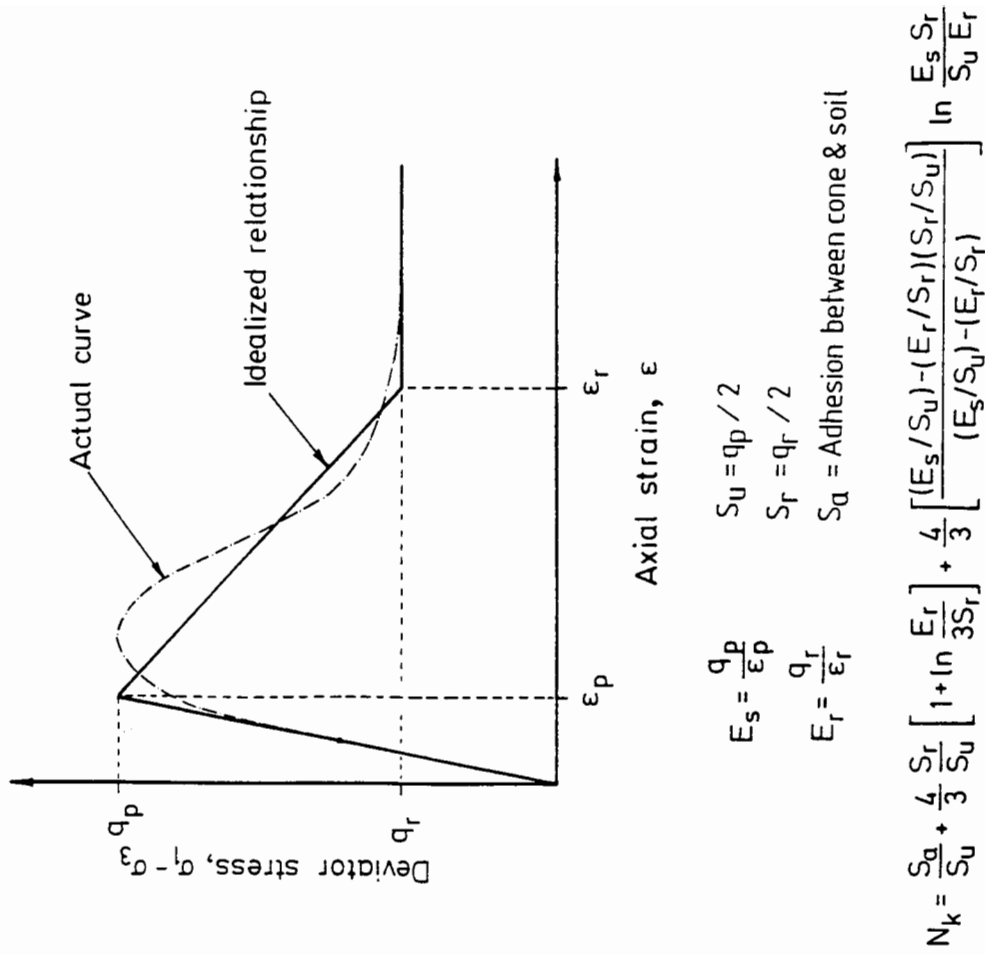


FIGURE 1.6 LADANYI AND EDEN SOLUTION FOR  $N_k$

FIGURE 1.5 COMMON PIEZOCONE CONFIGURATIONS

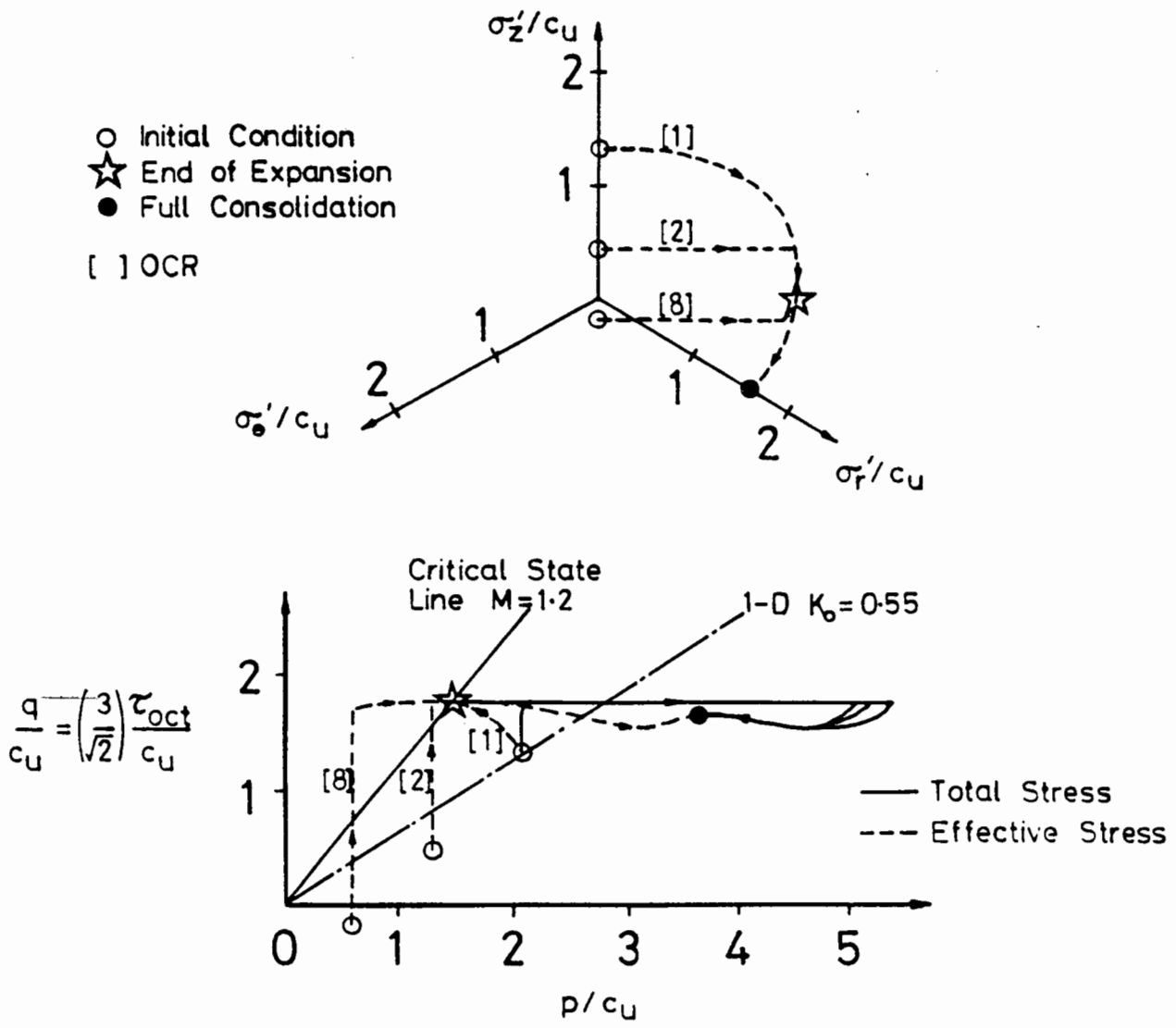


FIGURE 1.7 PREDICTED STRESS PATHS FOR CYLINDRICAL CAVITY EXPANSION  
 After Randolph, Carter and Wroth (1979)

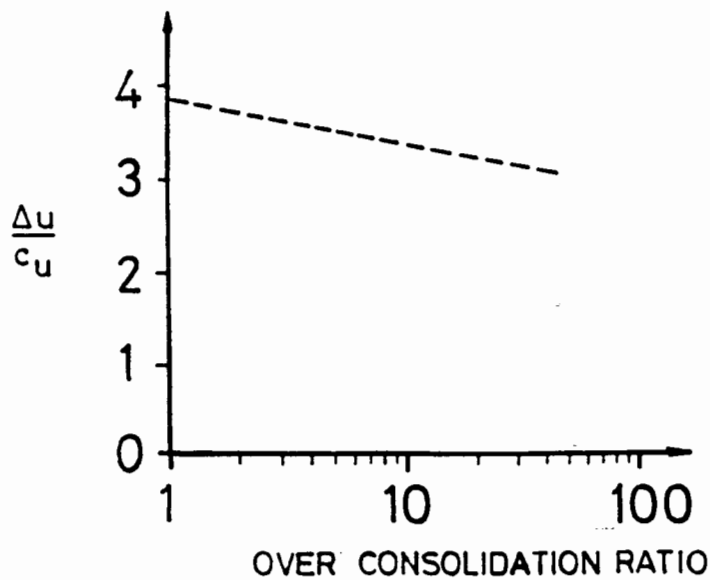


FIGURE 1.8 PREDICTED TREND OF  $(\Delta u_{max}/c_u)$  WITH OCR  
 After Randolph, Carter and Wroth (1979)

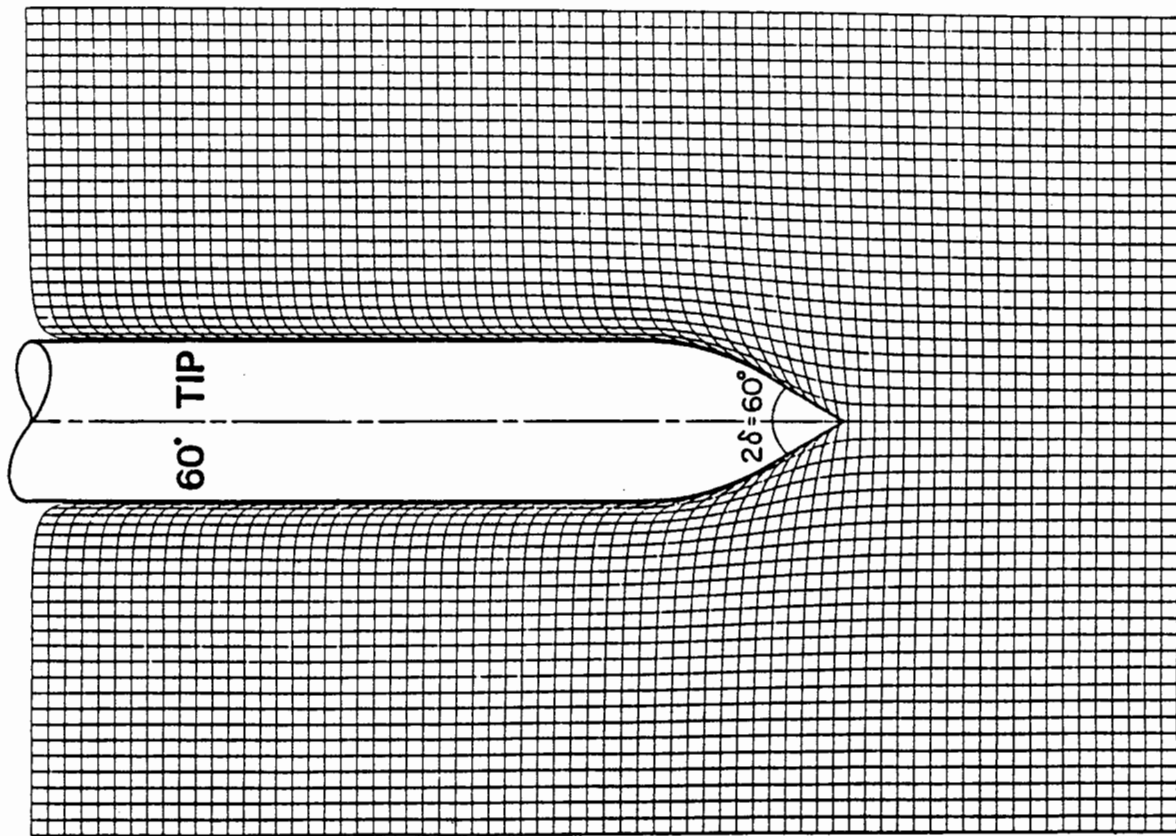
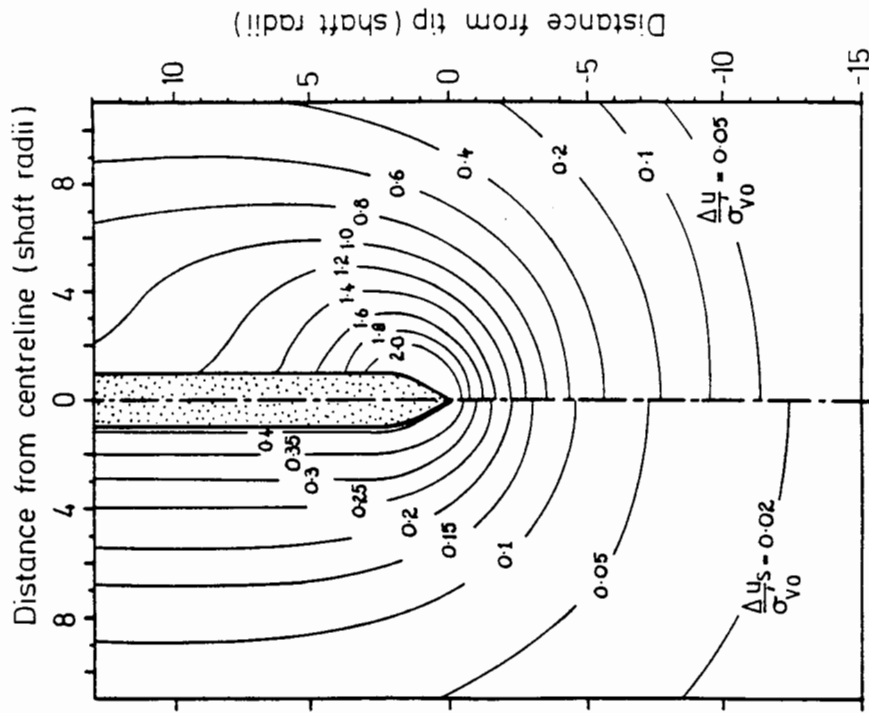
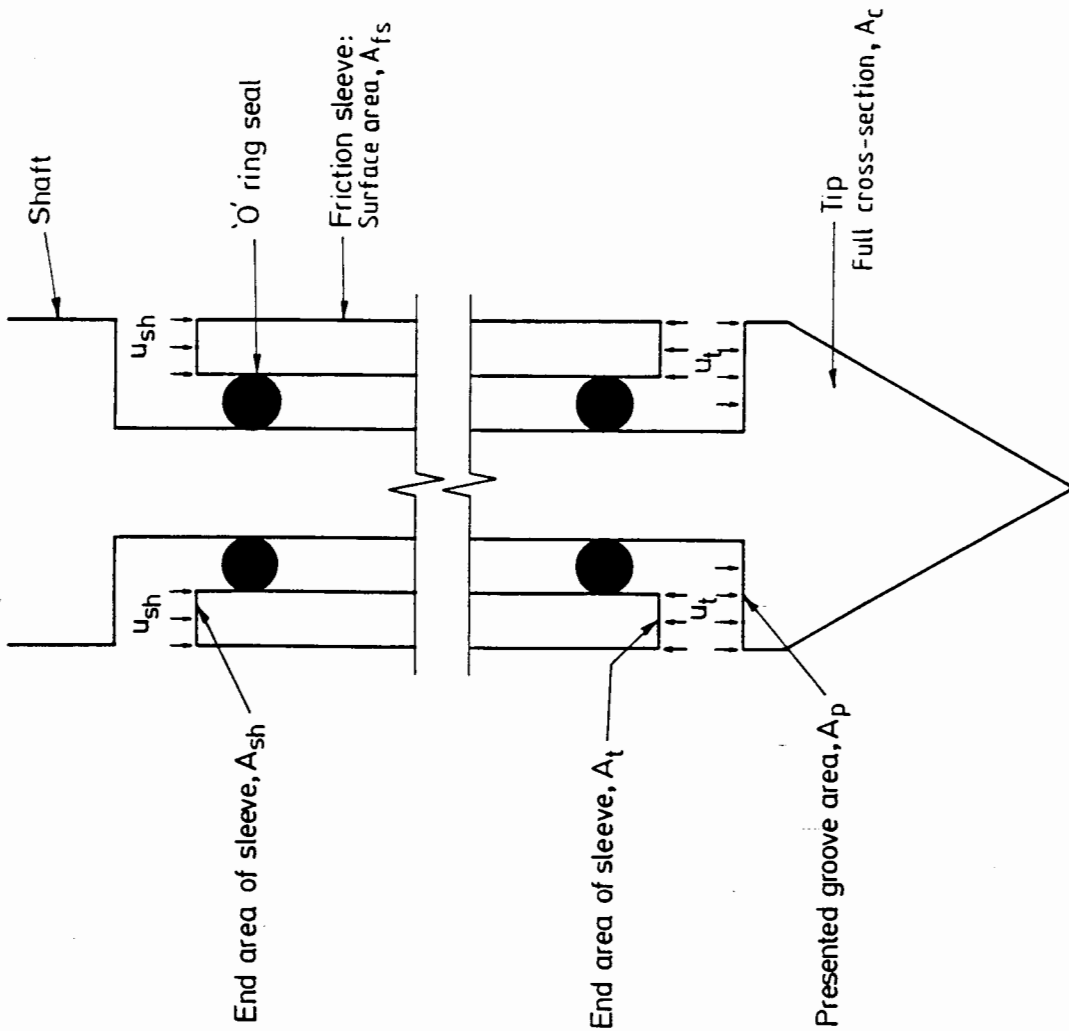


FIGURE 1.9 APPROXIMATE SOLUTION FOR STREAMLINES AROUND PENETROMETER  
After Baligh and Levadoux (1980)



$\Delta u_s$  = Excess pore pressure due to shear only  
 $\Delta u$  = Total excess pore pressure =  $\Delta u_s + \Delta \sigma_{oct}$

FIGURE 1.10 PREDICTED PORE PRESSURE DISTRIBUTION AROUND PENETROMETER  
After Levadoux and Baligh (1980)

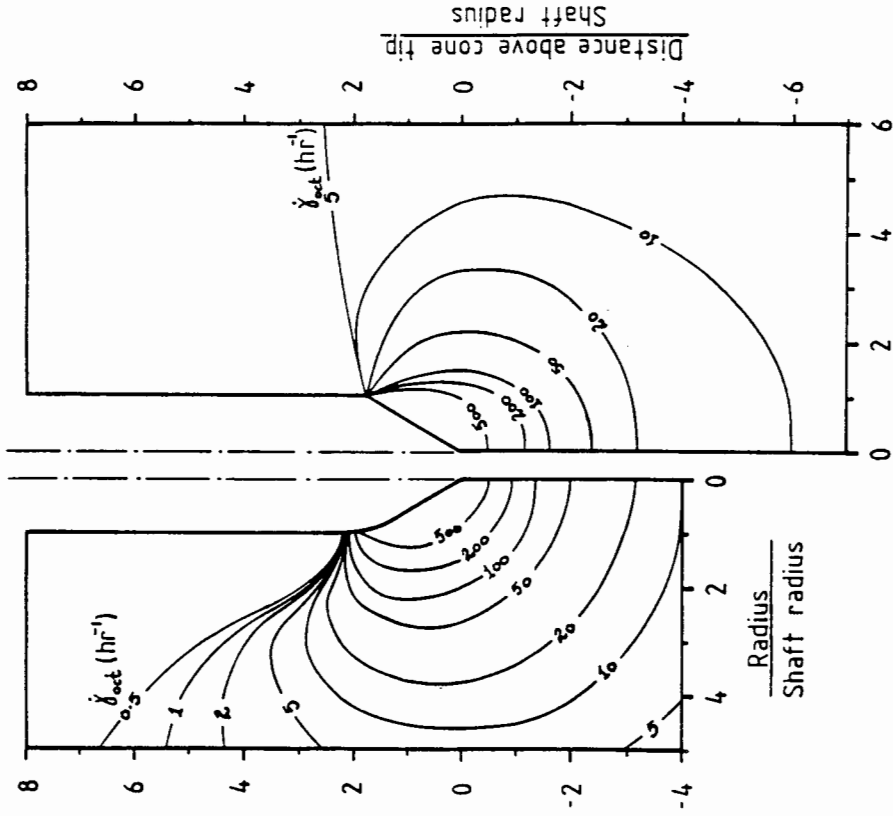


If the grooves are completely flooded the following corrections apply:

$$q_c (\text{corrected}) = q_c (\text{measured}) + \frac{u_t A_p}{A_c} = qt$$

$$f_s (\text{corrected}) = f_s (\text{measured}) + \frac{u_{sh} A_{sh} - u_t A_t}{A_{fs}}$$

FIGURE 1.11 CORRECTION OF PENETROMETER DATA FOR PORE PRESSURE EFFECTS



(a) Levadoux and Baligh (1980)

(b) Tumay, Acar, Cekirge and Ramesh (1985)

Note:  $\dot{\gamma}_{ext} = \frac{2}{3} [(\epsilon_r - \epsilon_t)^2 + (\epsilon_x - \epsilon_t)^2 + (\epsilon_s - \epsilon_t)^2]^{1/2}$

FIGURE 1.12 PREDICTED STRAIN RATES AROUND PENETROMETER

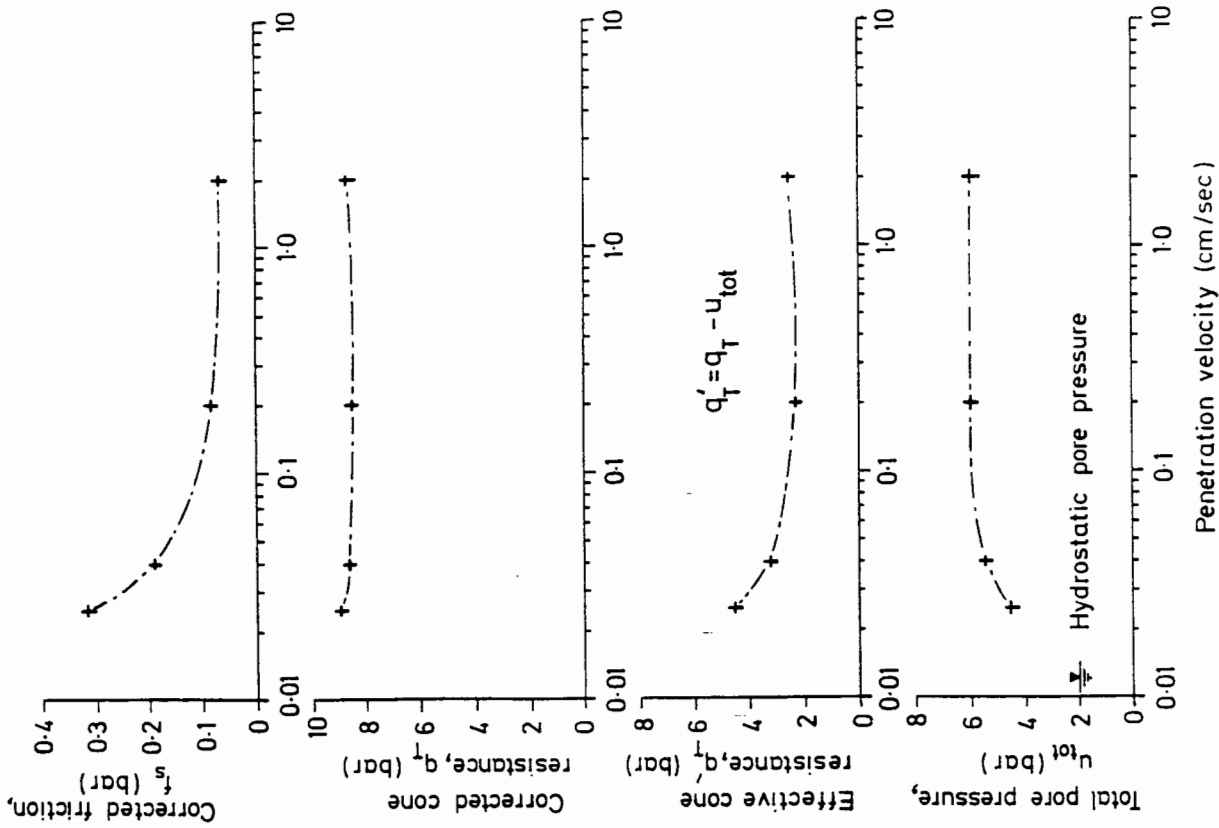
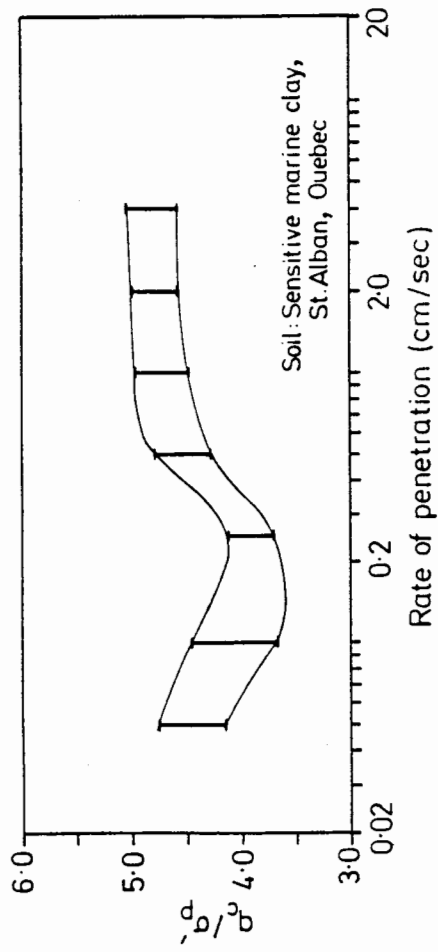
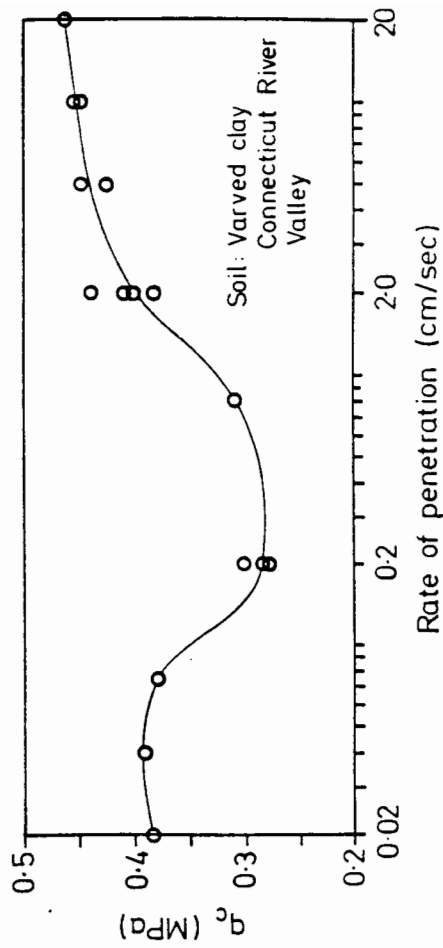


FIGURE 1.13 PENETROMETER MEASUREMENTS WITH PARTIAL DRAINAGE  
After Campanella, Robertson and Gillespie (1981)



a) After Roy et al (1982 b)



b) After Bembem and Myers (1974)

FIGURE 1.14 VARIATION OF CONE RESISTANCE WITH RATE FROM FIELD DATA

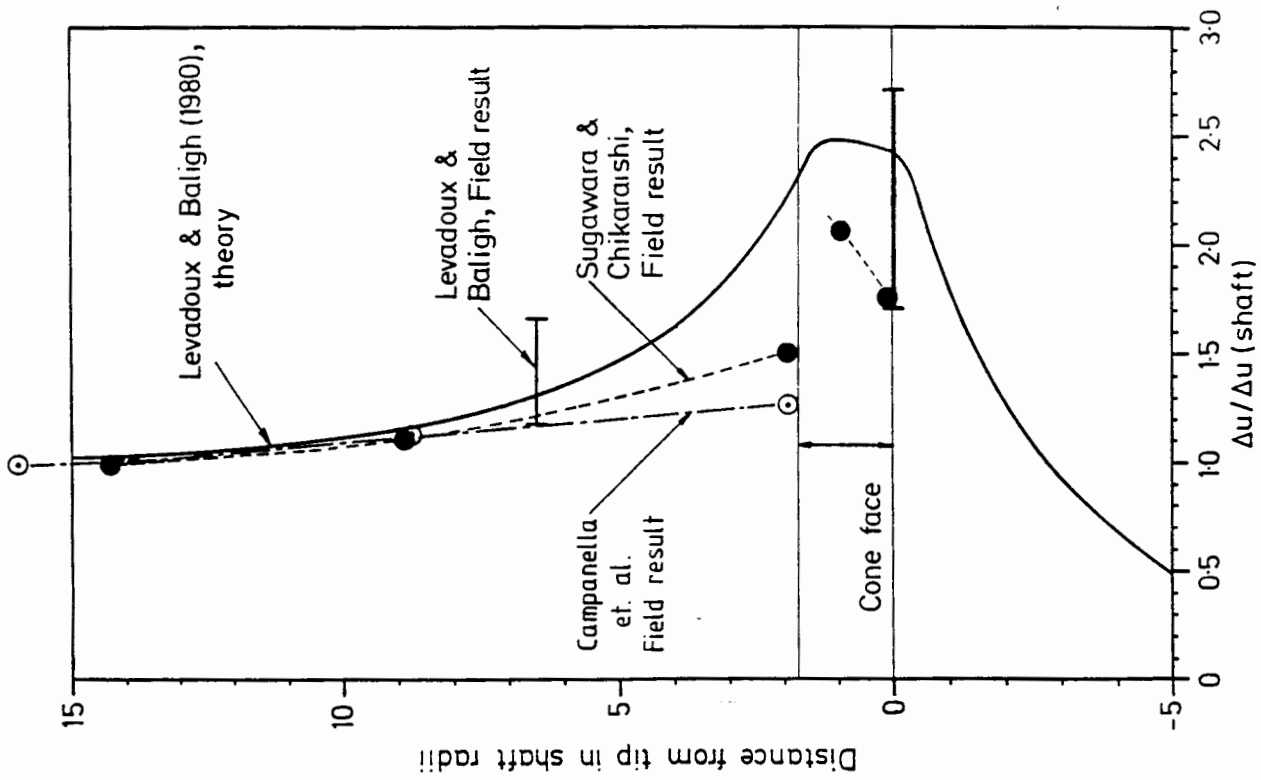
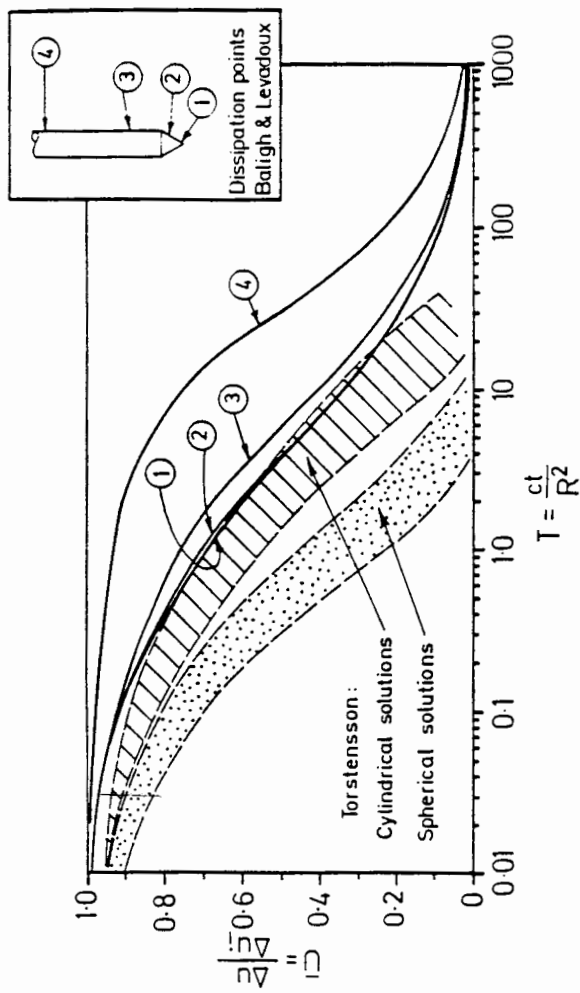
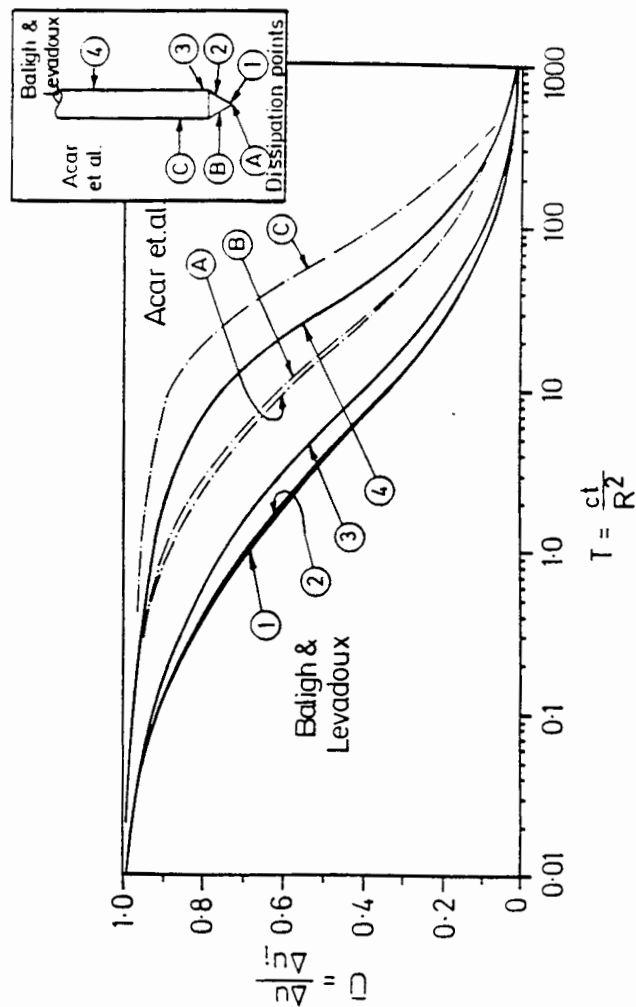


FIGURE 1.15 VARIATION OF PORE PRESSURE ALONG PENETROMETER SURFACE



a) Torstensson compared with Baligh and Levadoux



b) Acar et al. compared with Baligh and Levadoux

FIGURE 1.16 THEORETICAL SOLUTIONS FOR PORE PRESSURE DISSIPATION

## 2. INVESTIGATIONS INTO THE EFFECT OF TANK CONFINEMENT

### 2.1 Introduction

From the outset of the project it was decided the investigation into cone penetration behaviour should primarily be conducted in the laboratory rather than in the field. The major advantages of a laboratory investigation lie in the ability to control the homogeneity and the stress history of the soil with precision. Thorough and high quality sampling of the soil for secondary testing (e.g. triaxial tests) is also considerably easier from the laboratory clay "cake".

However the drawback to laboratory testing as compared to field testing lies in the imposed boundary conditions. In order to maintain a clay cake (other than a slurry) in a normally consolidated state appropriate effective stresses must be maintained on all its surfaces. This requirement dictates that the clay cake must be enclosed in some form of cell. For one-dimensional vertical consolidation of the clay from a slurry it is of practical importance that the top and bottom boundaries of the soil are inflexible and that the radial boundary is rigid. The importance of vertical drainage only is discussed by Nageswaran

and Houlsby (1984). These boundary conditions are only approximately met in the laboratory with consolidation cells of finite stiffness. However the boundary conditions required to model field behaviour during a CPT are much more complex. If the CPT may be crudely modelled as a cylindrical cavity expansion it may be seen that neither the vertical nor the radial stresses remain constant during penetration. The vertical stress is seen to increase only in the zone of plastic behaviour around the cavity (or penetrometer). This region may extend from 10 to 16 radii from the penetrometer centre line (with  $G/c_u = 100$  to 250). Outside this region lies the elastic zone in which no increase in vertical stress is predicted. The radial stress increases as the cavity expands, this increase being proportional to the inverse of the radius squared outside the plastic zone. Thus the radial stress increase reduces rapidly with increasing radius from the penetrometer but remains finite.

For the top and bottom of the cake four types of boundary are practical. These are a rigid no-displacement boundary (Rnd), a rigid constant mean stress boundary (Rcms), a flexible no mean displacement boundary (Fnmd) and a flexible constant stress boundary (Fcs). The practical choices for the radial boundary are more limited being either rigid no displacement (Rnd) or flexible constant stress



(Fcs). Not all the possible combinations of boundary are practical as the cake requires vertical stability.

Some of the different cells used for this type of testing in clays are listed in Table 2.1. Where doubt exists over the boundary condition this is shown with a question mark. The cells used for the present study are included for comparison.

Authors	Boundary Condition			Cell diameter	Nature of Study
	Top	Bottom	Radial	Probe Diameter	
Almeida & Parry (1985)	Rcms?	Rnd	Rnd	85.0 & 66.9	Model Penetrometer
Chandler & Martins (1982)	Rnd	Rcms	Fcs	6.8	Shaft friction of drilled-in pile
Smits (1982)	Fcmd?	Rcms	Rnd	16.1	Full scale penetrometer
Steenfelt et al (1981)	Fcmd	Rcms	Fcs	13.2	Model pile
Present Study	Fcs	Rnd	Rnd	51.4, 88.6 & 39.6	Model Penetrometer

**TABLE 2.1 BOUNDARY CONDITIONS OF CELLS  
FOR PENETRATION TESTS**

From the table it may be seen that Chandler and Martins and some researchers at Cambridge University have used flexible radial stress control. In these instances the clay cake has been consolidated from a slurry in a rigid cell, removed from this cell and reconsolidated in a second 'triaxial' cell to higher stresses in order to minimise the disturbance. The preferable method of consolidating the slurry into a membrane through which radial stresses could be controlled does not appear to have been perfected to date. The transfer of clay cakes between cells imposes rather severe limits on the maximum size of cake and this is reflected in the cell to probe diameter ratios obtained.

Although radial constant stress boundaries were considered for the present project the theoretical and practical drawbacks led to the adoption of the boundaries shown in Table 2.1. It was apparent however that the effect of different boundary conditions and the relative sizes of probe and cell were not well documented. It was decided to evaluate the effect of differing probe to tank diameter ratios on rigid walled tanks by a small scale experimental series together with numerical and theoretical calculations.

## 2.2 Small Scale Equipment

The principal objective of the small scale series of tests was to measure the change in radial stress at the cell wall due to probe penetration at the centre of a cell. These values were then compared with the radial stress increases predicted by cylindrical cavity expansion. One size of cell was used with a variety of probe sizes. Two forms of end boundary were investigated, these being rigid constant mean stress and flexible constant stress boundaries both combined with rigid no displacement boundaries on the opposite face.

The cell ( Figure 2.1 ) consists of a perspex tube (138mm internal diameter x 6mm wall thickness) inside which runs a dural piston. An O-ring provides a pressure tight seal between either side of the piston. The perspex tube is sealed onto a base plate at the bottom and at the top onto a retaining ring and top plate assembly. The cell is held together with three external tie rods.

The piston is designed to consolidate the soil by upward movement. A port in the baseplate allows fluid pressure to be applied under the piston and

water is strongly recommended in favour of gas pressure for this purpose. Drainage of the clay above the piston is axial and from both faces. A 3mm Vyon filter lies on top of the piston and this is drained through a port in the piston and out of the cell via a flexible tube and a port in the baseplate.

There are two designs of top plate and both provide for sample drainage. The stress control top plate can be used to produce either a no overall volume change or a constant stress top boundary condition. The conditions are imposed via a neoprene membrane by water pressure in a cavity above. The cavity is either connected to an air-water interface for stress control or isolated by closing a tap thus allowing no volume change. A flexible 1mm thick Vyon filter is located between the membrane and the soil. Drainage from this filter is through a fitting in the membrane into a flexible tube which runs through the cavity and out through the top plate. The alternative top plate is solid. Both plates have a central port which accommodates a range of plugs. The plugs either carry a total stress transducer for use during consolidation or sleeve the different sizes of probe during penetration.

A pair of Druck PDCR22 pressure transducers are mounted in the cell wall at a position 75mm below the top surface of the soil sample. One of these measures the radial stress exerted on the cell wall while the other measures pore pressure. Due to the limited wall thickness the transducers are mounted on an exterior dural split ring and sealed into the cell wall with O-rings. For the radial total stress measurements the transducer face should be mounted flush with the inside of the cell wall. This creates difficulty because the transducers have flat faces while the cell wall is curved. In practice the transducer is mounted so that the face is tangent to the inner surface of the cell. On the opposite side of the cell a small Vyon filter is mounted flush with the cell wall and pore pressures are measured in a saturated chamber behind it.

Four solid probes and a pore pressure probe may be used in the cell. The solid probes have a  $60^\circ$  included tip angle and the following diameters:

Probe diameter (mm)	$\frac{\text{Cell diameter}}{\text{Probe diameter}}$
11.11 (7/16")	12.4
7.94 (5/16")	17.4
4.76 (3/16")	29.0
3.18 (1/8")	43.5

TABLE 2.2 SMALL SCALE PROBE SIZES

The pore pressure probe (Figure 2.2) has a diameter of 11.11mm and a 60° porous tip. The porous tip is machined from Aerolith 10 ceramic filter with a mean pore size of 25µm. The porous section of tip ends just below the cone shoulder to avoid this point. The pore pressure are measured with a Gaeltec 3Ea pressure transducer mounted just above the filter inside the body of the probe.

The probe is driven into the cell at a constant rate by a heavy duty electric stepper motor. The motor pinion drives onto a vertical rack. The lower end of the rack has a Sangamo D95 500N load cell attached to it measuring the total resistance to probe penetration. The probes screw into the base of load cell. Four penetration rates are provided by the stepper motor controller between 6.5 and 20.0mm/sec. The majority of tests were performed at 20mm/sec.

The output from the load cell, pore pressure probe and wall mounted transducers are recorded against time on a four channel chart recorder.

### 2.3 Small Scale Testing Procedures

The clay cakes used for the small scale testing were consolidated from a slurry. This was mixed at water contents of either 100% or 120%. The wetter

slurry was more pourable and thus easier to load into the cells but gave rather shallow samples.

Before loading the slurry into the cells the cell walls were thoroughly greased with silicon grease or water pump grease. The latter appeared to reduce O-ring stiction. The importance of greasing the cells well was demonstrated by two tests in which the cells were not greased. Large vertical variations in water content and shear strength were produced in these tests. In well greased cells excellent uniformity was achieved as shown by detailed water content testing.

The drainage lines were flushed through with water and a 5cm depth of water placed on top of the piston. The Vyon filter was de-aired in water under vacuum and placed on top of the piston. Initially a paper filter was used on top of the Vyon to prevent filter clogging but this proved to be unnecessary. The slurry was then tremmied into the cell up to the level of the wall mounted transducers.

The pore pressure housing was installed at this point. The filter and housing body had been saturated in water under vacuum and the pressure transducer sealed into the housing under water. It proved difficult to maintain a high degree of saturation during the brief installation period

using water as the saturating medium. In general the dissipation of pore pressures during consolidation appeared to be indicated accurately by the unit but the response was too sluggish to follow rapid changes during probe insertion. This difficulty led to the use of glycerin in pore pressure transducers on the larger scale tests.

Having mounted the pore pressure housing the cell was now filled with the remaining slurry. The top filter was positioned and the top plate fitted without its central plug. The piston was then generally raised until the air was expelled from the top of the cell. The central plug complete with total stress transducer was fitted. The vertical pressure were increased to a maximum of 500kPa in steps and primary consolidation was complete in less than 24 hours. However the cells were normally left under pressure for five to seven days to allow the rate of secondary consolidation to reduce significantly. The consolidated depth of cake was around 140-150mm depending on consolidation pressure.

At this stage the port in the top plate was removed and an adapter plug screwed in to sleeve the probe selected for the test. For the early tests a clearance of approximately one probe radius was provided by these plugs. However it was found that



soil extruded into this annular gap during penetration thus altering the intended boundary conditions and significantly changing the radial stress response. Adaptor plugs that were a loose sliding fit to their probes were used for later tests.

Having fitted the adaptor plug the penetration unit was bolted onto the top plate and the probe attached. The boundary control conditions were checked. If a solid top plate was used the piston was held at a constant pressure to provide a rigid constant mean stress boundary at the base of the cake. If the pressure control top plate was used the pressure inlet to the water beneath the piston was closed to produce a rigid no displacement bottom boundary. The pressure acting on the top plate was recorded with a pressure transducer in-line to the water filled cavity. This pressure was matched in an air-water interface and the line between this and the top plate opened. The use of a self bleeding regulator for control of the air water interface enabled flexible constant stress top boundary conditions to be imposed during the penetration test.

For a number of tests the pore pressure probe was used. The tip of this instrument was left in

deaired water under vacuum for 24 hours. The pressure transducer was then screwed into the tip under water in a small cap which was only removed once the probe was screwed onto the load cell immediately prior to penetration. Despite the care taken to maintain saturation this was not always successful using these procedures.

#### 2.4 Results of Experimental Study on Confinement Effects.

The tests described above were all performed on Speswhite kaolin clay with the following properties:

Liquid Limit LL	66%
Plasticity Index PI	33%
Specific gravity G <sub>s</sub>	2.65
Peak $\phi'$	23°
Coefficient of consolidation $c_v$	0.5mm <sup>2</sup> /sec
Slope of virgin consol line	0.25
Slope of swelling line	0.05
Normally consolidated rigidity index $I_r = G/c_u$	150-250*

**\*NOTE:** These values were measured in standard CIU triaxial tests from initial loading and unload-reload loops. Displacements were measured external to the cell on the loading ram.

**TABLE 2.3 PROPERTIES OF SPESWHITE KAOLIN**

The test series is given in Table 2.4

Test Number	Cell Number	Cell dia Probe dia	Rate (mm/s)	w/c (%)	$p'$ (kPa)	Vane shear strength (kPa)	Notes
SC1	1	12.4	10.0	41.5	460	73	a b
SC3	2	12.4	6.5	43.0	-	57	b
SC4	1	12.4	20.0	42.9	375	58	b
SC5	2	12.4	20.0	41.9	456	67	b
SC7	3	12.4	10.0	55.8	68	8.8	
SC8	4	12.4	10.0	42.0	444	67	
SC9	2	12.4	10.0	41.0	463	78	
SC10	1	12.4	20.0	43.0	460	61	a
SC12	3	12.4	20.0	40.7	488	80	a
SC15	2	12.4	20.0	44.2	332	48	a
SC17	1	12.4	20.0	50.2	138	24	a
SC18	1	12.4	20.0	45.8	304	41	a
SC20	4	12.4	35.0	40.3	-	94	a c
SC22	1	29.0	20.0	45.8	284	38	
SC23	1	43.5	20.0	-	-	-	d
SC24	4	29.0	20.0	43.2	376	58	
SC25	3	43.5	20.0	-	-	-	d
SC26	1	43.5	20.0	42.9	459	67	
SC27	3	43.5	20.0	41.9	456	68	
SC28	1	17.4	20.0	41.7	488	73	
SC29	3	17.4	20.0	51.3	175	25.3	e

**TABLE 2.4 GENERAL DATA FOR SMALL SCALE CONFINEMENT EFFECT TEST DATA**

General notes to Table 2.4

1. All above series were performed on fully saturated normally consolidated clay.
2. Cells 1 and 3 were equipped with radial stress transducers. Cells 2 and 4 were used to provide extra penetration resistance data.
3. Vane tests were all conducted immediately after depressurisation of cell and removal of top plate. Vane strengths were reduced by approximately 25% on depressurisation (see Section 4.3).

Lettered notes to Table 2.4

- a. Pore pressure probe used for this test.
- b. Large diameter entry port.
- c. Test unsuccessful due to pinion slippage on motor shaft.
- d. Cell not greased.
- e. Flexible constant stress top boundary.

Ten of these tests gave useful information on the behaviour of the radial stresses during penetration. Measured radial stress profiles with depth of probe penetration are shown in Figure 2.3. The analysis of this data is shown in Table 2.5. These results are plotted in non-dimensionalized form in Figure 2.4, together with the results from the larger scale tanks (Section 4) and the results of a cylindrical cavity expansion analysis in an unrestricted soil domain. This analysis is described in Section 2.5.

The test performed with a flexible constant stress top boundary (SC29) fits into the pattern of results observed from tests with a rigid constant mean stress lower boundary shown on Figure 2.4.

Test Number	R/a	$c_{ui}$ (kPa)	$\Delta\sigma_r$ (kPa)	$\frac{c_{ui}}{\sigma_{vo}}$	$\frac{\sigma_{ro}}{\sigma_{vo}}$	$\frac{\Delta\sigma_r}{\sigma_{ro}}$	$\frac{\Delta\sigma_r}{\sigma_{vo}}$	$\frac{\Delta\sigma_r}{c_{ui}}$
SC1	12.4	132	175	0.29	0.52	0.74	0.38	1.33
SC4	12.4	107	265	0.29	0.61	1.16	0.71	2.48
SC10	12.4	106	198	0.23	0.59	0.73	0.43	1.87
SC12	12.4	146	192	0.30	0.82	0.48	0.40	1.32
SC17	12.4	40	128	0.29	0.84	1.20	1.01	3.20
SC28	17.4	128	196	0.26	0.67	0.59	0.40	1.53
SC29	17.4	35	95	0.20	0.74	0.74	0.54	2.71
SC22	17.4	73	157	0.26	0.88	0.63	0.55	2.15
SC26	43.5	107	80	0.23	0.66	0.26	0.17	0.75
SC27	43.5	123	61	0.27	0.70	0.17	0.13	0.50

**TABLE 2.5 ANALYSED DATA FROM CONFINEMENT EFFECT TEST SERIES**

The symbols used in Table 2.5 are as follows:

- R = cell radius
- a = probe radius
- $\sigma_{ro}$  = radial stress at end of consolidation
- $\sigma_{vo}$  = vertical stress at end of consolidation
- $\Delta\sigma_r$  = Increase in measured radial stress due to probe insertion
- $c_{ui}$  = In situ shear strength calculated from water content and CIU triaxial data (see Section 4.3).

It is of interest to supplement the data obtained from the 138mm diameter perspex cells with that obtained from the 580mm and 1000mm diameter tanks used in the main series. These data are given in Table 2.6 and plotted in Figure 2.4.

Test Number	$c_{ui}$ (kPa)	R/a	$\Delta\sigma_r$ (kPa)	$\frac{\Delta\sigma_r}{\sigma_{ro}}$	$\frac{\Delta\sigma_r}{c_{ui}}$
A3-1	65	51.4	47	0.26	0.72
A4-1	114	51.4	60	0.25	0.53
A5-1	121	51.4	77	0.29	0.64
B1-1	109	51.4	69	0.26	0.63
B2-1	66	51.4	55	0.29	0.83
B3-1	117	51.4	95	0.34	0.81
C1-1	84	88.6	27	0.13	0.32
C2-1	87	39.6	87	0.33	1.00

**TABLE 2.6 RADIAL STRESS MEASUREMENTS  
FROM LARGE SCALE TANKS**

**Note:** Undrained shear strengths in this Table refer to in-situ values (i.e. prior to depressurization)

## 2.5 Calculations of Confinement Effect.

A fully satisfactory calculation for the effect of the imposed laboratory boundary conditions during penetration has not been derived. In lieu of this, lower and upper bound calculations have been performed which give a degree of insight into the system behaviour.

An obvious lower bound solution is that of the cylindrical cavity expansion for an infinite soil domain. For this solution to correctly model cylindrical expansion inside the tank the tank wall would have to have the same rigidity as the clay from the radius of the wall outwards. In practice the steel or perspex wall is much more rigid than this calculation assumes.

The cylindrical cavity expansion solution developed by Professor C. Sagaseta was used for this analysis. This solution considers the soil to be linear elastic-plastic with a Von Mises yield criterion. Anisotropic initial stresses are incorporated together with shear forces at the cavity wall. The following input parameters were used for the present analysis:

- 1) Rigidity index  $I_r = 100$  and  $250$  (see Section 2.4)
- 2) Initial stress ratio  $\Delta_o = \frac{\sigma_{vo} - \sigma_{ho}}{2c_u} = 0$  to  $1$
- 3) Adhesion factor at cavity wall  $a = \frac{\sigma_z}{c_u} = 0.3$  to  $0$ .

The results of this calculation are shown in Figure 2.4. Of the three variables the rigidity index is the only significant parameter in the analysis. The effect of varying the initial stress ratio can be plotted but is small and variations in adhesion factor have very little effect on the radial stress increase. The predicted radial stress increases are less than those measured at the cell wall especially for larger tank to probe diameter ratios.

The upper bound calculation has been approached in steps. The first step was to assume all expansion to be radial and the soil to be incompressible. The required radial displacement of the shell may be calculated to accommodate the volume of the probe.

From the elastic properties of the shell the radial stress on the shell may then be determined. The radial stresses so calculated are greatly in excess of those measured.

Two refinements of this calculation have been performed. In the first a crude method to include the actual soil compressibility was followed. There the soil was taken to have a bulk modulus (K) but no shear modulus (G) as if it were a fluid. Again the expansion was taken to be radial, confined by the shell. The undrained bulk modulus of the soil is given by

$$K_u = \frac{(1 + e)}{(e/K_w) + (1/K_s)} + K'$$

where  $e$  = void ratio

$K_w$  = bulk modulus water

$K_s$  = bulk modulus soil solids

$K'$  = drained bulk modulus of soil skeleton

$$K' = \frac{2}{3} G \frac{(1 + \nu')}{(1 - 2\nu')} \quad \text{where } \nu' = \text{drained Poisson's ratio of approximately } 0.3$$

The drained bulk modulus appears in the above equation because soil skeleton deformation is initiated by differential volume changes of the fluids and solids. As this movement is different to that required by conventional drainage the  $K'$  term may require some modification but its influence is small in the overall expression.



Taking  $G/c_u = 200$  and considering the range of shear strength between 20 kPa and 100 kPa ( $e = 1.35$  to  $1.05$ ), the calculated range of undrained bulk modulus is from  $3.6 \times 10^6$  kPa to  $4.3 \times 10^6$  kPa. The increase in stress corresponding to a decrease in soil volume is given by

$$\Delta\sigma_r = \frac{\Delta V}{V_o} K_u = \frac{(a^2 - r_1^2 + r_o^2)}{r_o^2} K_u \quad (\text{eqn 1})$$

where  $a^2 =$  probe radius

$r_o =$  original tank radius

$r_1 =$  expanded tank radius

Consideration of the hoop strain in the shell gives

$$\Delta\sigma_r = \frac{2t E_{\text{wall}}}{2r_o} \frac{(r_1 - r_o)}{r_o} \quad (\text{eqn 2})$$

where  $t =$  wall thickness

$E_{\text{wall}} =$  Young's modulus of wall

Equations (1) and (2) may be solved by eliminating

$\Delta\sigma_r$  and solving the resulting quadratic for  $r_1$ .

Substitution of  $r_1$  back into either equation produces

$\Delta\sigma_r$ . This method of calculation produced the radial stresses shown in Table 2.7

Tank Material	$E_{\text{wall}}$ (GPa)	$t$ (mm)	$r_o$ (mm)	$a$ (mm)	$\frac{r_o}{a}$	$\Delta\sigma_r$ (kPa)
Steel	210	17	290	5.64	51.4	960
Steel	210	17	500	5.64	88.6	230
Steel	210	17	500	12.62	39.6	1170
Perspex	3.1	6	69	5.56	12.4	846
Perspex	3.1	6	69	3.97	17.4	432
Perspex	3.1	6	69	2.38	29.0	155
Perspex	3.1	6	69	1.59	43.5	69

**TABLE 2.7 RESULTS OF BULK MODULUS EXPANSION  
CALCULATIONS FOR  $K_u = 4 \times 10^6$  kPa**

The results of this unsophisticated analysis are interesting as the predicted radial stress increase in the perspex cell with the smallest probe diameter is rather closely matched (compare Tables 2.7 and 2.5). In the two tests concerned the top and radial boundaries were fixed and the bottom boundary was intended to be a rigid constant mean pressure boundary. Tests with larger diameter probes in the perspex cell and tests with the penetrometers in the steel cells with their flexible constant stress top boundaries produced much lower measured radial stress increases than those predicted in Table 2.7. The probable reason for this difference in behaviour lies in the detail of the rigid constant mean stress boundary in the perspex cell. This boundary is provided by a piston sealed moderately tightly

against the cell wall by an O-ring. It is likely that the effects of static friction on this seal combined with a rather low increase in vertical stress due to a very thin probe penetrating the tank to caused the piston to act as a rigid no displacement boundary in this case. However in the case of larger probes the piston acted as intended and the flexible boundary was also able to respond effectively in both types of cell. This observation sounds a note of caution over the use of rigid constant mean stress boundaries for this sort of problem especially in view of the difficulty of checking their correct operation.

The effects of confining a cylindrical cavity expansion within a stiff (but not rigid) shell were studied with the help of Dr. H. Burd. Use was made of his large displacement plane strain program PLATE6. Details of the formulation of this program are given in Burd and Houlsby (1985). A horizontal plate (Figure 2.5) representing a quadrant of the tank in plan was used. The plate consisted of 84 six-noded plane strain triangles with 3 three-noded membrane elements on the outside of the mesh modelling the tank wall. The soil model was linear elastic-plastic and the shell linear elastic. The mesh generating program for this problem and the data plotting routines were written by the present author. The

cavity expansion was from an initial radius ( $r_i$ ) to a final radius ( $r_f$ ) where:-

$$r_f = 4r_i$$

The case of the  $1\text{cm}^2$  penetrometer in the 580mm diameter tank was specifically considered and the area increase of the cavity set equal to  $1\text{cm}^2$ . 400 displacement steps were used to expand the cavity and a 3 point Gauss rule employed corresponding to 'full' integration. The program was run five times with a constant value of soil Young's modulus but a Poisson's ratio increasing from 0.30 to 0.49. The results of these analyses are shown in Figures 2.6 to 2.8. It may be noted that the value of Poissons ratio for undrained shear strengths of 20kPa to 100kPa lies between 0.4994 and 0.4977 approximatley. However such high values could not be used in the finite element program due to resultant problems with numerical stability.

It may be observed from the results of the finite element calculations that the tank wall has little effect on a cylindrical expansion in a compressible soil ( $\nu = 0.3$ ). However as the compressibility is reduced the effect of the wall increases, raising all the stresses throughout the soil by an equal amount for each given Poissons ratio. The magnitude of

stress change (radial, vertical or hoop) from the cavity to the wall remains almost unchanged by increasing Poisson's ratio. From Table 2.6 it can be seen that the average measured value of  $\Delta\sigma_r/c_u$  is around 0.7 for the case being modelled. This corresponds to a Poisson's ratio of approximately 0.45 in the plane strain analysis. A plane strain analysis with a compressible soil may not be an inappropriate model for the radial behaviour in the tanks as the vertical movement of soil in the prototype can be seen as a loss of volume or "pseudo-compressibility" in the radial direction.

The calculations were extended with the help of C.I. Teh. Use was made of his finite element program FEM15. This program has a large strain formulation and can analyse axially symmetric problems with anisotropic initial stresses. The mesh used for this exercise is shown in Fig. 2.9. The soil was modelled with 28 cubic strain triangles and the tank wall with a further four of these triangles. The soil model was linear elastic-plastic and the wall linear elastic. As in the previous calculations a four-fold radial expansion was used. Using this formulation reasonable numerical stability was obtained with a value of  $\nu = 0.495$  (see Figs. 2.10 to 2.13).

A more satisfactory numerical model would result from the application of a constant stress upper boundary to a deeper mesh of the form shown in Figure 2.9. However, this form of analysis has not been possible to date.

Three main conclusions can be drawn from the work on the effect of tank confinement on CPT behaviour in clay. Firstly the measurements of radial stresses on the tank wall produced stress changes that were considerably greater than those predicted in the field, even for large values of tank to probe radius. This is probably due to the tank walls confining the radial movement of the soil to a greater degree than would have occurred under field conditions. However, there is evidence that rigidity indices at low shear strains are considerably higher than those used in the above study. Use of high rigidity indices would narrow the gap between the analytical and experimental results. The magnitude of stress increase may be influenced by the soil stiffness if the cell wall has relatively low rigidity.

Secondly the numerical studies of plane strain cavity expansion confined by a stiff (but not rigid) radial boundary demonstrated that the radial stress increase at the boundary acts in a similar fashion to a cell pressure increase in an undrained triaxial test. All the principal stresses within the soil are increased by this boundary radial stress increment. However, once this increase is subtracted the stress distribution is practically unaffected by the wall. Under field conditions some rise in radial stress would be expected at any finite radial distance from

a penetration event. However, the above studies suggest that CPT results from radially confined chamber tests may give a lower bound to the corresponding field behaviour if the radial stress increase measured at the cell wall is subtracted from the penetrometer pore pressures and total stresses.

The third conclusion drawn from the small cells was that both flexible constant stress boundaries and rigid constant mean stress boundaries on one end of the clay cake lead to similar measured radial stress increases at the cell wall during penetration events. This may indicate that the far field behaviour during penetration is primarily radial expansion. Notwithstanding this observation it was felt that a flexible rather than a rigid pressure controlled boundary was preferable for the main series of tests. This was because the flexible boundary produces conditions that are closer to field conditions than the rigid boundary and the correct functioning of such a boundary is easier to check.

It is clear that the relatively rigid tank walls do alter the stress and strain fields around the penetrometer. However the known boundary conditions and soil properties will enable the laboratory condition to be modelled numerically and thus compared to field conditions.

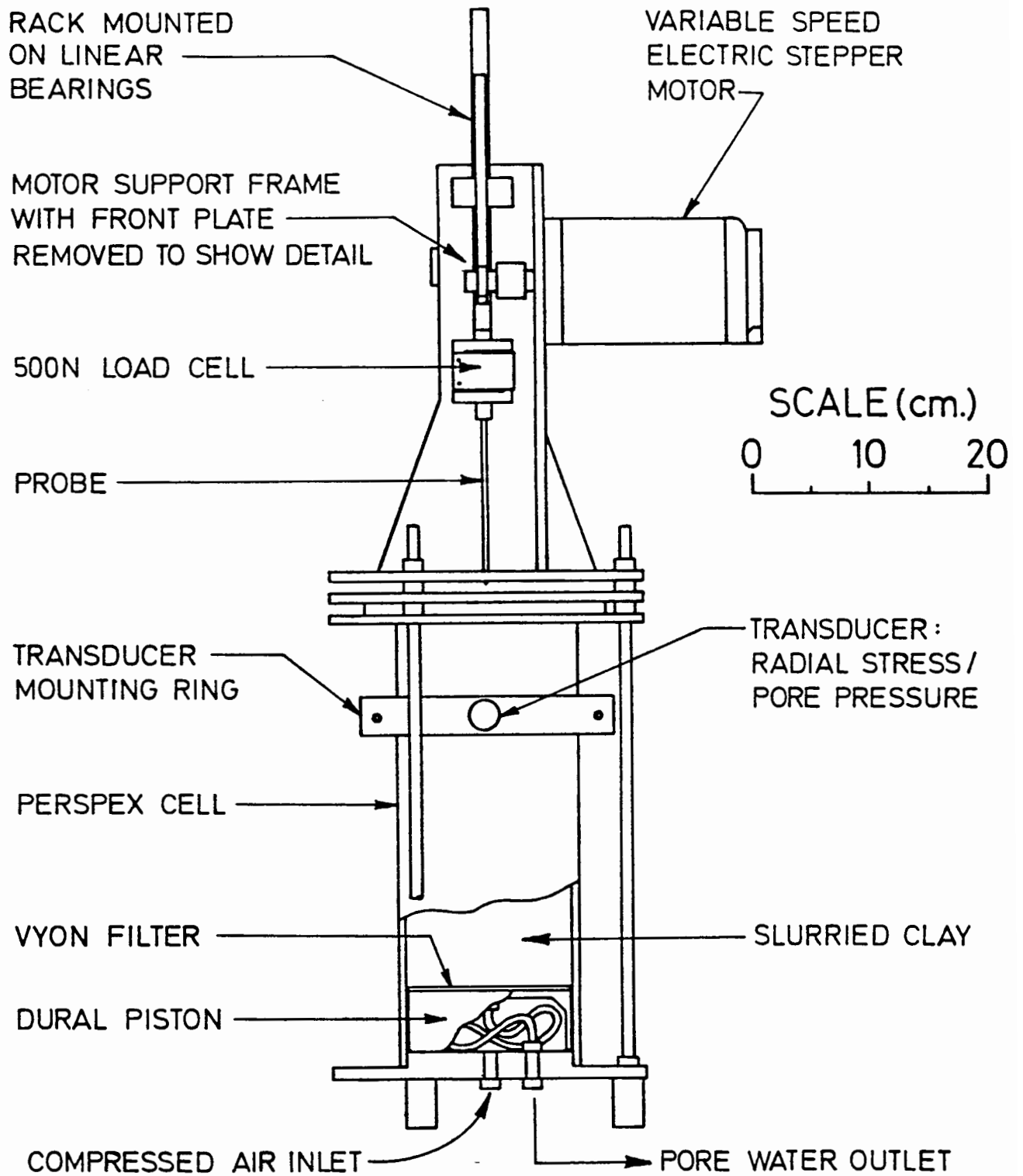


FIGURE 2.1 SMALL CELL ASSEMBLY



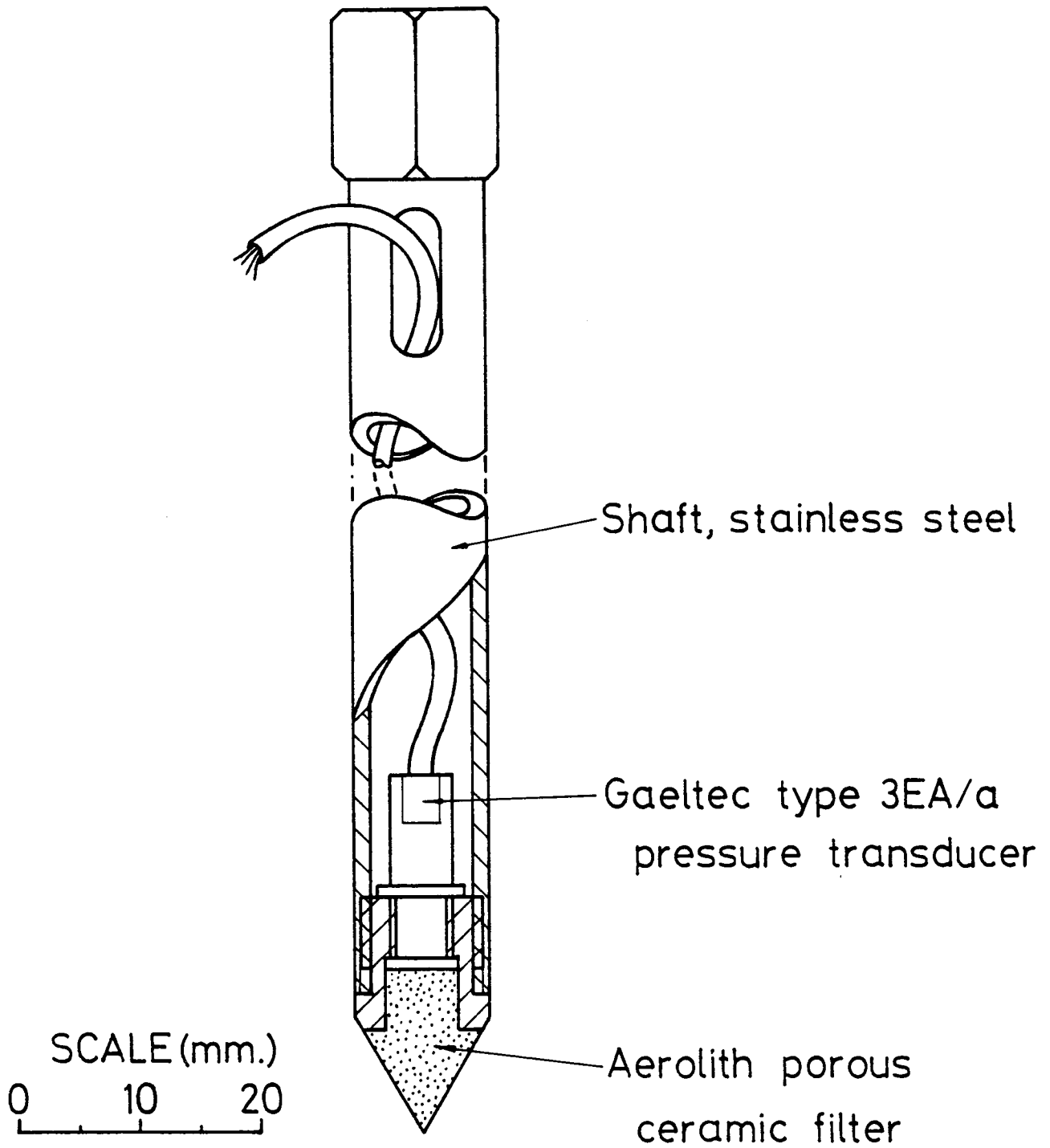
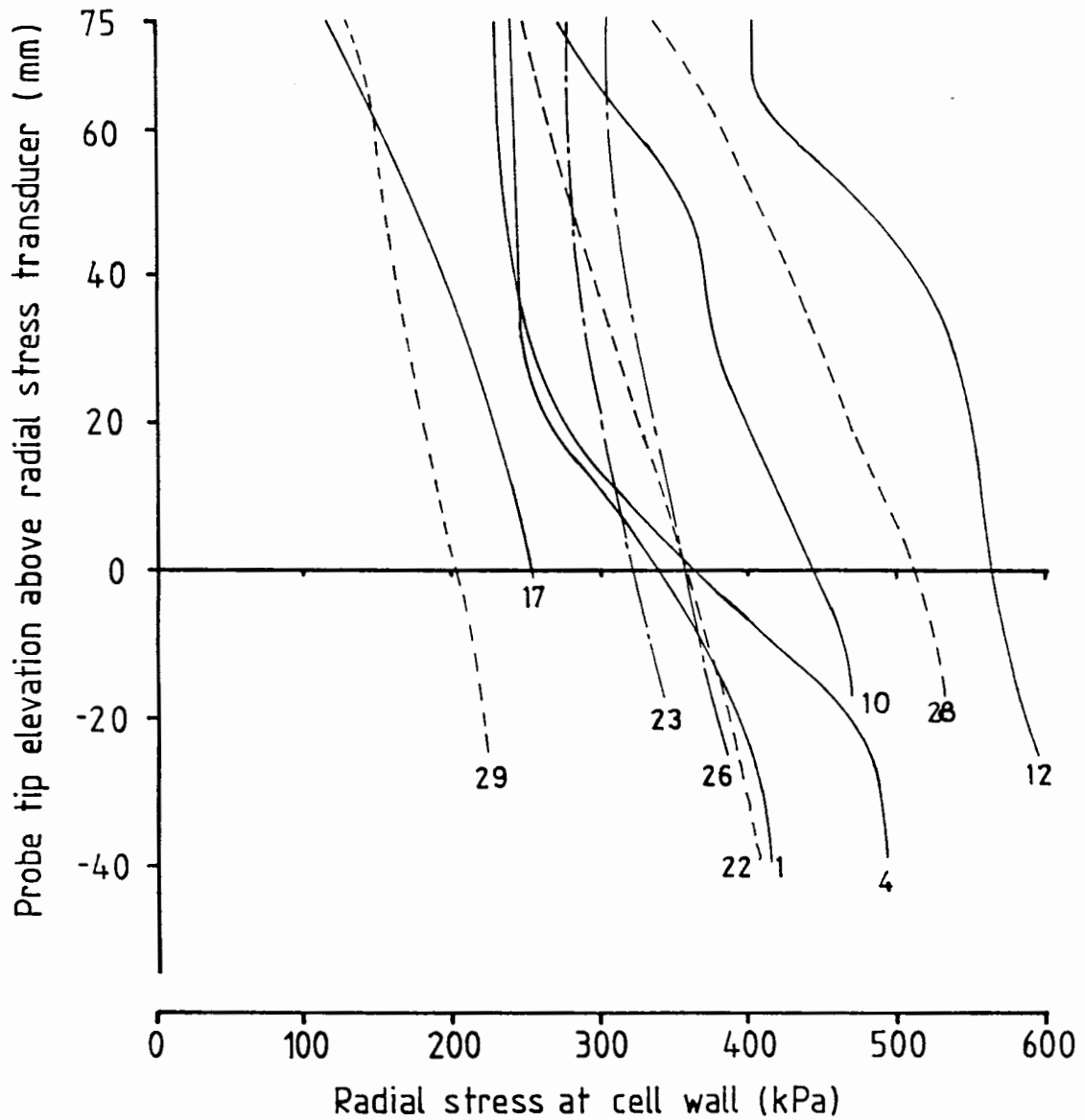


FIGURE 2.2 PORE PRESSURE PROBE



Note: Test number given at end of each trace

<u>KEY</u>	
Line	<u>Cell diameter</u> <u>Probe diameter</u>
—————	12.4
- - - - -	17.4
- · - · -	43.5

FIGURE 2.3 RADIAL STRESS DATA

CYLINDRICAL CAVITY EXPANSION SOLUTIONS

from program CAVEX written by Sagasetta (1984)

- $G/c_u = 250$  Initial stress ratio,  $\frac{\sigma_{vo} - \sigma_{ro}}{2c_u} = 0$  to 1
- - -  $G/c_u = 100$

EXPERIMENTAL DATA

- <sup>40</sup> Small scale (SC) test with in situ shear strength (kPa)
- Large scale test

$c_u = 50$  kPa

— Trend of small scale data

- - - Trend of large scale data

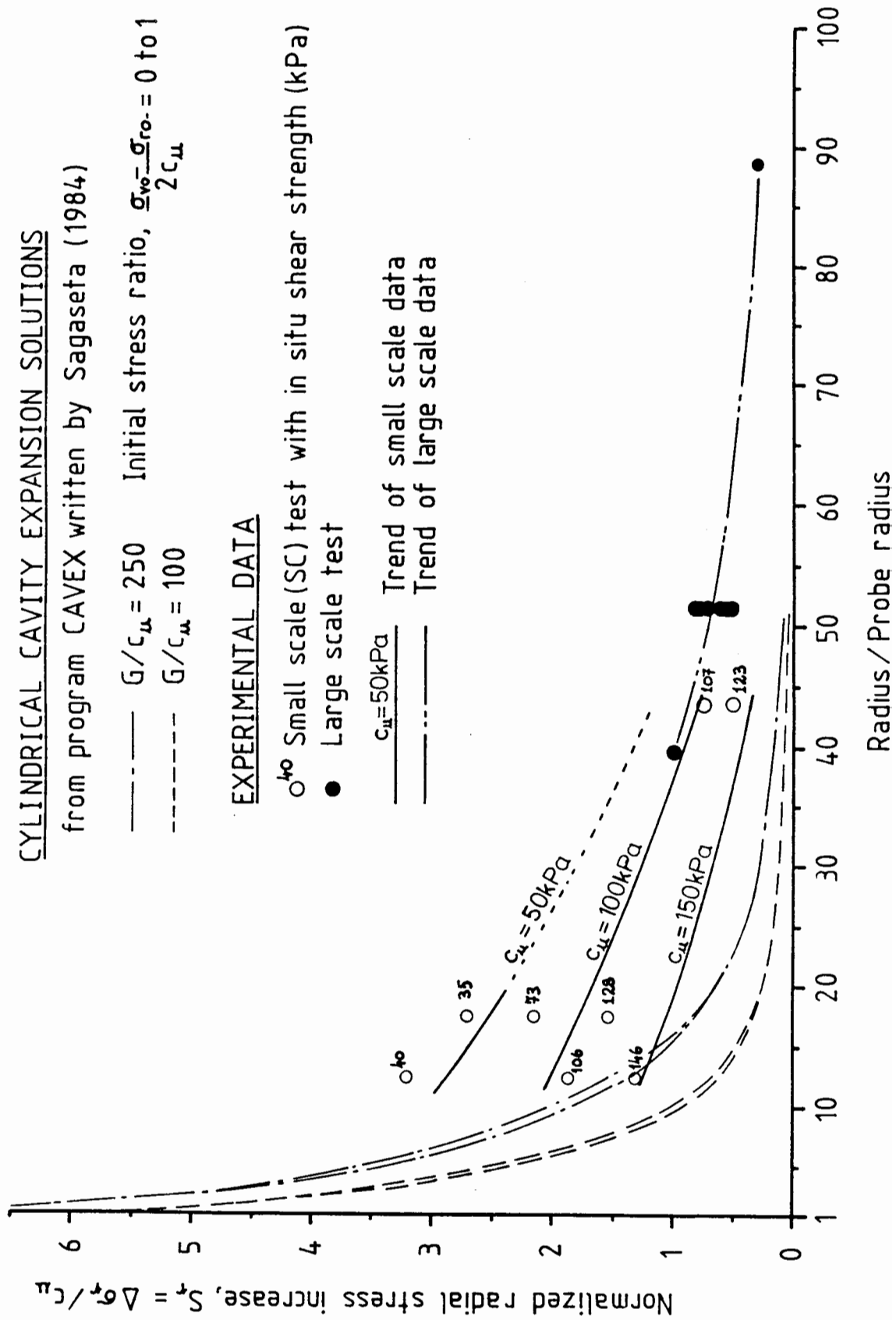
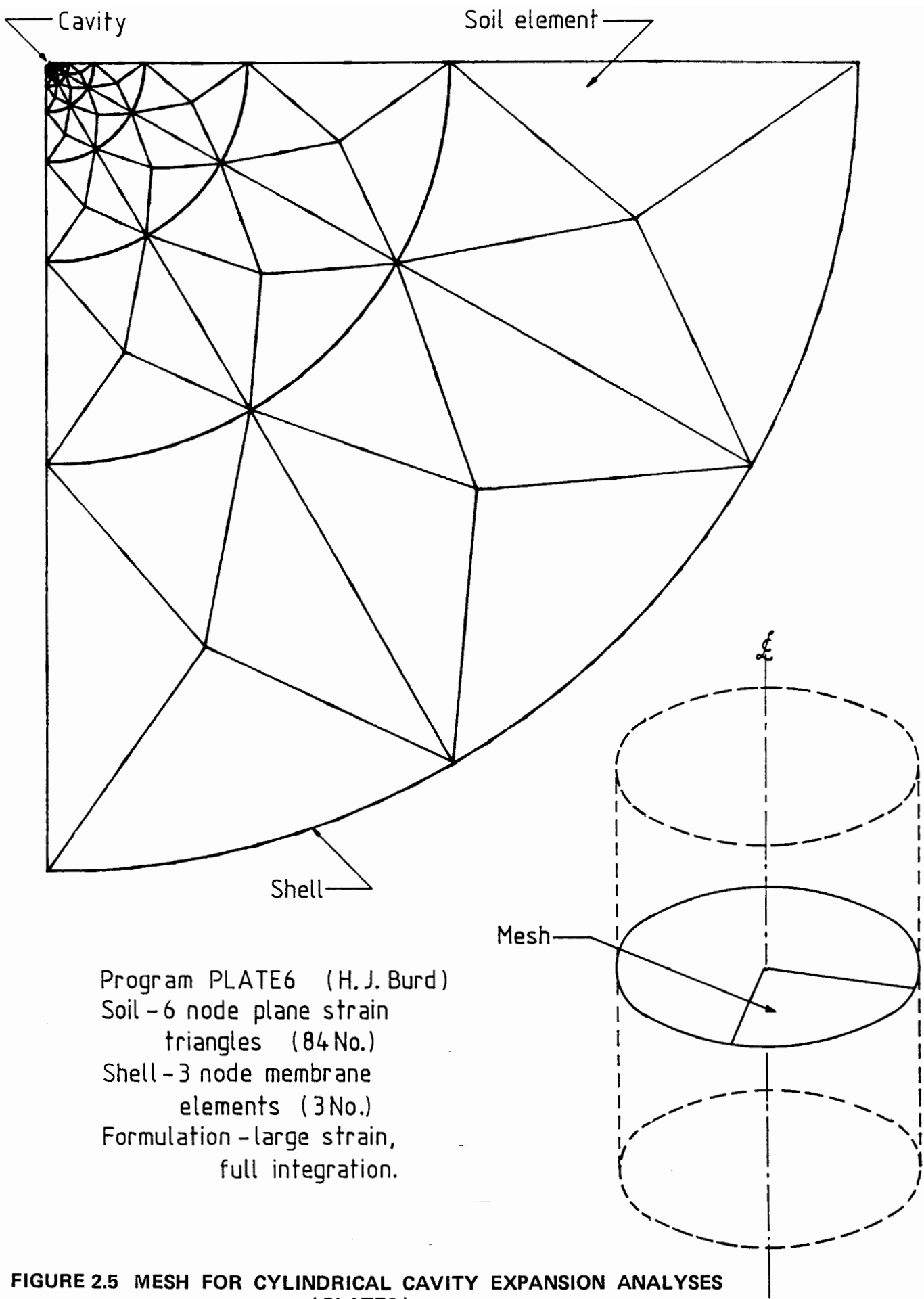
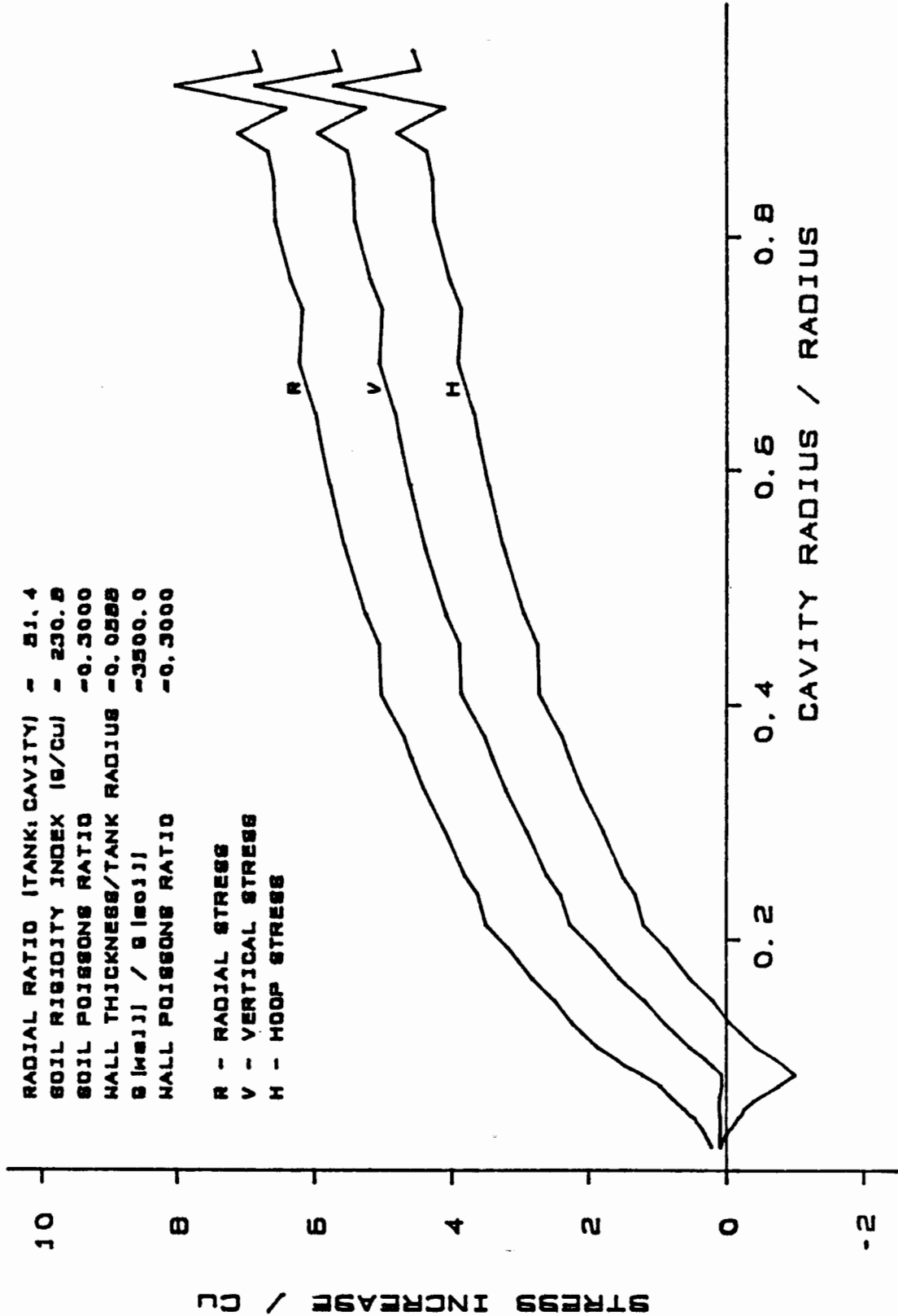


FIGURE 2.4 NORMALIZED RADIAL STRESSES

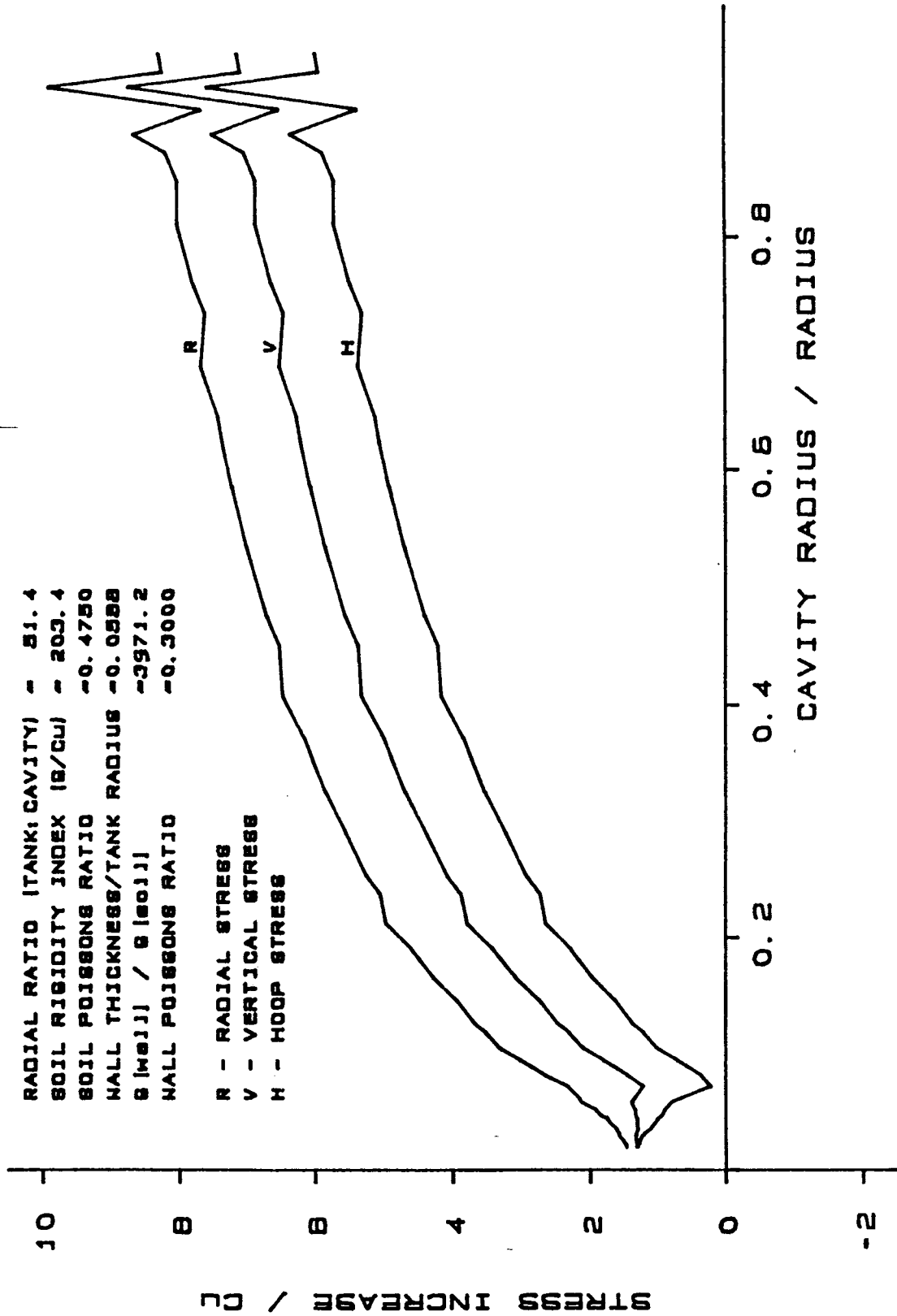


**FIGURE 2.5 MESH FOR CYLINDRICAL CAVITY EXPANSION ANALYSES (PLATE6)**



PLANE STRAIN CONFINED CAVITY EXPANSION RESULTS

FIGURE 2.6 NORMALIZED STRESS CHANGE : PLATE6 (  $\nu = 0.300$  )



PLANE STRAIN CONFINED CAVITY EXPANSION RESULTS

FIGURE 2.7 NORMALIZED STRESS CHANGE : PLATE6 ( $\nu = 0.475$ )

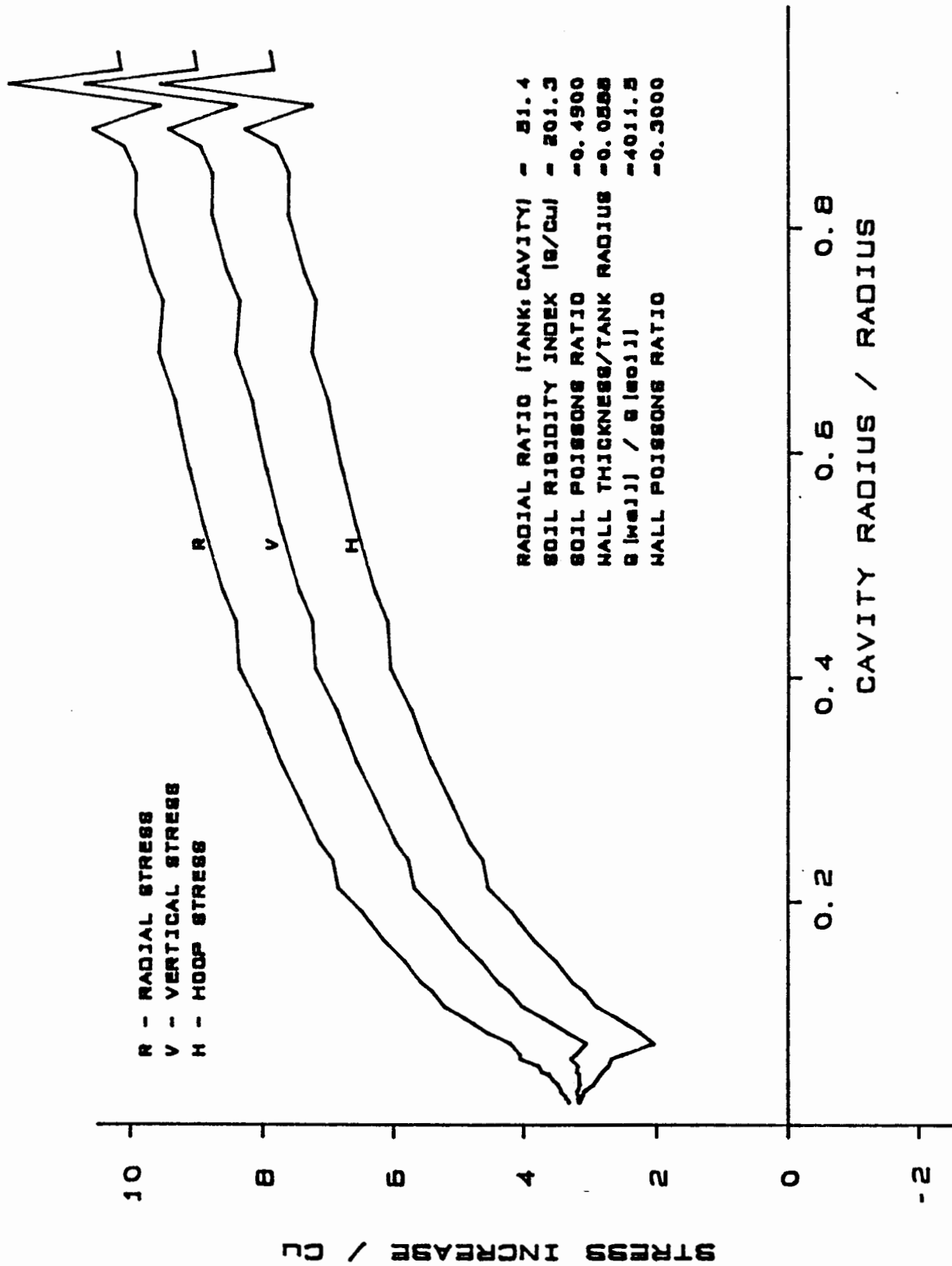
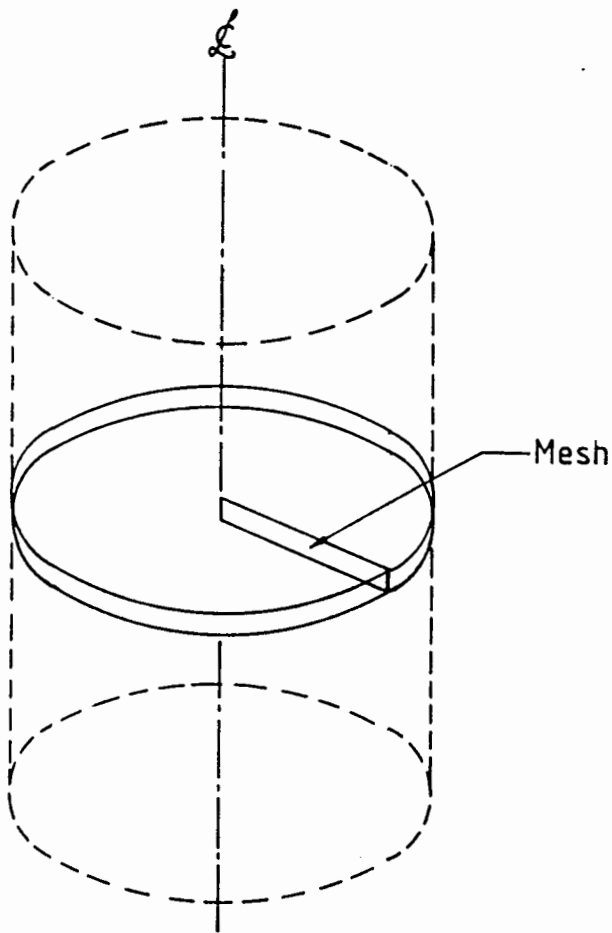
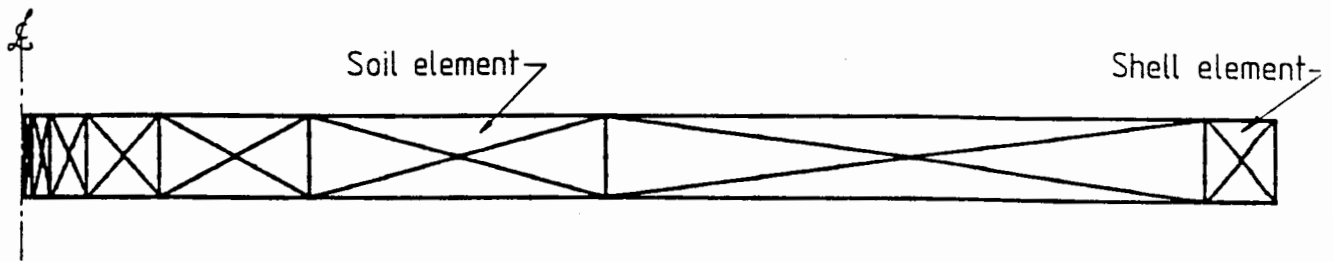


FIGURE 2.8 NORMALIZED STRESS CHANGE : PLATE6 (  $\nu = 0.490$  )

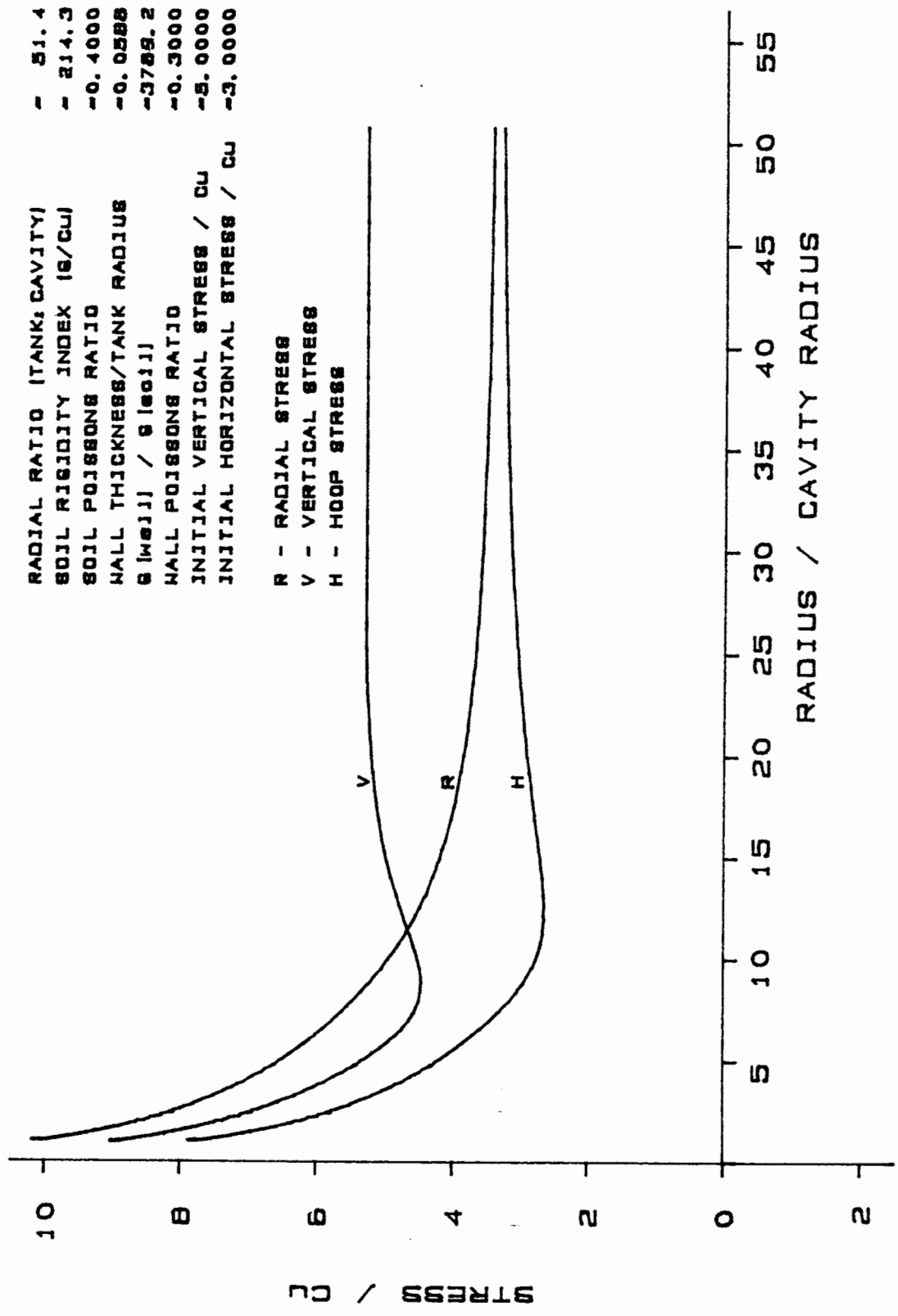
PLANE STRAIN CONFINED CAVITY EXPANSION RESULTS



Program FEM15 (C.I.Teh)  
 Soil - 15 node cubic strain  
 triangles (28 No.)  
 Shell - 15 node cubic strain  
 triangles (4 No.)  
 Formulation - large strain,  
 full integration.

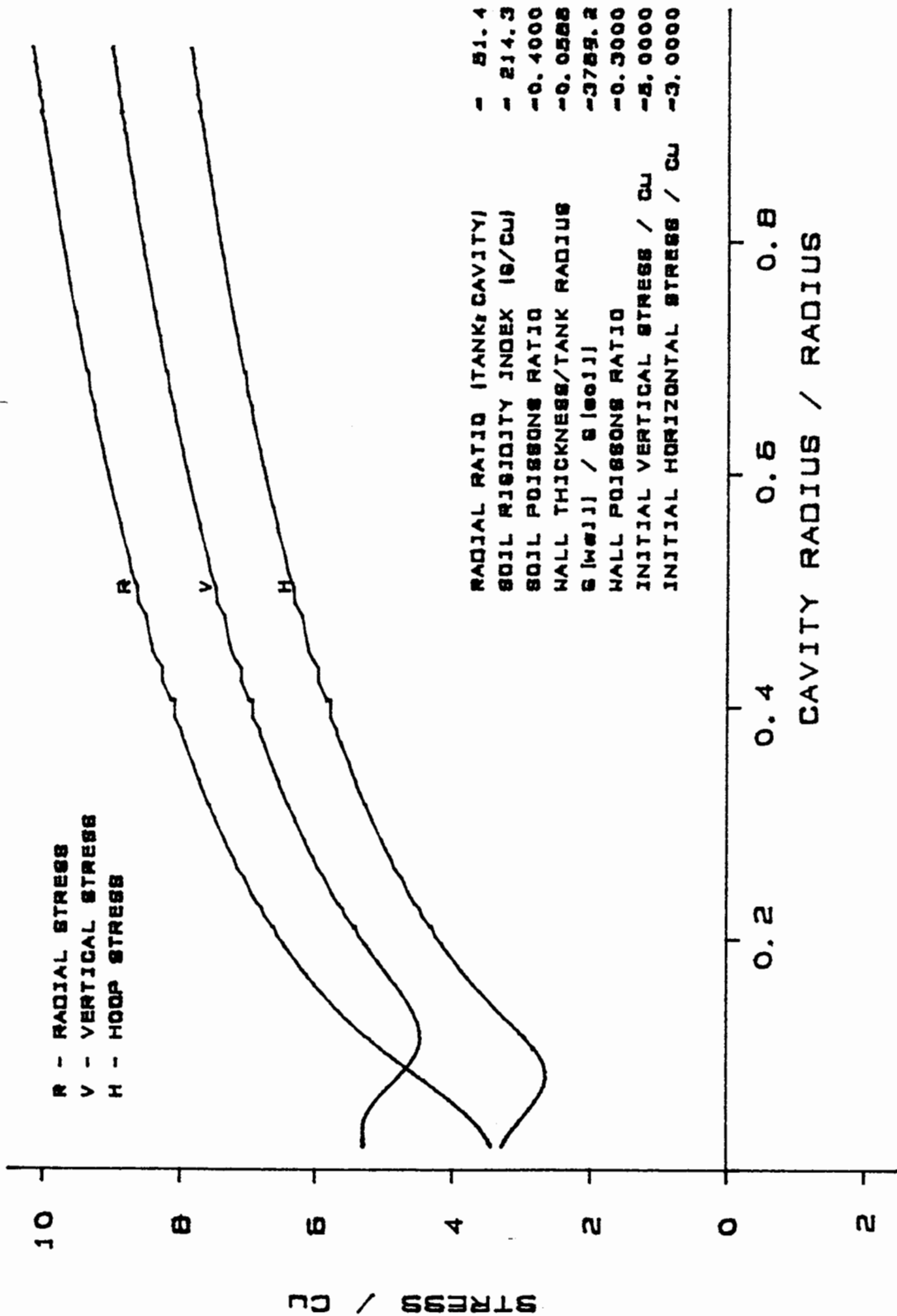
**FIGURE 2.9 MESH FOR CYLINDRICAL CAVITY EXPANSION ANALYSIS  
 ( FEM15 )**





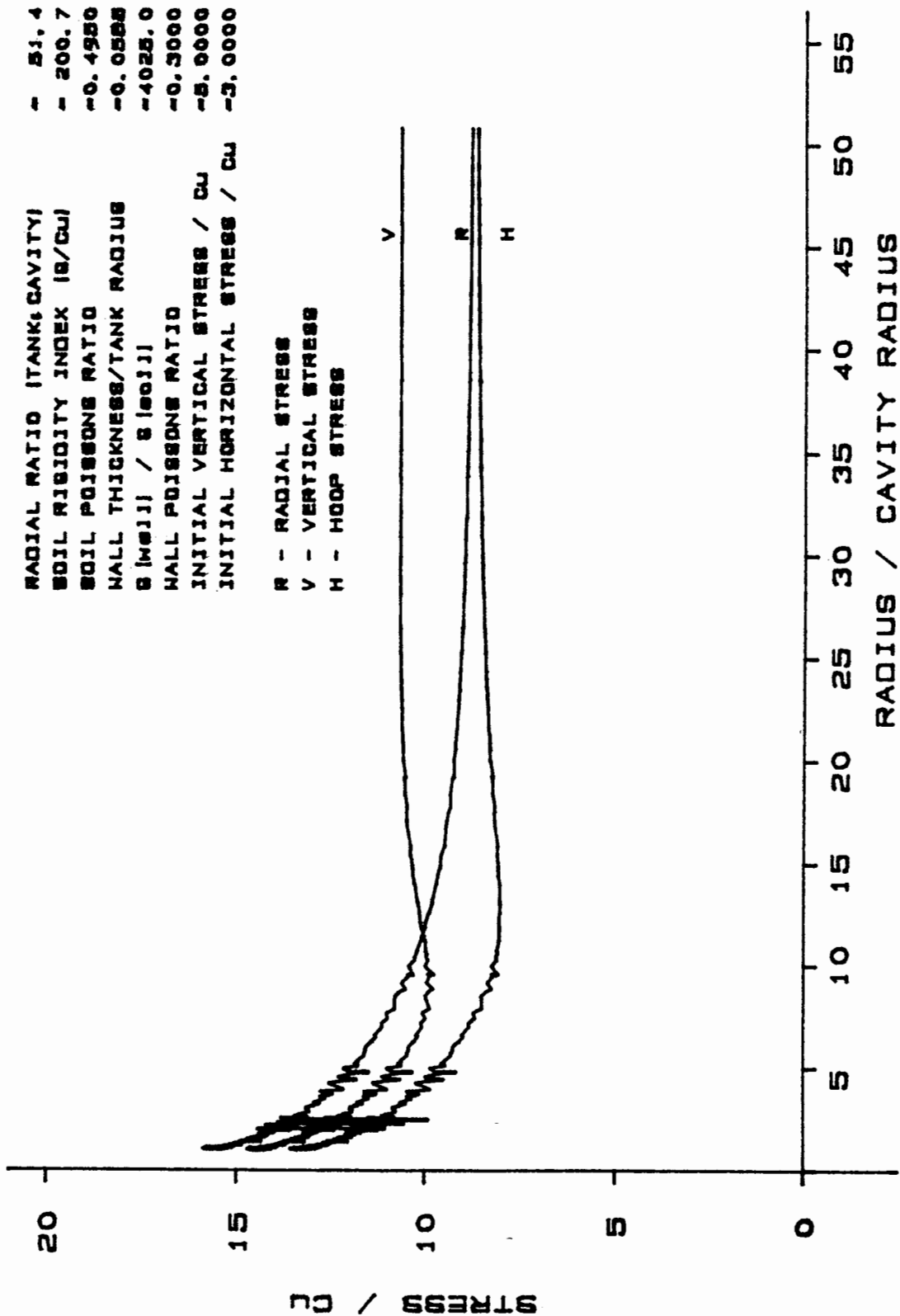
PLANE STRAIN CONFINED CAVITY EXPANSION RESULTS

FIGURE 2.10 NORMALIZED STRESSES : FEM15 (  $\nu = 0.400$  )



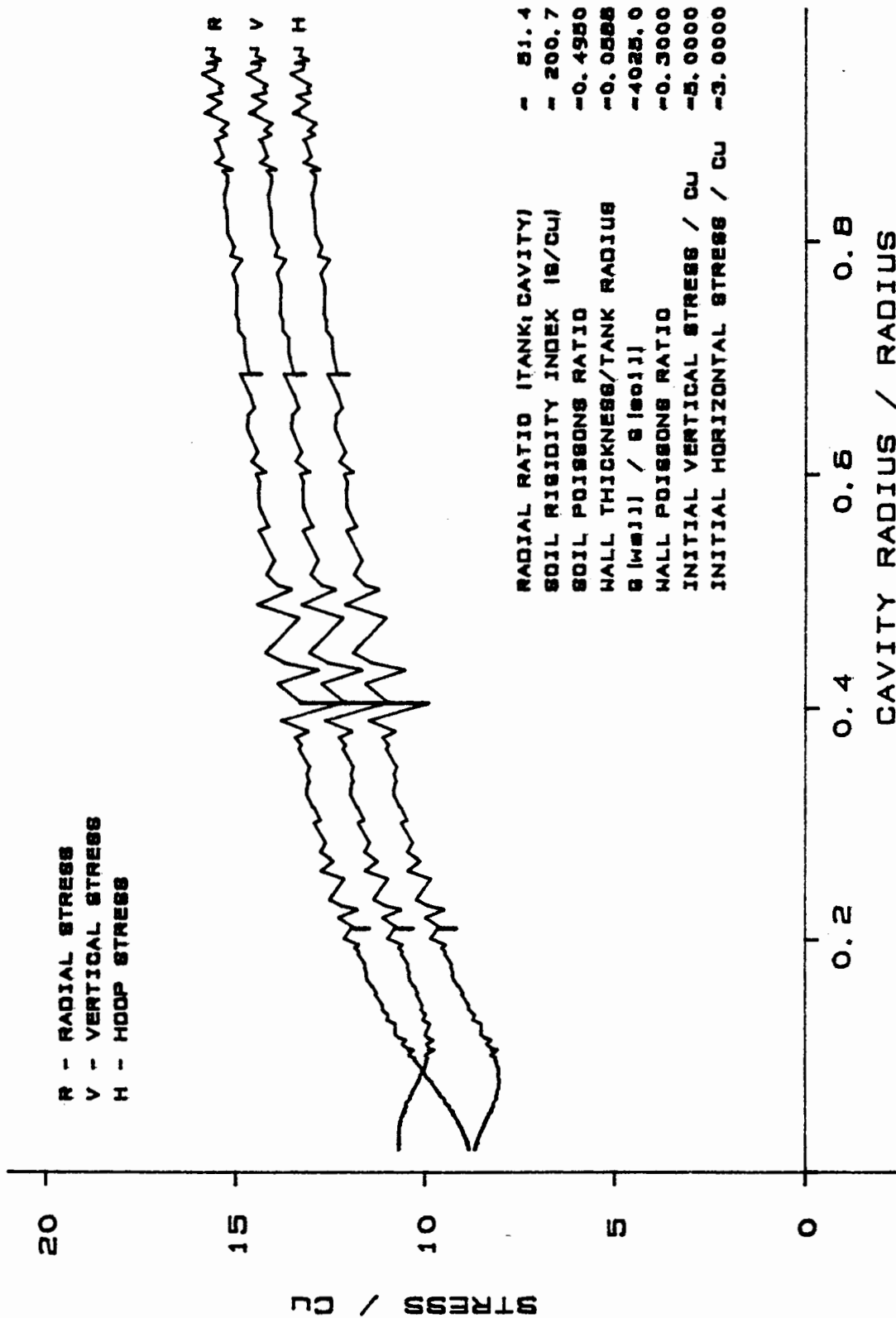
PLANE STRAIN CONFINED CAVITY EXPANSION RESULTS

FIGURE 2.11 NORMALIZED STRESSES : FEM15 (  $\nu = 0.400$  )



PLANE STRAIN CONFINED CAVITY EXPANSION RESULTS

FIGURE 2.12 NORMALIZED STRESSES : FEM15 ( $\nu = 0.495$ )



PLANE STRAIN CONFINED CAVITY EXPANSION RESULTS

FIGURE 2.13 NORMALIZED STRESSES : FEM15 (  $\nu = 0.495$  )

### 3. LARGE SCALE EQUIPMENT AND TESTING PROCEDURE

#### 3.1 Introduction

As the experimental work into the effect of radial confinement proceeded it became apparent that the confining effect of the rigid tank boundaries could not be entirely eliminated within a reasonable scale of tank. It was therefore decided to produce tanks which had the greatest practical tank to probe diameter ratio ( $R_{\text{tank}}/R_{\text{pen}}$ ). A diameter ratio of between 40:1 and 50:1 was chosen. In order to reduce the physical size of tanks two sizes of small scale penetrometer were used with  $5\text{cm}^2$  and  $1\text{cm}^2$  cross-sectional areas. This led to the production of two sizes of tank with diameters of 580mm and 1000mm.

The requirement for penetration rates of up to 2m/s necessitated the use of a hydraulic system to drive the penetrometer. The handling of a hydraulic ram and associated hoses on top of the consolidation tank required the maximum of clear working space. In order to provide this the consolidation tanks were designed with an internal piston which moved up the bore of the tank, consolidating the sample from its base.

The high velocity of penetration also required a rapid data logging system to record penetration events.

The equipment system is shown schematically in Fig. 3.1 and is described in detail in the following sections.

### 3.2 Consolidation Tanks

Three large consolidation tanks have been built. Tanks 'A' and 'B' have internal diameters of 580mm and heights of 1.1m. Tank 'C' (Fig. 3.2) has an internal diameter of 1000mm and an outside height of 2.0m. Both sizes of tank operate in the same manner.

The tank shell is cylindrical with a machined bore. The shell is equipped with ports that allow the insertion of pore pressure transducers into the upper portion of the tank and the measurement of total radial stresses at the tank wall. At either end the shell has a machined flange and rebate that enable the top and bottom plates to be clamped on using a Victaulic ring and seal (Fig. 3.3).

The Victaulic ring is divided into three sections. These are held together by three bolts lying tangential to the ring's circumference. As the joints require so few bolts installation of the end plates is considerably quicker than for a comparable bolted flange. The moulded rubber seal is located in an annulus between the ring and the tank. It seals under positive pressures and vacuum pressures inside the tank. In order to ensure the correct functioning of the seal a 6mm gap is required between the shell and the end plates. This is maintained by a series of M5 socket head bolts tapped into the ends of the shell.

The top plate of each tank contains five access ports and supports a flexible membrane on its under side (Fig. 3.4). The membrane is fabricated from a 1mm thick neoprene sheet stiffened at its edge and around the port holes with thin sheets of glass reinforced neoprene. The reinforcement is glued to the membrane using an industrial adhesive "Chelsea 391" combined with a chemical cross-linking agent "Tridur KA". This produces a flexible bond with high peel strength. The use of the reinforcing material enables the membrane to be clamped firmly to the

spacers at the ports and edge of the plate without extrusion of the membrane under pressure or tearing of the membrane in service. The spacers hold the membrane 35mm below the top plate. The gap between the membrane and top plate is water filled and linked to a pressure control and measurement system mounted on the outside of the tank. This system enables either constant stress or zero displacement conditions to be maintained on the top face of the soil sample.

A Vyon porous plastic filter is located below the flexible membrane to enable sample drainage from the top face. To ensure maximum flexibility for this filter it is only 1mm thick and has a series of slits cut through it radial to each port. Four brass "buttons" are located in the flexible membrane. These contain a central drainage hole and accommodate Lee-Instac flexible tube fittings in their upper surface. The flexible tubes connect the buttons to the underside of the top plate. Drainage holes are provided through the top plate and the expelled pore water is drained into a constant head tube mounted on the outside of the tank. Drainage to a constant head tube ensured that a known small positive initial pore pressure condition could be maintained in samples once consolidation was complete.

Each top plate has a central access port and four



peripheral ports spaced at half the tank radius from the centre line. Each port has an internal diameter of 25.3mm which provides a sliding fit for penetrometers with a  $5\text{cm}^2$  cross-section. The upper portion of each port is threaded M30 to enable brass plugs to be screwed into the port. There are three types of plug:

1. Blank plug
2. Blank plug incorporating a pressure transducer
3. Penetrometer adaptor plug.

All the plugs end flush with the bottom of the membrane retaining ring and incorporate an 'O' ring seal. The penetrometer adaptor plug has an axial hole of 11.3mm diameter running through it which provides a sliding fit for penetrometers of  $1\text{cm}^2$  cross-sectional area. On the upper face of the top plate there are four M14 holes around each port. These enable the penetration frame to be bolted onto the top plate.

The base plate of each tank has the same thickness as the top plate. The base plate has fittings which enable pressurized water to enter the tank, expelled porewater to leave the tank and the operation of a pressure transducer and a system to measure the piston displacement.

The piston itself is of hollow construction (Fig. 3.5). It functions by travelling vertically up the bore of the tank under water pressure thereby applying a consolidation pressure to the clay above the piston. The piston depth is 320mm for the larger tank and 195mm for the smaller tanks. Each piston has four circumferential grooves machined into its wall to accommodate a pair of seals and a pair of bearing rings. The seals are of 0.5" Quadring section. The bearing rings are 1.5" wide by 0.125" thick and made of a low friction fabric reinforced plastic, Tufcot T100G. The bearing rings prevent the seals from becoming nipped. The underside of the piston has dished air traps machined into it. These are vented through the piston and sealed with plugs screwed into the piston face. These vents enable the air trapped under the piston to be expelled during the filling of the water system. In the centre of each piston is a port designed to carry a PDCR 10DF pressure transducer. This waterproof transducer has its face flush with the top of a 3mm thick Vyon filter lying on top of the piston. This enables measurements of the total vertical stress on the base of the sample to be made for comparison with the vertical stresses measured at the top of the sample. Drainage from the bottom

filter is provided through the piston. The expelled pore water passes into an Enots 8mm diameter spiral tube attached to the underside of the piston at one end and the base plate at the other end. After passing through the base plate the water is piped into the constant head tube on the side of the tank.

The displacement of the piston is measured by a multi-turn potentiometer and self winding cable drum (Fig. 3.6). This system is bolted to the upper surface of the tank base plate and is designed to operate under 10 bar water pressure. A nylon sheathed Bowden cable passes from the self-winding drum, round a pulley and is attached to the underside of the piston. As the piston moves so the drum unwinds or reels in. The rotation of the drum is recorded by the potentiometer which is located in a water-tight housing.

The water pressure required to drive the piston in each tank is produced by a Madan Uni-Cub Model 'A' air driven hydraulic pump. A range of water pressures between 270kPa and 1200kPa can be achieved depending on the air regulator setting. The pump ratio is approximately 3:1 and the output is 27.5ml per stroke.

Optimum pump performance has been obtained by tapping a pressure relief valve and reservoir return line into the high pressure side of the system. This enables the pump to maintain continuous operation and total stress fluctuations on the sample are typically 2-3kPa. It has been found to be necessary to fit oil mist lubricators into the pumps' regulated air supply lines to prevent pump seizure (Fig. 3.1).

Details of the tanks' dimensions are given in Table 3.1.

	Tank 'A'	Tank 'B'	Tank 'C'
Shell Height (w/o studs) (mm)	1012	1012	1850
Piston Height (mm)	195	195	320
Shell Internal Diameter (mm)	580.87 - 580.97	580.49 - 580.75	1001.01 - 1001.27
Top Plate Thickness (mm)	47.25	47.85	65.68
Pressure Chamber Thickness (mm)	34.55	34.15	36.32
Base Plate Thickness (mm)	48	48	66
Depth of pore pressure and total stress port below shell rim	Port 1	135	209.5
	Port 2	225	409.5
	Port 3	315	609.5
Maximum initial sample depth (mm)	780	780	1495
Number of mixes to fill tank	3	3	14

**TABLE 3.1 TANK DIMENSIONS**

### 3.3 Penetrometers

Two sizes of penetrometer were supplied by Fugro B.V. The penetrometers are referred to by their cross-sectional area as  $5\text{cm}^2$  and  $1\text{cm}^2$  piezocones. Two penetrometers of each size have been built.

The  $5\text{cm}^2$  piezocones have a diameter of 25.23m and are intended primarily for use in the 1000mm diameter tank. In this tank the probe to tank diameter ratio is 1:39.6. The external configuration of the instrument is shown in Fig. 3.7(a). Tip resistance and sleeve friction are measured together with pore pressure at four locations as follows:

- 1) Mid-height on the cone face
- 2) On the cone shoulder
- 3) Mid-height on the friction sleeve
- 4) Immediately above the friction sleeve

Inside the  $5\text{cm}^2$  penetrometer are two strain gauged loadcells. The loadcell nearest the tip measures the force on the tip and the loadcell further from the tip measures the combined force from the tip plus the friction sleeve. Each loadcell contains four pairs of orthogonal strain gauges equally spaced around the circumference, together with temperature compensating resistors. The gauges are a standard Micro Measurements

type and comprise a full bridge with a resistance of  $180 \Omega$  in each arm. In order to minimize heat generation in the gauges the input voltage is kept to 3V D.C. Both load cells have a capacity of 10kN which is equivalent to an end bearing of 20MPa. The measured end bearing is typically only 5% of this value. Output for both loadcells is approximately 0.45mV/V FSO which leads to typical loadcell outputs of 70-150 $\mu$ V in the current experiments.

The pore pressures are measured with Kyowa PS-10KB miniature strain gauge transducers. These have a 10 bar range with a 15 bar burst pressure. They are powered at 3V D.C. and produce a full scale output of approximately 3mV. The filters on the cone surface are marked "1" to "4" (Figs. 3.7a). They serve as a rigid interface between the pore water in the soil and the saturating fluid (glycerin) inside the penetrometer in which the pore pressure measurements are made. The filters are made from Aerolith porous ceramic. Filter "1" has a width of 3mm, filter "2" a width of 3.5mm and filters "3" and "4" a width of 4mm.

The  $1\text{cm}^2$  piezocones have a diameter of 11.3mm. This gives tank to probe diameter ratios of 51.4:1 and 88.7:1 for the 580mm and 1000mm diameter tanks

respectively. There are two alternative configurations for this penetrometer and these are shown in Fig. 3.7(b). Tip resistance together with one pore pressure measurement can be recorded. By changing the tips pore pressure can be measured either on the face of the cone or on the shoulder.

The filter widths are 2mm on the cone face and 2.5mm on the shoulder. The load cell and pressure transducer are similar to those used in the 5cm<sup>2</sup> design. The load cell has a capacity of 10kN which is equivalent to an end bearing of 100MPa. The measured end bearing is typically only 1% of this value. However, the load cell design is severely constrained by the small diameter of the probe and the need to provide sufficient volume of metal for adequate heat dissipation. Thus it is difficult to improve the sensitivity of these small penetrometers. When powered at 3V D.C. the typical loadcell output is approximately 75  $\mu$ V in the current experiments.

The total length of the 5cm<sup>2</sup> penetrometers is 850mm. This enables a maximum penetration of 670mm to be performed in the largest tank. The 1cm<sup>2</sup> penetrometers have a length of 730mm. These have a penetration of 350mm in the smaller tanks and 550mm in the 1m diameter tank.

### 3.4 Hydraulic Driving System

Due to the requirement of driving probes into the tanks at up to 2m/s an insertion system power output of just under 100kW is required. To provide this a hydraulic system was designed (Fig. 3.8). The system makes use of an accumulator which discharges oil at high pressure to a double-acting ram via flow control valves. The valves are pre-set to the required flow rate and are internally compensated for pressure changes. On completion of the test the ram is instroked directly by the pump.

The pump is a Heypac air driven hydraulic power pack (HP40-BN-R1-21). It is driven from the laboratory compressed air supply and pumps oil from the reservoir into the accumulator to a maximum pressure of 165 bar (2400 psi). A pressure relief valve prevents over pressurization of the accumulator.

The accumulator is a Fawcett Engineering 18 litre capacity model. The nitrogen bag is precharged to 138 bar and this pressure rises to 165 bar when the accumulator is fully pressurized. In order to out-stroke the ram oil is released from the accumulator through either of two flow control systems.



For slow penetration in the range 20mm/s to 200mm/s solenoid valve S2 is operated. This activates the rapid opening of the pilot operated relief valve R2. Oil then flows through a pressure compensated flow control valve F3. This valve is a Fluid Controls type 2F75 1/2" restrictive style two port model. If rates of between 200mm/s and 3.5m/s are required solenoid valve S1 is operated which opens the pilot relief valve R1. The oil flow is then divided and passes through two flow control valves F1 and F2. These Fluid Controls Type 2F77 valves are larger versions of valve F3 having 1" diameter ports.

The controlled flow of oil passes to the ram through two 1.5" diameter "flexible" hoses. Oil leaving the ram is taken through two more of these hoses back to tank. Hose of this diameter is required to reduce friction losses and prevent turbulence. The hoses are connected to the ram through swivel couplings to aid manoeuvrability. The ram itself has a 2" (50.8mm) bore with a 1" (25.4mm) diameter rod. It has high speed seals and is cushioned at both ends.

The return flow to tank is controlled by a pressure relief valve (R3) set to operate at 14 bar line pressure. This valve prevents premature movement of the ram on the outstroke and enables the ram to be simply instroked by the operation of solenoid valve S3.

### 3.5 Logging System and Instrumentation

The full instrumentation and logging system is shown in Fig. 3.9. The instrumentation may be considered as follows:

1. Measurement of pore water pressure in the soil mass. Up to three Gaeltec type 3Ea transducers may be installed in any tank.
2. Measurement of total stresses on the tank boundaries. Up to 6 Druck PDCR22 and PDCR10DF transducers may be installed on the larger tank or 4 transducers on the smaller tanks.
3. Measurement of piston displacement. One potentiometer is installed in each tank.
4. Penetrometer instrumentation (see above). On the 5cm<sup>2</sup> probe two load cells (L1 and L2) and four pore pressures (P1-P4) require logging. The 1cm<sup>2</sup> penetrometer gives data from one load cell (L1) and one pore pressure transducer (P1).
5. Measurement of penetrometer displacement. A Sakae 10 turn precision potentiometer mounted on the hydraulic ram performs this measurement. It has a linearity of better than  $\pm 0.02\%$  giving a displacement measurement accuracy of  $\pm 0.2$ mm.

The measurement of pore water pressures within bodies of soil is commonly accomplished with Druck PDCR81 transducers. However, experience at Oxford has shown that these transducers are difficult to de-air fully and that they can be unreliable in operation. For the measurement of pore pressure changes during rapid events such as cone penetration it is essential that the transducers are fully de-aired. To overcome these problems an alternative transducer type has been adapted for pore pressure measurement. The design is based on the Gaeltec 3Ea transducer with the addition of a thread and shoulder on the front and a spanner flat on the rear of the body. A Druck filter mounted in a perspex holder is screwed onto the front of the transducer under glycerin after having been independently saturated. The transducers are of the half bridge type. A Gaeltec circuit board is connected to each transducer. This board contains the balancing and temperature compensation resistors, transforms 10V D.C. into  $\pm 5V$  A.C. to power the transducers and provides offset and amplification facilities to the output signal. The output of each unit has been calibrated to produce  $1mV/kPa$  with zero offset. Transducers have been purchased in the 3 bar and 5 bar ranges.

The Gaeltec transducers with an output of around 300mV and the Druck PDCR22 and PDCR10DF with outputs of 75-100mV can be read into the data logger without the need for additional amplification. The two potentiometers in the system, measuring penetrometer ram displacement and consolidation tank piston displacement, likewise require no amplification having a  $\pm 10$ V D.C. output. However, the penetrometer outputs are low and require stable front end amplification before being passed to the data logger. Outputs from the pore pressure transducers are around 3mV. This is amplified x 100 using an Oxford University multi-channel amplifier system designed by Mr. S. Oldham. The penetrometer loadcell outputs are around 75-150  $\mu$ V for the current experiments. A 1K amplification of these signals requires a very stable amplifier and the Fylde type FE-255-DA unit has proved to have the required performance. The calibration of the penetrometers is conducted with the same amplifiers, cabling and power supply that are used during actual laboratory penetration.

The outputs from the various transducers and potentiometers are then connected to a 3D data acquisition system. This unit, the "Analogue Express", is a 16 channel parallel analogue to digital converter with a

memory mapped interface to a Commodore C-64 micro-computer. The main features of the system are that it combines high sampling rates, high resolution and the simultaneous reading of all channels. The maximum sampling rate is dependent on the number of channels being read. For only one channel the maximum sampling rate is 13.889 kHz. During laboratory experiments between 7 and 16 channels are logged at maximum rates of 4.63kHz to 2.31kHz respectively. (Table 3.2). The sampling rate can be reduced for logging slower penetration events.

The conversion resolution is full 12 bit which gives a resolution of 0.025% of full scale. The signal conversion itself is accomplished with separate sample and hold amplifiers and A to D convertors for each channel, thus enabling the simultaneous reading of all channels. The Analogue Express passes the data to the C-64 where they are stored in a pre-assigned area of memory as channel number and value pairs. In order to achieve the high sampling rates required the storage of these data is performed under the control of the Analogue Express rather than under the C-64's own operating system.

The C-64 uses two programs to control the data logging, these being "BOBLOG" and "MMAPDRV.C-64". BOBLOG is a BASIC program which controls the setting

up of the logging system and the timing of slow logging stages. MMAPDRV.C-64 is a machine code program which drives the A to D convertors. BOBLOG enables any combination of channels from 0 to 15 to be read. The delay between fast scans is selected and may be any value between the minimum shown in Table 3 to a maximum of 1.573 seconds. Likewise the number of fast scans is selected at any value up to the maximum shown in Table 3.2. In addition to the fast scanning sequence, up to ten stages of slower scanning may be selected with delays of between 1 second and 999 seconds per scan. Each stage of the slow scanning takes ten readings of each selected channel. BOBLOG also allows up to ten single shot calibration scans before and after the experiment. Once the data have been acquired they may be viewed in digital form on the VDU, output to a chart recorder and stored on disk for transfer to the Departmental VAX computer for processing.

Correct triggering for the fast logging stage of the experiment is important. This is achieved with an external trigger linked directly to the Analogue Express. The trigger may be activated by the penetrometer ram potentiometer or by a hand-held battery driven unit.

Number of Channels logged	Minimum delay time (ms)	Maximum scan rate (kHz)	Maximum number of fast scans
1	0.072	13.889	8072
7	0.216	4.630	1050
8	0.240	4.167	904
9	0.264	3.788	790
10	0.288	3.472	699
11	0.312	3.205	624
12	0.336	2.732	562
13	0.360	2.778	510
14	0.384	2.604	465
15	0.408	2.451	426
16	0.432	2.315	392

**Table 3.2. LOGGING SYSTEM - FAST SCANNING PERFORMANCE**

### 3.6 Tank preparation

The tank preparation is the same for both diameters of tank. The apparatus is initially separated into its main components, base plate with piston, shell and top plate. The bore of the shell is cleaned of old clay and grease. A generous coating of Castrol Water-Pump Grease is then applied, particular attention being given to the lead-in at the base of the shell.

The Water-Pump Grease seems to be less prone to setting around the seals than the alternative silicon grease and is also less costly.

The connections between the piston and the base plate are checked. These are the spiral drainage line, the piston vertical stress transducer electrical connection and the connections to the piston displacement transducer. The piston displacement transducer is powered up and the zero displacement reading checked to ensure that the potentiometer has sufficient turns available to measure the full experimental piston displacement. Once these checks are complete the piston is located centrally on its base plate.

The lower Victaulic Seal is now lubricated with Victaulic Lubricant and positioned below the rim of the base plate. Grease is applied to the piston Quadring seals and these are located in their grooves. Care must be taken to use the correct pair of seals for each tank. Lightning Banding (a form of giant Jubilee clip) is now used to hold the Tufcot bearing strips in their grooves on the piston. The banding is positioned around the bottom edge of each strip to facilitate removal in the next stage of assembly.



The shell is lifted on the overhead crane and lowered over the piston, removing the Lightning Banding as each bearing strip enters the shell. A lifting frame has been built to facilitate the lifting of the 1m diameter shell. With the shell in position the Victaulic Seal is moved up over the joint between shell and base plate, one lip of the seal being located on each flange (see Figure 3.3). The three sections of the Victaulic Ring are now bolted together around the joint forming a pressure and vacuum tight seal.

The water level in the appropriate header tank is checked and topped up if required. The brass vent plugs in the face of the piston are removed and the space under the piston pumped full of water by the Uni-Cub water pump. Then the pump is isolated from the tank by closing the tank inlet valve. A vacuum is applied to the water under the piston and trapped air bubbles drawn out. The vent plugs are replaced and the bottom Vyon filter placed ontop of the piston.

The constant head tube is bolted to the lifting lugs on one side of the tank and the transducer supply block and pressure bag control unit bolted onto the opposite lugs. The total stress transducer(s) are located in the shell wall and the pore pressure ports are sealed. Finally the bottom sample drainage line

is connected between the base plate and the constant head tube. The tank is now ready to receive the clay slurry.

### 3.7 Slurry mixing procedure

The clay used for all the laboratory experiments was Speswhite kaolin from the English China Clay Co. To obtain a uniform sample the kaolin was mixed in a ribbon blade mixer. In order to remove air bubbles a vacuum was applied during mixing. A water content of approximately twice the liquid limit was used to provide a pumpable slurry which could be placed without the formation of shears and which would exhibit no stress-history "memory" when consolidated. Details of the mixer are given in Gue (1984).

The mixing procedure is as follows. The mixer is washed out and the seals checked. The mixer drain is then closed. Two bags of kaolin are weighed (approximately 50 kg). The weight of the empty bags (0.7 kg) is subtracted and the volume of water to produce a water content of 120% is calculated (approximately 60l). The volume of water is measured into the mixer and the kaolin powder added on top. The powder is hand mixed into the water. A smear of slurry is then placed round the lid flange to aid sealing and the

lid is clamped down. After having closed the mixer air vent, the vacuum pump is started. The safety screw is wound in and the mixer started. When a vacuum of 90 kPa (30 ft H<sub>2</sub>O) has been reached the vacuum line valve is shut and the pump switched off. The slurry is mixed for 1½ to 2 hours with the vacuum maintained between 84 and 90 kPa. Higher vacuums cause the water to boil at room temperature.

Once the mix is complete the mixer is stopped and the vacuum gradually released. The lid is opened and a water content sample taken. The mixer drain is opened and the slurry pump started. The slurry is initially pumped into a bucket to clear the line of water and dilute slurry. Once uniform slurry is being delivered the hose is transferred into the tank. Optimum performance is obtained with the end of the hose just submerged under slurry. Care has to be taken at the mixer to prevent air from being sucked into the mixer drain. When the full batch has been pumped into the tank the mixer drain is closed and further batches of clay mixed as above. Three batches are required to fill the small tanks and 14 batches to fill the large tank.

In between pumping the surface of the clay slurry is covered with polythene to prevent evaporation. This procedure was found to be preferable to leaving a layer

of water on the slurry surface as this extra water appeared to lead to the formation of softer zones at batch interfaces in the consolidated samples. In addition a spade was used gently to stir up the sample after the placing of each mix, care being taken to avoid air entrainment.

### 3.8 Top plate preparation and fitting

The top plate of each tank includes a flexible rubber membrane on its lower surface (see Section 3.2). It is necessary to ensure that the space above this membrane is filled with water and de-aired prior to fitting the top plate onto the tank.

It is first necessary to check that the four drainage lines through the top plate are unobstructed. This may be done by blowing through them. If the lines are blocked this must be rectified before proceeding.

Using the lifting points on the top plate it is then placed onto the membrane support former. The former is clamped onto the top plate with G-clamps and prevents the membrane from excessive stretching during filling. The top plate is now tilted to an angle of approximately  $30^{\circ}$  from the horizontal so that one of the pressure control ports is at the lowest point of the plate and the other is at the highest. The top plate is then filled with dyed

water through the lower port. The water is dyed to indicate any leakage into the top filter and to aid observation of air bubbles in the translucent pressure lines. Some water is allowed to flow out through the tube connected to the upper port. The tap on the line to the upper port is then closed and the plate is rocked and tapped with a soft faced hammer to dislodge any trapped air pockets. Once the air has been expelled the tap on the input line is closed thus sealing the cavity. The plate is now levelled and the former removed. The plate is lifted and the top Vyon filter fitted underneath the membrane with aluminium fingers.

The top Victaulic seal is now lubricated and fitted onto the top flange of the shell below the rim. The top plate is lowered into position on top of the tank, the Victaulic seal located and the Victualic Ring clamped up. The drainage lines are connected from the top plate to the constant head tube and the closest top plate pressure control line is connected to its control system. The tank is now ready for consolidation to commence.

### 3.9 Sample consolidation

Due to the use of pressure tight seals on the piston the full required vertical consolidation pressure

can be applied from the start of consolidation. However if pore pressure transducers are to be installed only 80% of the final consolidation pressure is applied initially, the pressure being increased after transducer installation.

Before loading is applied to the slurry the hydraulic pump is started and the pressure relief valve on the dumphine adjusted to provide the minimum pressure fluctuation at the selected consolidation pressure. Once satisfactory running is achieved on the pump the tank inlet valve is opened and drainage from both ends of the sample commences. The piston displacement together with total soil stresses on the piston, tank wall and top plate are recorded on a chart recorder. On the top plate the water pressure behind the flexible membrane is recorded together with the vertical stress on one of the plugs in the rigid penetration ports. The flexible membranes usually exhibit very slight leakage with time (typically 5 to 10 ml/day). This leads to a transfer of stress from the bag to the rigid ports if the loss is not corrected. Such a condition produces uneven stresses on the top of the sample and hence uneven consolidation. To avoid this regular checks of the pressures are required with careful use of the top plate pressure control system to eliminate any out of balance pressures.

Due to fluctuations in pumping pressure and rather poor pump reliability when being used for long periods large capacity air-water interfaces are used to maintain consolidation pressure once the piston displacement is virtually complete.

### 3.10 Pore Pressure Transducer Installation

Once piston movement is complete and the horizontal total stress has fallen to approximately  $K_0 \sigma_v$  the installation of pore pressure transducers is possible. It is important that the transducers are saturated before installation. With the current design the transducer filter in its perspex holder is first placed under vacuum for a day. The filters are then lowered into glycerin still under vacuum. The vacuum is then released and the filters stored under glycerin until required. The transducer body is placed into the glycerin and a syringe used to remove any air bubbles. The filter cap may then be screwed onto the transducer. The output of the transducer is monitored during this operation as it is easy to generate high pressures on the transducer by excessively rapid assembly.

The transducer is installed into the tank without reducing the consolidation pressure. The appropriate port on the tank wall is opened by unscrewing the cap and removing the bung and plug. A horizontal hole is then drilled radially into the clay cake to a distance

10mm short of the final transducer location. The pore pressure transducer is then removed from the glycerin and pushed into the bored hole using a purpose made inserting tool. The transducer is carefully pushed to the required depth while the pore pressures are monitored to prevent over-ranging. The insertion tool is then removed a split bung fitted onto the transducer cable and the port resealed. Extra cable is introduced into the hole in this operation thus minimising any tendency for the wire to exert a pull on the transducer under further consolidation.

Once all the required transducers have been inserted the consolidation pressure is increased by 25%. This increase is effective in closing the wire entry hole and minimising the effects of disturbance.

### 3.11 Penetrometer Saturation

In order to obtain good quality pore pressure data from the penetrometers complete saturation of the piezometric system is required. Poor saturation leads to a sluggish response and some apparent reduction in the magnitude of the pore pressure recorded. Glycerin was used to saturate the penetrometers as saturation was easy to maintain with this fluid.



The saturation procedures differ for the two sizes of penetrometer. The smaller  $1\text{cm}^2$  piezocone has a detachable tip and filters. The tips and Aerolith filters for this device are placed dry in a vacuum chamber and held under vacuum for approximately 24 hours. Without releasing the vacuum the tips and filters are transferred into a beaker of glycerin. The vacuum is then released. In order to ensure saturation the glycerin is heated to approximately  $60^\circ\text{C}$  and returned to the vacuum chamber for a further 30 minutes. The penetrometer, minus its tip, is clamped vertically tip uppermost and a saturation cup sealed onto its shaft. The cup is filled with glycerin and a small syringe is used to remove all air bubbles around the transducer face and threads. A length of dental floss is used to expel air from the groove behind the tip and ensure the groove is free from dirt. The required tip and filter are now transferred with tweezers into the cup ensuring that a thick film of glycerin remains over the items. The tip plus filter is screwed onto the penetrometer. A sheet of cling film is placed over the cup, eliminating air bubbles, and the penetrometer inverted. It is then submerged in a small bath of glycerin and the cup is removed. The  $1\text{cm}^2$  piezocone penetrometer is now ready for use.

The 5cm<sup>2</sup> piezocone cannot be saturated in a similar method as the filters cannot be removed without exposing the strain gauged load cells. This means that the penetrometer must be saturated in its assembled form. The penetrometer is sealed into its calibration and saturation chamber. This is then evacuated over-night. The penetrometer is moved to a vertical position, tip uppermost. Without reducing the vacuum warm glycerin is then sucked into the chamber, flooding it from the bottom upwards. A quantity of glycerin is allowed to flow through the chamber to flush out any possible bubbles. The penetrometer is then subjected to a number of cycles of vacuum followed by return to atmospheric pressure. The penetrometer output during these cycles is monitored on a chart recorder. If the output of one or more channels is sluggish or creeps under constant pressure conditions this suggests incomplete saturation. When successful saturation is achieved the penetrometer is removed from its saturation chamber under glycerin in a transfer bath. It is stored in this bath until required for testing.

### 3.12 Penetration Testing

Penetration testing in the laboratory is a fairly

complex operation as a number of different items of equipment need to be controlled.

The first step is to prepare the logging system. The data channels to be read, together with the fast and slow logging rates and duration, must be set. In addition to being connected to the logger the penetrometer outputs are also connected to a Y-T chart recorder. This serves as a back-up to the logger and also provides the best zero output data for the different transducers.

The driving system is now saturated by bleeding the ram with the pump running and the main valves open. Eye protection must be worn when bleeding the ram. The performance of the system is checked by driving the ram out at slow speed and checking the linearity of the displacement vs time plot on the chart recorder. The appropriate flow control valves are then set for the required penetration rate.

The tank inlet valve is now closed isolating the water filled space under the piston. All drainage lines from the sample are closed. The top pressure boundary control system is checked to ensure the appropriate valves are open and that the pressure is

being controlled by a venting type regulator. The required penetration port on the tank top plate is now opened.

If a  $1\text{cm}^2$  penetrometer is being used a sleeve is screwed into the port. The driving ram and frame are now aligned over the port with a mandrel and bolted to the top plate. A 25mm thick neoprene bush between the frame and the top plate introduces some flexibility into the system to prevent equipment damage from imperfect alignment. A syringe is used to fill the port with water. The piezocone is removed from its bath and pushed into the port until the tip is at soil level. The ram is advanced and the penetrometer coupled to it.

A slightly different procedure is required for the  $5\text{cm}^2$  penetrometer in the 1m diameter tank due to head room restrictions. This tank rests on heavy duty shifting skates. These are used to position the tank so that the ram will not foul on the overhead crane-way. The required port is opened and the penetrometer slid into it. The ram and frame are now positioned over the penetrometer and bolted through the rubber bush to the top plate as before. The ram is advanced and the penetrometer coupled to it.

All the valves on the driving system are now closed and the accumulator brought up to full working pressure (165 bar). At this point the appropriate solenoid valve for fast or slow discharge is operated and the logger trigger activated. The penetrometer is now driven into the sample and dissipation of pore pressures follows. Oil pressure on the ram is maintained throughout this period. Once dissipation is complete the return solenoid valve is activated, the outstroke valve is closed and the ram is instroked by the oil pump.

The penetrometer is uncoupled from the ram and removed for cleaning and resaturation. Filters are cleaned with a pressurized water spray and grooves with dental floss. The ram and frame are repositioned and the port plug replaced.

### 3.13 Post-penetration Soil Testing

Three CPTs are usually performed in each clay cake leaving two ports available for vane tests. Work on small scale cells demonstrated the importance of performing vane tests before unloading the clay (see Section 4.3). These tests are therefore

performed in the larger tanks under the same total stress conditions as the CPTs. A Pilcon hand vane is used for these tests. This vane has been calibrated against known values of torque and the readings indicated on the instrument corrected accordingly. The BS1377 formula has been used to convert torque into shear strength:

$$\text{Torque} = \pi c_{uv} \frac{D^2 H}{2} \left( 1 + \frac{D}{3H} \right)$$

where

$$\begin{array}{l} D = \text{vane diameter} = 19.2\text{mm} \\ H = \text{vane height} = 28.7\text{mm} \end{array} \left. \vphantom{\begin{array}{l} D \\ H \end{array}} \right\} \text{Small Vane}$$

$c_{uv}$  = vane undrained shear strength

This formula assumes the full shear strength to be developed across the ends of the cylindrical shear surface.

The head is rotated at a rate of 0.05 revolutions/s. After each vane test the soil is augered out to the depth of the test with a 3/4" diameter auger. The shaft of the vane is then oiled before pushing the instrument deeper into the soil for another test.

Once the vane tests are completed the tank is depressurized and the water under the piston drained out. This allows the piston and clay cake to descend onto the base plate. The lower Victaulic Joint is then unbolted and the shell complete with top plate is removed. Water content samples are taken from the clay at this stage to give a thorough indication of any sample variability.

In addition thin-walled oiled brass tubes of 38mm internal diameter are pushed vertically into the soil at selected elevations. These samples are waxed and transferred to an incubator at 2°C prior to triaxial testing. On each cake a number of unconsolidated undrained triaxials are performed at varying cell pressures. Additional samples may be used for isotropically consolidated undrained triaxial testing. Oedometer testing may also be performed.

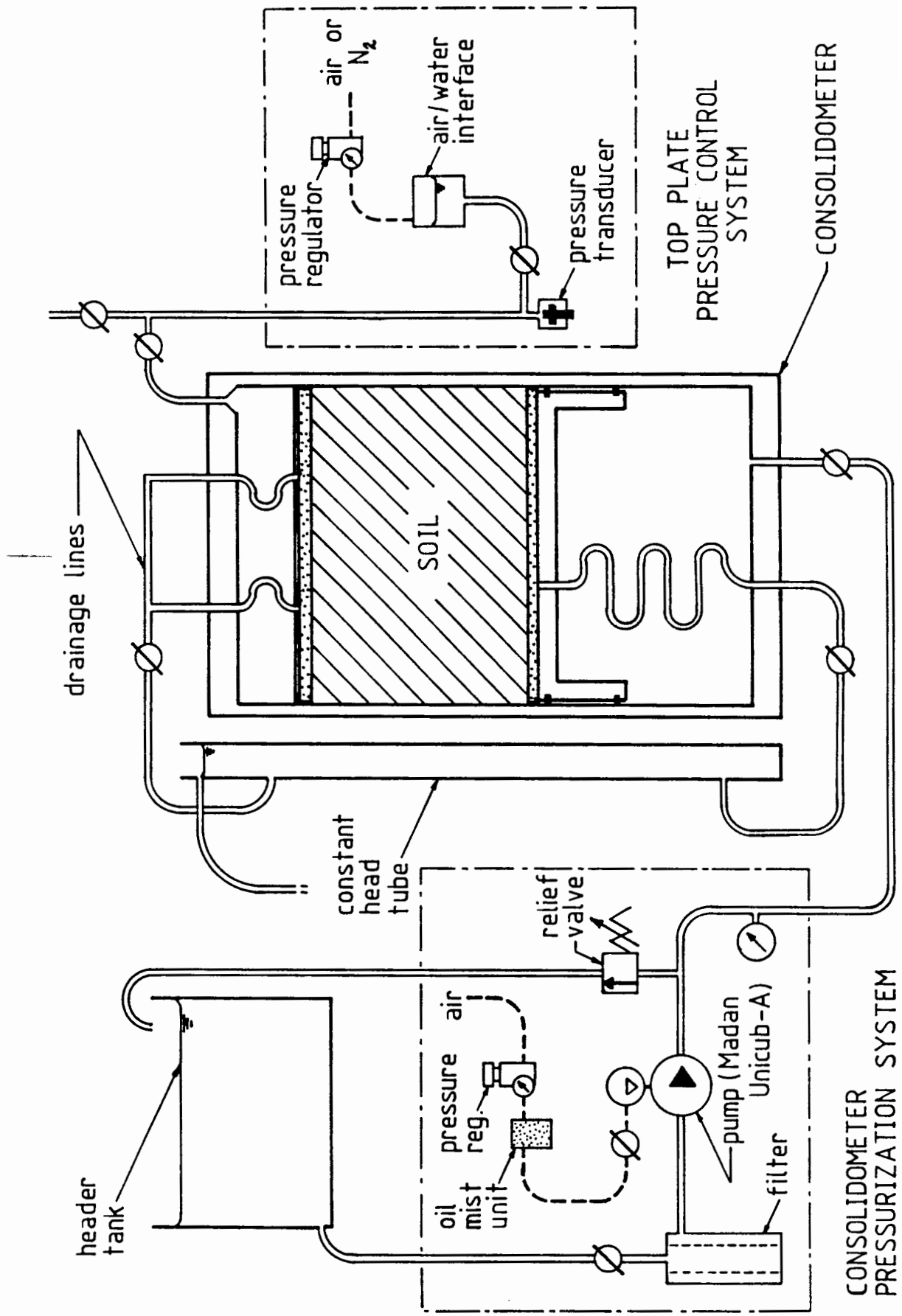


FIGURE 3.1 LARGE SCALE CONSOLIDOMETER SYSTEM



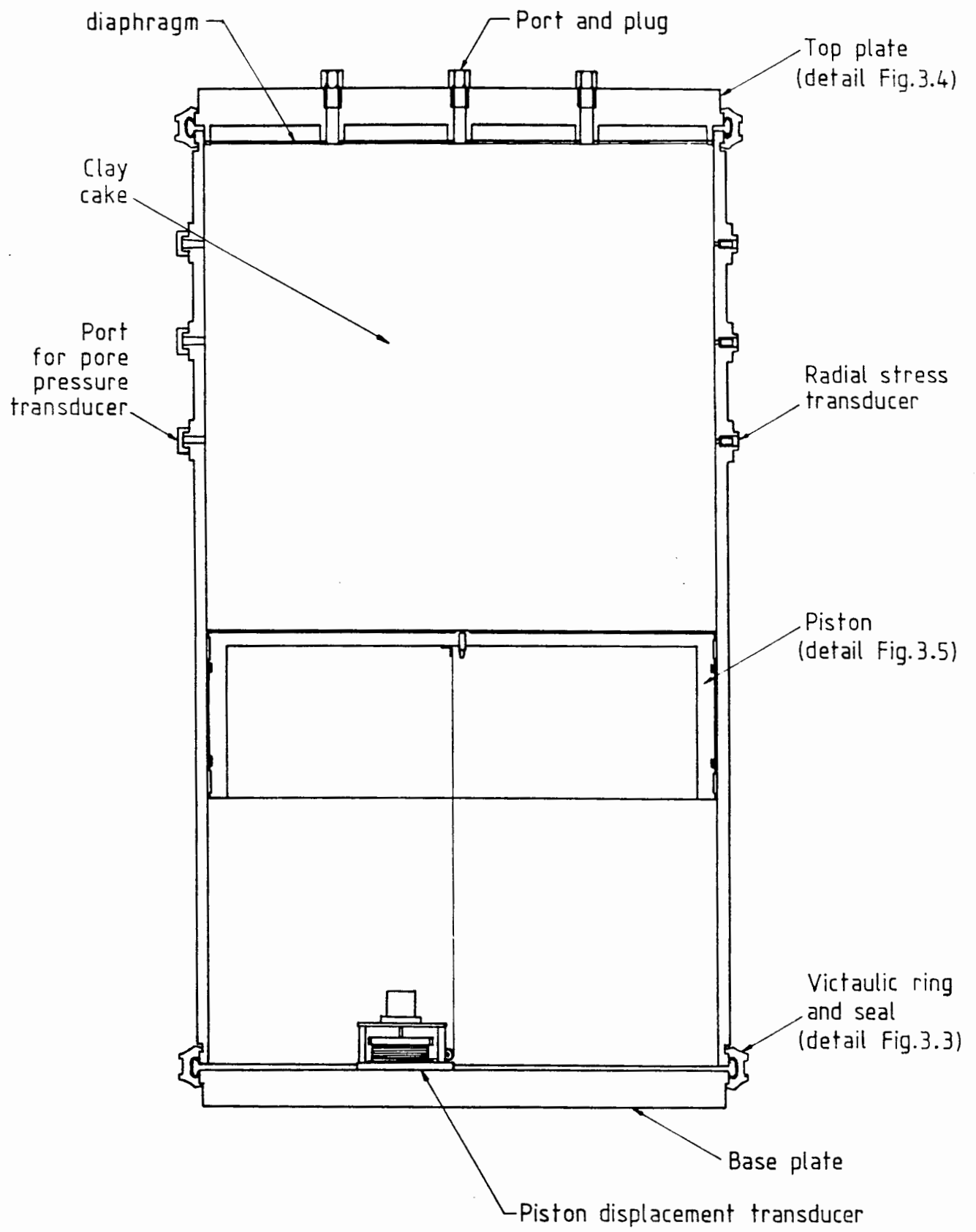


FIGURE 3.2 LARGE TANK DETAIL

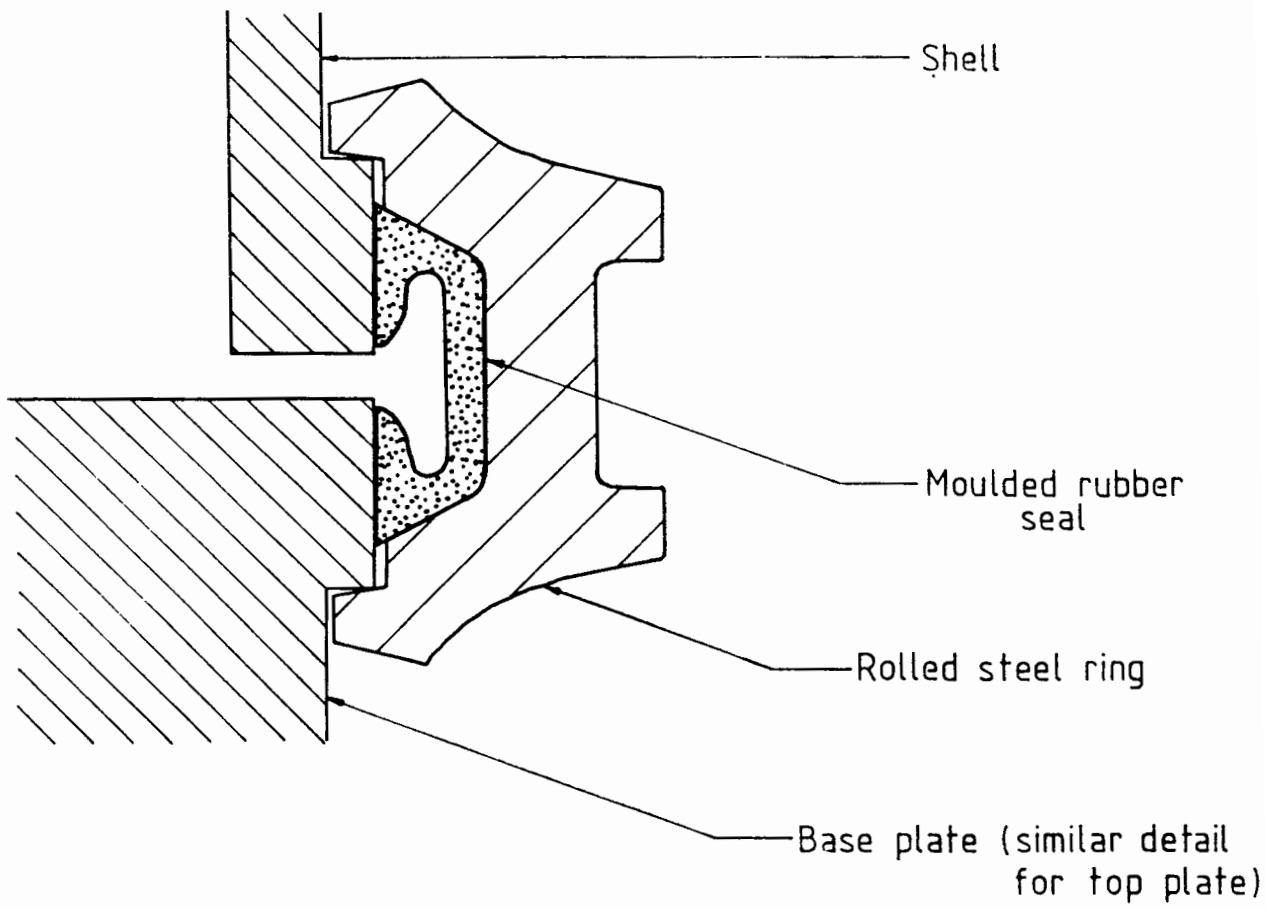


FIGURE 3.3 VICTAULIC SEALS

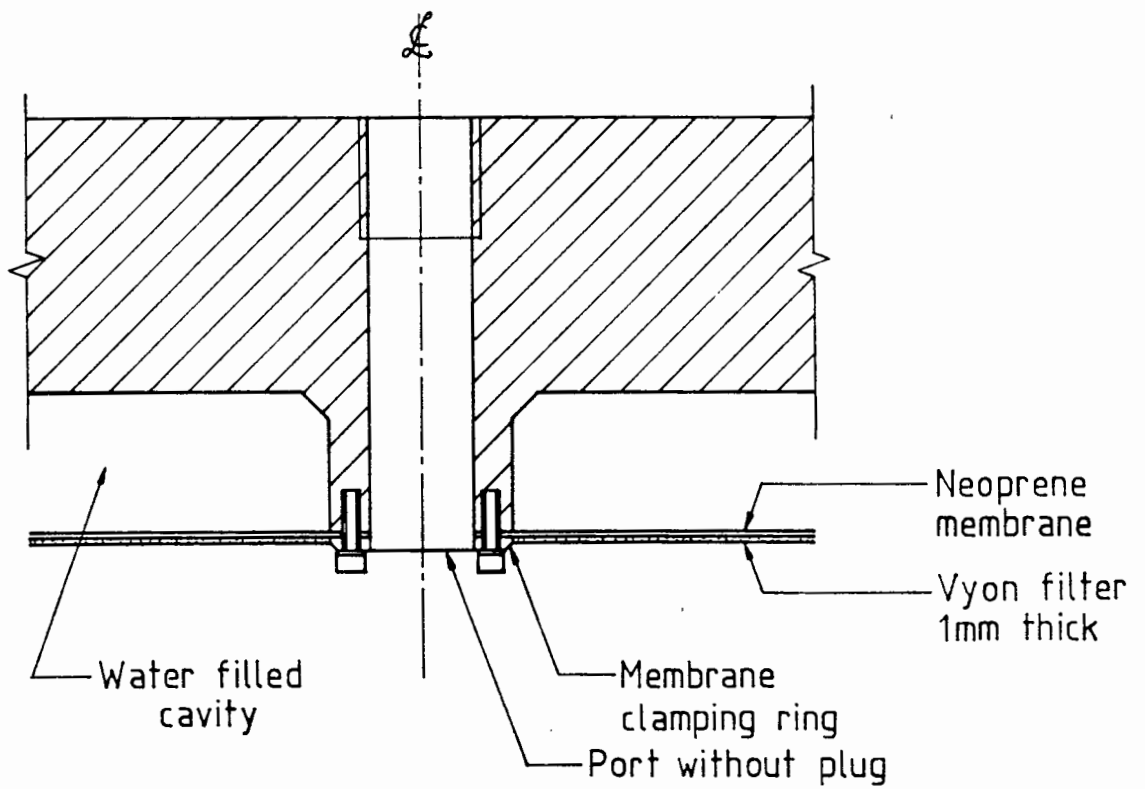


FIGURE 3.4 LARGE TANK TOP PLATE

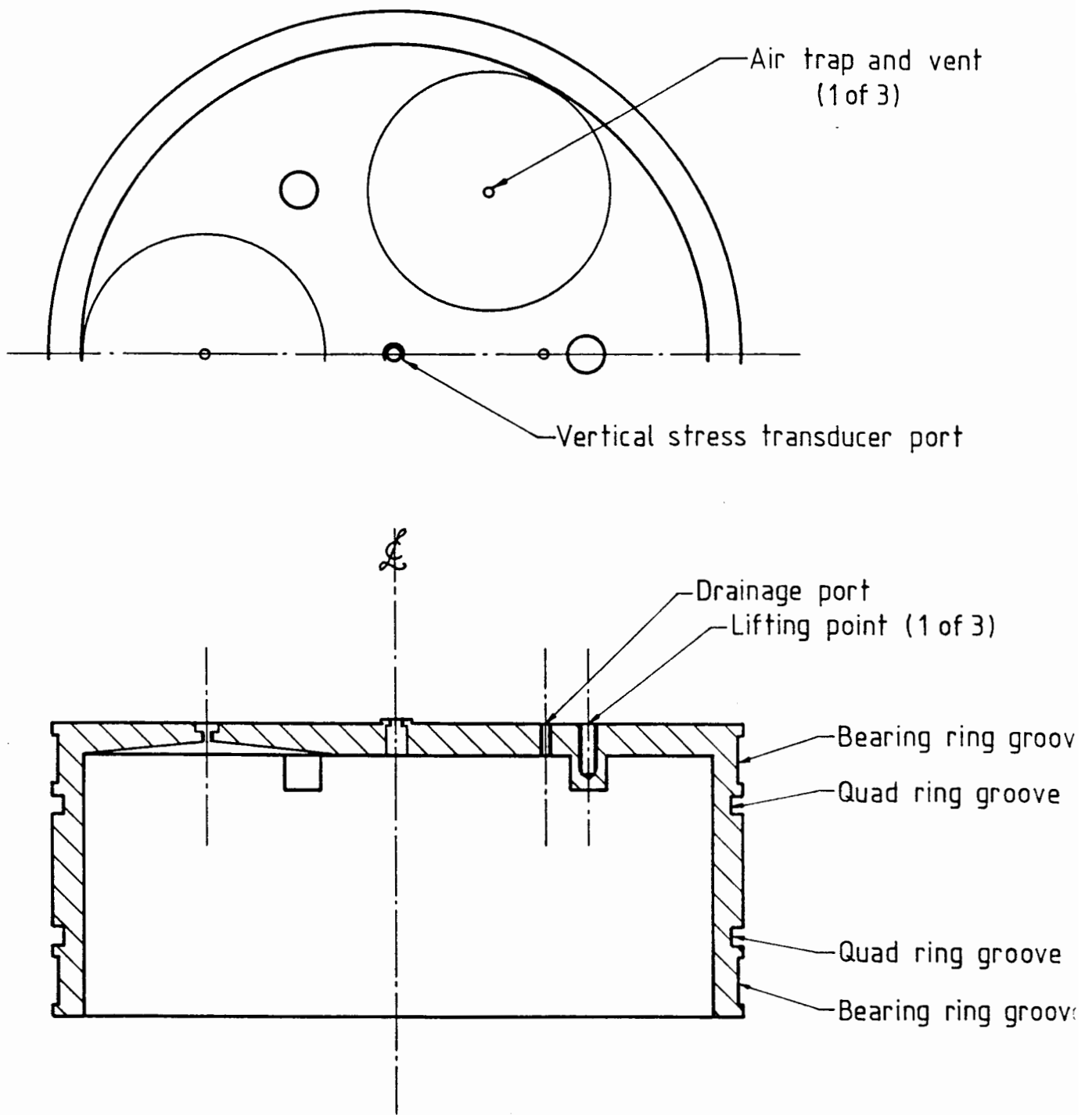


FIGURE 3.5 HOLLOW PISTON

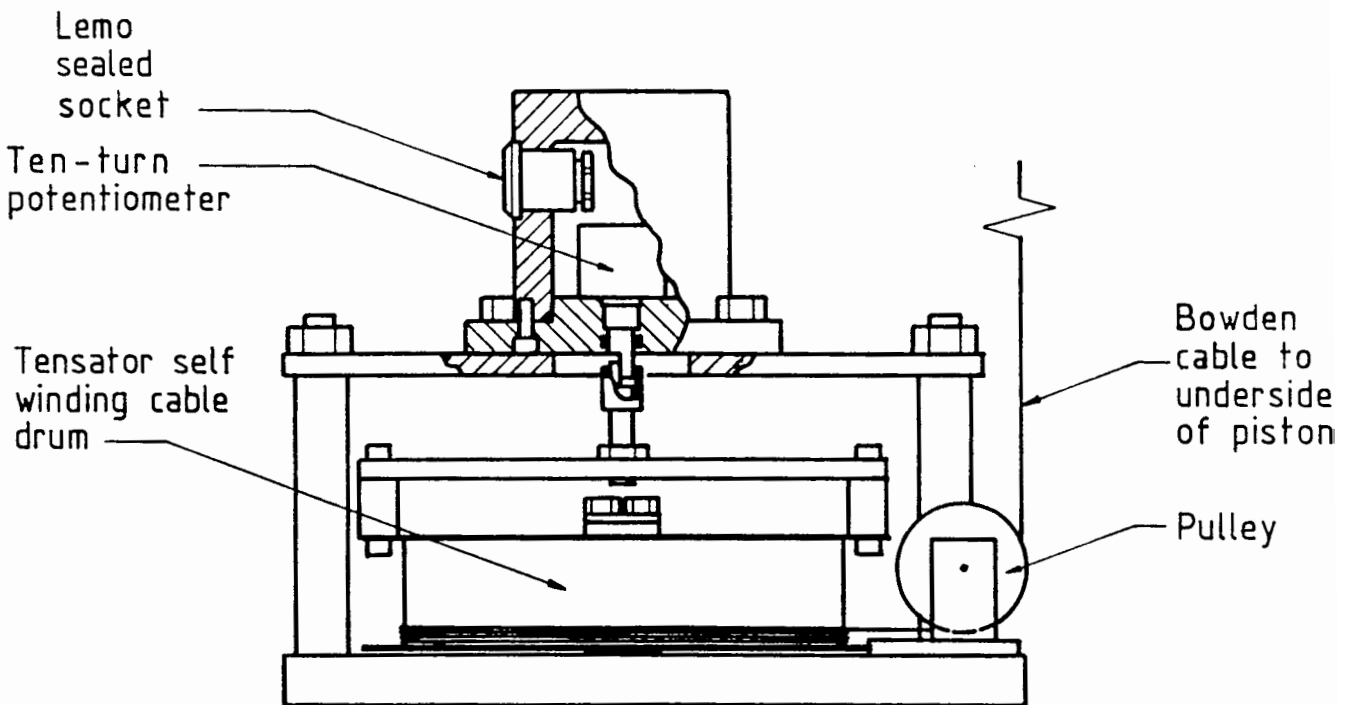
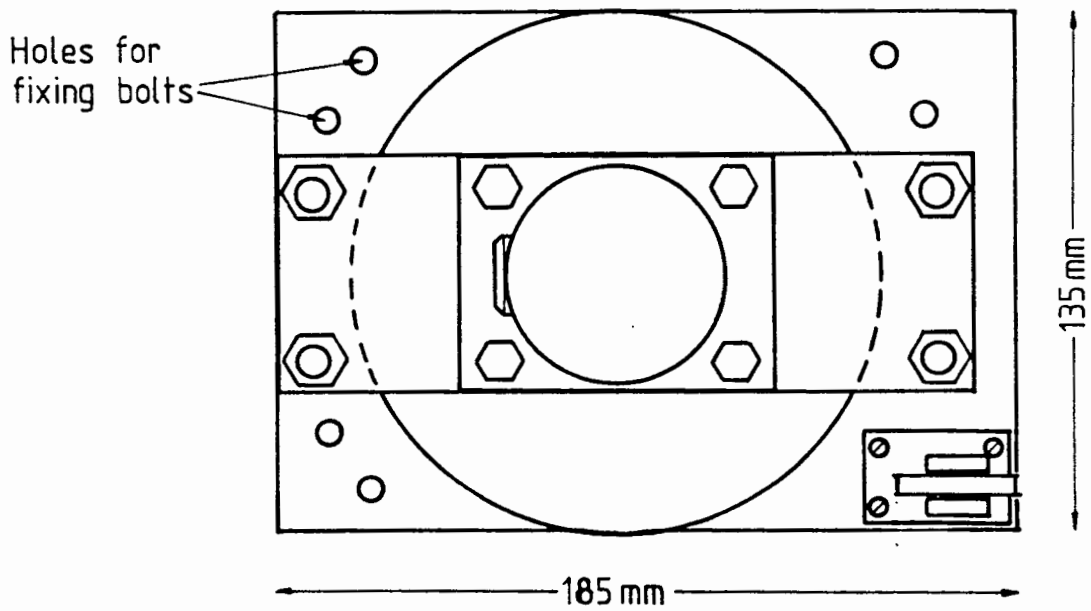
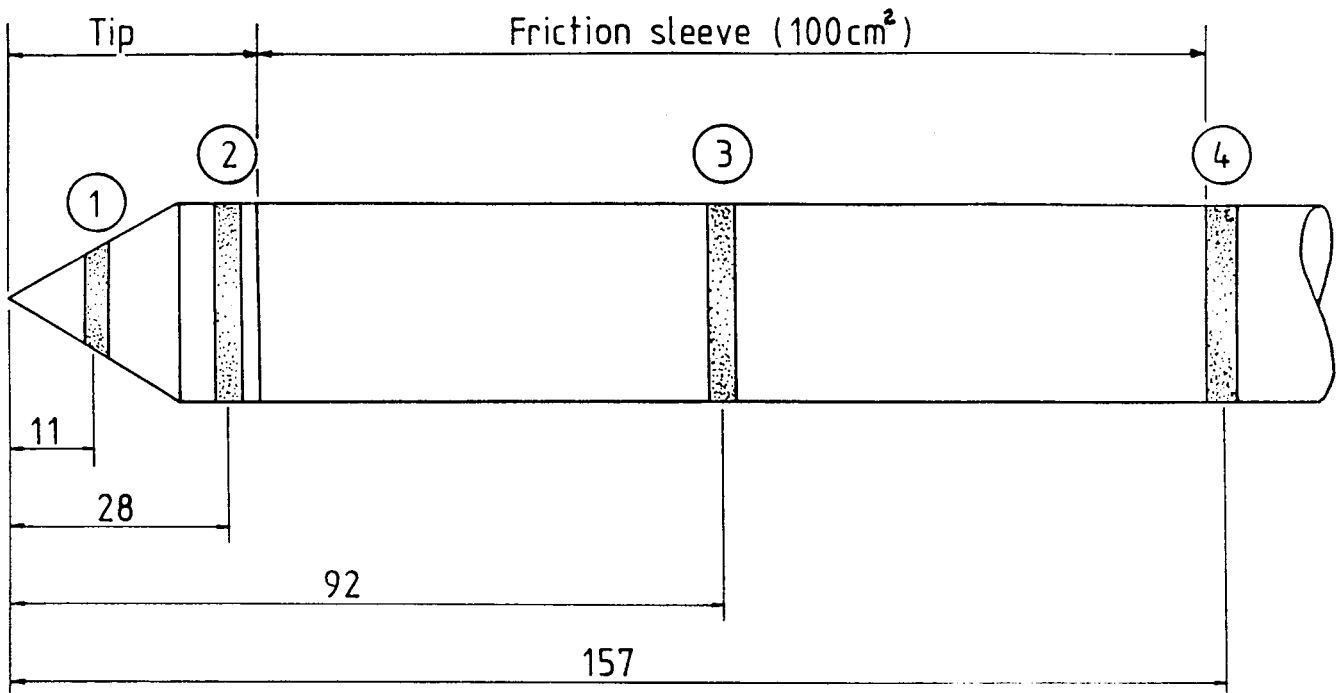


FIGURE 3.6 PISTON DISPLACEMENT TRANSDUCER

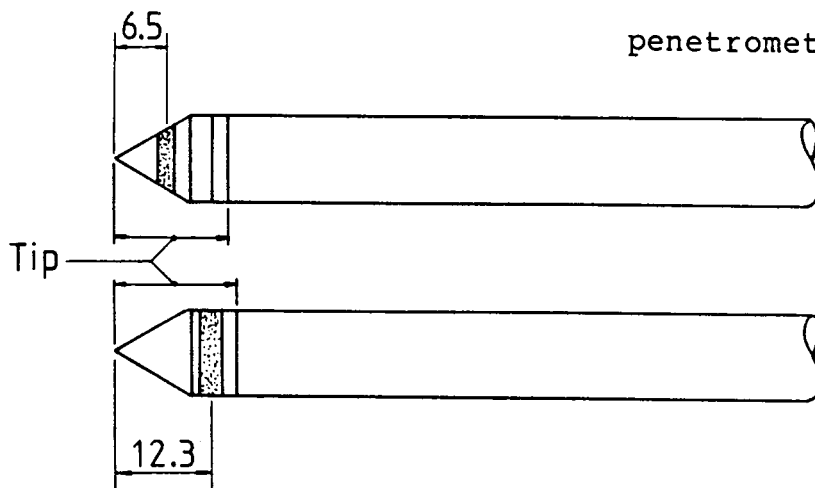


5 cm<sup>2</sup> PIEZOCONE

Cone-002  $\alpha = 0.4480$

Note: All linear dimensions  
in millimetres

$\alpha = \frac{\text{groove cross-section area}}{\text{penetrometer cross-section area}}$

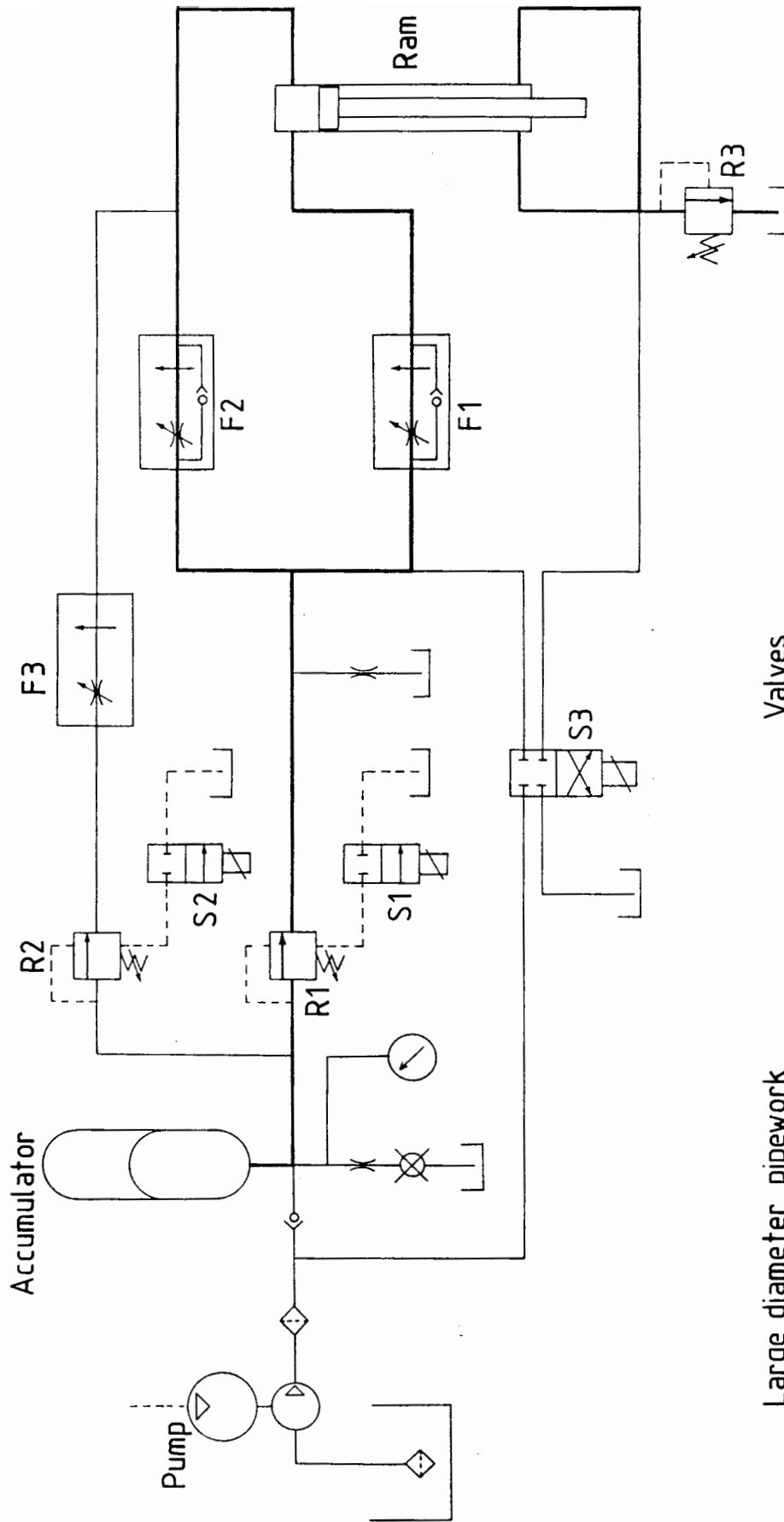


1 cm<sup>2</sup> PIEZOCONE (with alternative tips)

Cone-003  $\alpha = 0.4664$

Cone-004  $\alpha = 0.4693$

FIGURE 3.7 EXPERIMENTAL PIEZOCONE PENETROMETERS ( 1 cm<sup>2</sup> & 5 cm<sup>2</sup> )



Valves  
 F1, F2, F3 - Pressure compensated flow control valves  
 R1, R2, R3 - Relief valves  
 S1, S2, S3 - Solenoid valves

Large diameter pipework shown with bold line

FIGURE 3.8 HYDRAULIC CONE INSERTION SYSTEM

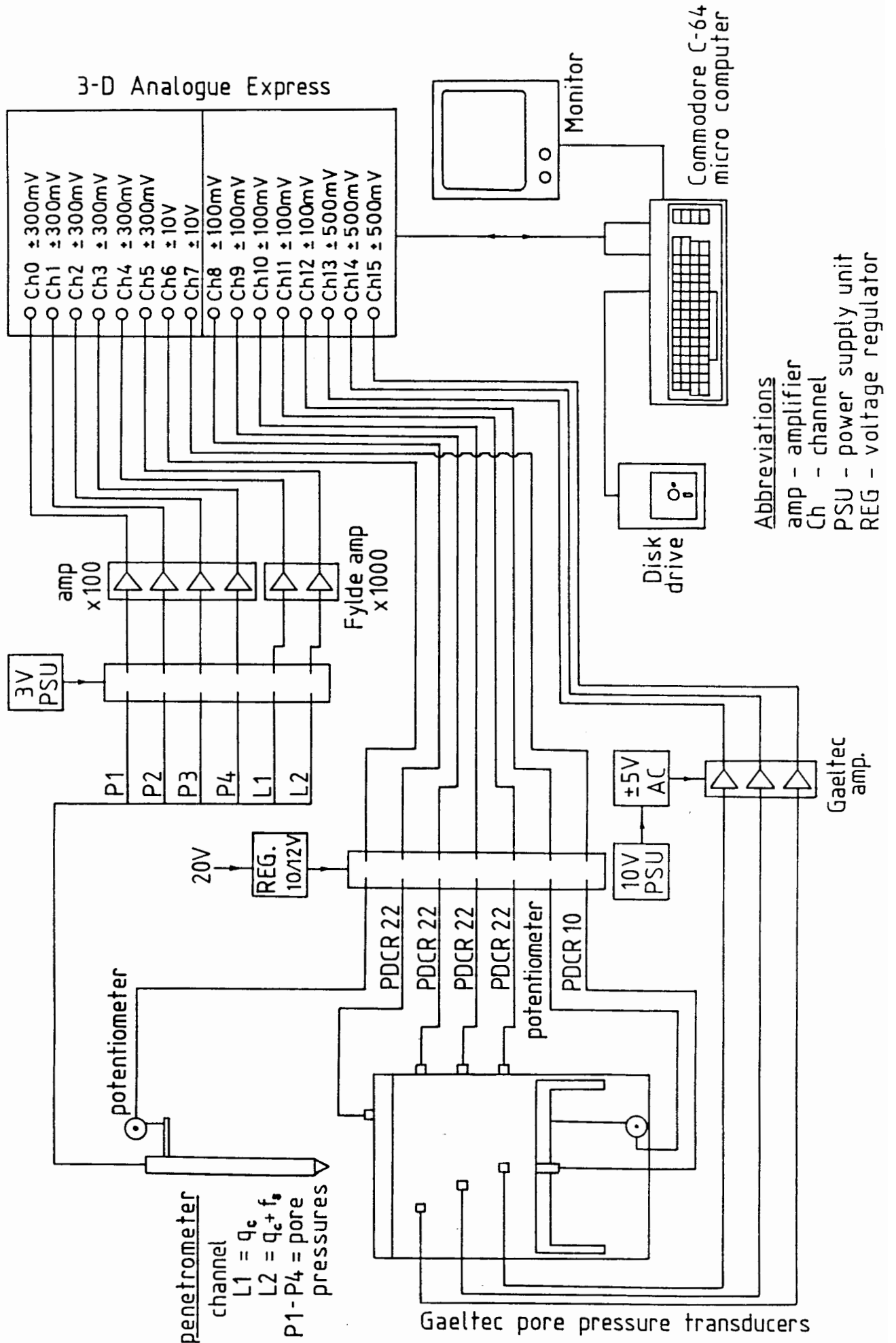


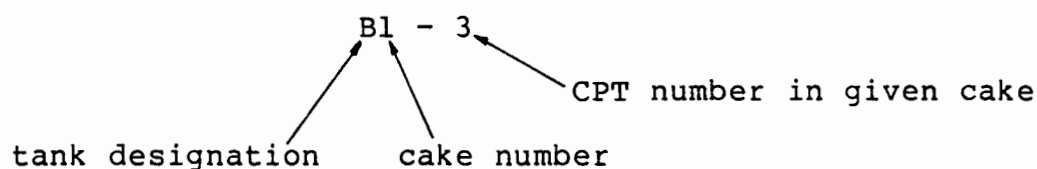
FIGURE 3.9 LABORATORY INSTRUMENTATION SYSTEM

#### 4. LARGE SCALE LABORATORY TESTING RESULTS

In this Chapter the parameters for the large scale laboratory testing series are presented. The quality of the data is then examined before presenting the detailed laboratory testing results.

##### 4.1 Large Scale Test Series

The large scale test series are shown on Tables 4.1 and 4.2. The designation of the tests is as follows:





high velocity CPTs were performed in normally consolidated cakes over the full range of shear strengths.

The water content and shear strength profile of each cake are shown in Figures 4.1 to 4.8. The cone penetration profiles are shown in Figures 4.9 to 4.28. It should be noted that apart from Tests A4-3 (and the unsuccessful B3-2) all the tests performed with the  $1\text{cm}^2$  penetrometers had the pore pressure measurement on the cone shoulder (see Figure 3.7). Factors affecting the quality of the penetration data are discussed in Section 4.2.

Test Series	Consolidation Time (days)	Vertical Stress $\sigma_{vo}$ (kPa)	Horizontal Stress $\sigma_{ho}$ (kPa)	Water Content (%)	OCR $\frac{\sigma'_{v \max}}{\sigma'_{vo}}$
A3	28	300	181	46.1-47.4	1.07
A4	12	512	245	42.0-42.9	1.00
A5	16	597	262	41.0-42.9	1.00
B1	17	446	268	42.0-43.2	1.29
B2	40	303	192	45.1-46.1	1.03
B3	69	548	284	42.9-43.9	1.03
C1	78	325	214	44.0-45.9	
C2	102	376	268	44.0-44.9	1.00

TABLE 4.1 GEOTECHNICAL DATA ON CLAY CAKES

Test Designation	Cone Size (cm <sup>2</sup> )	Cone Serial No.	Penetration Rate (mm/s)	Comments
A3-1	1.0	F1CW-001	44	
A3-2	1.0	"	42	
A4-1	1.0	F1CW-001	27	
A4-2	1.0	"	26	
A4-3	1.0	"	26	
A5-1	1.0	F1CW-003	31	No data obtained during penetration
A5-2	1.0	"	33	
A5-3	1.0	"	313	
B1-1	1.0	F1CW-003	33	
B1-2	1.0	"	35	
B1-3	1.0	"	32	
B2-1	1.0	F1CW-004	101	
B2-2	1.0	"	109	
B2-3	1.0	"	48	
B3-1	1.0	F1CW-004	250	Failure of data logging system Failure of data logging system Failure of flexible membrane after test
B3-2	1.0	"	2500	
B3-3	1.0	"	26	
C1-1	1.0	F1CW-003	29	Raised pore pressure in soil due to leakage below piston Failure of data logging system
C1-2	1.0	"	31	
C1-3	1.0	"	250	
C1-4	1.0	"	3210	
C2-1	5.0	F2.5CW-002	25	Failure of flexible membrane after test
C2-2	5.0	"	238	

TABLE 4.2 CPT SERIES - GENERAL DATA

#### 4.2 Data Quality

The quality of data obtained from the penetrometers, the cell instrumentation and the post CPT soils testing requires evaluation. The recording of data from the pore pressure transducers on the penetrometers was generally more satisfactory than from the load cells. The pore pressure transducers were usually operating at pressures close to their rated full scale output during penetration. The output signal was ten times larger than that of the load cells and hence the significance of electrical noise on the signal lines was reduced. These transducers proved insensitive to temperature changes of up to 30°C. The most significant factor affecting the quality of the penetrometer pore pressure data was the saturation of the piezometric system. The 1cm<sup>2</sup> penetrometers with their detachable filters were much easier to saturate than the 5cm<sup>2</sup> device. The saturation of the 5cm<sup>2</sup> assembled penetrometer was accomplished by the more complex procedure described in Section 3.11. The method worked well for an initially completely dry instrument. However, it was less successful in the resaturation of a partially saturated penetrometer. It is suspected that this was due to the difficulty of drawing trapped air bubbles out of the glycerin. The degree of saturation

of the piezometric system affects its response time, better saturation being required for faster tests. For well saturated CPTs the accuracy of the data presented is better than + 1%.

The load cell data was of rather lower quality for two main reasons, those of zero stability and signal noise. The load cell zeros were affected by temperature changes, the problem being particularly severe for the smaller instruments. It was found that powering the  $1\text{cm}^2$  instrument at 10V produced a temperature rise in excess of  $15^{\circ}\text{C}$  on the outside of the instrument in air. In order to reduce this heating the penetrometers were powered at 3V for all tests except the A3 series. This reduced the measured external temperature rise in air to less than  $2^{\circ}\text{C}$ , but also reduced the load cell output voltages to 30% of their former value. It may be noted that the heat generation of the load cell should be proportional to the square of the voltage while the output is directly proportional to the input voltage. The reduction in voltage improved the performance of the original  $1\text{cm}^2$  penetrometer (FlCW-001) however significant zero changes were still experienced when the external temperature was altered. A very careful rearrangement of the temperature compensation by Fugro B.V. resulted

in improved performance from subsequent  $1\text{cm}^2$  instruments (F1CW-003 and -004). For these penetrometers an external temperature change still produced a spike in output but the original value was restored in less than 0.1 sec. This response time may still be seen as rather marginal for fast penetration in the smaller tanks. The  $5\text{cm}^2$  penetrometer had considerably better load cell zero stability than the  $1\text{cm}^2$  equivalent although indentical strain gauges were used on both. The reasons for this difference lie in the small radius and low cross-sectional area of the cylindrical load cell in the  $1\text{cm}^2$  instrument.

Due to the low output of the load cells during penetration (typically  $30\mu\text{V}$  to  $50\mu\text{V}$ ) difficulties were experienced with noise levels on the signal lines. At low penetration velocities the amplified output was recorded on a 6 channel y-t chart recorder. This system acted as a mechanical filter as the pens were unable to respond to high frequency noise. However, the data logger used for high speed tests and for up to 16 channels of data had a very short conversion time of  $15\mu\text{s}$ . Significant noise levels were captured by this system. The use of electronic filters to remove this noise was rejected in case significant information was lost in fast penetration events. Instead various numerical filters were employed in the data analysis, the most satisfactory proving to be a simple averaging procedure.

When the fluctuations in loadcell output at the start of a test are excluded an accuracy of around  $\pm 5\%$  may be assigned to the load cell data presented.

The quality of data obtained from the cell instrumentation was variable. The measurement of the vertical stresses acting on the top plate of the tanks was considered to be of high accuracy. The Druck PDCR 22 transducer installed in a port in the top plate uses a silicon diaphragm and strain gauges which produce a high signal output combined with a very stiff response. Applying a measured back pressure to these transducers to produce a null reading demonstrated a measuring error of less than 0.2% when recording soil normal pressures on a flat surface. A similar transducer was used to record fluid pressure behind the flexible membrane and the balancing of these two pressures led to a highly accurate assessment of the stresses acting across the top surface of the tank.

A waterproof silicon diaphragm transducer was used to record vertical stresses at the base of the clay cake. The transducer was mounted into a button in the centre of the piston face. The button was machined to a 3mm upstand to match the surrounding Vyon filter and the transducer diaphragm was flush with the

button surface. However, this transducer recorded stresses that were rather higher than expected probably due to the mounting attracting some stress concentration in the overlying clay.

The least satisfactory boundary stress measurements were the radial stress transducers. As noted in the small scale perspex cells, small radial displacements of the transducer face substantially affect the measured total stress. Limited evidence from tank C suggests that the magnitude of the measured radial stress increase ( $\Delta\sigma_r$ ) is less affected by small variations in the location of the transducer face than the initial measured radial stress ( $\sigma_{r0}$ ). Hence the ratio ( $\Delta\sigma_r/c_u$ ) has been used in preference to ( $\Delta\sigma_r/\sigma_{r0}$ ) when considering this data.

The Gaeltec pore pressure transducers used for this experimental series did not contain on-board temperature compensation. This resulted in zero drift when the transducers were installed in the clay cakes. The absolute accuracy of pore pressure measurement was typically  $\pm 10$  kPa. However, the measurement of the pore pressure increase during penetration was more accurate with an error of around  $\pm 2$  kPa providing the system was well saturated.

### 4.3 Shear Strength Measurements

The evaluation of piezocone data against soil shear strength forms a major part of the present study. It is therefore necessary to make a careful analysis of the shear strength data obtained, considering the relationship of the recorded data to the in-situ shear strength and the uniformity of the results.

The radial and vertical uniformity of consolidation achieved in the cells was determined by examining water content distributions. Three samples were consolidated in the 138mm diameter cells with varying drainage arrangements and boundary types. All the samples show a high degree of water content uniformity with the extreme variation in water content being  $\pm 0.5\%$  (Fig. 4.29). The provision of a flexible top boundary with zero overall displacement produced samples of the same uniformity as the rigid top plate cells.

This degree of uniformity is seen in the water content profiles obtained in the larger tanks (e.g. Fig. 4.8). For each cake water content samples have been obtained from at least two vertical profiles at <sup>different</sup> radii from the centre. The results are as tightly banded as those from the small cells.



The uniformity of water content indicates uniformity of void ratio as the clay was fully saturated. As the total stresses applied have maintained normally consolidated conditions (except for Sample B1), the uniformity of void ratio indicates the existence of uniform shear strengths in the samples.

Three methods were used to evaluate soil shear strengths. Vane tests were performed with a Pilcon vane before and after depressurization of the sample, "quick" unconsolidated undrained triaxial tests (QUU) and isotropically consolidated undrained triaxial tests (CIU) were performed.

The vane test is often regarded as a "strength index" test rather than a fundamental shear strength test. Uncertainties of interpretation exist due to disturbance on vane insertion, the complex distribution of shear resistance across the ends of the vane, possible strength anisotropy effects, rapid drainage of the very thin shear zone and marked rate effects. In this report a simple analysis has been used to convert the torque measured in the vane test into a shear strength ( $c_{uv}$ )

$$c_{uv} = \frac{6T}{\pi (3HD^2 + D^3)}$$

(see Section 3.13) where  $T$  = torque  
 $H$  = vane height  
 $D$  = vane diameter

Vane tests were conducted on samples consolidated in the small cells before and immediately after depressurization (Table 4.3). The results indicate a reduction in shear strength of approximately 30% within a few minutes of unloading. Similar results are reported by Kirkpatrick and Khan (1984b). The effect is probably due to the inability of the clay to maintain negative pore water pressures of equal magnitude to the in-situ mean effective stress before stress relief. The data in Table 4.3 show that the vane shear strength continues to fall with time. Kirkpatrick and Khan noted the same effect over longer time spans. These authors note that the effect is particularly severe for kaolin and may be rather less for smaller grained clays (e.g., illites).

The measurement with vane tests of large strength reductions due to stress relief is of significance for the measurements of shear strength in the triaxial apparatus. Kirkpatrick and Khan demonstrated that the percentage strength reduction measured by triaxial and vane tests is very similar. The QUU triaxial tests performed on specimens from each clay cake would therefore be expected to yield values of

Time	Average Vane Shear Strength (kPa)	$\frac{\text{Vane Shear Strength}}{\text{Initial Vane Shear Strength}}$
Before depressurization	65	1.00
1 min after depressurizing	48	0.74
6 min after depressurizing	44	0.68

## General data:

Vane :	Pilcon, blade height	28.7mm
	diameter	19.2mm
	thickness	1.6mm
Sample :	Height	140mm
	Diameter	138mm
	Water Content	45.4%
	Initial $\sigma_v'$	433kPa

**TABLE 4.3 : EFFECT OF CELL DEPRESSURIZATION ON VANE SHEAR STRENGTH**

shear strength below the in-situ value (under active stress conditions). In addition the triaxial samples will have suffered a degree of sampling disturbance due to the intrusion and extrusion of the clay into the thin walled sampling tubes (see Hight et al 1985). The combined effects of stress relief and sampling disturbance are partially "counteracted" in the QUU test by the high rate of shearing (2% axial strain/min). This rate is 100 times that employed in the isotropically consolidated undrained triaxial tests (CIU) and may increase the QUU shear strength by up to 20%. Despite this, the CIU tests yield higher shear strengths at given water contents than the QUU tests.

The vane, QUU and CIU shear strength data are plotted on Fig. 4.30 against water content. The relationship between log depressurized vane shear strength and water content has been obtained by linear regression through 21 data points. This technique was not used to plot the relationship between pressurized vane shear strength or QUU shear strength and water content. This was because inconsistencies were introduced into these data by partial depressurization, sample disturbance, variable sampling and storage effects. These processes produced lower measured vane or QUU shear strengths in some cases. The relationships have instead been plotted through the peak shear strength values parallel to the log depressurized vane shear strength vs water content relationship. It should be noted that adopting this approach implies a constant ratio between the various shear strength measurements at any given water content or void ratio. The peak strength data from pressurized vane and QUU tests do not contradict this assumption. The CIU data has generally been obtained by consolidation to cell pressures higher than the mean effective in-situ pressures of the clay cakes (Table 4.4) and therefore provides data at relatively high shear strengths. Nevertheless the same straight line relationship between water content and log peak shear strength

Sample Number	Clay Cake	$\sigma_{vo}'$ (kPa)	$P_o'$ (kPa)	$P_c'$ (kPa)	$\frac{P_c'}{\sigma_{vo}'}$	$\frac{P_o'}{P_c'}$	$c_{cu}$ (kPa)	w/c (%)
A3a				394.0	0.76	0.56	128.0	41.8
A3b	A3	300	221	295.9	1.01	0.75	101.4	42.3
A3c				497.4	0.60	0.44	153.4	41.6
C2a				387.4	0.97	0.72	128.0	41.0
C2b	C2	376	278	292.4	1.29	0.95	92.9	42.1
C2c				494.8	0.76	0.56	142.5	40.3

**TABLE 4.4 SUMMARIZED DATA FROM CIU TRIAXIAL TESTS**

would be expected to hold at lower shear strengths as observed with the other types of strength test. The work of Kirkpatrick and Khan (1984a) indicates that the relationship of shear strength to water content is close to the insitu behaviour for CIU tests where the consolidation pressure  $p_c'$  is at least equal to the original vertical consolidation pressure (i.e. CIU tests A3a, A3c, C2a, C2c). For these samples the CIU strength may be around 6% less than the in situ undrained shear strength at the same water content. For CIU tests consolidated at pressures less than the original vertical consolidation pressure the discrepancy will be greater between in situ and CIU shear strength - water content relationships. Thus tests A3c, A3a, C2a and C2c may be expected to give shear strength-water content relationships close to the normally consolidated

in situ value. However, A3b with an OCR of 1.01 and C2b with an OCR of 1.29 should yield a progressively lower shear strength at their water contents. Reference to Figure 4.30 shows that this trend was observed. The in situ shear strength has been taken to be equal to the CIU shear strength at the measured water content. In order to calculate in situ shear strengths for the full range of clay cakes tested the water content vs log in situ shear strength relationship has been extrapolated from the experimental CIU data on a line parallel to the depressurized vane shear strength vs water content relationship (see Fig. 4.30).

The derived in situ strengths are compared to the values from vane and QUU tests in Tables 4.5 and 4.6.

Clay Cake	Water Content			OCR $\frac{P'_c}{\sigma'_{vo}}$	Undrained Shear Strength		
	mean $\bar{x}$ (%)	Std dev S (%)	S/ $\bar{x}$ (%)		$c_{uv}$ (kPa)	$c_{uu}$ (kPa)	$c_{ui}$ (kPa)
A3	46.6	0.7	1.5	1.07	41.5	48.5	65
A4	42.5	0.3	0.7	1.00	88.3	84.1	114
A5	42.1	0.5	1.1	1.00	92.1	90.1	121
B1	42.8	0.5	1.1	1.29	81.0	70.3	109
B2	46.5	0.4	0.9	1.03	43.1	-	66
B3	42.3	0.6	1.3	1.03	80.3	59.5	117
					70.2*		
C1	44.8	0.7	1.5	1.00	65.7	61.8	84
					53.7*		
C2	44.5	0.4	0.9	1.00	53.3*	52.3	87

\* Vane tests performed after sample depressurization

**TABLE 4.5 SHEAR STRENGTH AND WATER CONTENT OF CLAY CAKES**

Clay Cake	OCR	$\frac{C_{uv}}{C_{ui}}$	$\frac{C_{uu}}{C_{ui}}$
A3	1.07	0.64	0.75
A4	1.00	0.77	0.74
A5	1.00	0.76	0.74
B1	1.29	0.74	0.65
B2	1.03	0.65	-
B3	1.03	0.69	0.51
C1	1.00	0.78	0.74
C2	1.00	-	0.60

NOTE: Pressurized vane test results only have been used in this table.

$C_{uv}$  = Pilcon vane shear strength

$C_{uu}$  = QUU shear strength

$C_{ui}$  = Calculated in situ shear strength

**TABLE 4.6 RELATIONSHIP OF STRENGTH MEASUREMENTS TO CALCULATED INSITU STRENGTH**

#### 4.4 Cone Resistance at Lower Penetration Rates

The experimental cone resistance data recorded at penetration rates of 20mm/s to 50mm/s is presented in Table 4.7. The data has been analysed in two ways to produce a cone resistance factor ( $N_{kt}$ ). The first analysis uses the standard bearing capacity formula:

$$N_{kt} = q_t - \frac{\sigma_{vo}}{c_u}$$

where  $q_t$  = total cone resistance (corrected for pore pressure behind tip).

$\sigma_{vo}$  = initial vertical stress.

$c_u$  = undrained shear strength

The second analysis provides for an approximate correction of the cone resistance measured in the tanks to provide an estimate of the  $N_{kt}$  that would be obtained in an infinitely large tank (i.e. in situ). The correction is made by subtraction of the radial stress increase at the tank wall ( $\Delta\sigma_{rb}$ ) from the cone resistance. A discussion of the concept behind such a correction is given in Chapter 2. The amended equation is:

$$N_{kt}^{*}(\text{corrected}) = \frac{q_t - (\Delta\sigma_{rb} + \sigma_{vo})}{c_u}$$

In order to provide the most reliable estimates of  $N_{kt}$  from the experimental data those sections of the records in which  $q_c$  varies substantially due to electrical instabilities or localized variations in soil properties have been excluded from the analysis. The sections of each profile considered are given in Table 4.7.

It should be noted that all correlations have used the in situ shear strength calculated from the water content as detailed in Section 4.3, rather than the measured vane or QUU shear strengths.



For convenience the nett cone resistance ( $q_n$ ) has been used in Table 4.7 where:

$$q_n = q_t - \sigma_{vo}$$

Test No.	Rate (mm/s)	Penetration (mm)	$q_n$ (kPa)	$c_{uu}$ (kPa)	$c_{ui}$ (kPa)	$N_{kt}$ (in situ)	$N_{kt}^*$ (in situ)
A3-1	44	125 - 210	620	48	65	9.5	8.8
A3-2	42	135 - 200	625	48	65	9.6	8.9
A4-1	26	20 - 290	1258	88	114	11.0	10.5
A4-2	26	80 - 290	1228	88	114	10.8	10.2
A4-3	26	175 - 325	1238	88	114	10.9	10.3
A5-1	31	100	1283	87	121	10.6	10.0
		165	1353	94	121	11.2	10.5
		250	1383	97	121	11.4	10.8
A5-2	33	130 - 200	1373	95	121	11.3	10.7
B1-1	33	250 - 325	1304	84	109	12.0	11.3
B1-2	35	120 - 285	1314	84	109	12.1	11.4
B1-3	32	110 - 300	1344	84	109	12.3	11.7
B2-3	39	160 - 220	672	43	66	10.1	9.3
	56	275 - 315	712	48	66	10.8	10.0
B3-3	26	80 - 205	1302	82	117	11.1	10.3
		225 - 300	1382	88	117	11.8	11.0
C1-2	31	65 - 215	866	67	84	10.3	10.0
		215 - 343	866	67	84	10.3	10.0
		462 - 550	857	67	84	10.2	9.9
C2-1	25	190 - 272	876	48	87	10.1	9.1
		320 - 450	894	56	87	10.3	9.3

**TABLE 4.7 SUMMARIZED CONE RESISTANCE DATA  
FOR LOW VELOCITY SERIES**

#### 4.5 Pore Pressures During Penetration at Lower Penetration Rates.

The pore pressure data obtained from penetrometers advancing at rates of 20mm/s to 50mm/s has been correlated against shear strength as follows:

$$N_{\Delta u} = \frac{\Delta u}{c_u}$$

where  $N_{\Delta u}$  = Excess pore pressure factor  
 $\Delta u$  = Excess pore pressure above hydrostatic.

In similar manner to the analysis of the cone resistance data, a correction to the recorded pore pressures has been made to account for the effect of radial confinement.

$$N_{\Delta u}^* = \frac{\Delta u - \Delta \sigma_r}{c_u} = \frac{\Delta u^*}{c_u}$$

The results of these analyses are presented in Table 4.8a.

These data may be compared with the results obtained from using the piezoprobe (Fig. 2.3 and Section 2.2) in the 138mm diameter small scale perspex cells. The methods used for these tests are described in Section 2.3. Data from these tests is given in Table 4.8b. It is of interest to note that the values of  $N_{\Delta u}$  recorded in these small cells (tank/probe diameter = 12.4) are of a similar magnitude to those recorded on the cone face in the large scale tests A4-3 and C2-1.

The distribution of pore pressure along the cone has been determined by the 5cm<sup>2</sup> multi-pore pressure penetrometer (Test C2-1) and in a more limited fashion for the 1cm<sup>2</sup> exchangeable tip penetrometer (A4 series). The results of these analyses normalized with pore pressure at the cone face and above the friction sleeve are shown in Fig. 4.31.

A further analysis has been performed to determine the distribution of pore pressure in the clay cake during penetration. Insufficient data has been obtained to produce a complete distribution. However contours of  $\Delta u/c_u$  have been plotted with the available data on Figure 4.32.

Test No.	Rate (mm/s)	Penetration (mm)	Sensor Location	$\Delta u$ (kPa)	$\frac{\Delta u}{c_{ui}}$	$\frac{\Delta u^*}{c_{ui}}$
A3-1	44	125-210	Shoulder	545	8.4	7.7
A3-2	42	135-200	Shoulder	570	8.8	8.0
A4-1	26	150-275	Shoulder	1020	8.9	8.4
A4-2	26	100-260	Shoulder	920	8.1	7.5
A4-3	26	100-285	Cone Face	1140	10.0	9.5
A5-2	33	75-110 300-350	Shoulder Shoulder	1110 1210	9.2 10.0	8.5 9.4
B1-1	33	125-200 260-330	Shoulder Shoulder	892 1030	8.2 9.5	7.6 8.8
B1-2	35	125-325	Shoulder	965	8.9	8.2
B1-3	32	150-275	Shoulder	985	9.0	8.4
B2-3	56	300-350	Shoulder	575	8.7	7.9
B3-3	26	70 190 210-350	Shoulder Shoulder Shoulder	930 1020 1050	7.9 8.7 9.0	7.1 7.9 8.2
C1-1	29	100-280 410-480	Shoulder Shoulder	630 630	7.5 7.5	7.2 7.2
C1-2	31	200-360	Shoulder	605	7.2	6.9
C2-1	25	190-450 305-440 265-520 240-495	Cone face Shoulder Mid-sleeve Shaft	853 730 580 470	9.8 8.4 6.7 5.4	8.9 7.5 5.7 4.5

**TABLE 4.8a SUMMARIZED PENETROMETER PORE PRESSURE DATA FOR LOWER VELOCITY TESTS.**

Test No.	Rate (mm/s)	Sensor Location	w/c (%)	$C_{ui}$ (kPa)	$\Delta u$ (kPa)	$\frac{\Delta u}{C_{ui}}$
SC10	20	Cone face and tip	43.0	106	825	7.8
SC12	20		40.7	146	1100	7.5
SC15	20		44.2	90	850	9.4
SC17	20		50.2	40	390	9.8
SC18	20		45.8	73	670	9.2

**TABLE 4.8b SUMMARIZED PIEZOPROBE DATA FOR SMALL SCALE TESTS**

#### 4.6 Dissipation of pore pressures

Data obtained from the piezometric elements of the penetrometers after completion of the penetration stage of testing is shown on Figures 4.33 to 4.41. During the dissipation stage the penetrometers were held rigid with hydraulic pressure on the ram. Some tests dissipated to the original hydrostatic pore pressure while others dissipated to a slightly elevated final pore pressure. This was due to no drainage being permitted from the cake in the latter tests while drainage was provided from both faces for the remainder. The drainage conditions are shown in Table 4.9. The tests which had free drainage conditions at the lower cake filter showed the pore pressures dissipating to the original hydrostatic values. Where drainage was not permitted the final pore

Test No.	Drainage	Test No.	Drainage
A3-1	None	B2-1	Base
A3-2	None	B2-2	Base
A4-1	None	B2-3	Base
A4-2	None	B3-1	Base & Top
A4-3	None	B3-2	None
A5-1	Base & Top	B3-3	None
A5-2	None	C1-1	Base & Top
A5-3	None	C1-2	Base & Top
B1-1	None	C1-3	Base & Top
B1-2	None	C1-4	Base & Top
B1-3	None	C2-1	None
		C2-2	None

**TABLE 4.9 DRAINAGE CONDITIONS FOR CLAY CAKES DURING AND AFTER PENETRATION**

pressure was typically 60 kPa above hydrostatic. However when the normalised excess pore pressure ( $U$ ) is plotted against logarithm of time no difference between the two drainage conditions can be detected.

It may be noted that the normalized excess pore pressure is defined by:

$$U = \frac{\Delta u}{\Delta u_i} = \frac{u - u_f}{u_i - u_f}$$

where  $u$  = pore pressure

$u_f$  = final pore pressure

$u_i$  = pore pressure at start of dissipation

Comparing the results of the dissipation analysis on each cake shows that very similar behaviour was observed at each location. The normalized data from all the tests has been plotted on Fig. 4.42. Despite the wide range of consolidation pressures and tank sizes the data from the shoulder of the  $1\text{cm}^2$  penetrometer are fairly similar.

The tip dissipation is up to twice as rapid as that from the shoulder. The dissipation times at the cone face and shoulder locations for the  $1\text{cm}^2$  penetrometer were between five and ten times faster than those of the  $5\text{cm}^2$  device. Radial or spherical dissipation theories suggest that the rate is dependent on the square of the cone radius and thus the larger penetrometer would be expected to take five times as long to reach any given degree of dissipation.

Of the methods proposed for the evaluation of the horizontal coefficient of consolidation ( $c_h$ ) from PCPT dissipation data, those due to Baligh and Levadoux (1980) and Torstensson (1979) are most widely used. The Baligh and Levadoux method has two advantages over that due to Torstensson. Baligh and Levadoux predict the dissipation behaviour for a

range of locations on the penetrometer surface. In addition this method is not dependent on a value of  $(G/c_u)$ . This parameter is difficult to select due to its strong variation with strain level.

The value of  $c_{h(\text{probe})}$  may be simply obtained by matching the non dimensionalized graph of  $U$  vs  $\log T$  (Fig. 1.16) to the experimental graph of  $U$  vs  $\log t$ .

As

$$T = (c_{h[\text{probe}]} t) / R^2$$

$$\log T = \log t - \log (c_{h(\text{probe})} / R^2)$$

$$\text{or, } \log (c_{h[\text{probe}]} / R^2) = \log t - \log T$$

Thus the displacement in the  $x$  direction required to match the curves represents the logarithm of  $(c_{h[\text{probe}]} / R^2)$ .

Using this method the following values of  $c_{h(\text{probe})}$  were obtained:

$$\begin{array}{l} 1\text{cm}^2 \text{ penetrometer } c_{h(\text{probe})} = 0.09 \text{ cm}^2/\text{sec} \\ 5\text{cm}^2 \text{ penetrometer } c_{h(\text{probe})} = 0.07 \text{ cm}^2/\text{sec} \end{array}$$



This value of  $c_h$  is applicable to the soil in an overconsolidated state according to Baligh and Levadoux. In order to obtain  $c_h$  for the normally consolidated soil the following correction is required:

$$c_{h(N/C)} = c_{h(\text{probe})} \times \frac{C_s}{C_c}$$

Restricted flow consolidation tests have been performed on horizontally and vertically cut samples to determine the ratio of  $C_c/C_s$  (Fig. 4.43). The horizontal and vertical samples gave similar results with  $C_c/C_s$  lying between 12.5 and 16.8 where  $C_c$  and  $C_s$  have been taken as tangent to the curves at the maximum effective stress applied. The calculated value of  $c_h$  is thus  $7 \times 10^{-3}$  to  $4 \times 10^{-3}$   $\text{cm}^2/\text{sec}$  with a mean value of  $5 \times 10^{-3}$   $\text{cm}^2/\text{sec}$ .

The value of  $c_v$  will not generally be the same as that of  $c_h$  the relationship being approximated by:

$$c_v = c_h \frac{k_v}{k_h}$$

where  $k_v$  = vertical permeability

and  $k_h$  = horizontal permeability

This assumes  $m_v$  equals  $m_h$ . The oedometer data from the horizontal and vertical samples suggests that  $k_h/k_v$  may be taken as unity. Hence the calculated value of  $c_v$  from the dissipation data is  $5 \times 10^{-3}$   $\text{cm}^2/\text{sec}$ .

The value of  $c_v$  has been independently calculated from the consolidation stages of the CIU triaxial tests shown on Figure 4.44. The method of analysis proposed by Bishop and Henkel (1962a) has been used in which

$$t_{100} = \frac{\pi h^2}{c_v} \quad \text{for single ended drainage}$$

where  $t_{100}$  = projected time to full consolidation on a root time vs volume change graph

$2h$  = sample height

This analysis produced the following range of values for  $c_v$  (Table 4.10):

Test no.	h (mm)	$t_{100}$ (min)	$c_v$	
			( $\text{mm}^2/\text{min}$ )	( $\text{cm}^2/\text{sec}$ )
A3a	39.6	102	48	$8.0 \times 10^{-3}$
A3b	38.1	100	46	$7.6 \times 10^{-3}$
A3c	38.2	154	30	$5.0 \times 10^{-3}$
C2a	37.4	142	31	$5.2 \times 10^{-3}$
C2b	37.6	121	37	$6.1 \times 10^{-3}$
C2c	38.0	137	33	$5.5 \times 10^{-3}$

**TABLE 4.10 VERTICAL COEFFICIENT OF CONSOLIDATION FROM CIU TRIAXIAL TESTS.**

The range of  $c_v$  from the triaxial tests agrees well with that calculated from the penetrometer dissipation data and thereby lends considerable confidence to this form of analysis for normally consolidated clay.

#### 4.7 Rate Effects

In order to study the effects of rate of penetration on the cone resistance and pore pressure data a number of tests were performed at higher rates. Due to various logging problems these were not all successfully recorded. The data obtained from tests at rates in excess of 50mm/s is shown in Tables 4.11 and 4.12. The definitions of  $N_{kt}$ ,  $N_{kt}^*$ ,  $N_{\Delta u}$  and  $N_{\Delta u}^*$  are the same as in sections 4.4. and 4.5. The calculated in situ shear strength ( $c_{ui}$ ) has been used for the correlations.

Test No.	Rate (mm/s)	Penetration (mm)	$q_n$ (kPa)	$c_{ui}$ (kPa)	$N_{kt}$ (in situ)	$N_{kt}^*$ (in situ)
B2-1	101	100-190	682	66	10.3	9.5
		250-300	717	66	10.9	10.0
B2-2	109	170-330	722	66	10.9	10.1
C1-4	3210	90-185	1225	84	14.6	14.3
		300-500	1243	84	14.8	14.5
C2-2	238	420-860	956	87	11.0	10.0

TABLE 4.11

SUMMARIZED CONE RESISTANCE DATA FOR HIGH VELOCITY TESTS.

The  $N_{kt}^*$  and  $N_{\Delta u}^*$  data have been plotted against the rate of test in Fig. 4.45. From this figure it may be seen that a substantial rise in  $N_{kt}^*$  is indicated for an increase in rate of two orders of magnitude, although only one successful test was carried out at the top penetration rate. If the data from Test C1-4 is typical of the values obtained at this penetration rate an increase in  $N_{kt}^*$  and thus in  $q_n$  of 40% is shown for a hundred fold increase in penetration rate from 20mm/sec. Such an increase is approximately double that expected from general observations of strength increase with rate in triaxial tests. The effect of a tenfold increase in rate on the increase in shear strength is generally quoted as between 5% (e.g. Bishop and Henkel, 1962b) and 10% (Richardson and Whitman, 1963). However data produced by Luger et al (1982) show a 17% increase in cone resistance for each tenfold increase in rate between 10mm/sec and 2m/s. These researchers also used kaolin and although detailed differences exist between their work and the present study the results are clearly similar. It is of interest to note that the rise in  $N_{kt}^*$  is not matched by a similar rise in  $N_{\Delta u}^*$ , as measured on the cone shoulder. The available data suggests a constant  $N_{\Delta u}^*$  at this location on the penetrometer with a value of  $8.25 \pm 1.0$ .

Test No.	Rate (mm/s)	Penetration (mm)	Sensor Location	$\Delta u$ (kPa)	$c_{ui}$ (kPa)	$N_{\Delta u}$ (in-situ)	$N_{\Delta u}^*$ (in-situ)
B2-1	101	100 - 175	Shoulder	550	66	8.3	7.5
		250 - 340		570	66	8.6	7.8
B2-2	109	150 - 240	Shoulder	550	66	8.3	7.5
		250 - 350		585	66	8.9	8.0
C1-4	3210	80 - 190	Shoulder	690	84	8.2	7.9
		300 - 400		730	84	8.7	8.4
		400 - 555		725	84	8.6	8.3
C2-2	238	420 - 660	Cone Face	770	87	8.9	7.9
			Shoulder	655	87	7.5	6.6

**TABLE 4.12 SUMMARIZED PORE PRESSURE DATA FOR HIGH VELOCITY TESTS**

If values of  $N_{kt}$  and  $N_{\Delta u}$  are considered with varying penetration rate the same trends emerge as noted for the corrected factors. The magnitude of the uncorrected factors is naturally somewhat greater than the corrected versions.

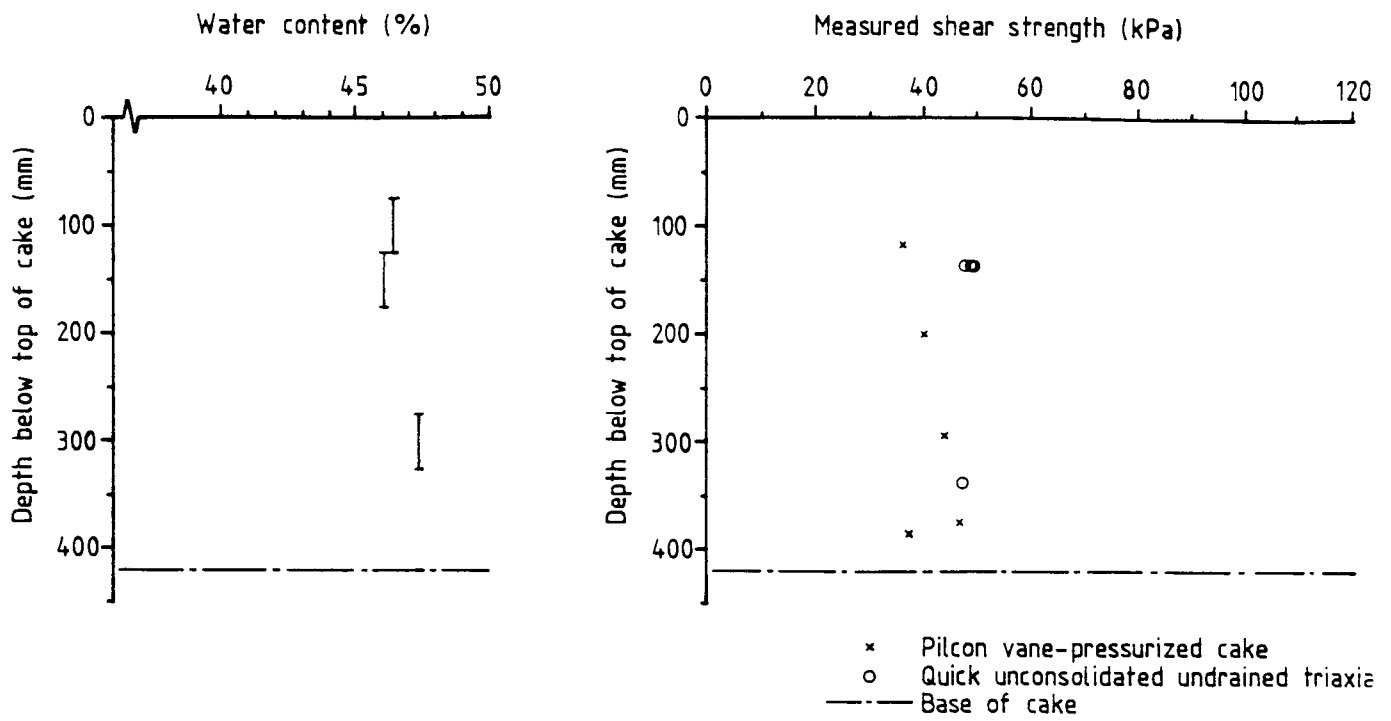


FIGURE 4.1 MEASURED STRENGTH & WATER CONTENT – CAKE A3

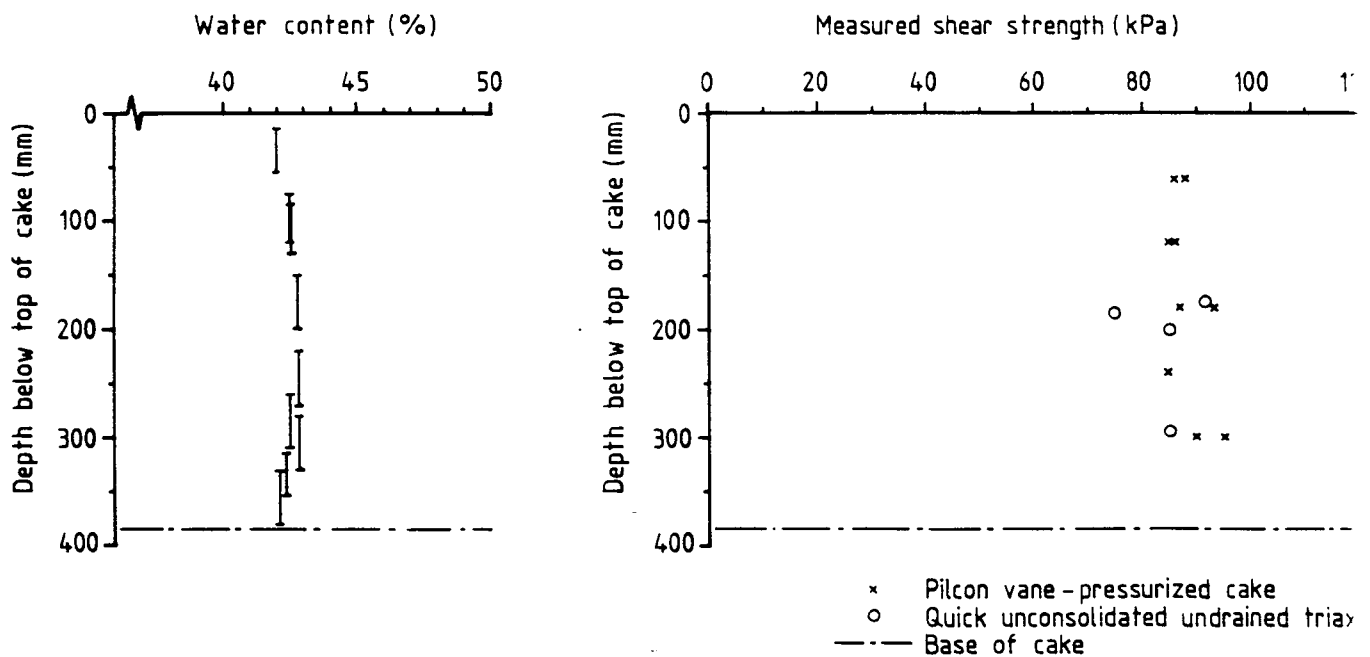


FIGURE 4.2 MEASURED STRENGTH & WATER CONTENT – CAKE A4

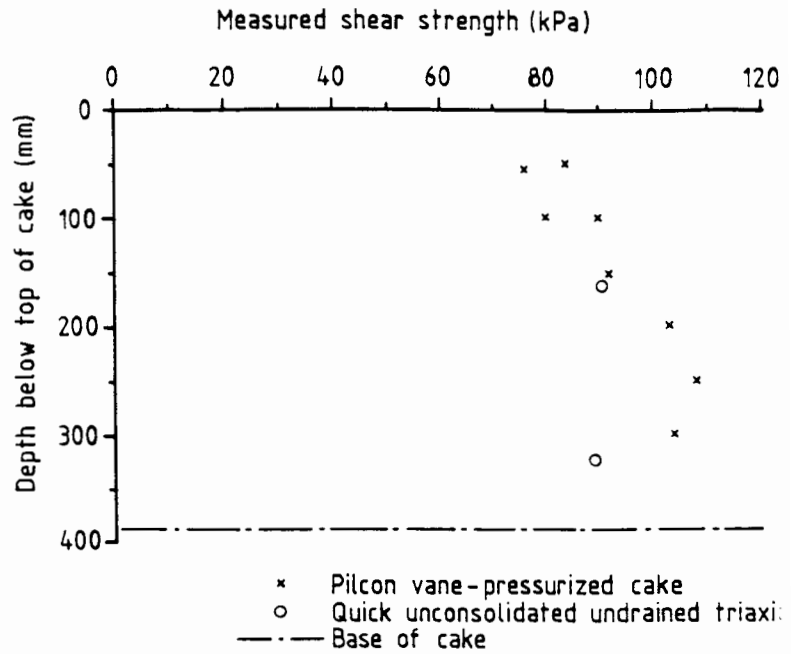
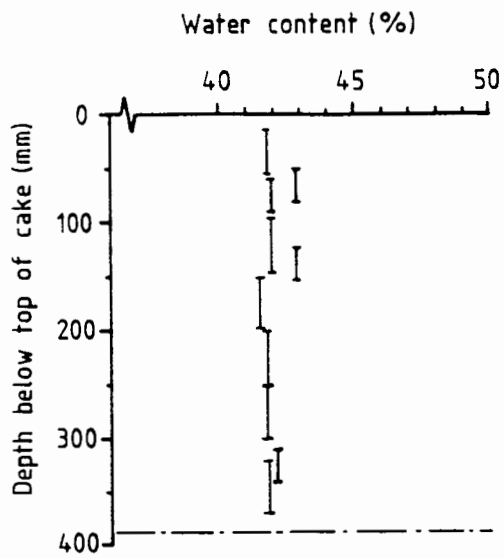


FIGURE 4.3 MEASURED STRENGTH & WATER CONTENT - CAKE A5

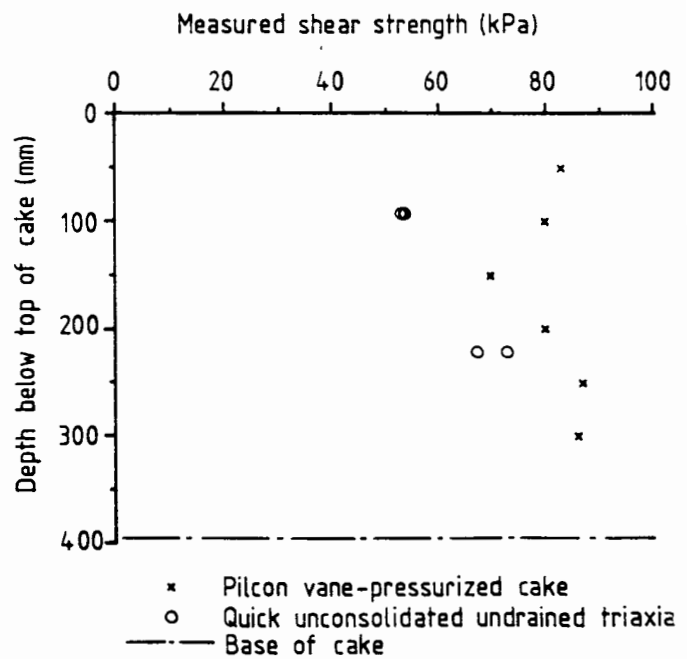
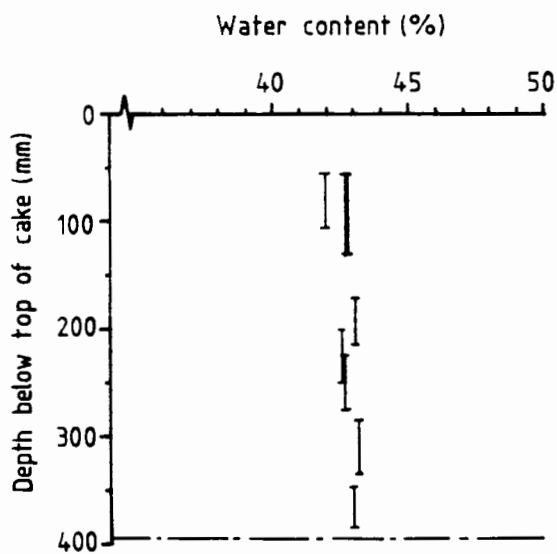


FIGURE 4.4 MEASURED STRENGTH & WATER CONTENT - CAKE B1

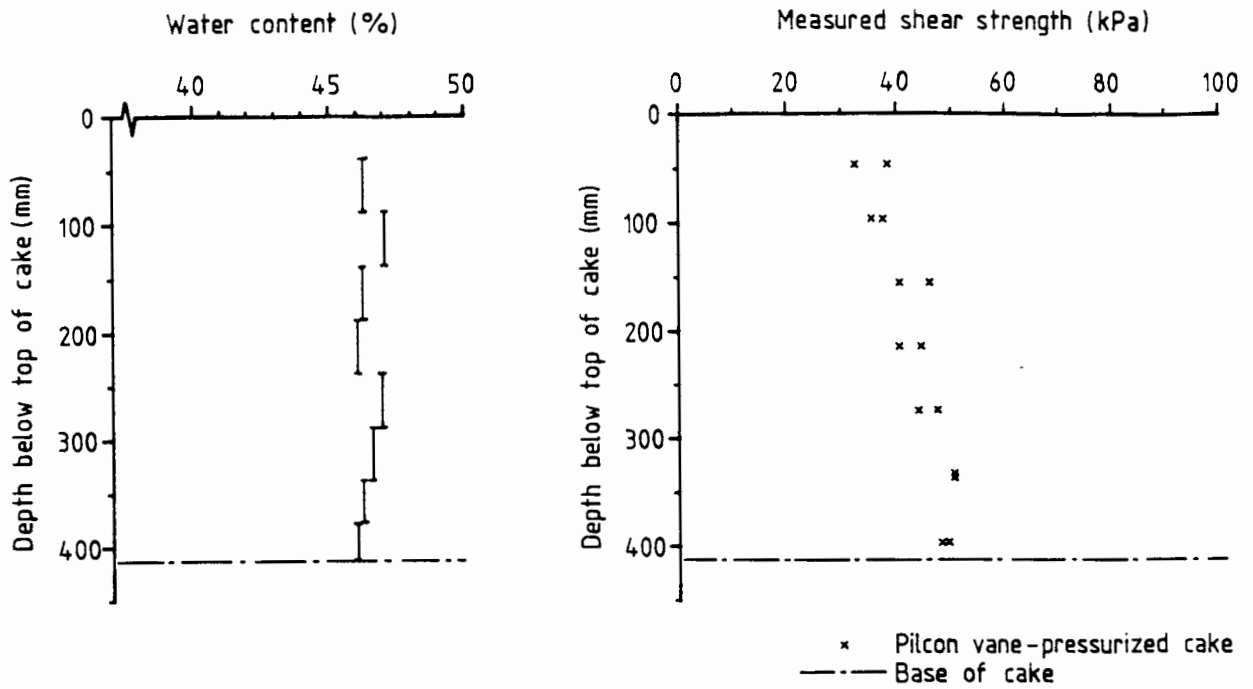


FIGURE 4.5 MEASURED STRENGTH & WATER CONTENT – CAKE B2

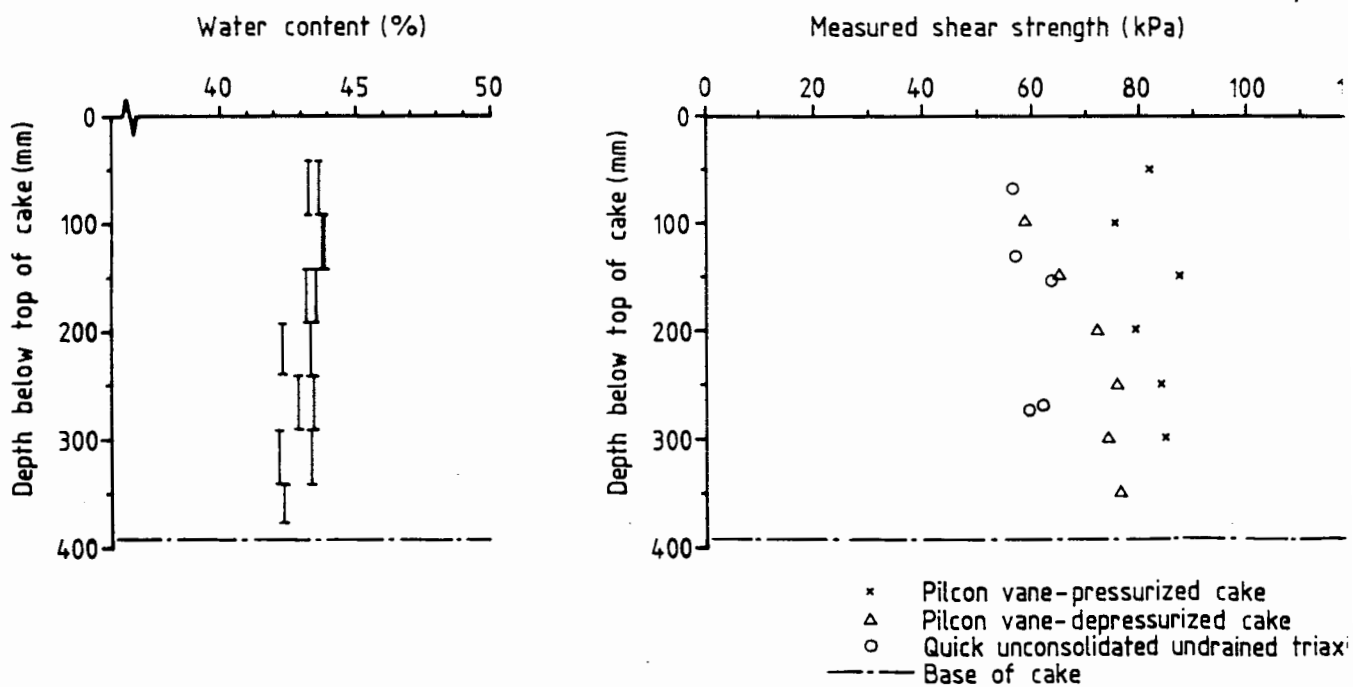


FIGURE 4.6 MEASURED STRENGTH & WATER CONTENT – CAKE B3



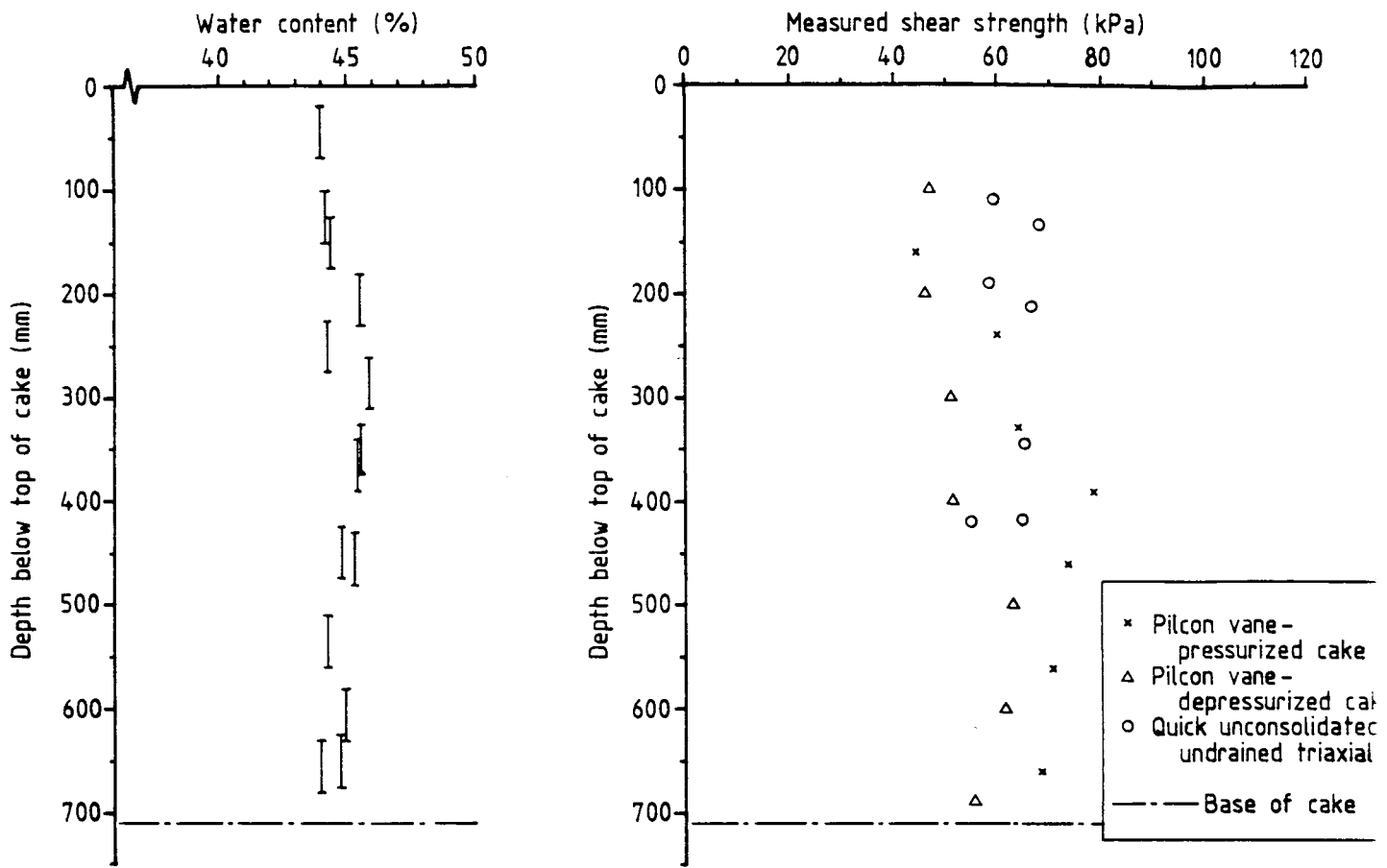


FIGURE 4.7 MEASURED STRENGTH & WATER CONTENT – CAKE C1

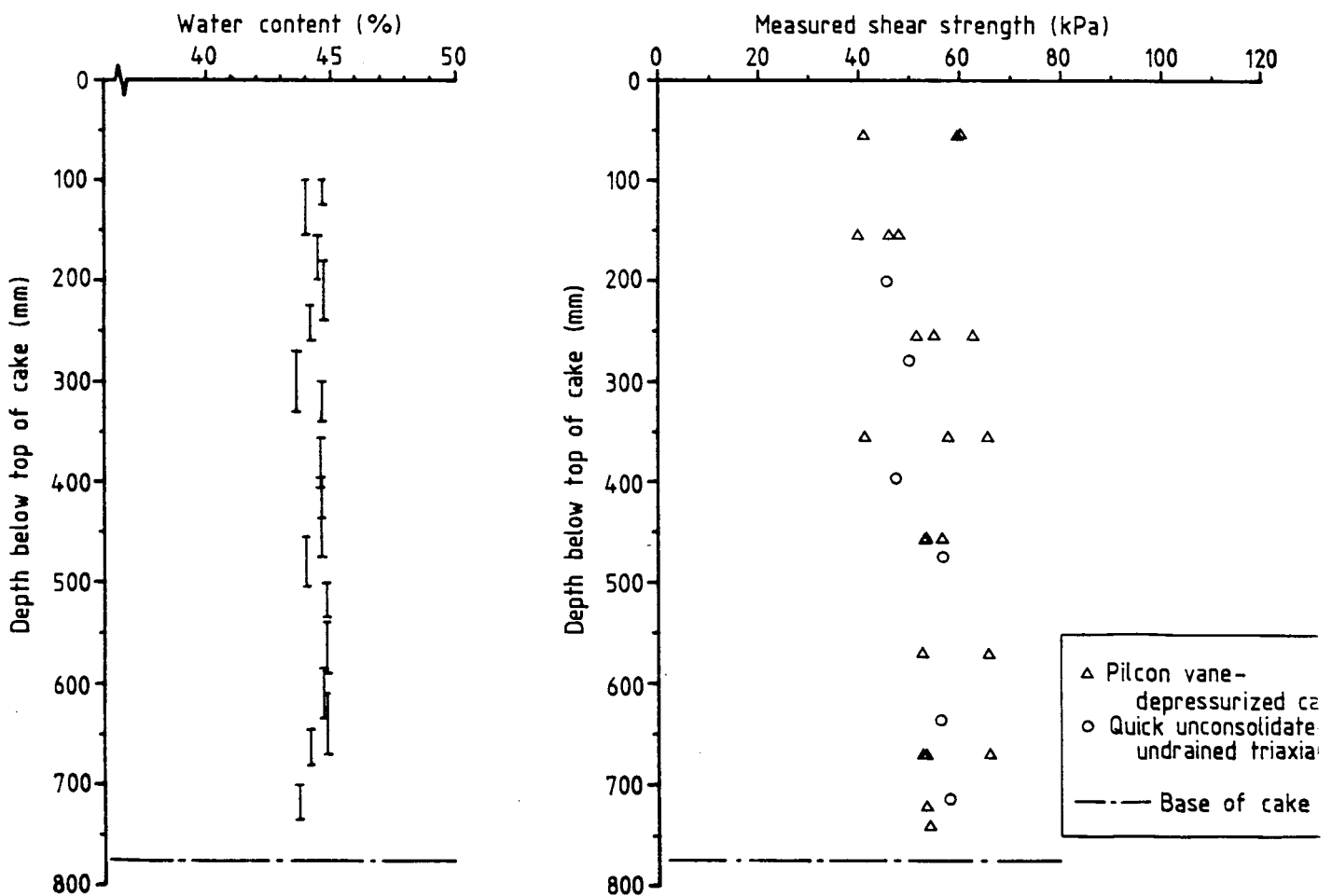


FIGURE 4.8 MEASURED STRENGTH & WATER CONTENT – CAKE C2

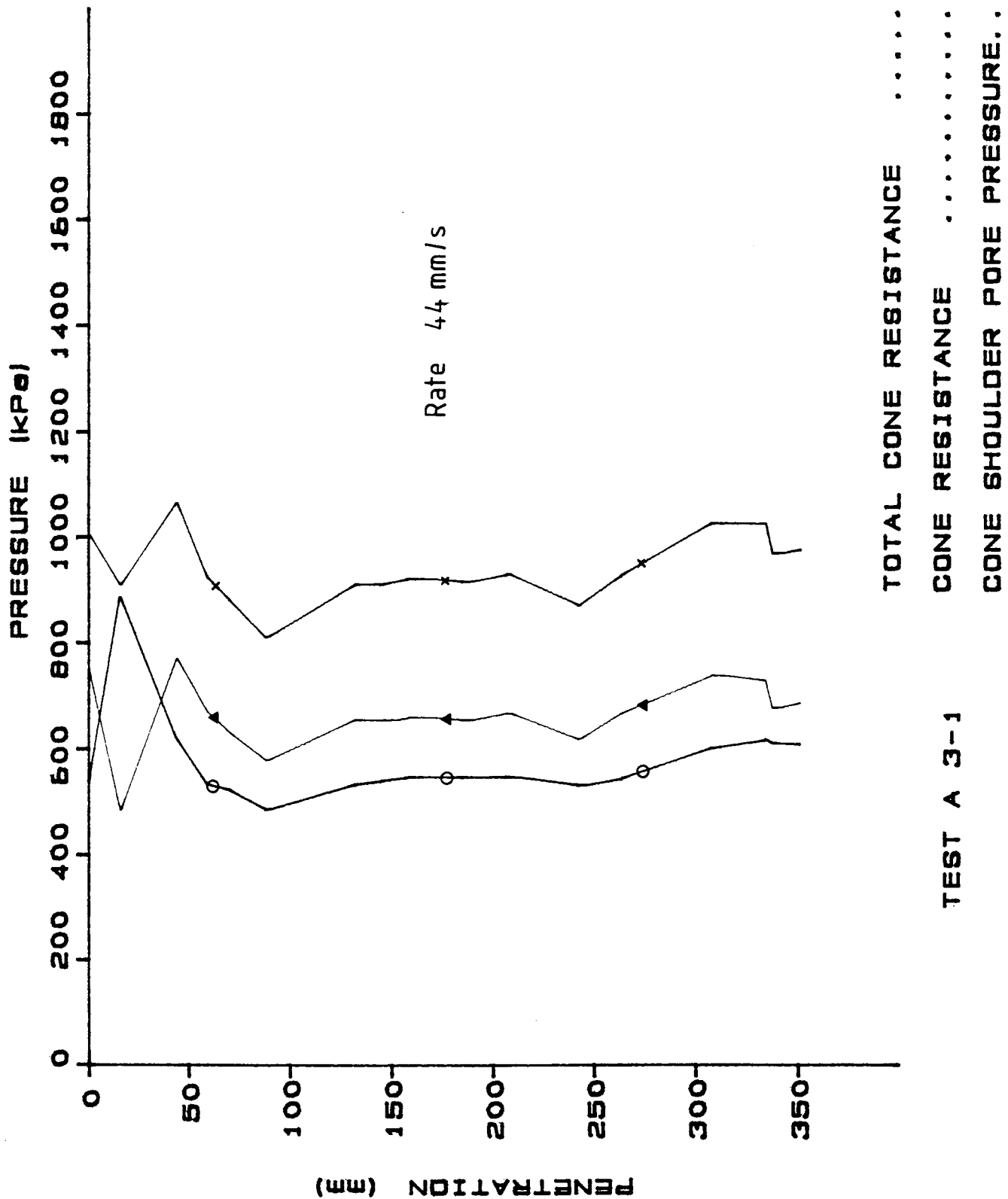
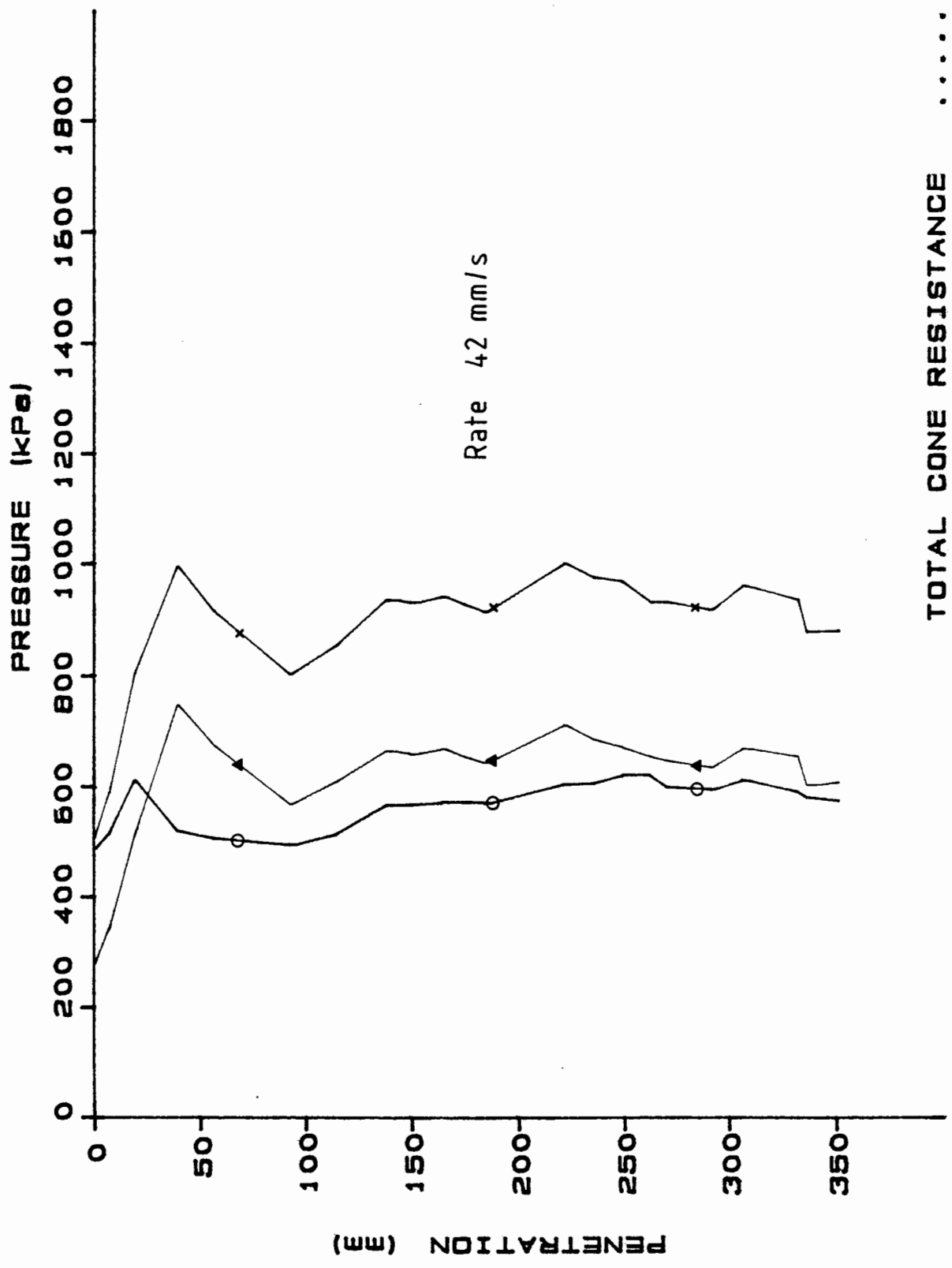


FIGURE 4.9 PENETRATION TEST DATA : TEST A3-1



TOTAL CONE RESISTANCE ..... x  
 CONE RESISTANCE ..... ▲  
 CONE SHOULDER PORE PRESSURE..... ○

TEST A 3-2

FIGURE 4.10 PENETRATION TEST DATA : TEST A3 - 2

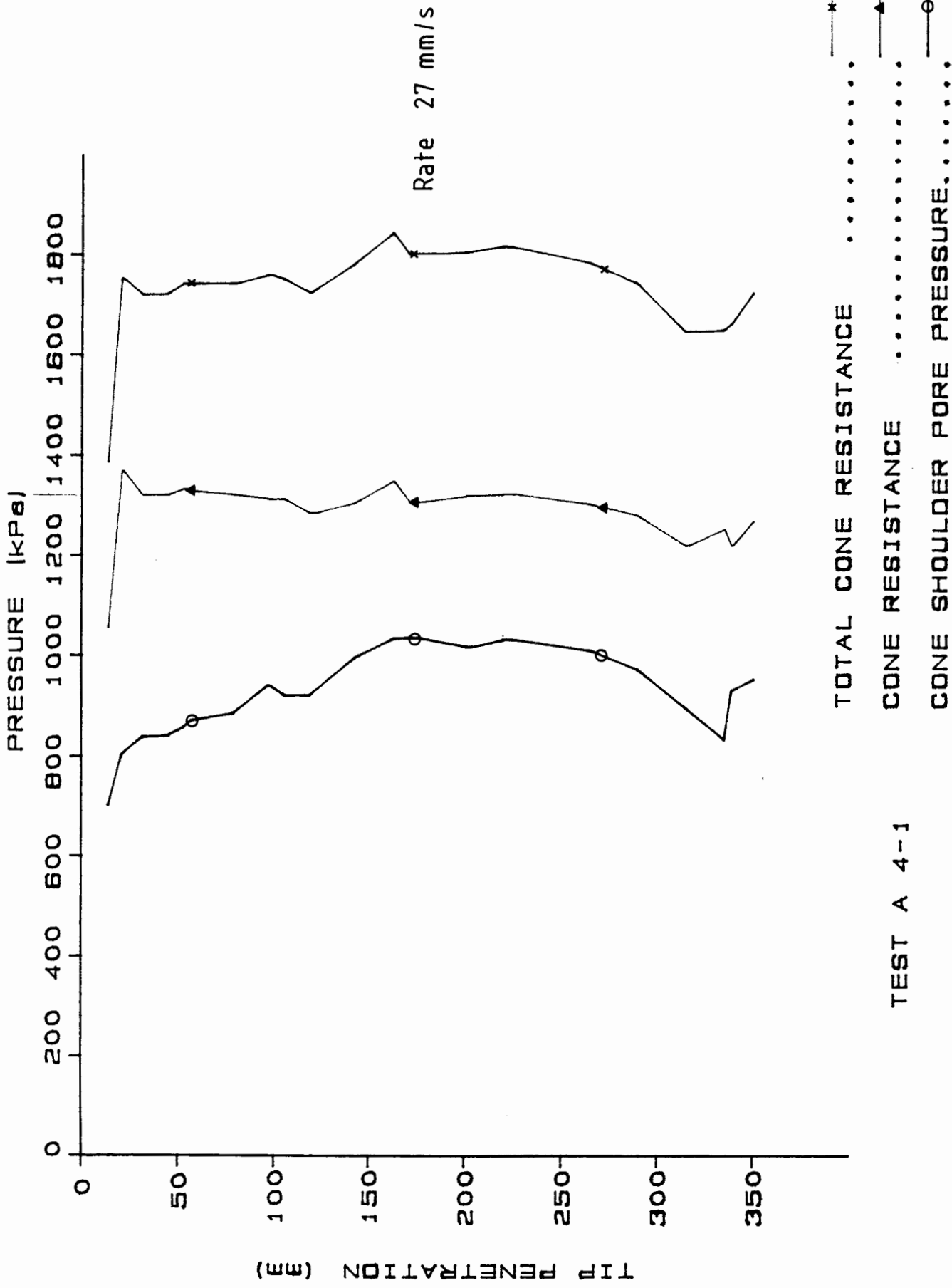


FIGURE 4.11 PENETRATION TEST DATA : TEST A4 - 1

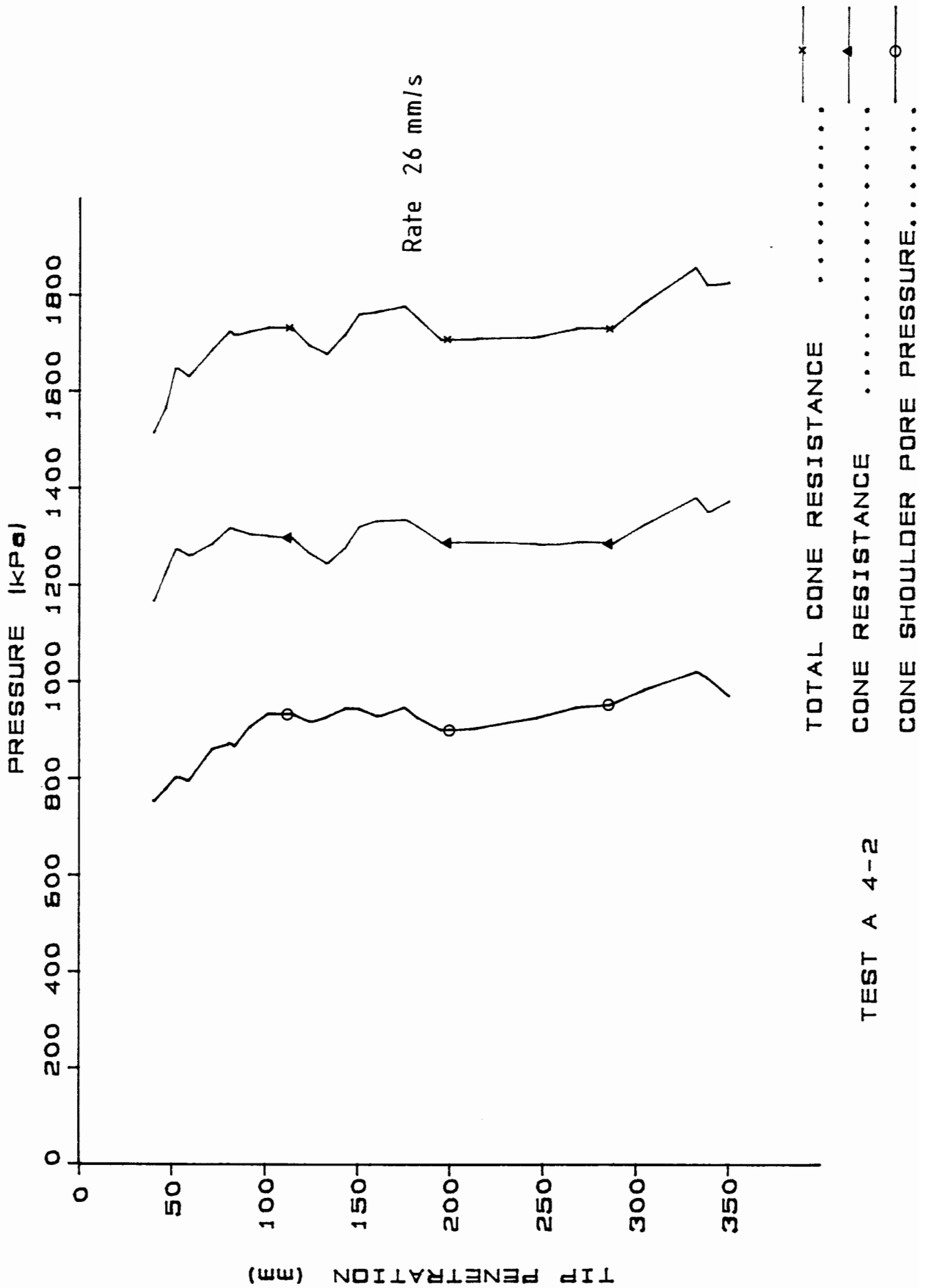


FIGURE 4.12 PENETRATION TEST DATA : TEST A4-2

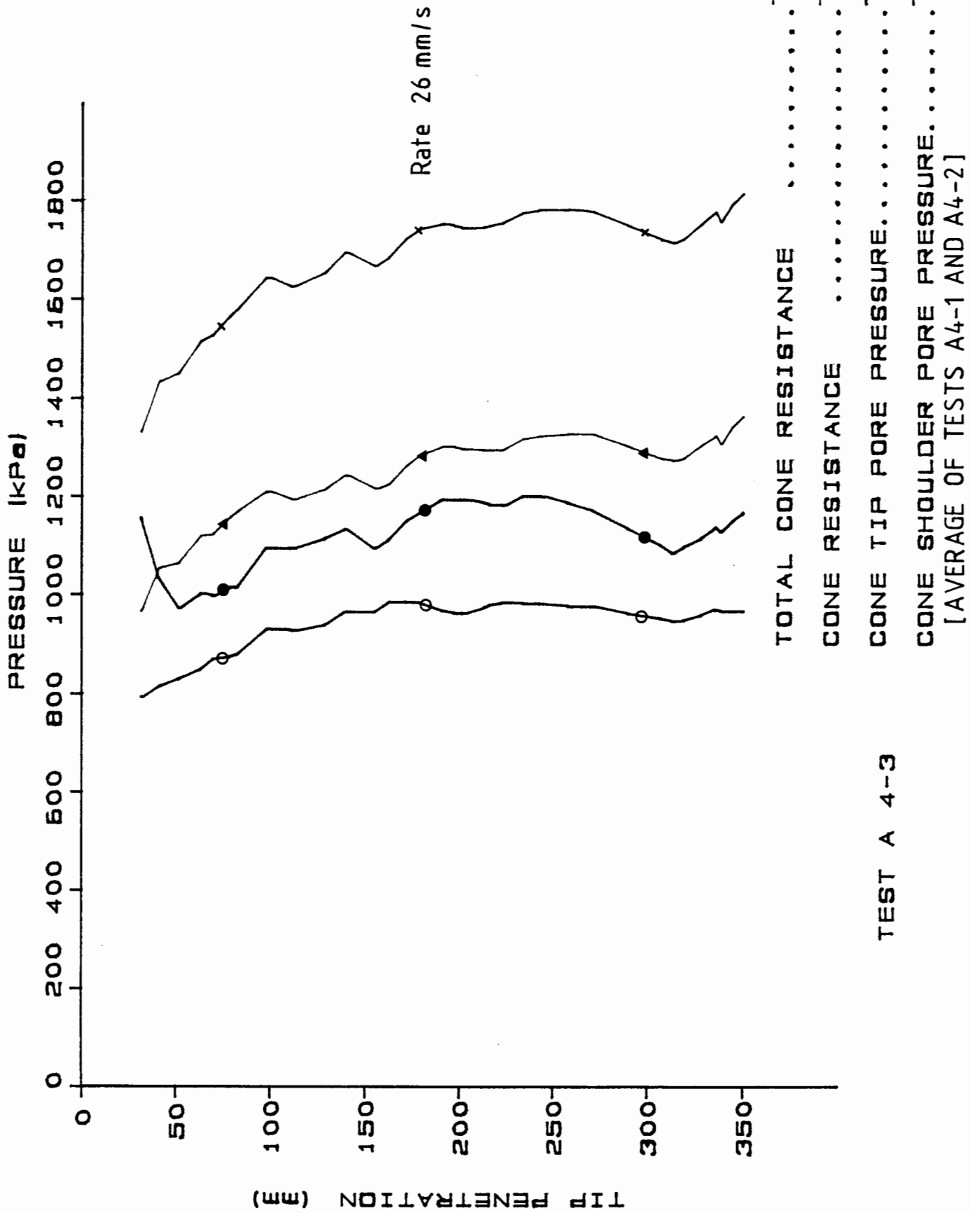
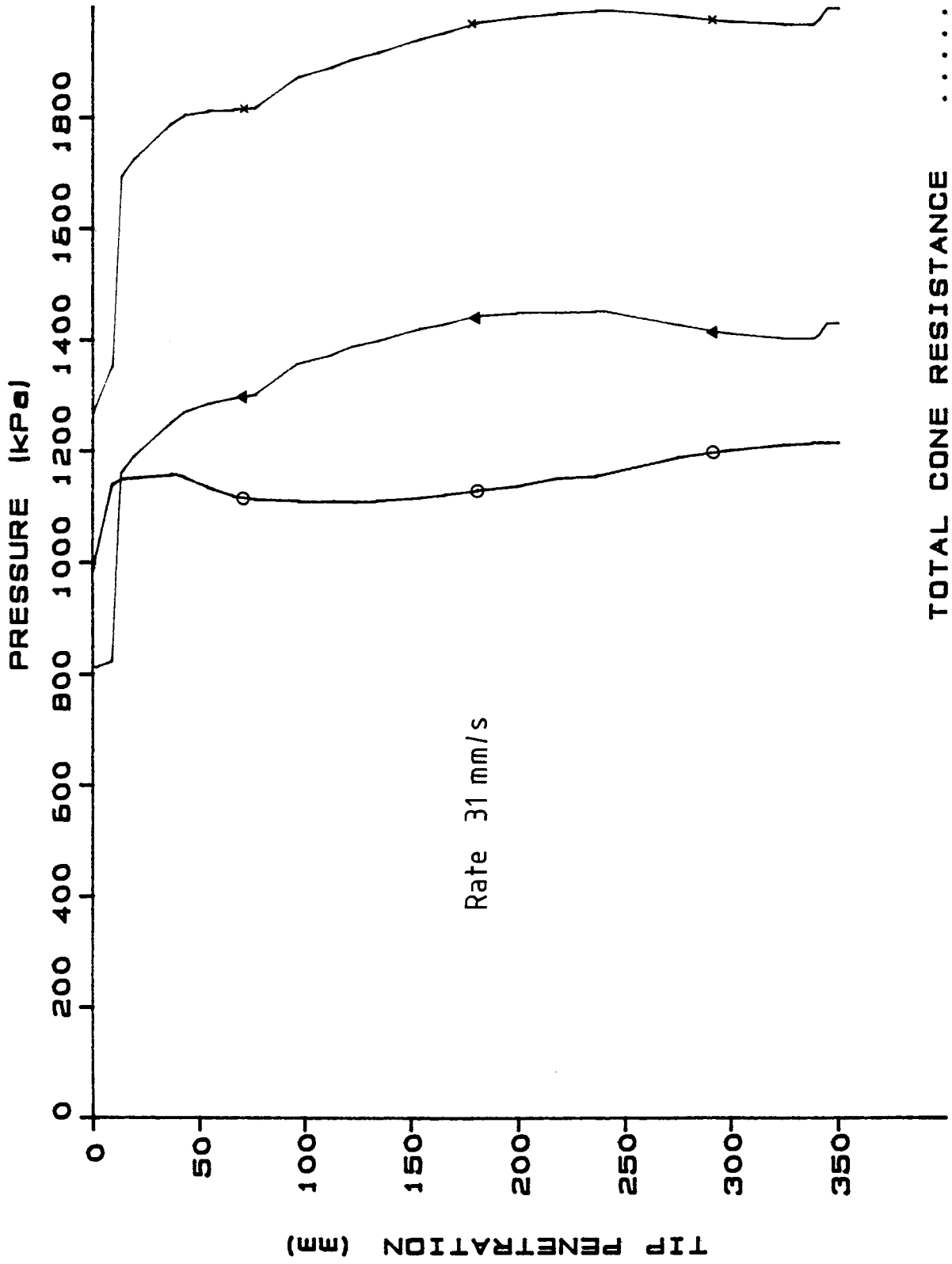


FIGURE 4.13 PENETRATION TEST DATA : TEST A4 - 3



x ..... TOTAL CONE RESISTANCE  
 ▲ ..... CONE RESISTANCE  
 ○ ..... CONE SHOULDER PORE PRESSURE

TEST A 5-1

FIGURE 4.14 PENETRATION TEST DATA : TEST A5 - 1

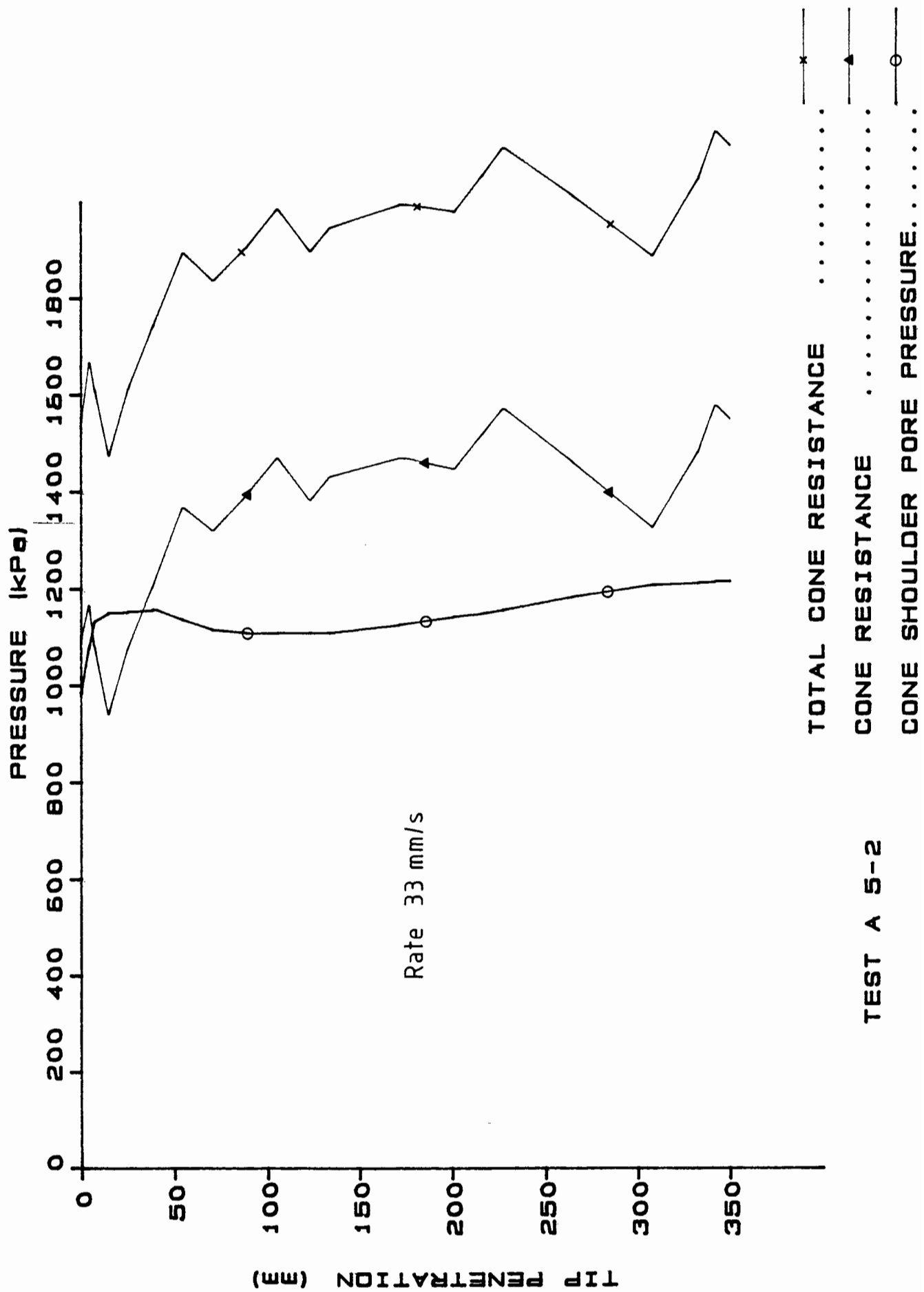


FIGURE 4.15 PENETRATION TEST DATA : TEST A5 - 2



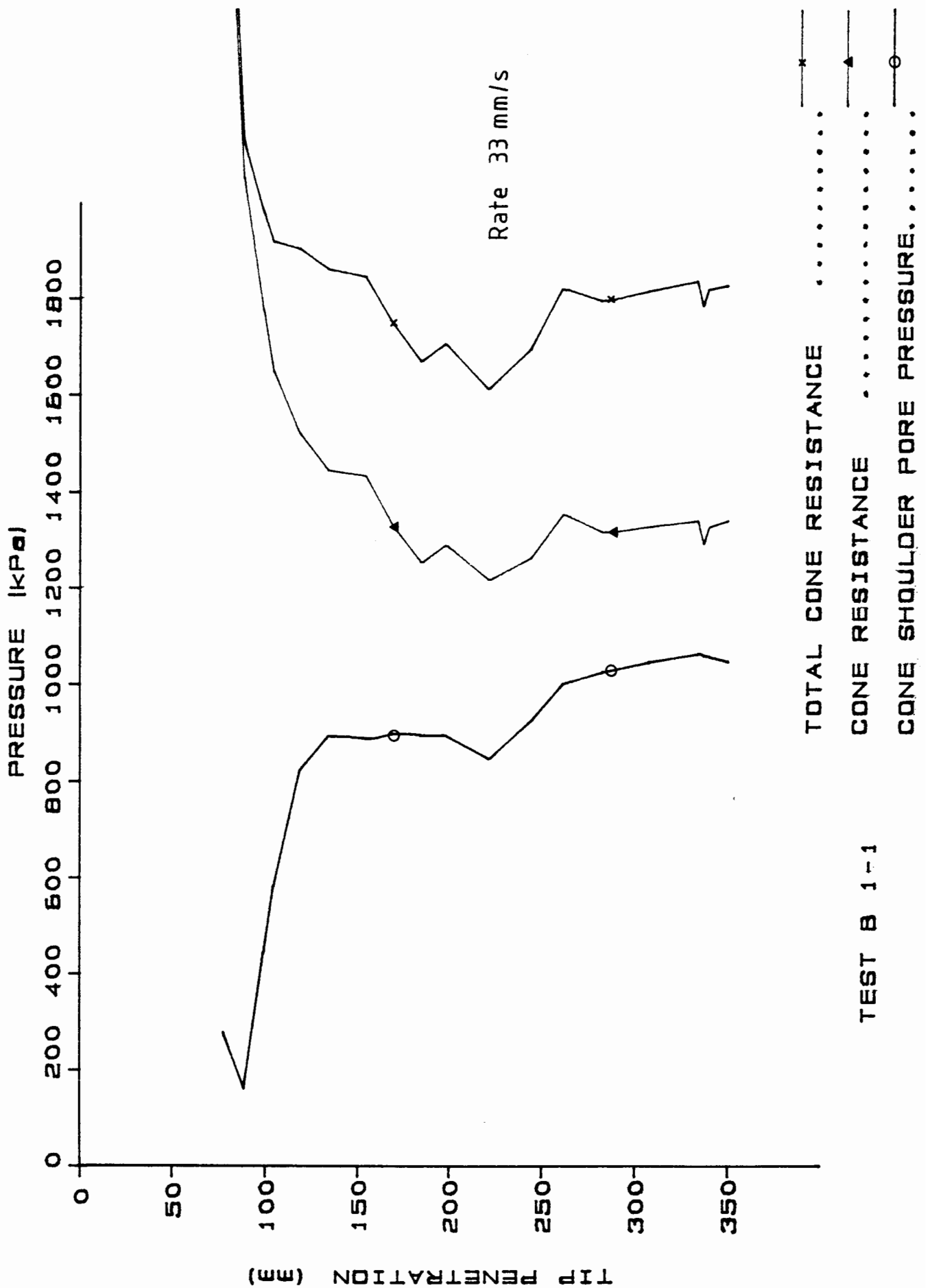


FIGURE 4.16 PENETRATION TEST DATA . TEST B1 - 1

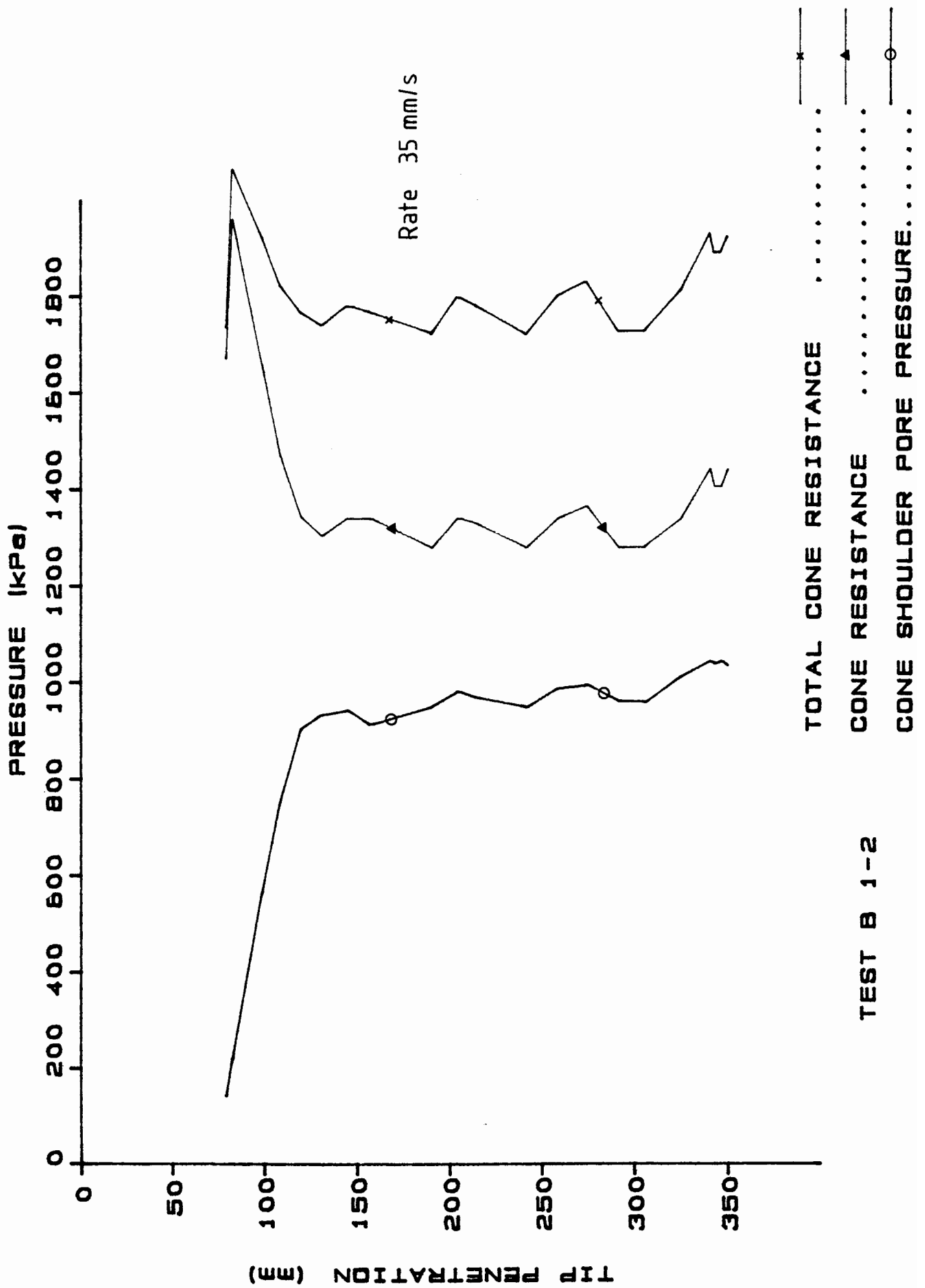


FIGURE 4.17 PENETRATION TEST DATA : TEST B1 - 2

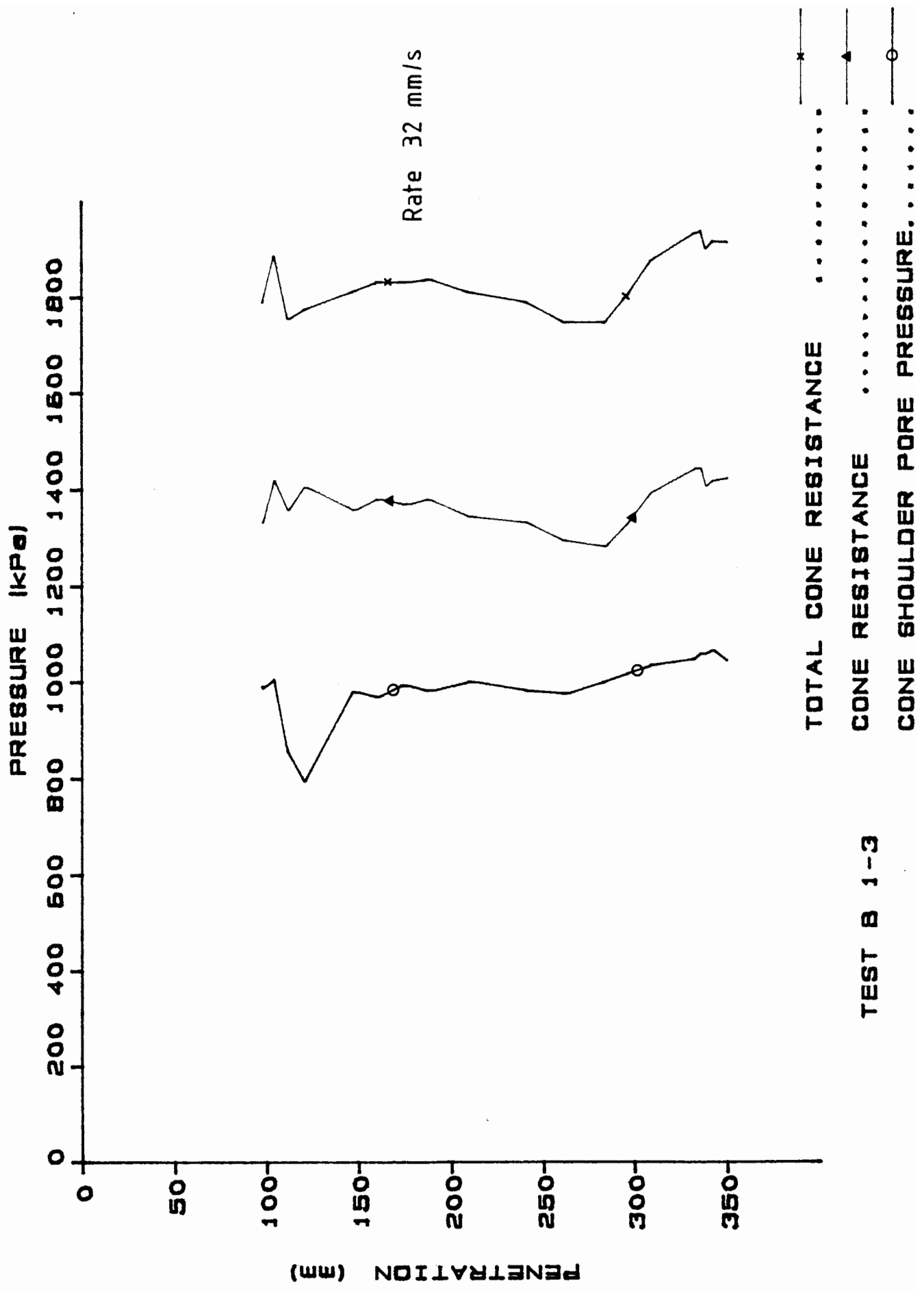


FIGURE 4.18 PENETRATION TEST DATA : TEST B1 - 3

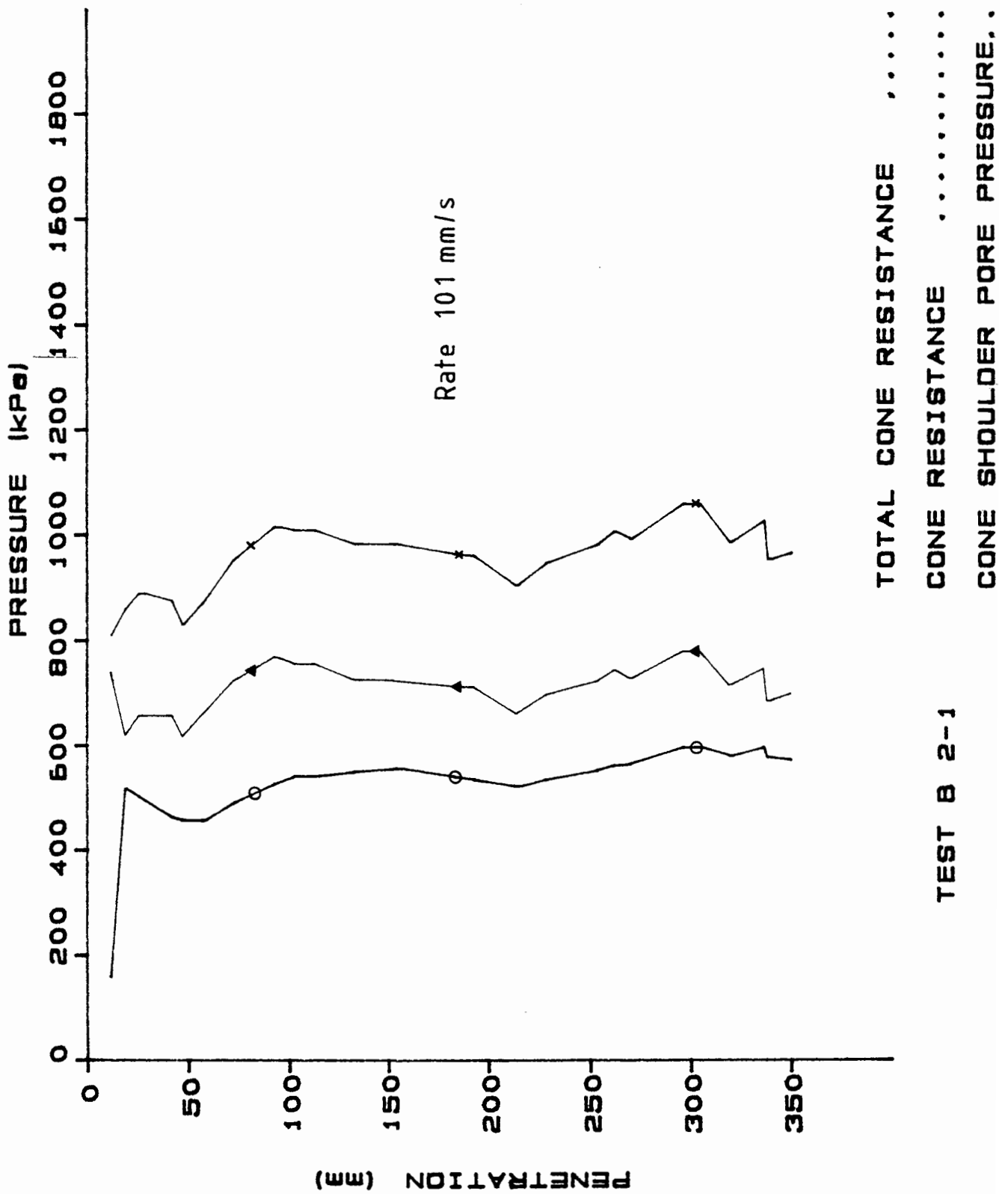


FIGURE 4.19 PENETRATION TEST DATA : TEST B2 - 1

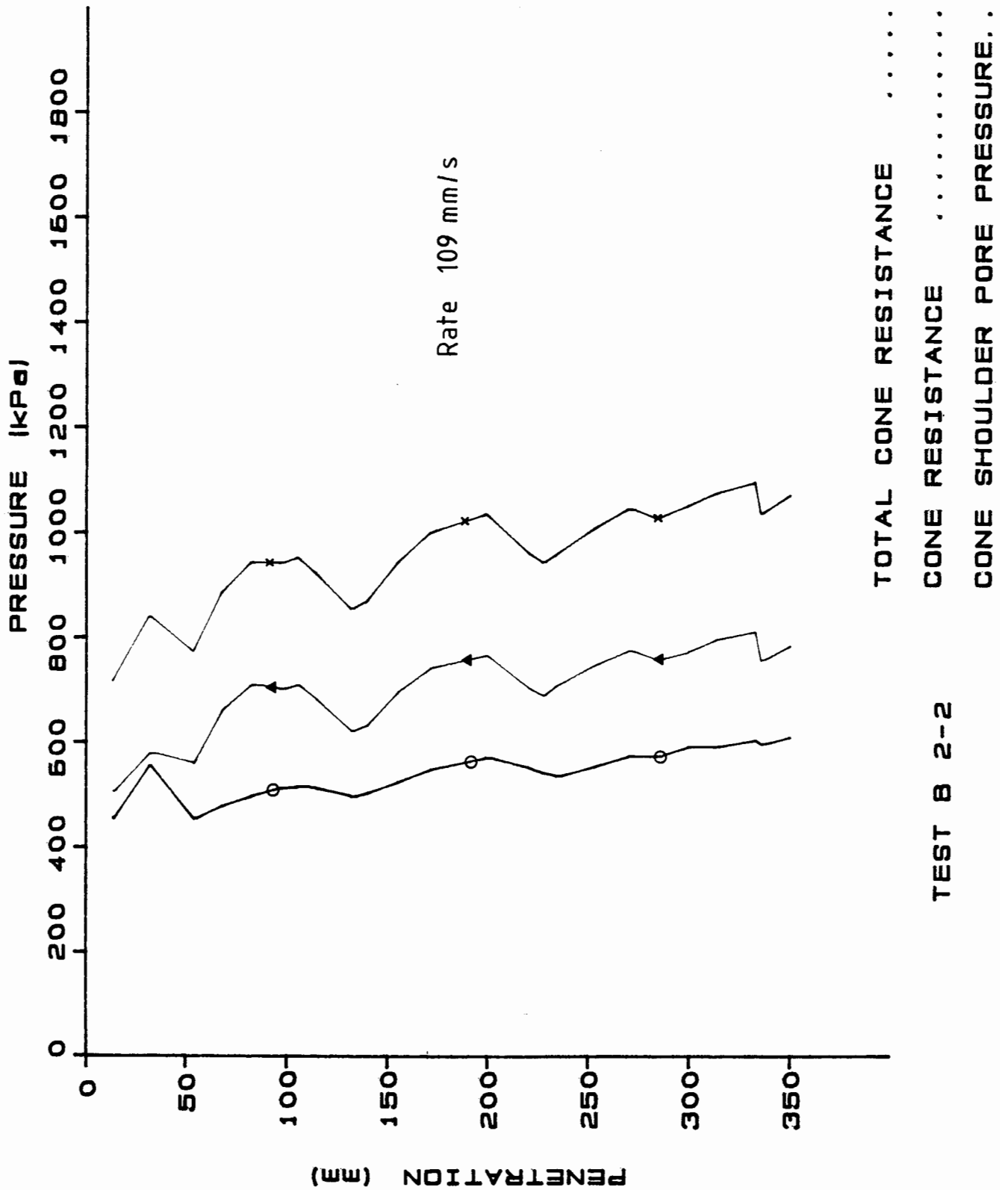


FIGURE 4.20 PENETRATION TEST DATA : TEST B2 - 2

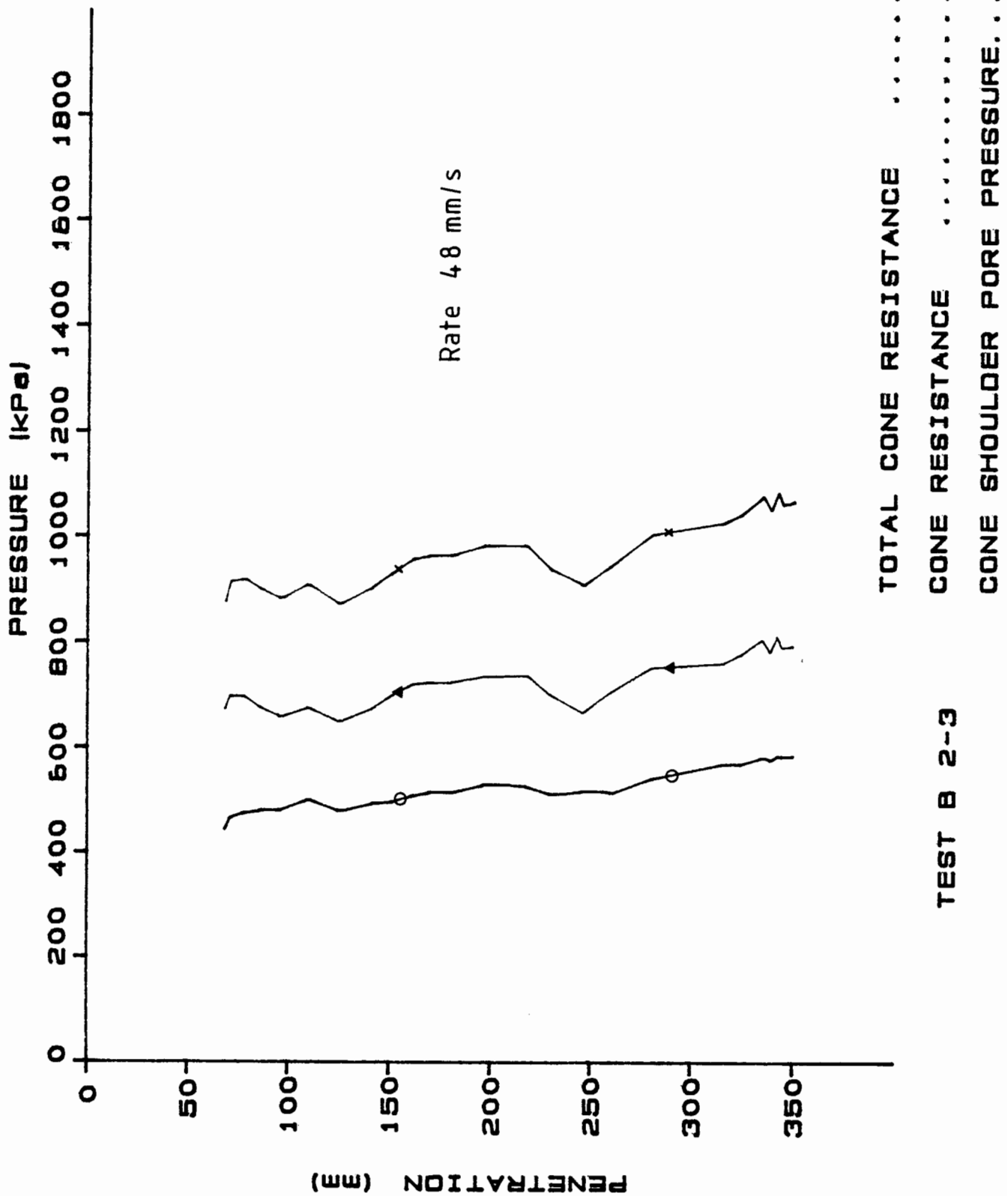


FIGURE 4.21 PENETRATION TEST DATA : TEST B2 - 3

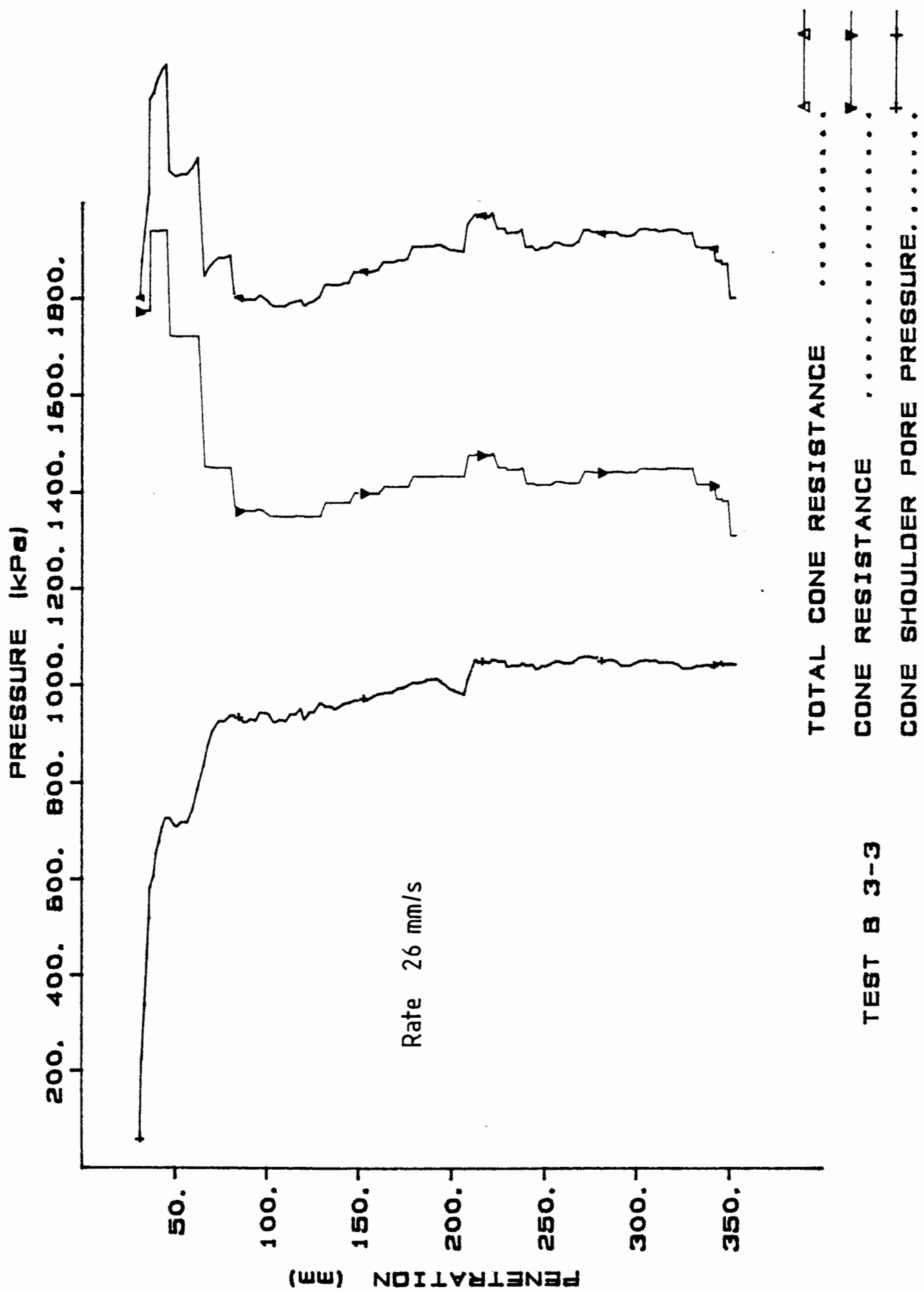


FIGURE 4.22 PENETRATION TEST DATA : TEST B3 - 3

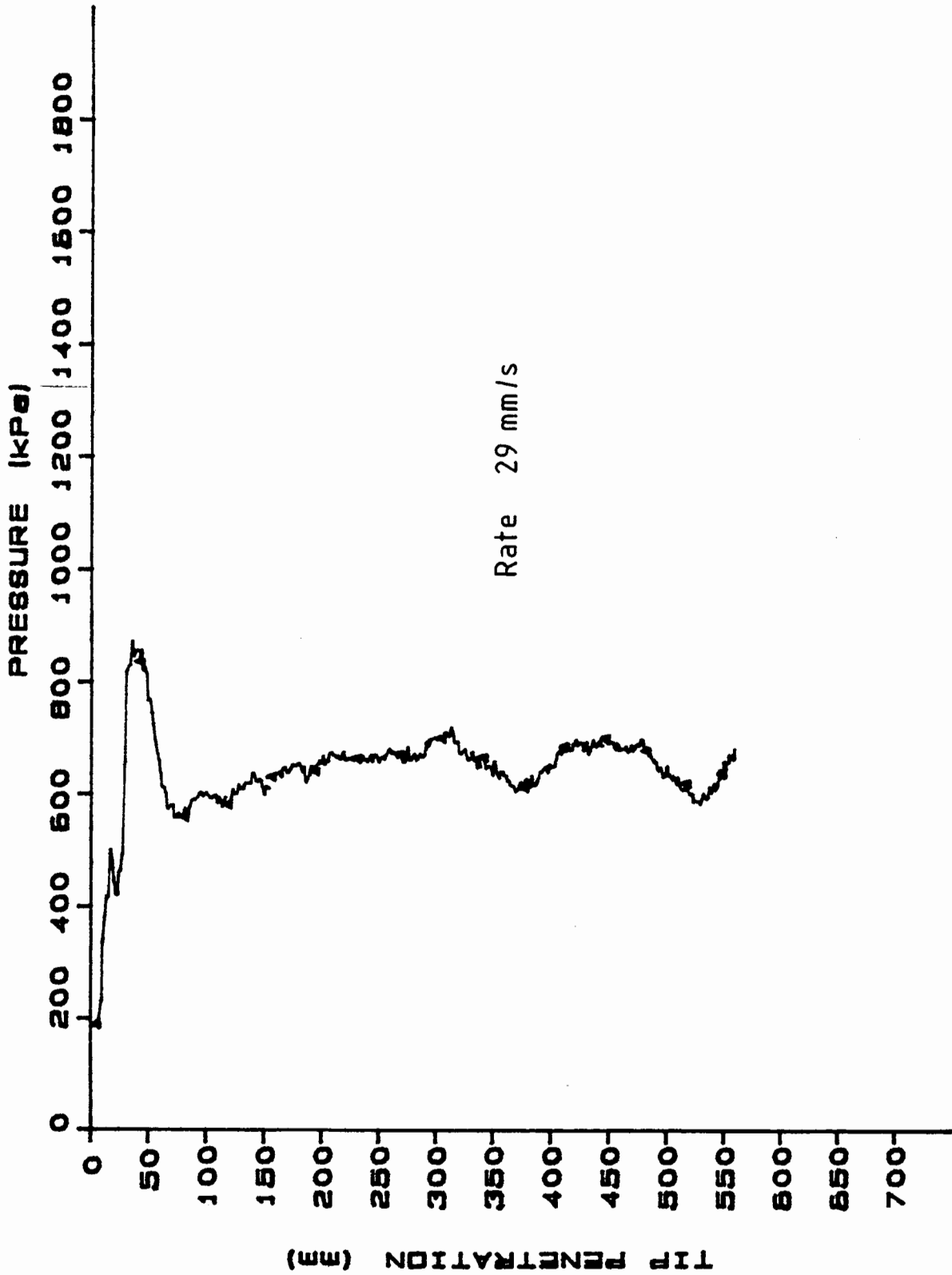
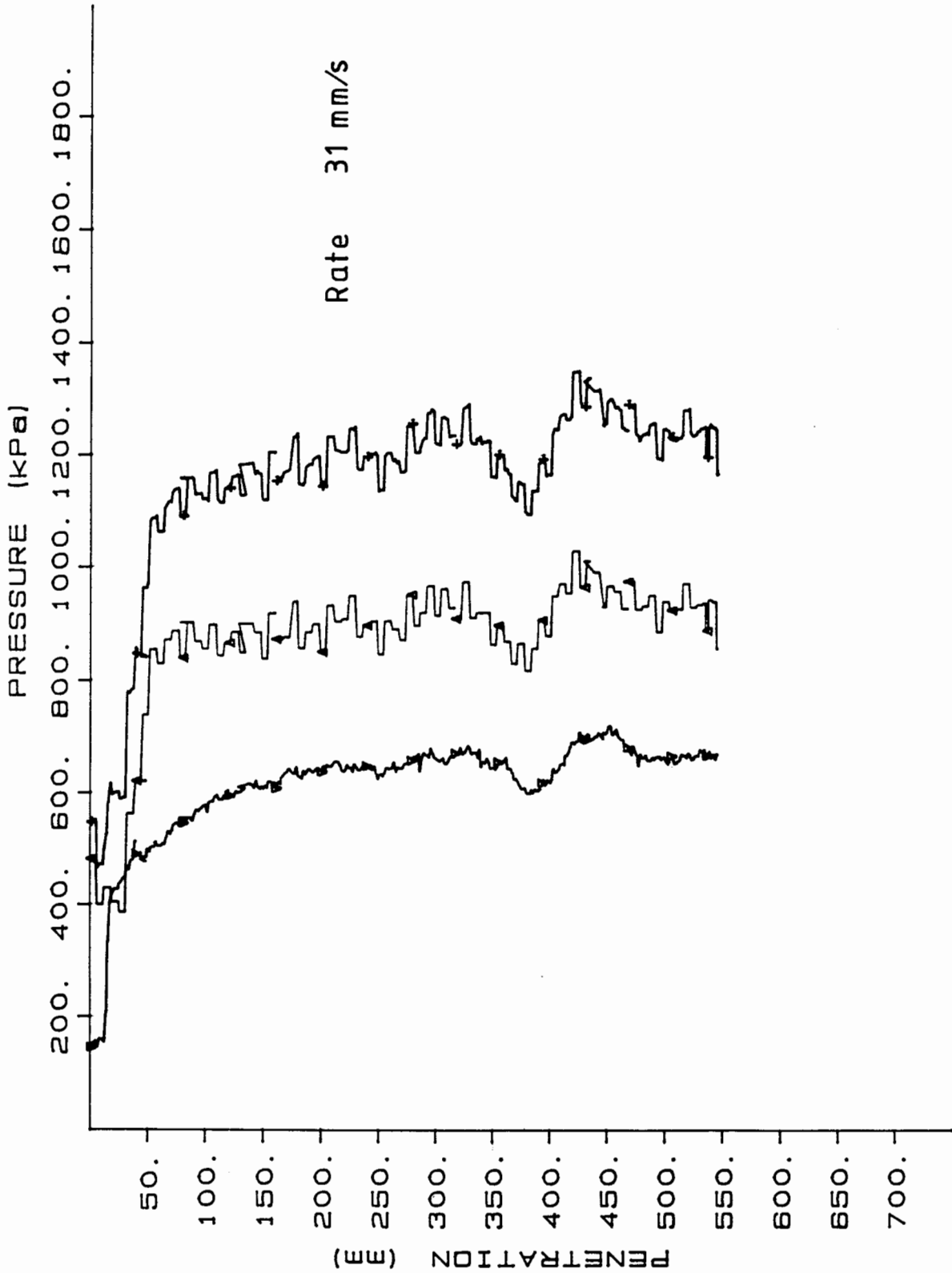


FIGURE 4.23 PENETRATION TEST DATA : TEST C1 - 1

TEST C 1-1

CONE SHOULDER PORE PRESSURE.....A





CONE RESISTANCE ..... ▲  
 CONE SHOULDER PORE PRESSURE..... ▼  
 TOTAL CONE RESISTANCE ..... †

TEST C 1-2

FIGURE 4.24 PENETRATION TEST DATA : TEST C1 - 2

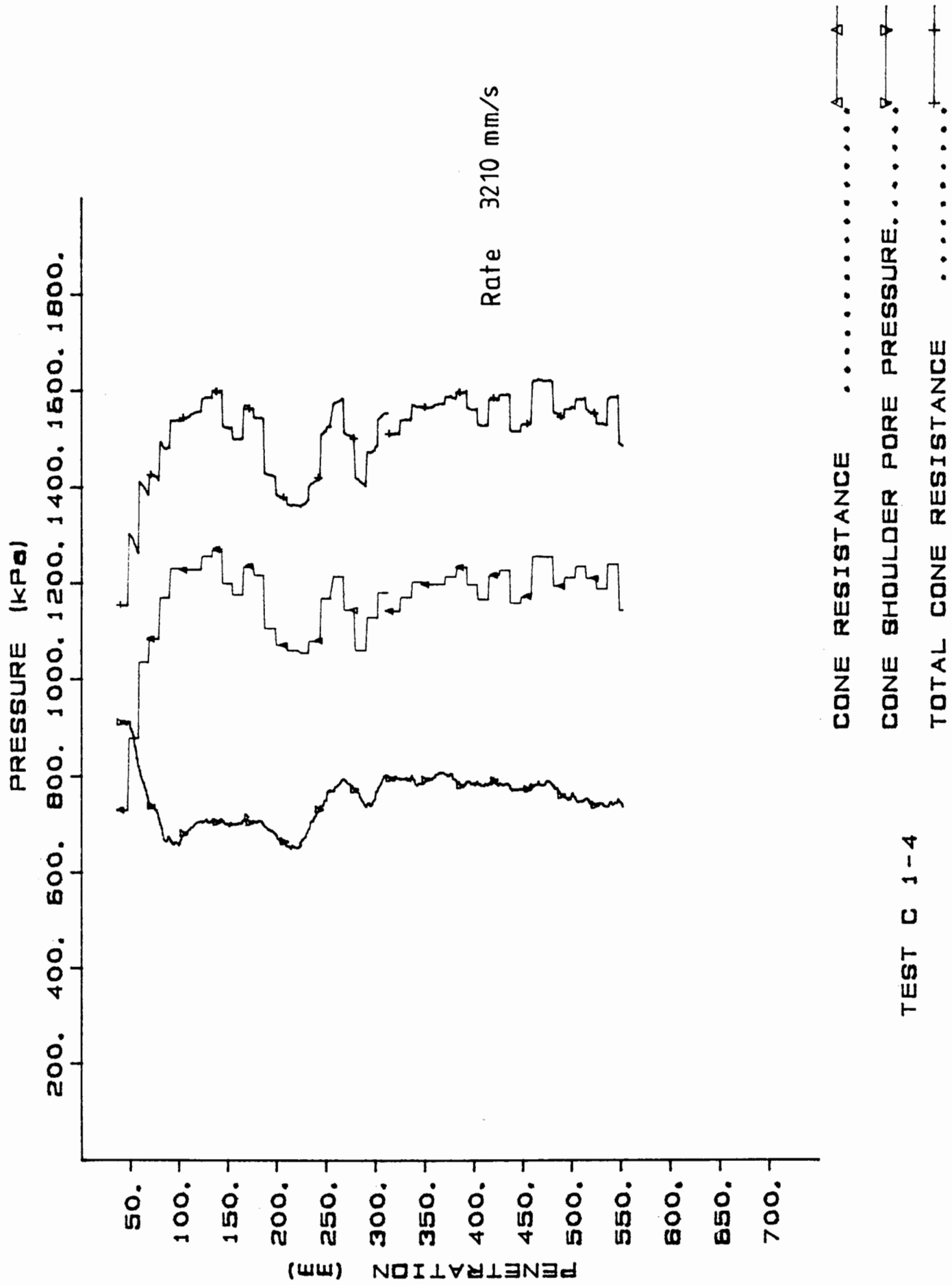
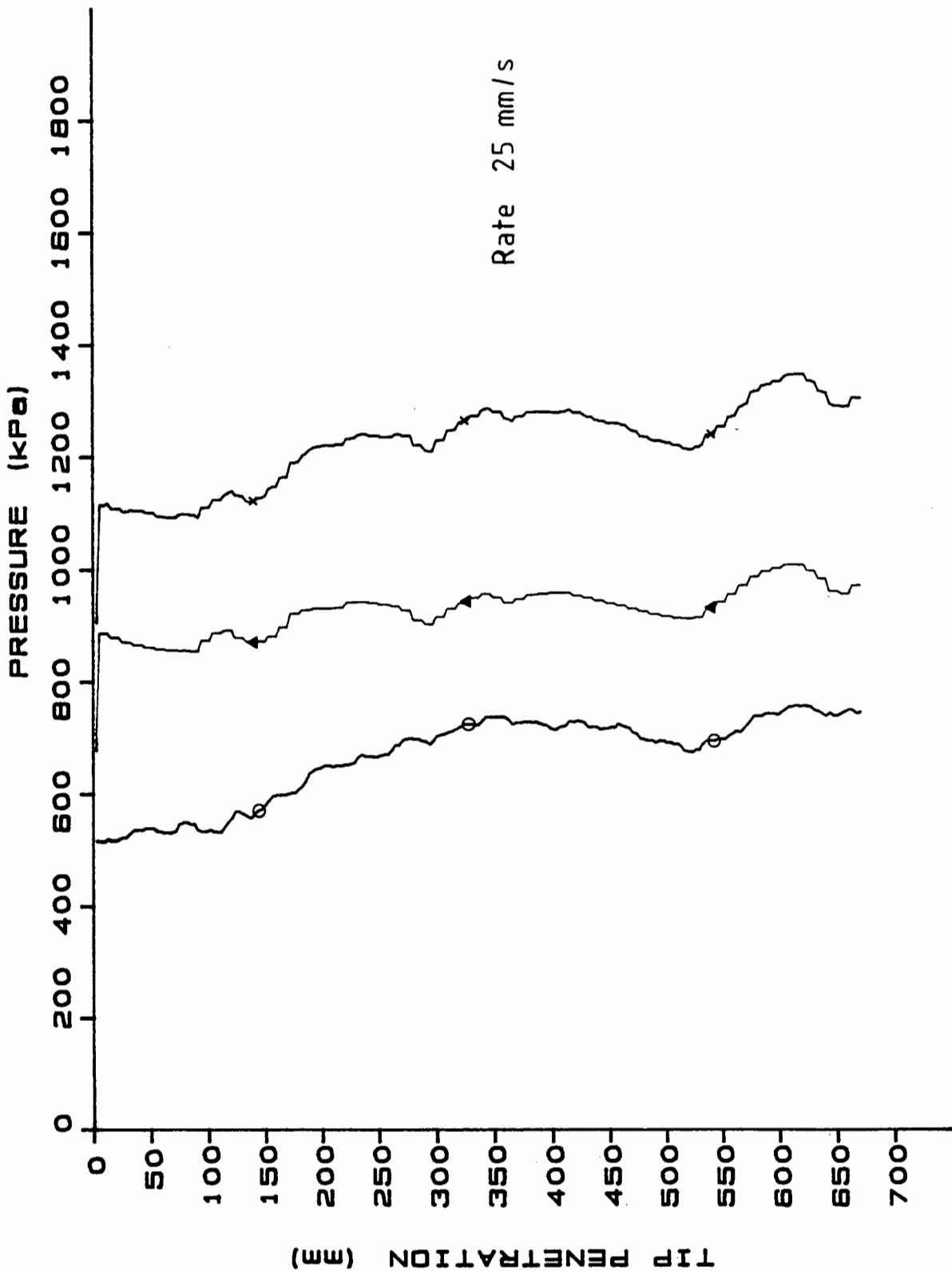


FIGURE 4.25 PENETRATION TEST DATA : TEST C1 - 4



TOTAL CONE RESISTANCE ..... \*  
 CONE RESISTANCE ..... ▲  
 CONE SHOULDER PORE PRESSURE..... ○

TEST C2-1

FIGURE 4.26 PENETRATION TEST DATA : TEST C2 - 1

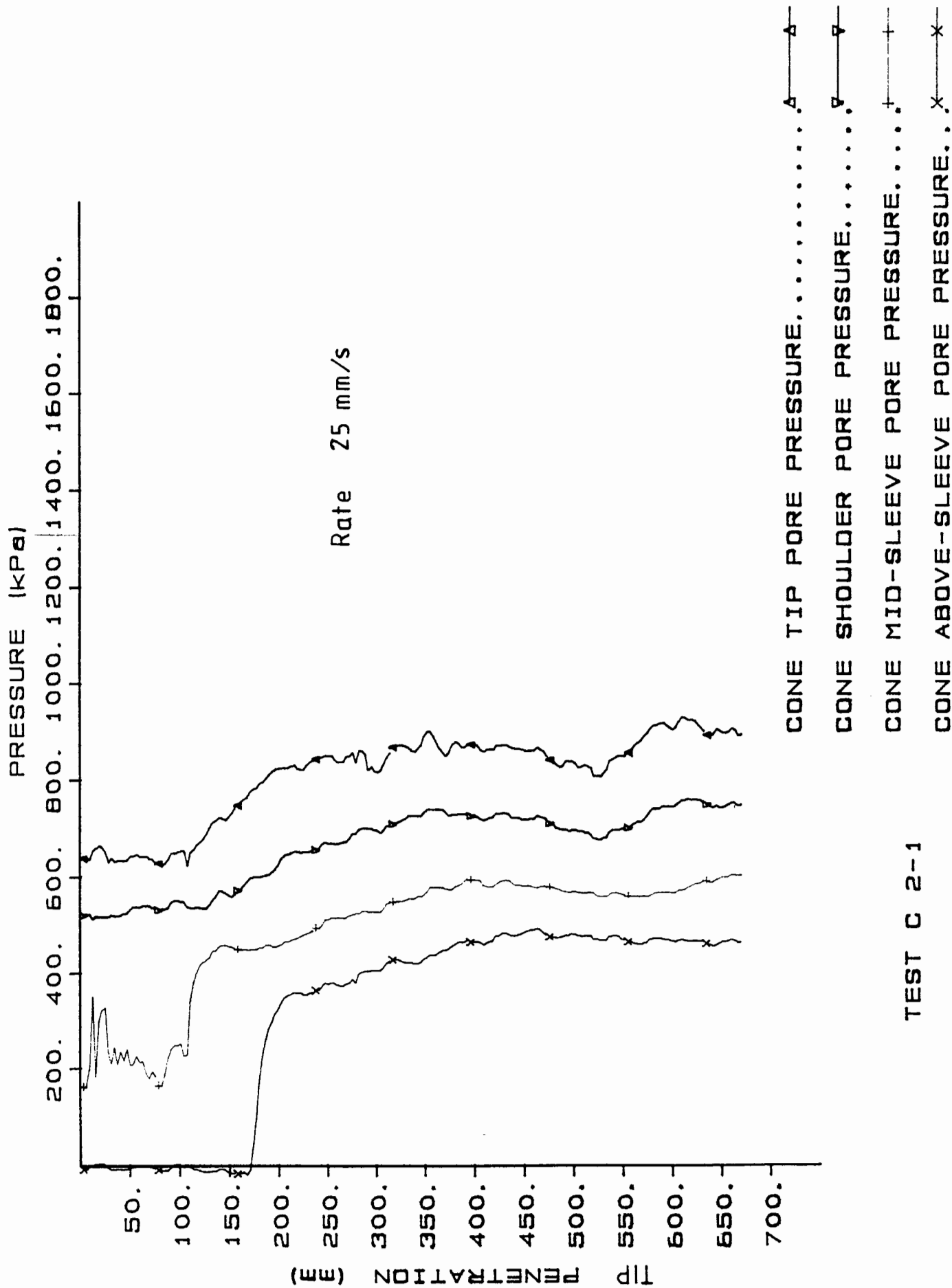
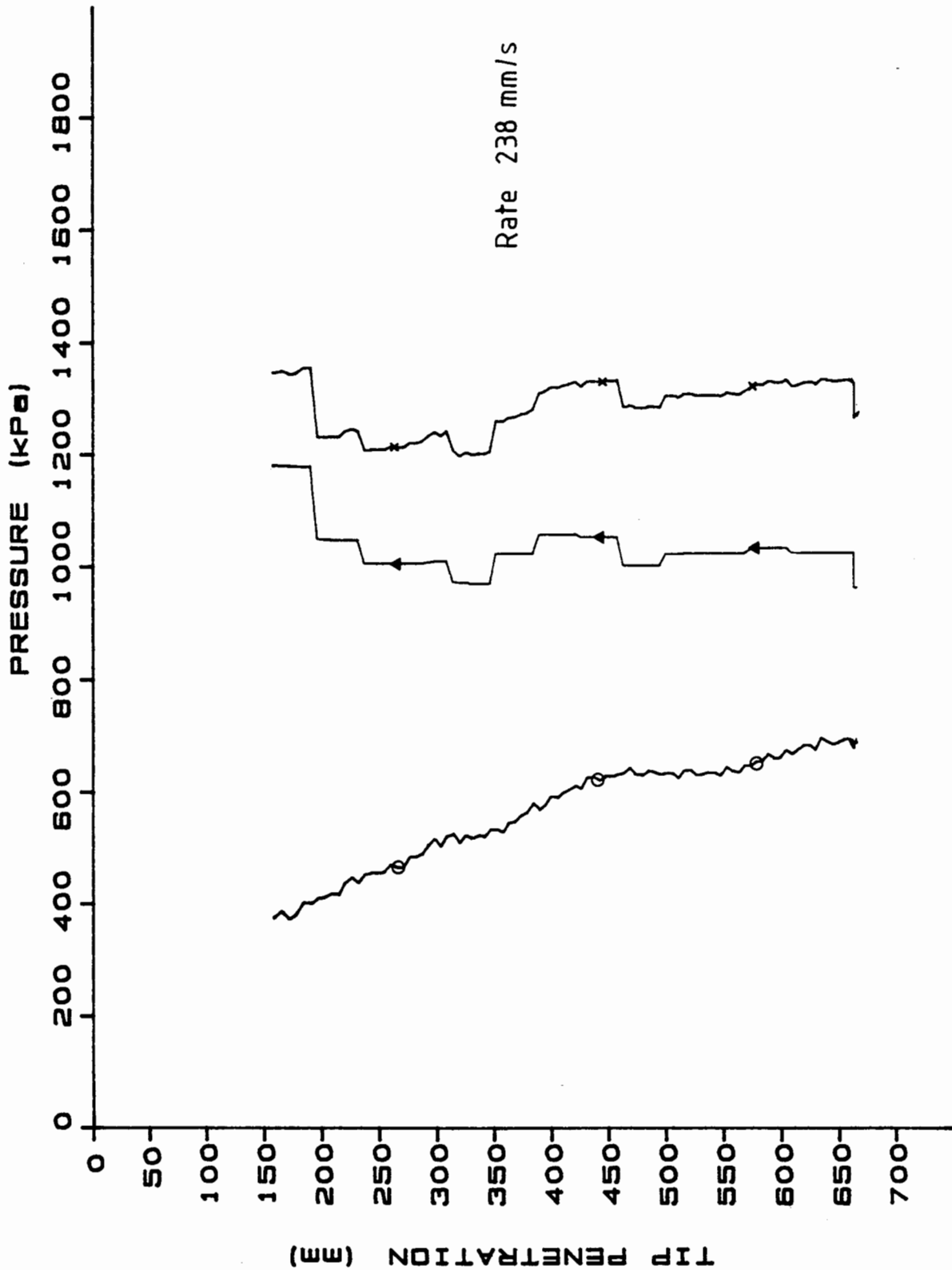


FIGURE 4.27 PENETRATION TEST DATA : TEST C2 - 1 (pore pressures)

TEST C 2--1

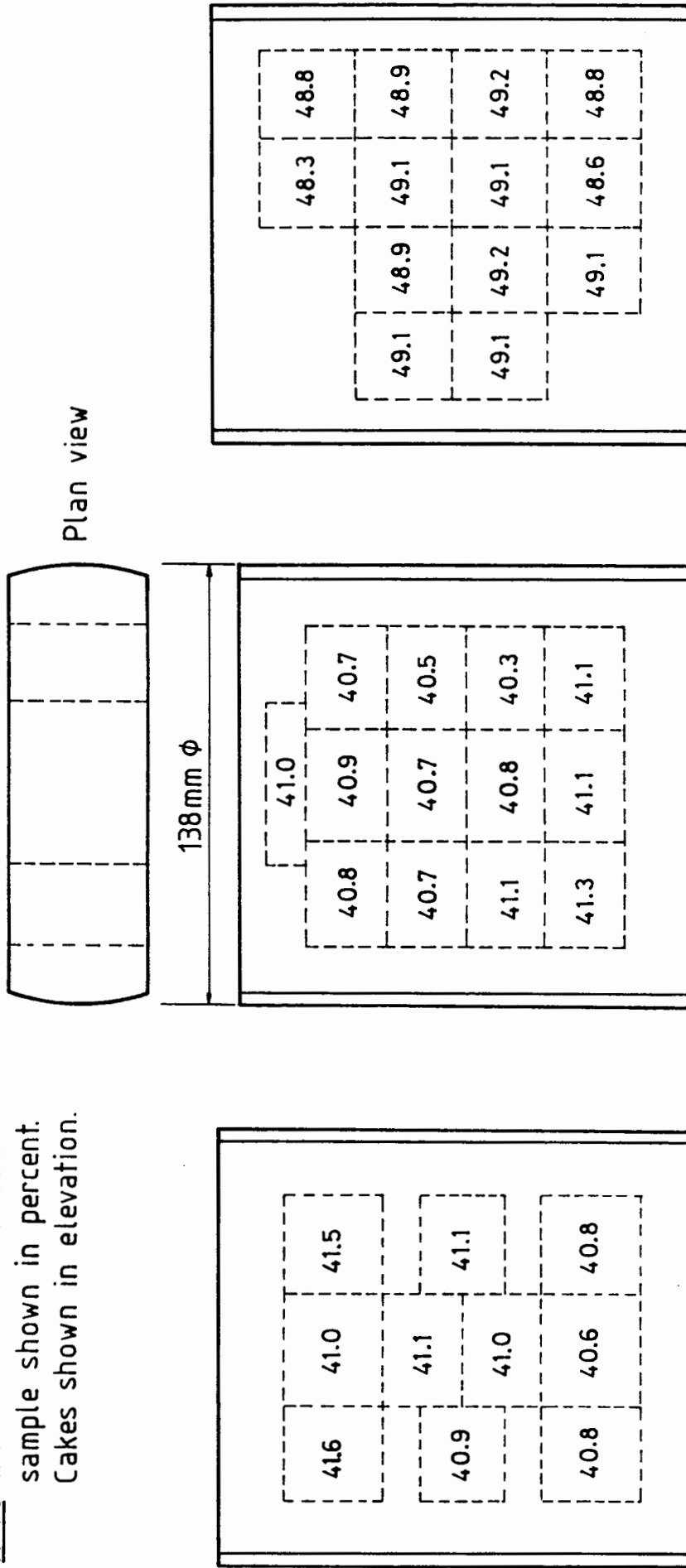


TOTAL CONE RESISTANCE ..... \*  
 CONE RESISTANCE ..... ^  
 CONE SHOULDER PORE PRESSURE..... o

TEST C2-2

FIGURE 4.28 PENETRATION TEST DATA : TEST C2-2

Note: Water contents of each sample shown in percent. Cakes shown in elevation.



(1) Rigid top plate, drainage to sump 800mm below cell

(2) Rigid top plate, drainage to constant head tube maintaining positive pore pressures

(3) Flexible top boundary, drainage to constant head tube maintaining positive pore pressures

FIGURE 4.29 WATER CONTENT DISTRIBUTIONS FOR CLAY CAKES CONSOLIDATED IN VARIOUS CELLS

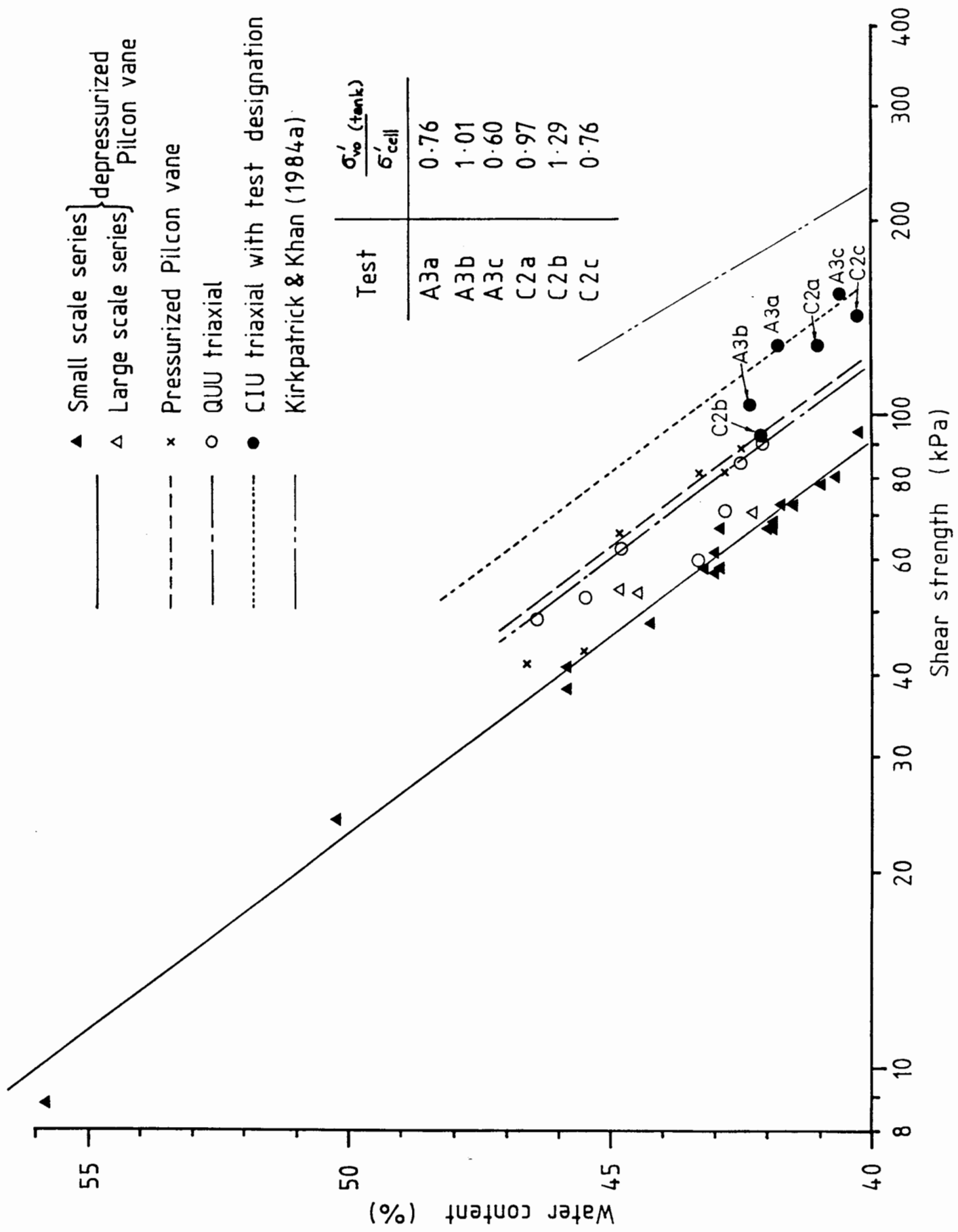
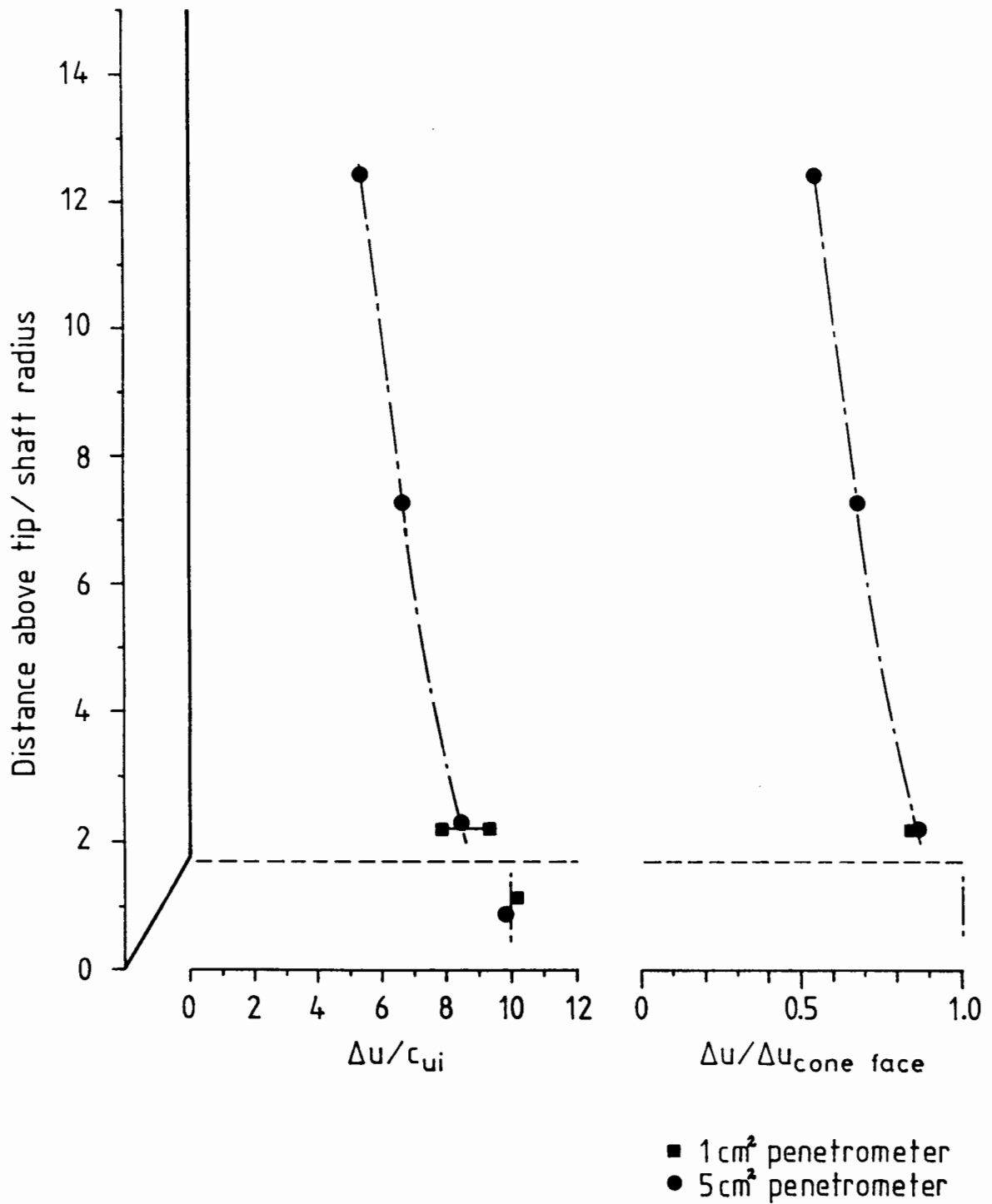


FIGURE 4.30 SHEAR STRENGTH vs WATER CONTENT RELATIONSHIPS



Notes: 1) Data from tests at 20-50mm/s  
 2) Values of  $\Delta u$  not modified for possible confinement effects

FIGURE 4.31 NORMALIZED EXCESS PORE PRESSURES ALONG PENETROMETER SURFACE



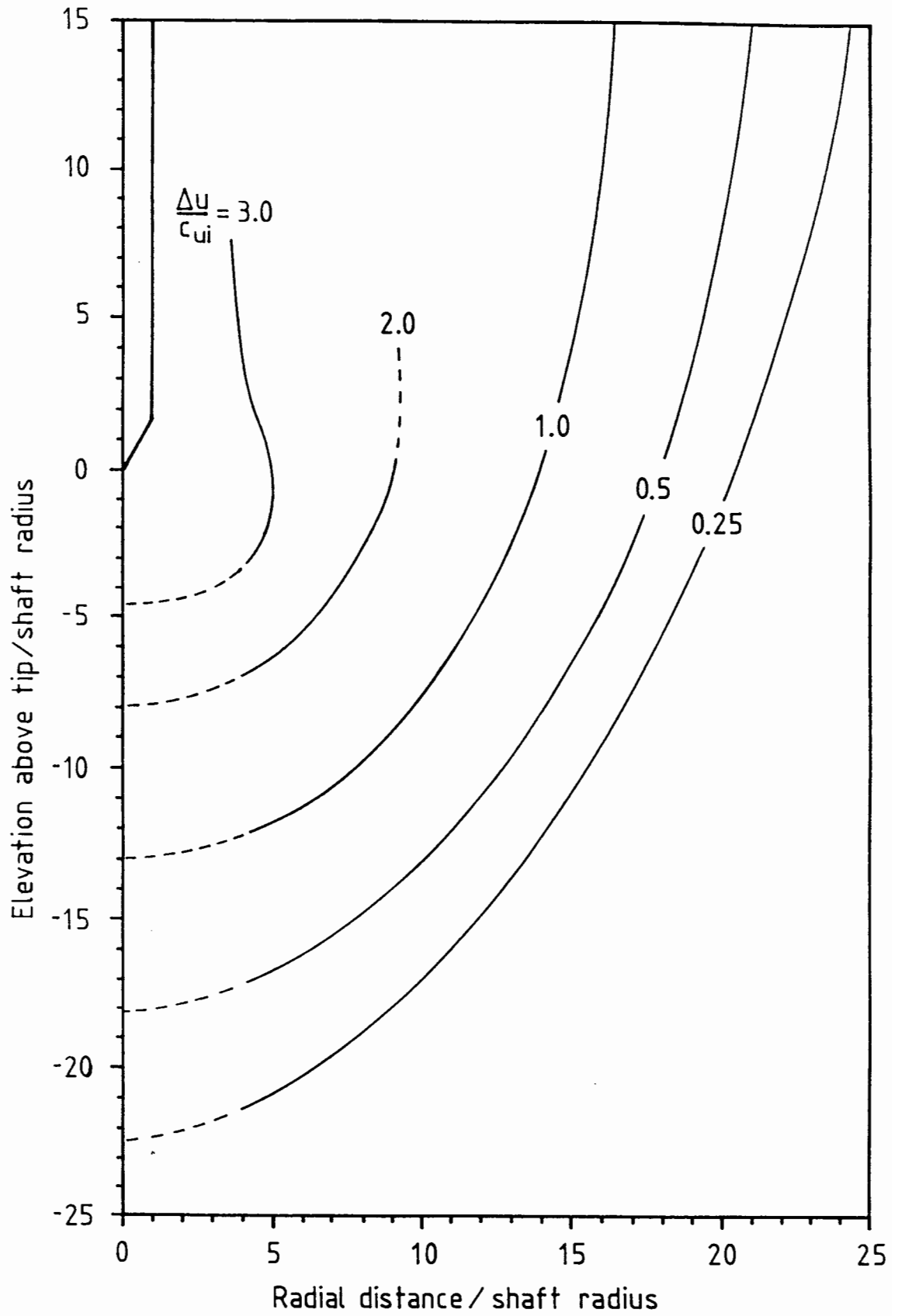


FIGURE 4.32 NORMALIZED EXCESS PORE PRESSURE DISTRIBUTION IN CAKE DURING PENETRATION

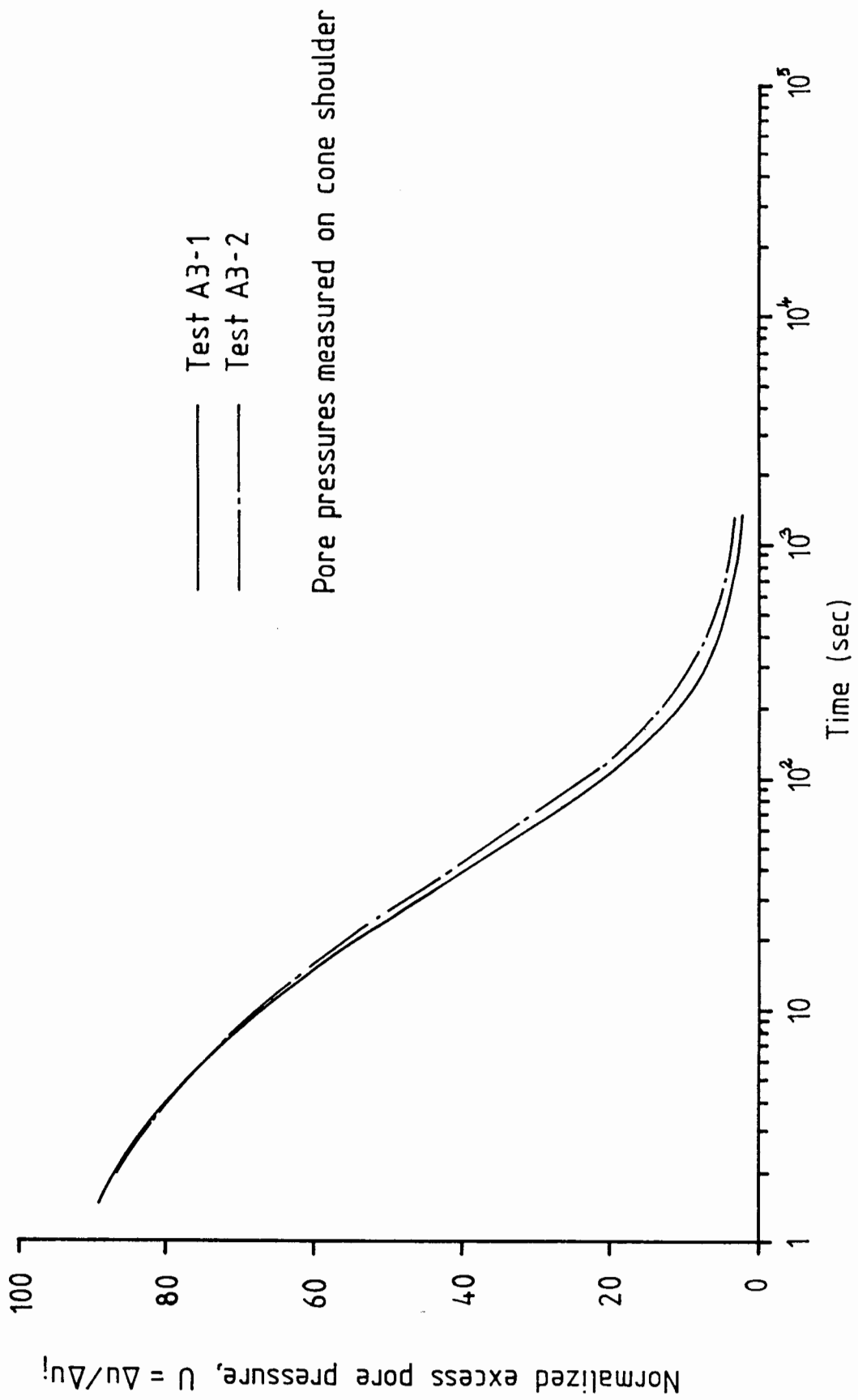


FIGURE 4.33 DISSIPATION DATA : A3 SERIES

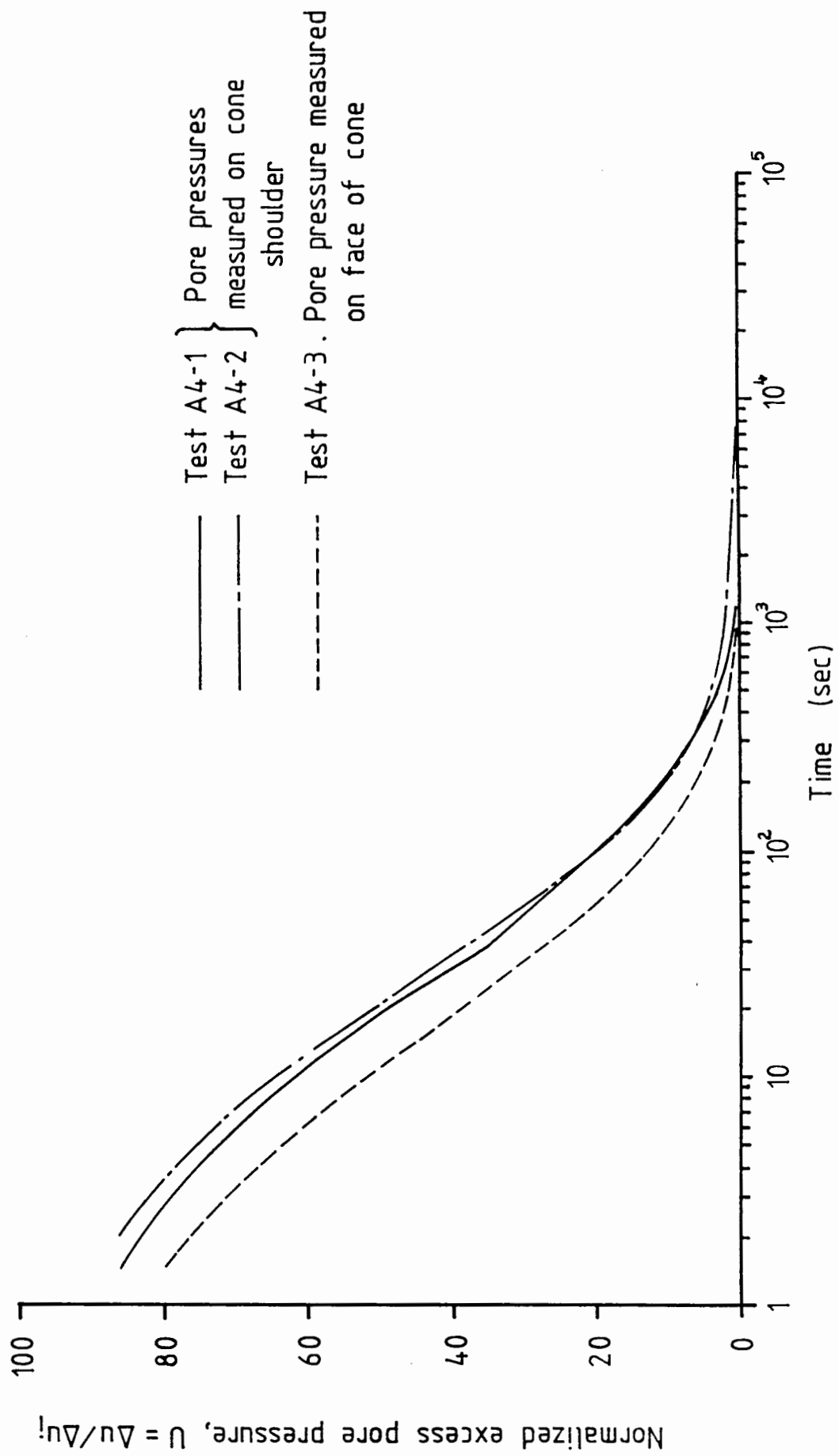


FIGURE 4.34 DISSIPATION DATA : A4 SERIES

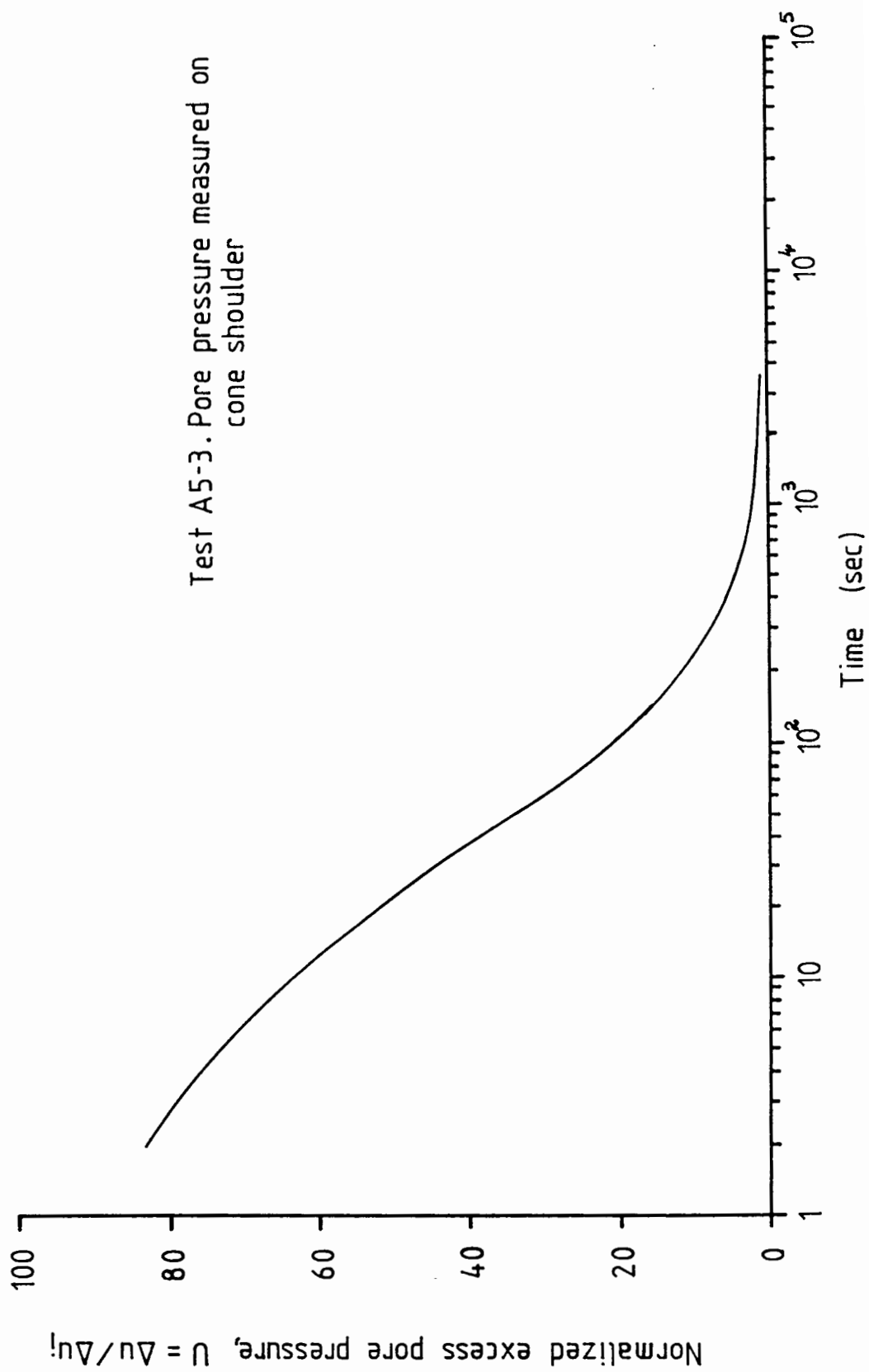


FIGURE 4.35 DISSIPATION DATA : TEST A5 - 3

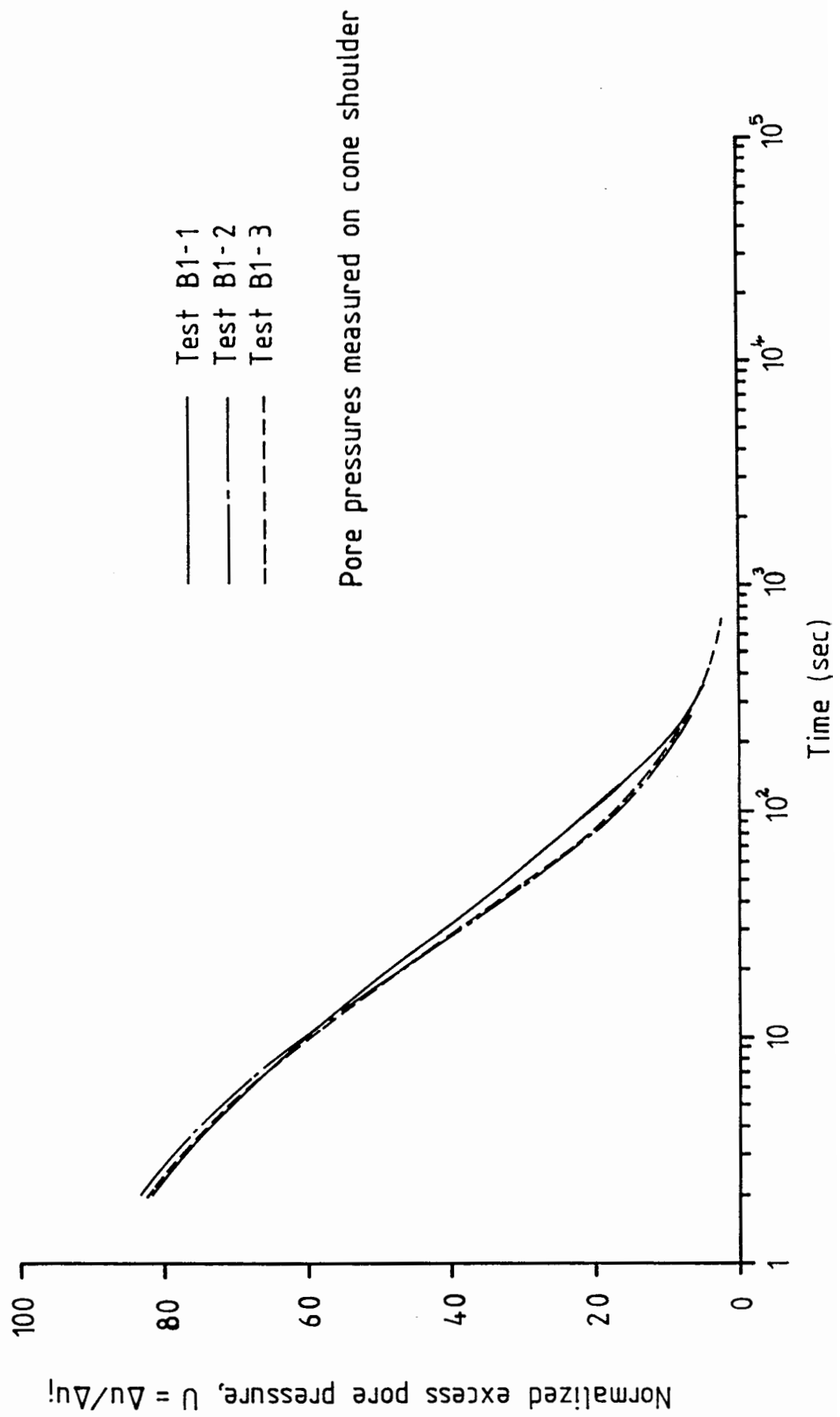


FIGURE 4.36 DISSIPATION DATA : B1 SERIES

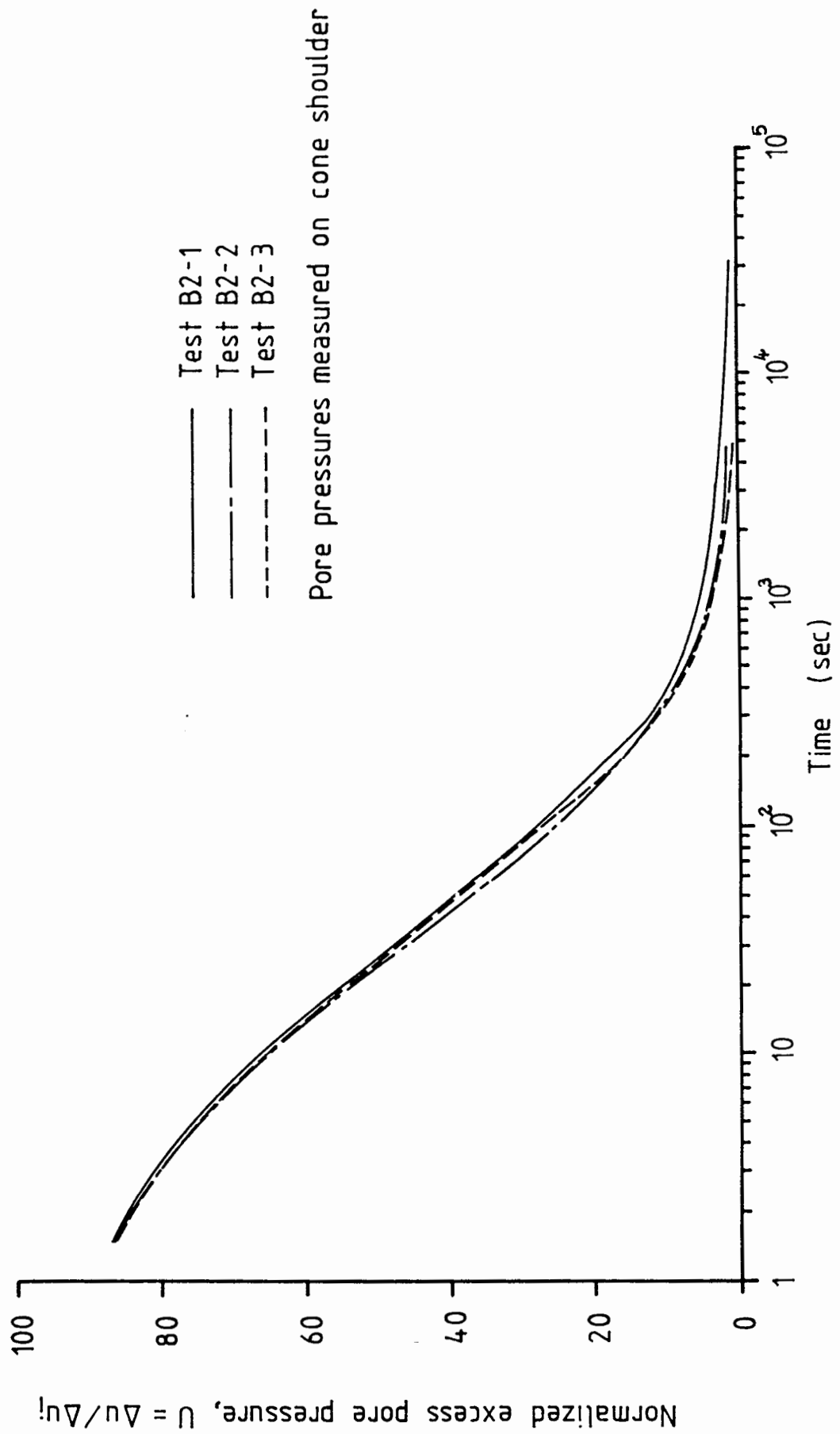


FIGURE 4.37 DISSIPATION DATA : B2 SERIES

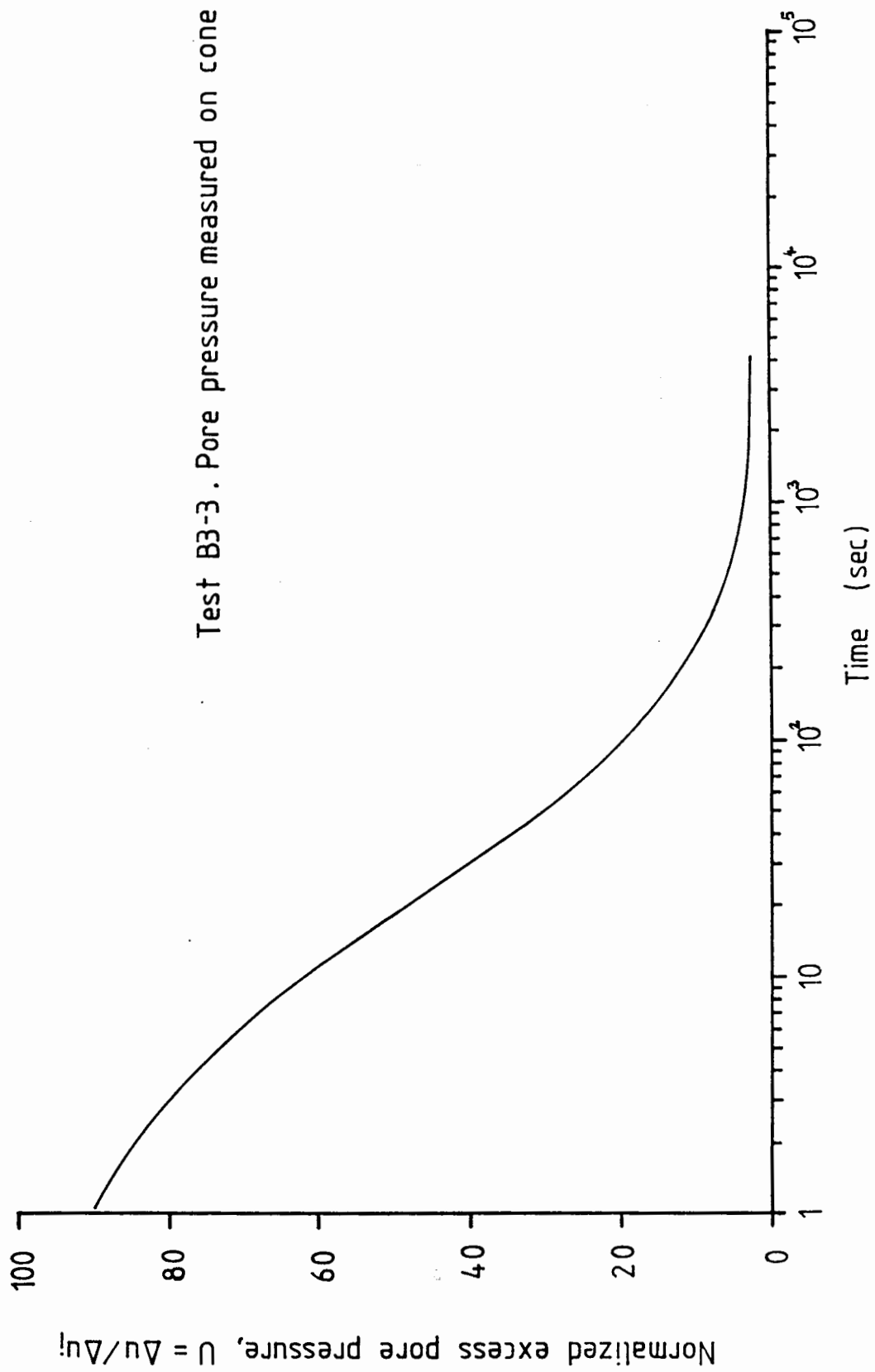


FIGURE 4.38 DISSIPATION DATA : TEST B3 - 3

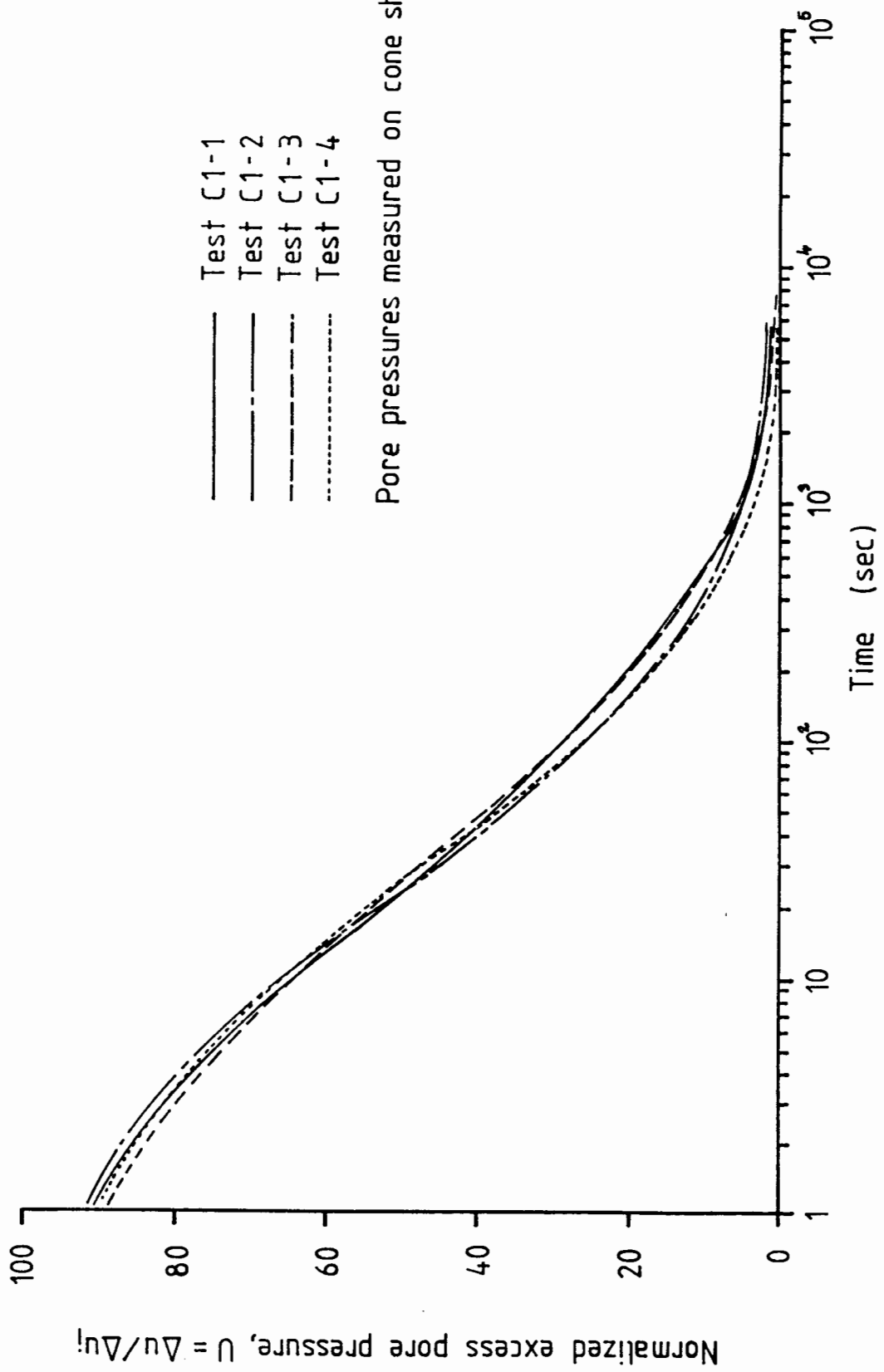


FIGURE 4.39 DISSIPATION DATA : C1 SERIES



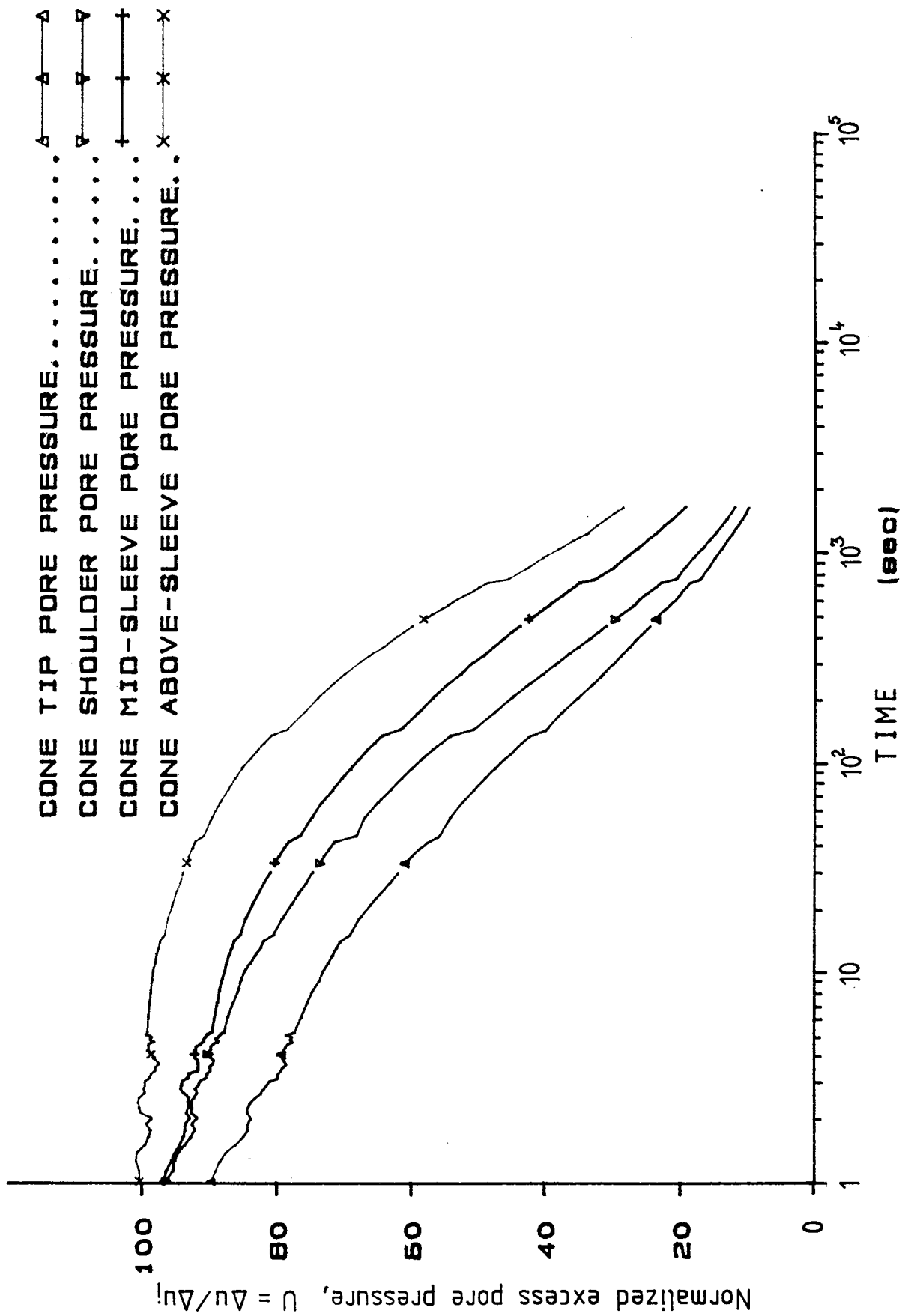


FIGURE 4.40 NORMALIZED PORE PRESSURE DISSIPATION DATA : TEST C2-1

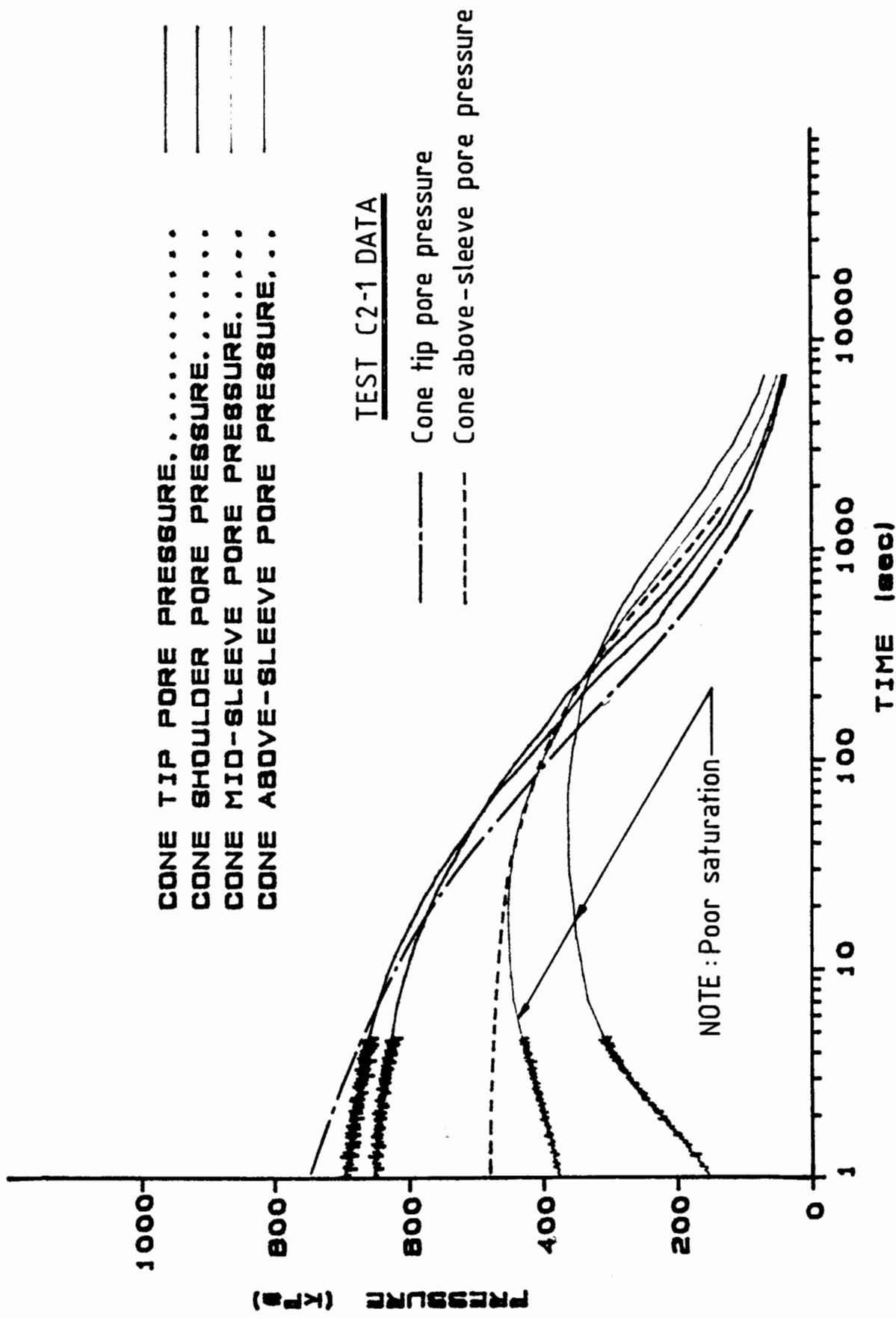


FIGURE 4.4| PORE PRESSURE DISSIPATION DATA : TEST C2 - 2

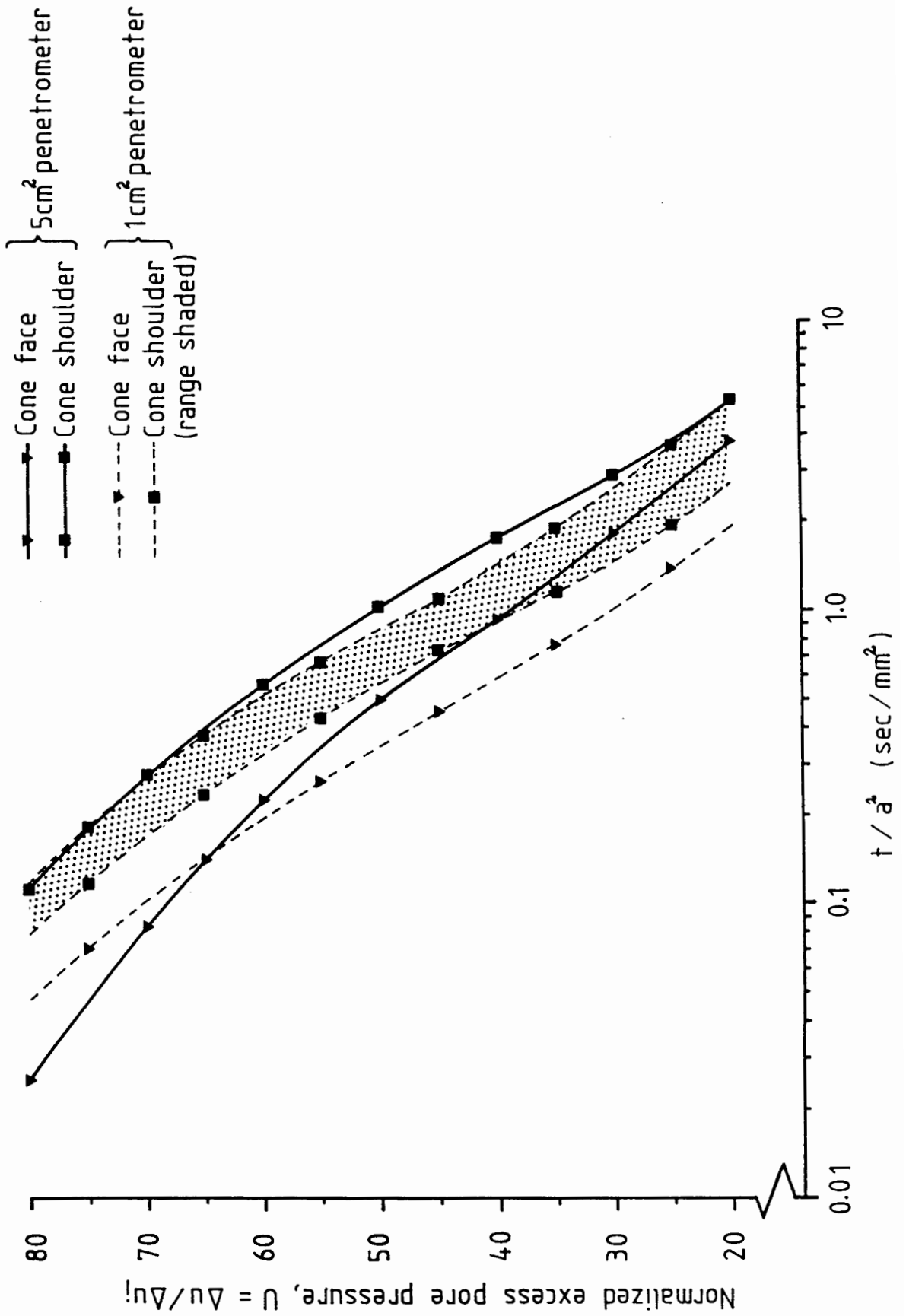
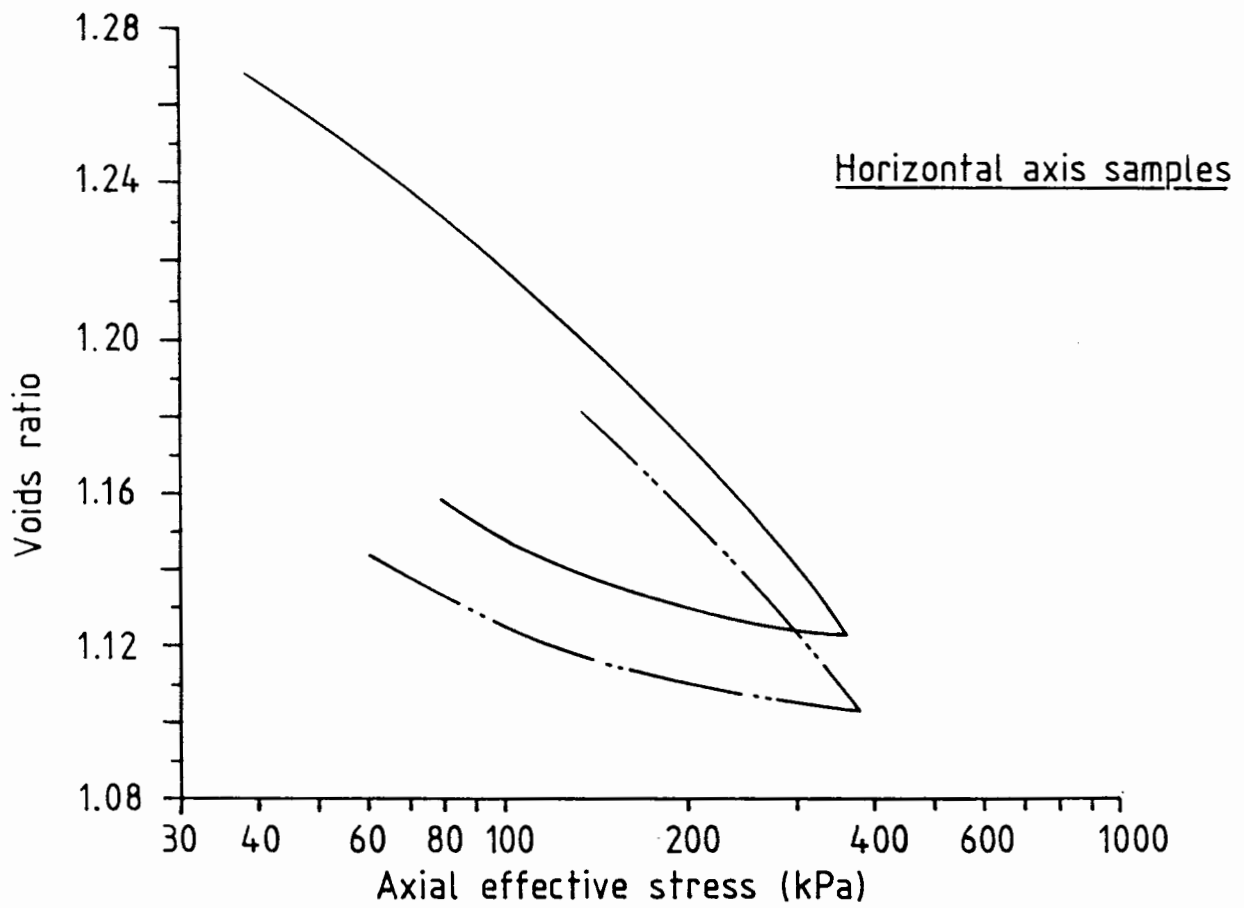
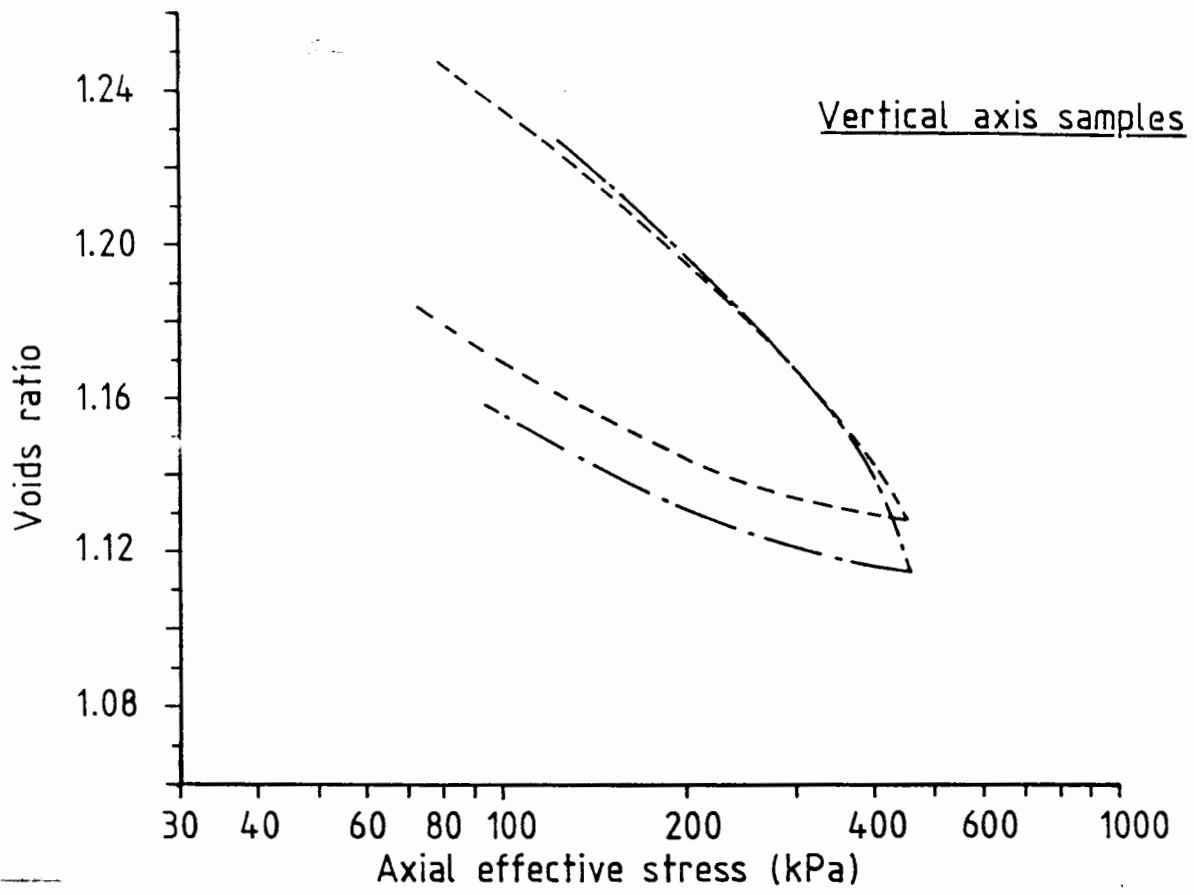


FIGURE 4.42 COMBINED DISSIPATION DATA



All samples obtained from cake C2

FIGURE 4.43 RESTRICTED FLOW CONSOLIDATION TEST DATA

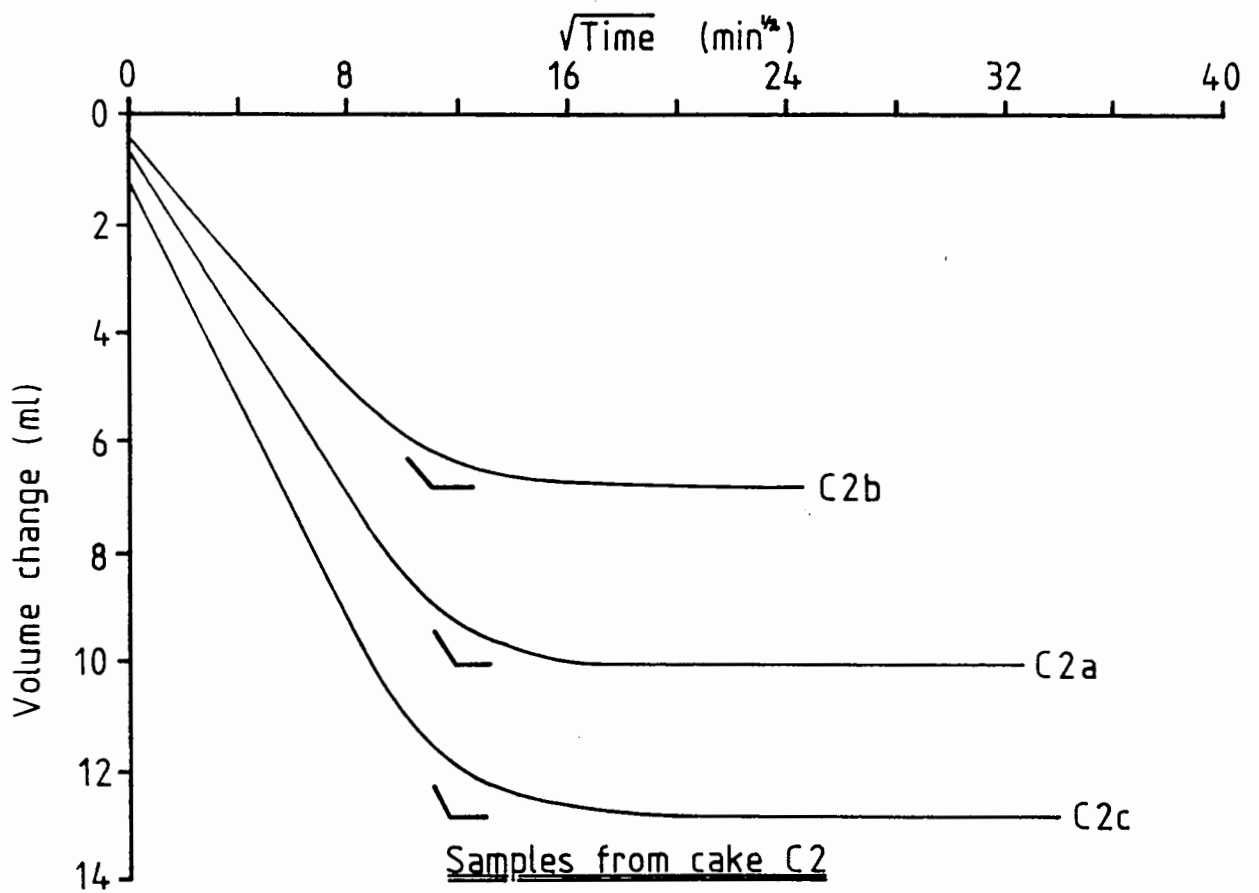
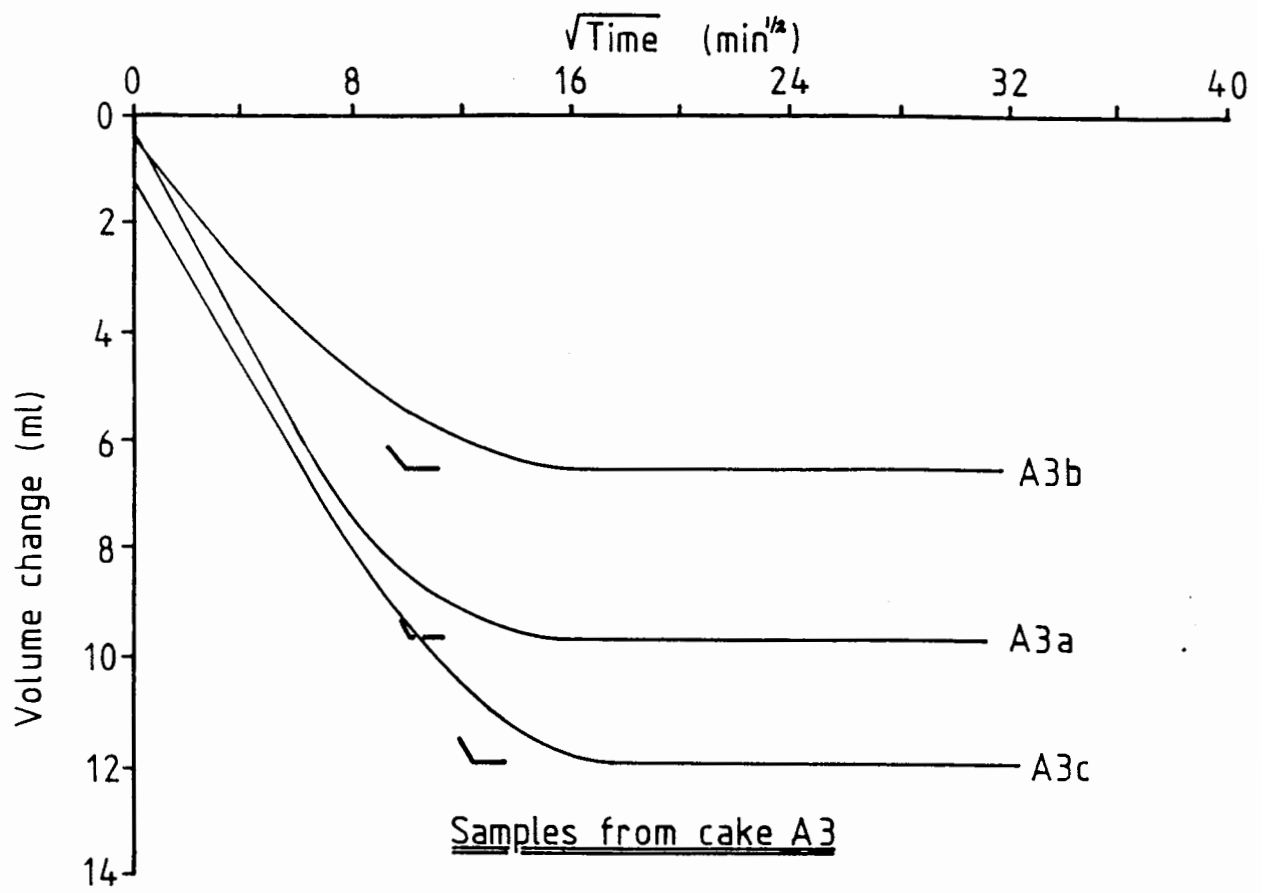
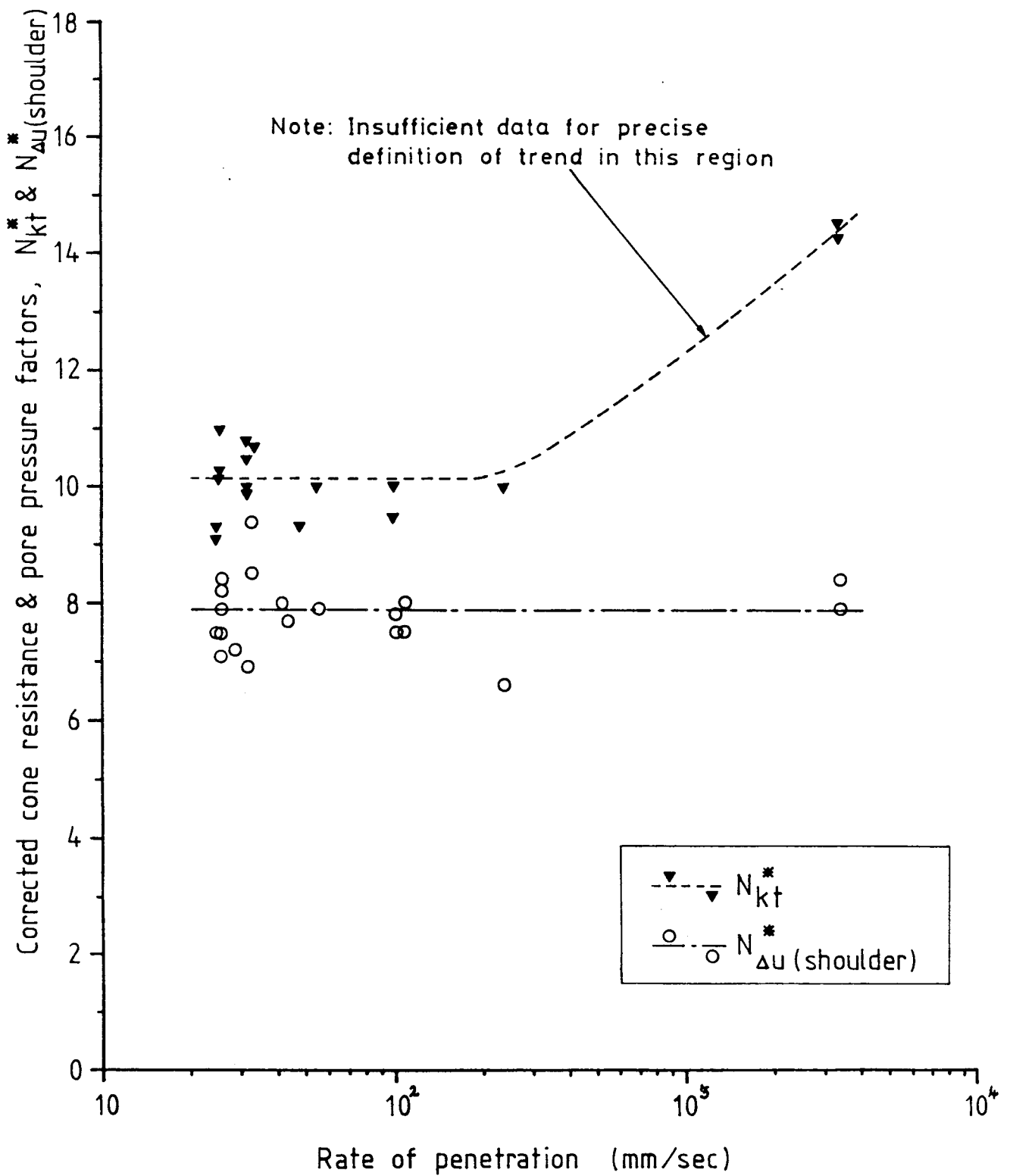


FIGURE 4.44 CONSOLIDATION OF TRIAXIAL SAMPLES



Notes: 1)  $OCR < 1.1$  for above data

$$2) \quad N_{kt}^* = (q_n - \Delta \sigma_{rb}) / c_{ui}$$

$$N_{\Delta u}^*(\text{shoulder}) = (\Delta u - \Delta \sigma_{rb}) / c_{ui}$$

FIGURE 4.45 VARIATION OF  $N_{kt}^*$  AND  $N_{\Delta u}^*$  WITH PENETRATION RATE

## 5. FIELDWORK

### 5.1 Introduction

In August 14th-16th 1986 fieldwork was undertaken jointly with Oxford Research Assistant Mr. T. Henderson. The aims of this work were as follows:

1. Investigate the possibility of scale effects between different sizes of penetrometer.
2. Obtain dynamic pore pressures and cone resistances in normally consolidated clay to compare with laboratory data.
3. Obtain dynamic pore pressure distributions from the multi-channel piezo-cone penetrometer to compare with laboratory behaviour.

For this work Fugro Limited made available one of their 20 tonne penetrometer trucks, a commercial  $10\text{cm}^2$  piezo-cone and an operator. Technicians Mr. S. Hoare and Mr. R. Sawala completed the site team.

In order to obtain data comparable to the laboratory series a normally consolidated clay site was required with a stratum depth of approximately 10m. From their extensive CPT records Fugro were able to identify a suitable site at Inchinnan to the west of Glasgow and the Scottish Development Agency kindly granted permission for its use.

## 5.2 Site Description and Geology

The site location is shown in Figure 5.1 and lies at O.S. map reference NS680471. The surrounding area is generally flat making it ideal for the location of Glasgow's Abbotsinch Airport which lies just over 1km to the south. Between the site and the airport lies the Black Cart Water which flows North East into the River Clyde approximately 3km distant. The site elevation is +7m AOD.

The depth of Quaternary deposits at this location is greater than that of much of the surrounding area because it lies in the buried river valley of the pre-glacial River Cart. Rock head is believed to lie at approximately -15m AOD sloping gradually to -30m AOD to the south and west (University of Strathclyde 1983). Overlying rockhead is probably a variable thickness of glacial lodgement till (boulder



clay). This has been observed by previous CPTs and boreholes in the vicinity, although the present site investigation did not penetrate to the base of the overlying Clyde Beds. The Clyde Beds at this location consist of grey and greyish-brown regularly banded silty clay. They are of late Devensian age being dated between 11,000 and 8,000 B.C. (Peacock 1981). Deposition of these clays began as the Devensian ice sheet retreated to the north during the Windermere Interstadial. It is believed that the Clyde estuary was initially dammed by the ice around Greenock and Dumbarton downstream from Inchinnan. The relative sea level at this time was around +25m AOD enabling sea water access to the site through the Lochwinnoch Gap to the south west. Initial deposition was thus probably in brackish water due to the large volumes of melt water flowing from the nearby ice-sheet. Conditions became estuarine as the ice sheet retreated further to the North-West and probably melted completely. Deposition slowed appreciably as vegetation became established on low ground but increased again after about 10000 B.C. during the final Loch Lomond stade (glacial period). By this time relative changes in sea level and crustal rebound had reduced sea level to a few meters above present levels. The increased deposition was due to solifluction, frost

action and the effects of reglaciation. The Loch Lomond glacier was halted at the Highland Boundary Fault (Sisson 1967) about 16km NW of the present site. There is a lack of post glacial deposits (younger than 8000 B.C.) probably indicating that the sea-level had fallen to approximately its present level by this time.

### 5.3 Site Investigation Equipment

The first phase of the investigation was carried out using the 1cm<sup>2</sup> and 5cm<sup>2</sup> Oxford piezocones (see Section 3.3) and a 10cm<sup>2</sup> Fugro piezocone (Figure 5.2). The Fugro piezocone measured tip resistance ( $q_c$ ) and pore pressure on the face of the cone. The full scale range of the tip resistance load cell was 5 tonne (equivalent to approx. 49MPa) and the maximum working pressure of the pore pressure transducer was 5 bar (0.5MPa). The filter stone for this penetrometer is made of Aerolith porous ceramic identical to that used in the Oxford instruments. The instrument has an  $\alpha$  factor\* of 0.27.

For this series of tests the Fugro penetrometer was connected to its normal signal conditioning and

\* where  $\alpha = \frac{\text{groove cross-section area}}{\text{penetrometer cross-section area}}$

recording system. The cone resistance and pore pressure traces were recorded on a two pen chart recorder.

The system used for the Oxford piezocones is shown in Figure 5.3. The penetrometers were connected to standard 10cm<sup>2</sup> sounding rods using adaptors designed by T. Henderson. The penetrometers' load cells and pore pressure transducers were independently powered at 3V D.C. Depth recording was by means of the Fugro depth encoder and signal conditioning unit. The output from this unit was routed through a step counter and trigger which provided for a 6 channel scan every 20mm. The penetrometer output was amplified and recorded on two systems. For the first of these the signals were digitized by the Analogue Express memory mapped data logger, the data being stored in the memory of a Commodore C-64. On completion of a penetration profile this data was transferred onto disk. The amplified penetrometer output was also recorded on a 6 channel Y-T chart recorder.

In the second phase of the site investigation Fugro made a borehole at the site using their hollow stem flight auger drilling system. This was combined with a push sampling technique using thin walled Shelby tubes with an internal diameter of 72mm.

#### 5.4 Borehole and Piezocone Data

The detailed site plan is shown on Figure 5.1.

The borehole produced 13 consecutive samples giving a complete recovery from 1.20m to 13.10m below ground level. These were sealed with wax on recovery. The samples were later tested at Fugro's laboratory under supervision of the author. Details of the material grading and Atterberg limits are given on Figure 5.4. In situ stresses and overconsolidation ratios have been determined from oedometer tests and density measurements. These are shown on Figure 5.5.

Details of the type of penetration test performed at each position are given in Table 5.1. All tests were performed at a penetration rate of 20mm/sec. The results of these tests are shown in Figures 5.6 to 5.8. On Figure 5.6 the combined values of  $q_c$  and  $q_t$  are plotted for the three  $5\text{cm}^2$  PCPTs. On Figure 5.7 the combined pore pressures are plotted for the  $5\text{cm}^2$  tests. Figure 5.8 shows the pore pressure and cone resistance data from the  $10\text{cm}^2$  PCPTs.

Test No.	Cone Type	Filter Locations	Saturating Fluid
A1	Fugro 10cm <sup>2</sup> friction cone	-	-
A2	Oxford 5cm <sup>2</sup> cone (002)	cone face shoulder mid-friction sleeve above friction sleeve	glycerin
B1	Oxford 5cm <sup>2</sup> cone (001)	cone face shoulder mid-friction sleeve	glycerin
B1A	Fugro 10cm <sup>2</sup> piezocone	cone face	water
B2*	Oxford 1cm <sup>2</sup> cone (003)	shoulder	glycerin
B3	Fugro 10cm <sup>2</sup> piezocone	cone face	water
C1	Oxford 5cm <sup>2</sup> cone (001)	cone face shoulder mid-friction sleeve	glycerin
C2	Fugro 10cm <sup>2</sup> piezocone	cone face	glycerin

\*NOTE: This test not reliable. Penetrometer lost in ground.

**TABLE 5.1 FIELD PENETRATION TESTING DETAILS**

### 5.5 Analysis of Field Data

The first aim of the field testing program was to examine whether the size of the penetrometer affected the measured pore pressures and total stresses. Although the 1cm<sup>2</sup> CPT cannot be regarded as reliable due to the gross deviation of the tip from the vertical, excellent data was obtained from the 5cm<sup>2</sup> Oxford

and 10cm<sup>2</sup> Fugro piezocones. This data firstly allows comparison between the cone face pore pressures for the two sizes (Fig. 5.9). There was close agreement between these pore pressures, the match being particularly good between 3m and 5m penetration and around 8m penetration.

The measured cone resistances ( $q_c$ ) are compared on Figure 5.9. These show the data from the 10cm<sup>2</sup> penetrometers to plot consistently higher than the values from the 5cm<sup>2</sup> penetrometers.

Total cone resistances ( $q_t$ ) for the two scales of instrument can be compared if pore pressures appropriate to the groove area can be calculated for the 10cm<sup>2</sup> piezocones. The similarity of pore pressures on the cone face between 5cm<sup>2</sup> and 10cm<sup>2</sup> scales enables the ratio of shoulder to cone face pore pressures observed for the smaller scale to be applied to the larger penetrometers at the same depths with reasonable confidence. Using this procedure the shoulder pore pressure values for the larger penetrometers have been calculated. The total cone resistance may then be calculated from:

$$q_t = q_c + a u_{sh}$$

where:

$u_{sh}$  = total pore pressure at penetrometer  
shoulder

$a$  =  $\frac{\text{area of groove}}{\text{total cone cross-sectional area}}$

The results for both sizes of penetrometer are shown on Fig. 5.9. It can be seen that the  $q_t$  values match well.

Figure 5.10a shows the normalised excess pore pressure distribution along the penetrometer shaft to vary considerably between 3m and 9m penetration. At the deeper penetration the reduction in excess pore-pressure up the shaft is rather more rapid. However, the major reduction in excess pore pressure occurs at the cone shoulder as was observed in the laboratory tests (Figure 4.40).

In Figure 5.10b this variation with depth is examined in more detail. Here  $\beta$  is plotted against depth where:

$$\beta = \frac{\Delta u_{\text{shoulder}}}{\Delta u_{\text{cone face}}}$$

The  $\beta$  factor is seen to rise fairly steadily with depth of penetration.

In Figure 5.10c  $\beta$  has been plotted against OCR. This plot shows  $\beta$  to decrease with increasing OCR. The laboratory value for  $\beta$  in normally consolidated clay is also shown on this plot and appears to be consistent with the field data.



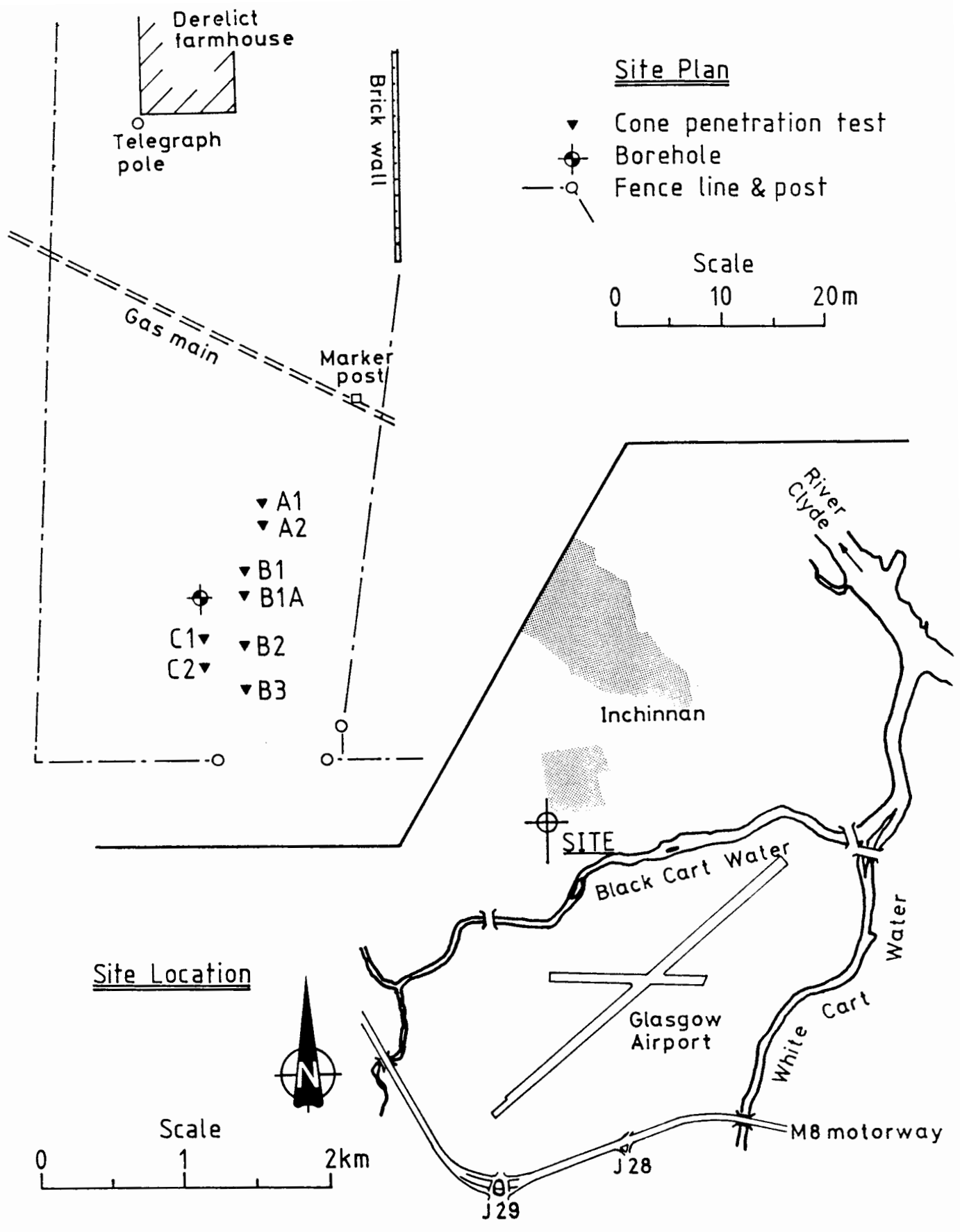


FIGURE 5.1 INCHINNAN SITE PLAN AND LOCATION MAP

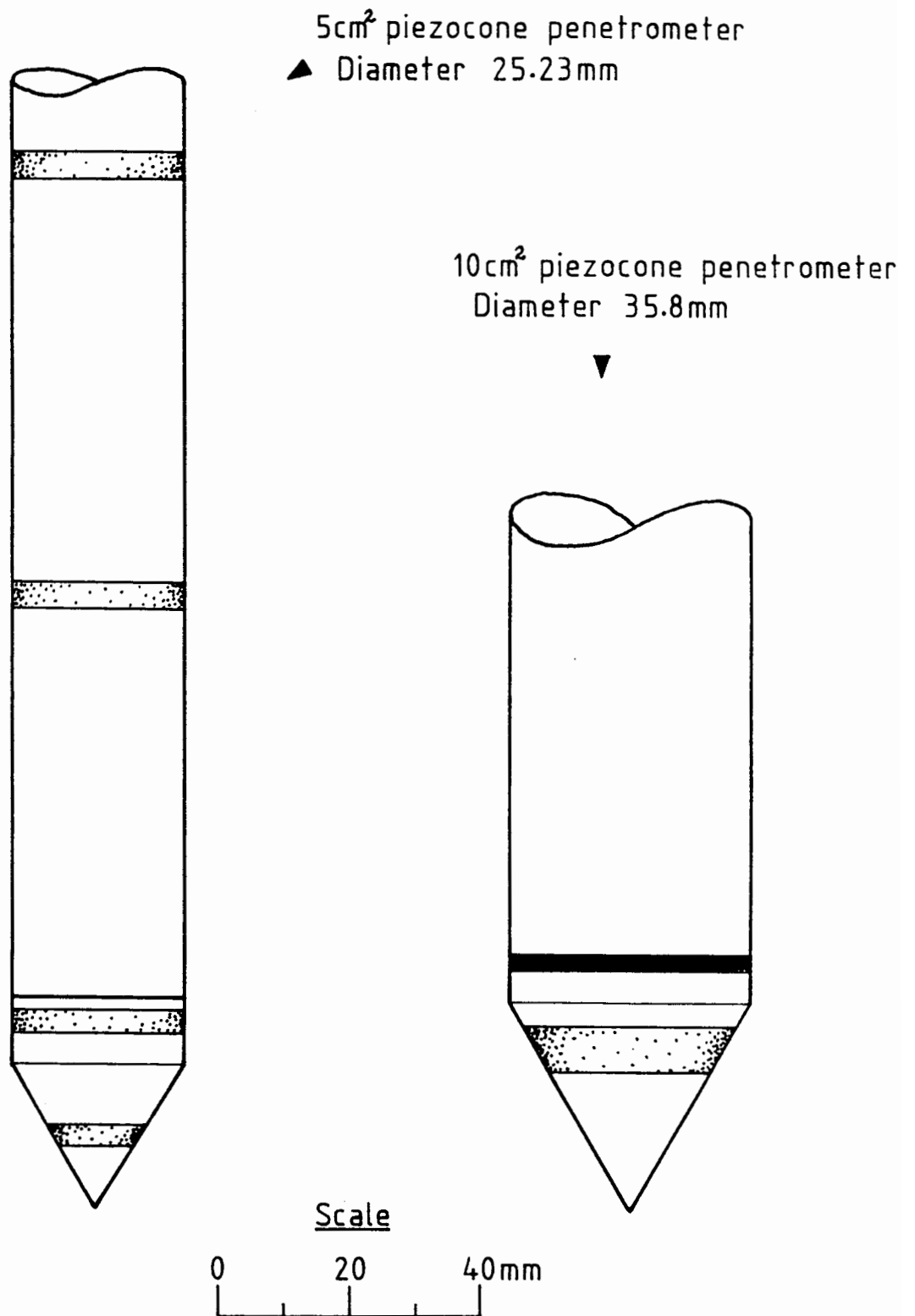


FIGURE 5.2 COMPARISON OF 5 cm<sup>2</sup> & 10 cm<sup>2</sup> PIEZOCONE PENETROMETERS

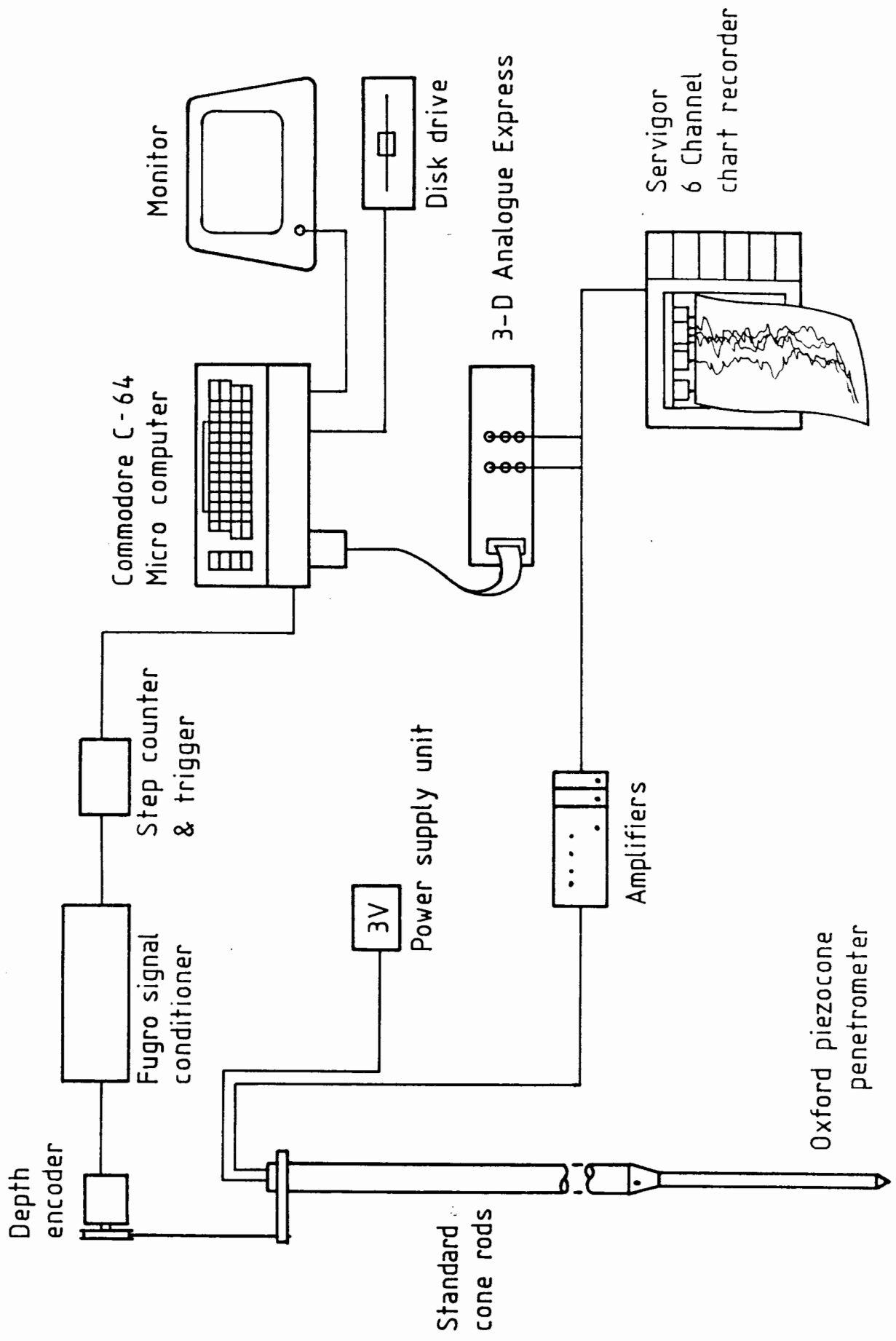


FIGURE 5.3 DATA LOGGING SYSTEM FOR FIELD TESTS

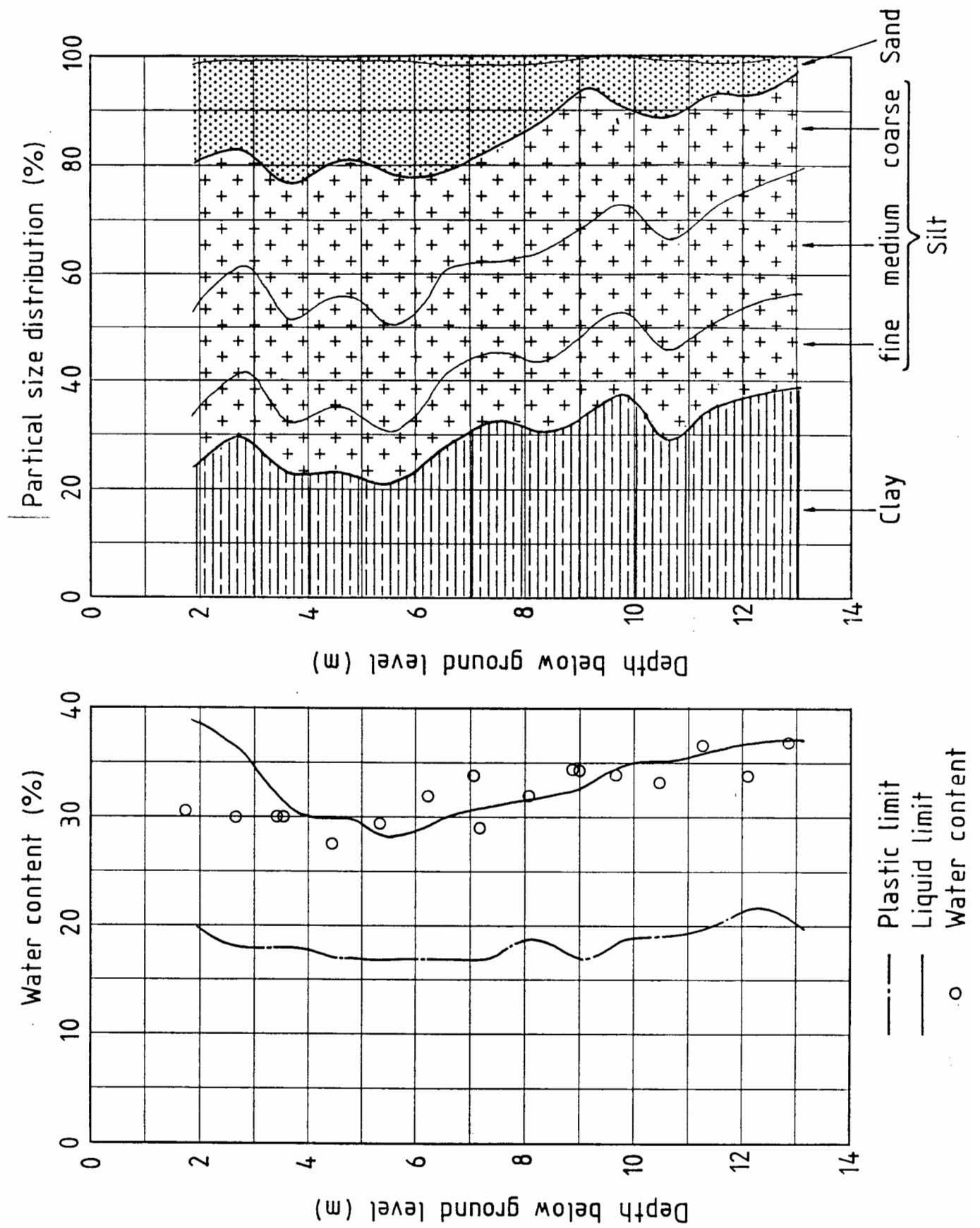
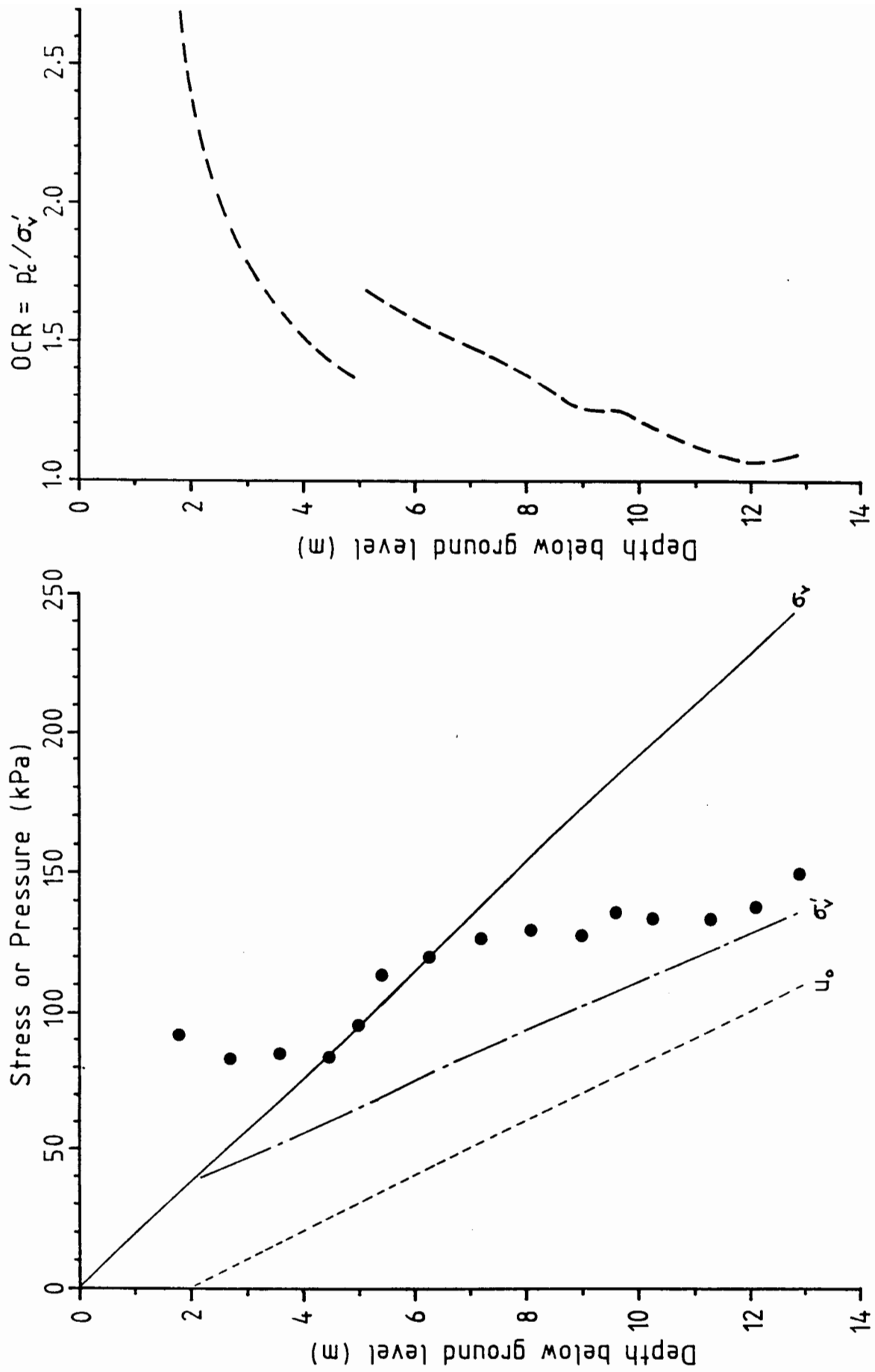


FIGURE 5.4 SITE PARTICLE SIZE DISTRIBUTION & INDEX PROPERTIES



- Effective vertical stress,  $\sigma'_v$
- preconsolidation stress,  $p'_c$

FIGURE 5.5 IN SITU STRESS DISTRIBUTION

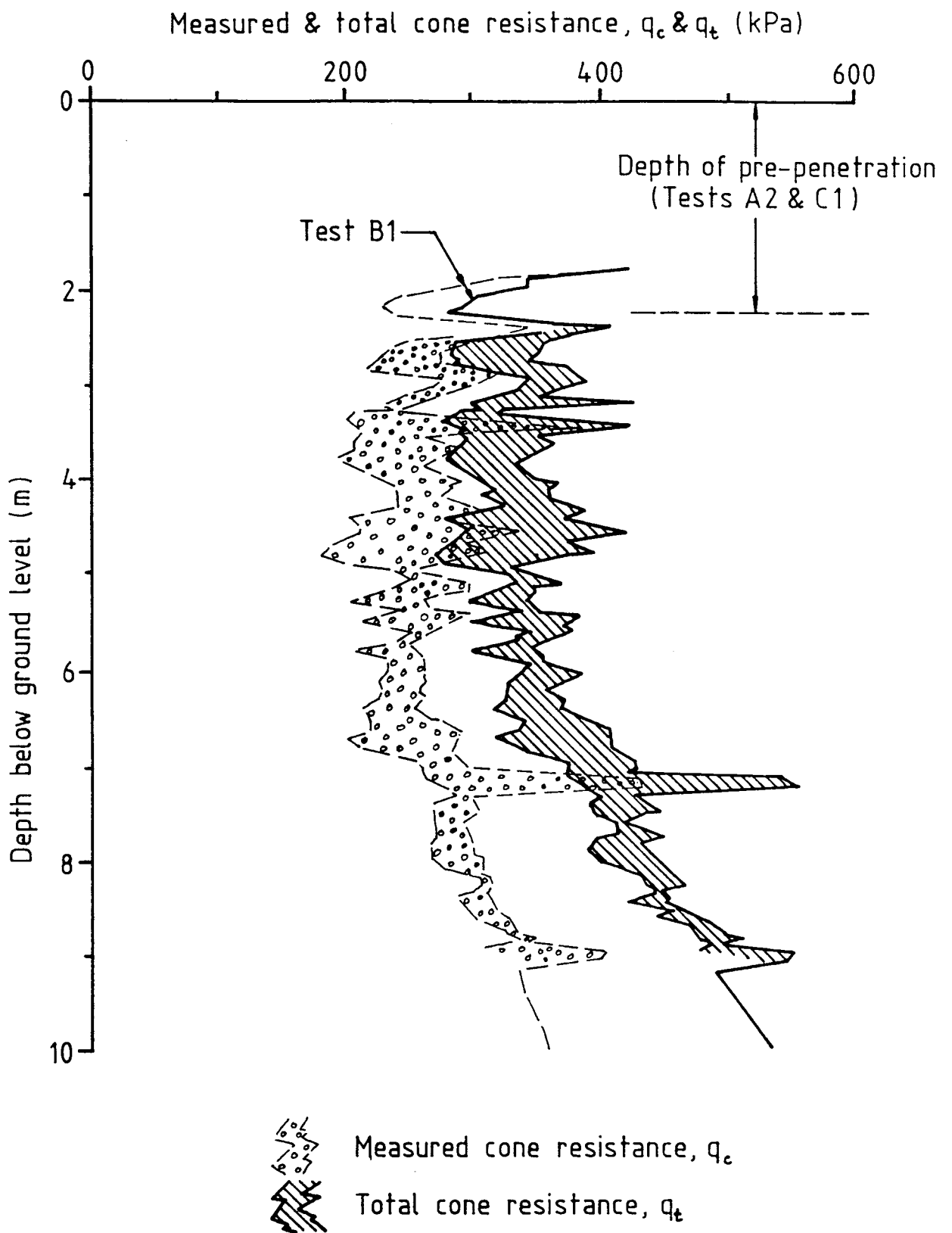


FIGURE 5.6 CONE RESISTANCE DATA : 5 cm<sup>2</sup> PCPTs

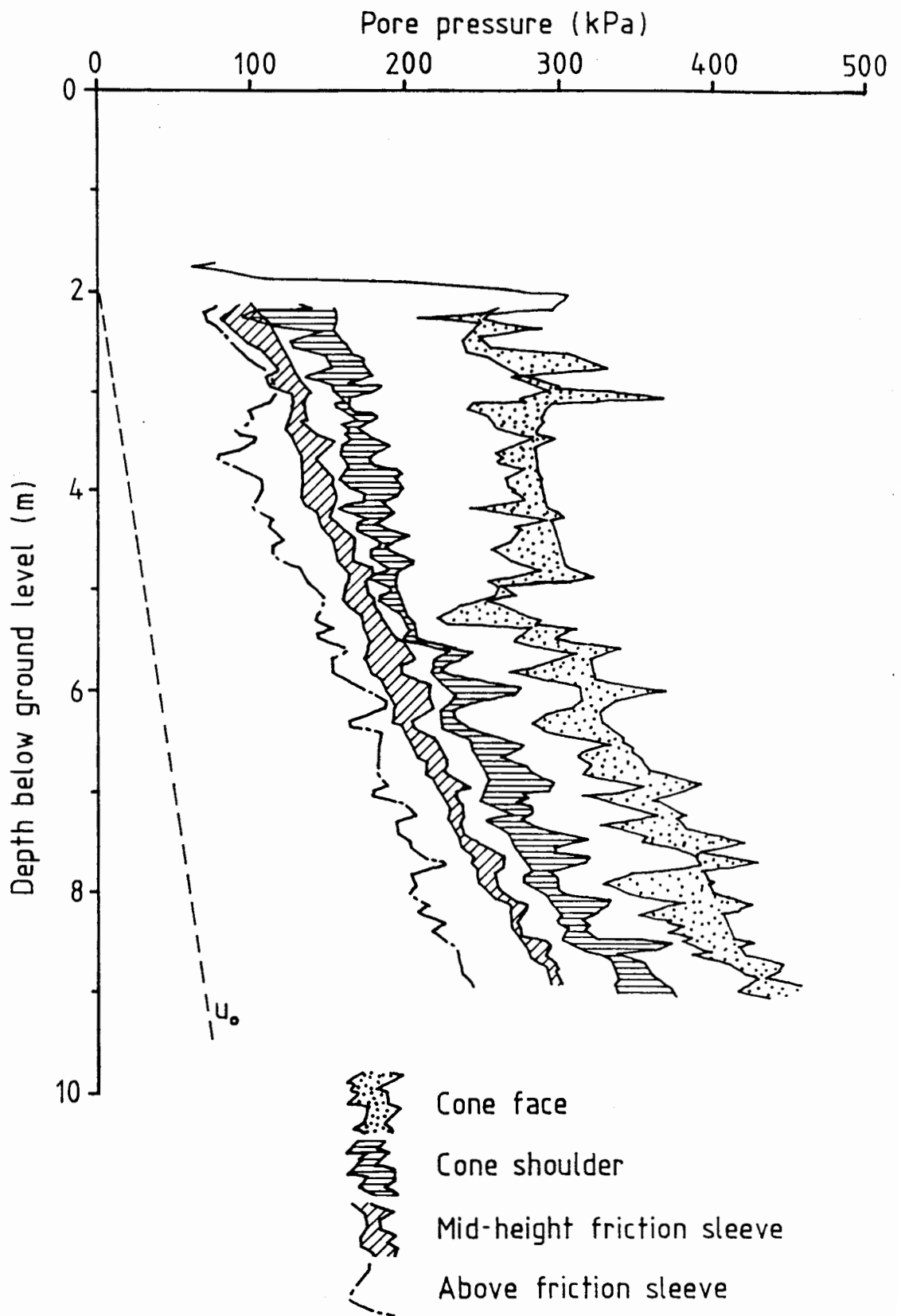


FIGURE 5.7 PENETRATION PORE PRESSURE DATA : 5 cm<sup>2</sup> PCPTs

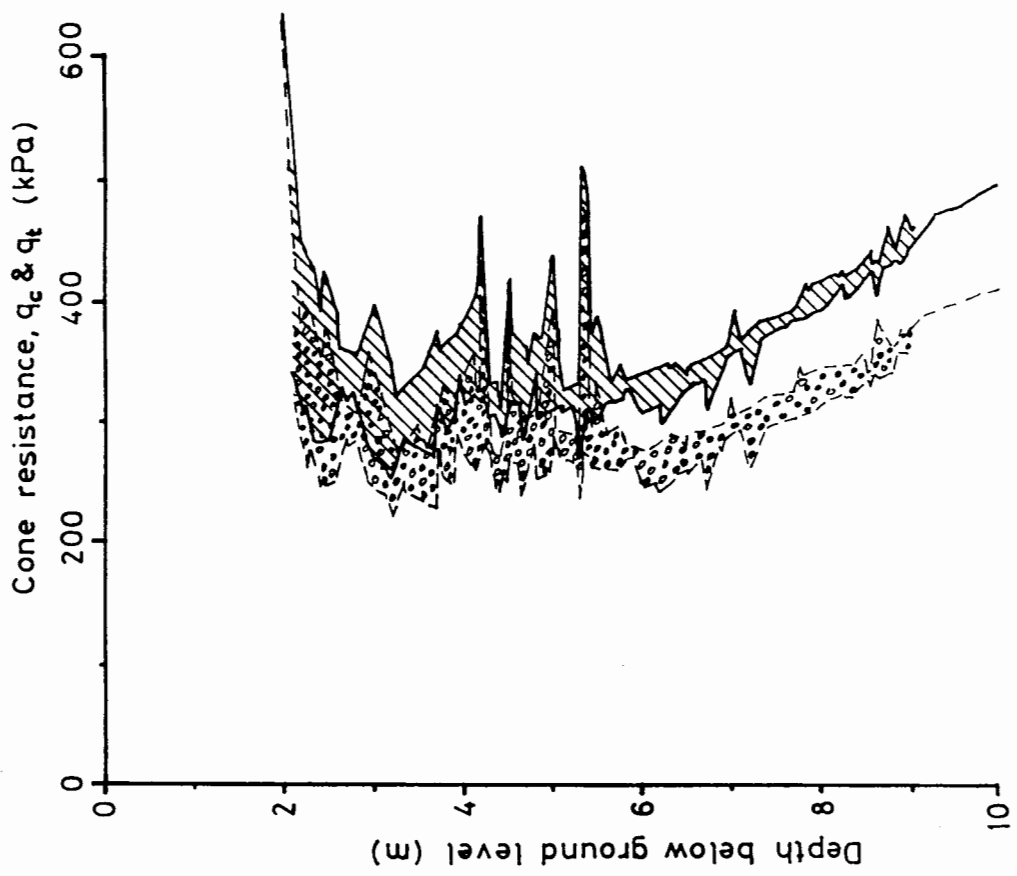
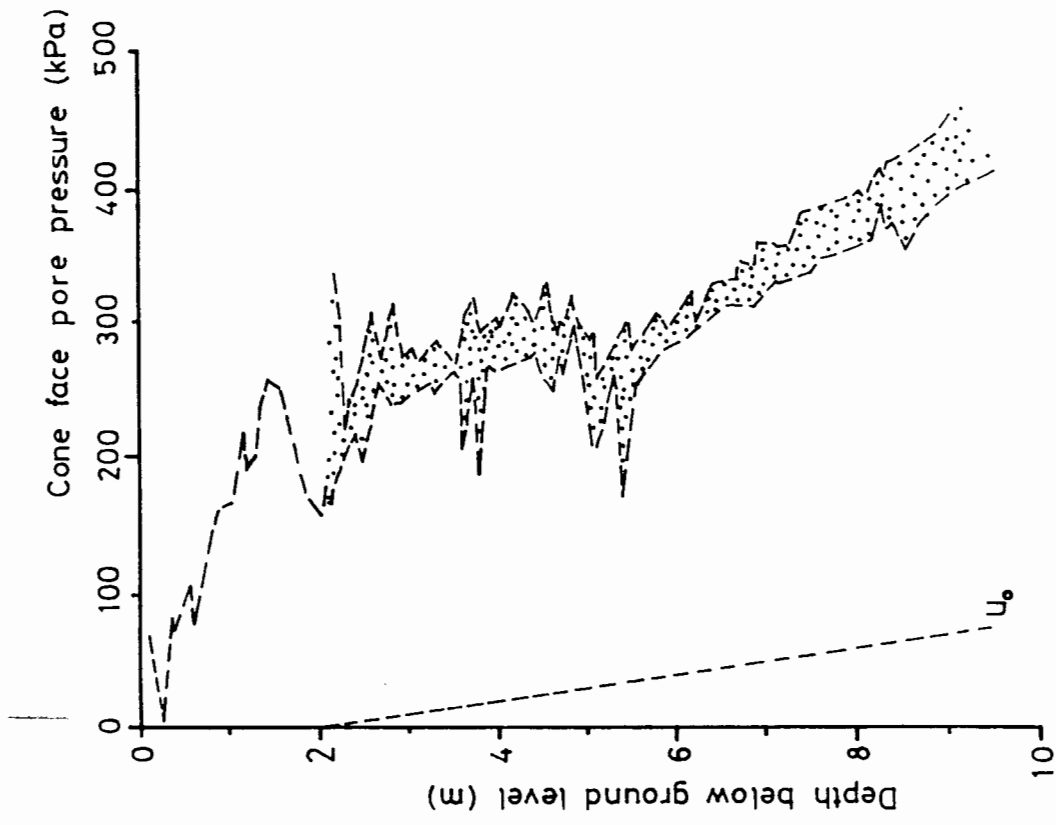
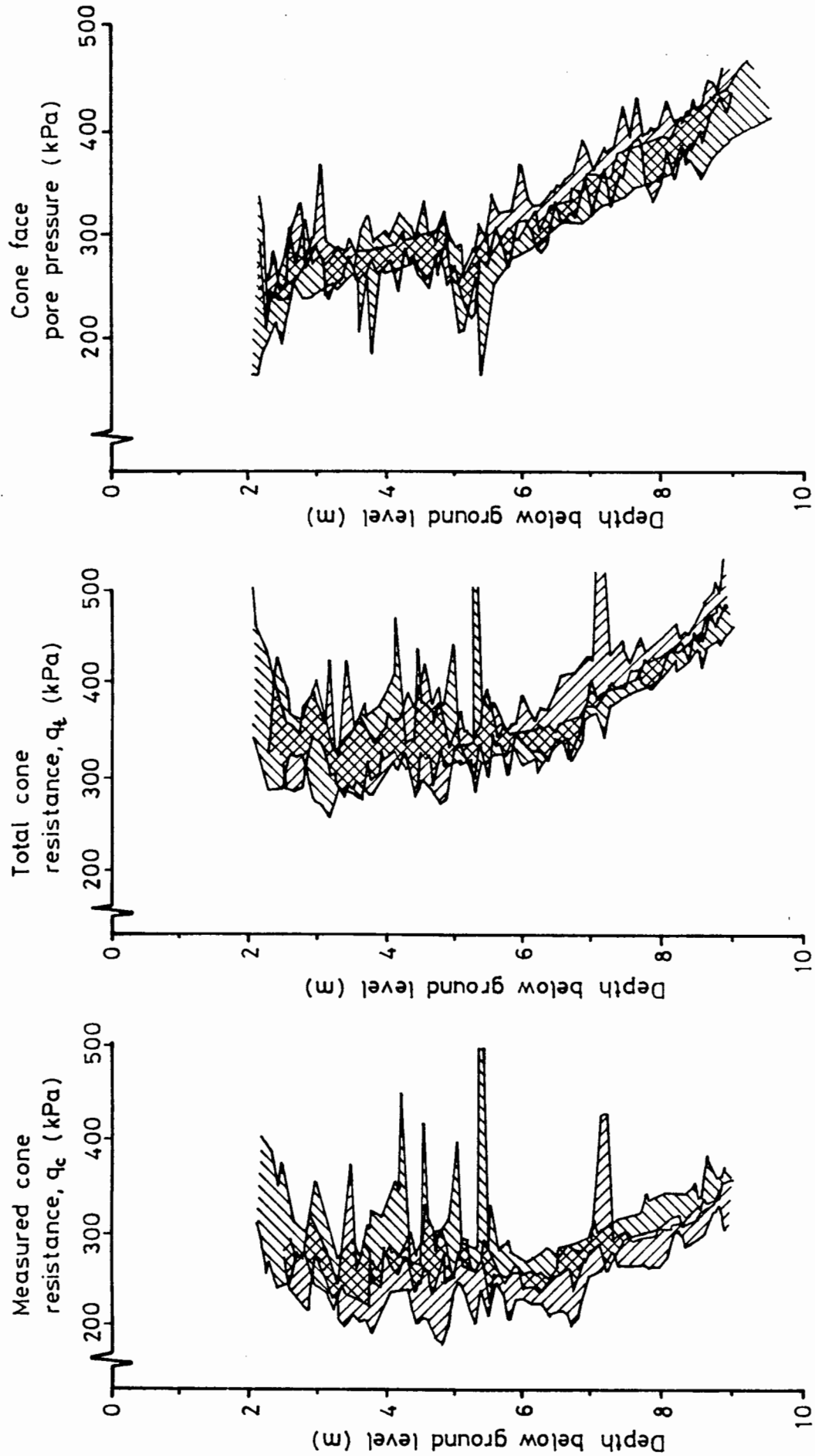


FIGURE 5.8 10 cm<sup>2</sup> PIEZOCONE PENETRATION TESTS







 5 cm<sup>2</sup> piezocone tests ( A2, B1 & C1 )  
 10 cm<sup>2</sup> piezocone tests ( B1A, B3 & C2 )

FIGURE 5.9 COMBINED PLOTS OF TOTAL CONE RESISTANCE & CONE FACE PORE PRESSURE

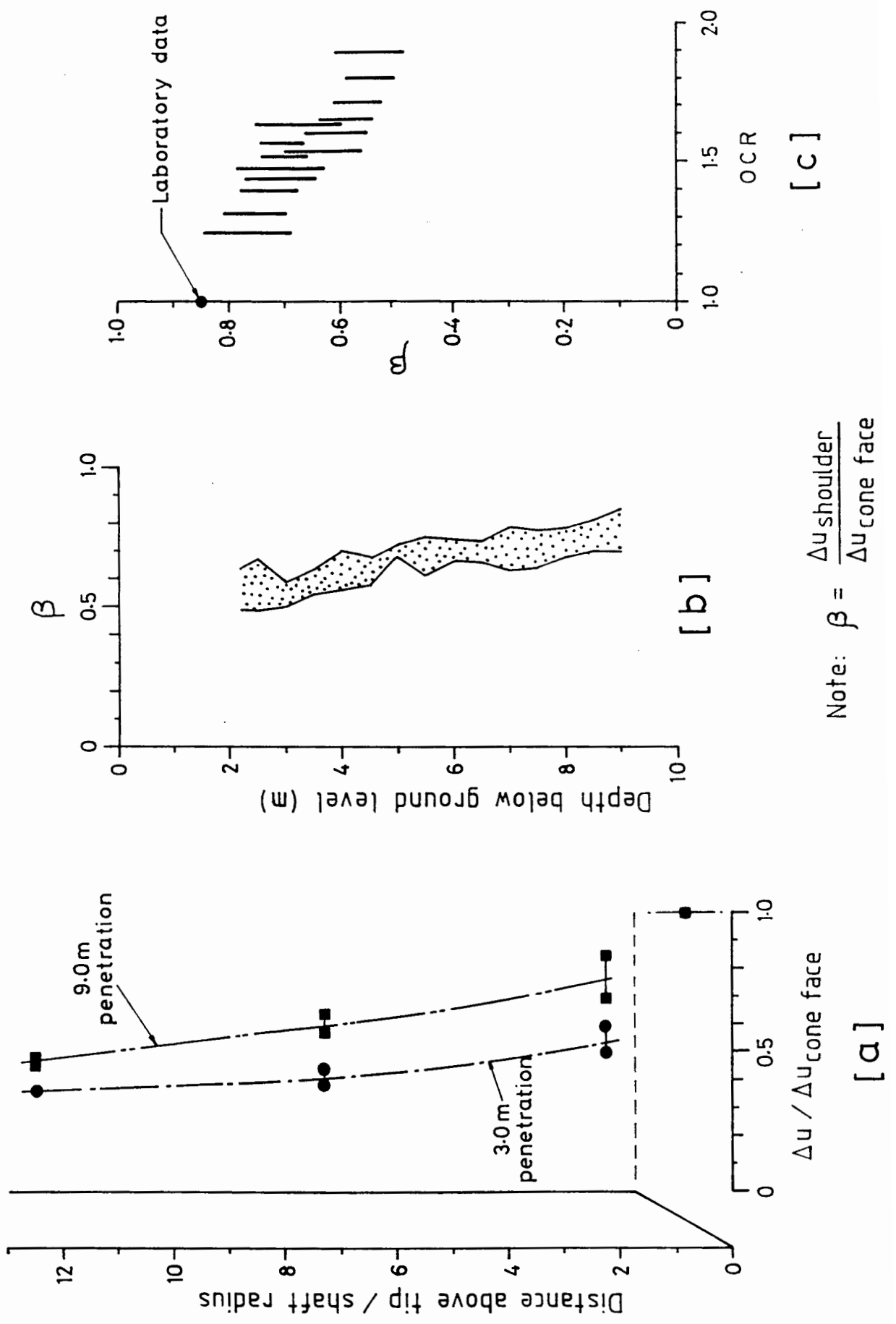


FIGURE 5.10 NORMALIZED EXCESS PORE PRESSURE DISTRIBUTIONS

## 6. CONCLUSIONS AND RECOMMENDATIONS

### 6.1 Introduction

The conclusions from this work have been divided into conclusions on fundamental piezocone behaviour and practical aspects of performing PCPTs. Recommendations for further analytical and practical work are also included in this chapter.

### 6.2 Fundamental Aspects of Piezocone Behaviour

It should be borne in mind that the conclusions drawn below relate primarily to PCPTs in normally consolidated clay. These are as follows:

- 6.2.1 The values calculated for  $N_{kt}$  and  $N_{\Delta u}$  are strongly dependent on sampling disturbance effects in the shear strength test used for the correlation. Where clays have undergone large changes in total stress due to sampling stress relief a considerable loss of strength may occur. This strength loss appears to increase with time between sampling and testing. Hence the shear strength from QUU triaxial tests may substantially under estimate the in situ undrained compressive shear strength.

Although this effect is particularly severe for kaolin it is known to exist for other less permeable clays. Consolidation of the clay back to the in situ effective stress state largely restores the in situ properties. It is therefore concluded that PCPT results should be correlated against CIU triaxial peak shear strength calculated at comparable voids ratios or CAU triaxial peak shear strength for samples consolidated to the in situ horizontal and vertical effective stresses.

6.2.2 From the laboratory tests  $N_{kt}$  has an upper bound value of  $10.6 \pm 0.6$  and a lower bound value of  $10.0 \pm 0.6$  for normally consolidated kaolin and penetration rates between 20mm/s and 50mm/s.

These values exceed those quoted by Almeida and Parry (1985) in normally consolidated kaolin ( $N_{kt} = 6.9$ ) but are lower than their value for normally consolidated Gault clay ( $N_{kt} = 13.2$ ). The reasons for these differences are not clear.

The values from the present study are slightly above those obtained from theoretical analyses which lie in the range 7.5 to 10 depending on the assumed failure mechanism and soil proper-

ties. Two possible explanations for this are that the CPT produces high rates of shear strain around the penetrometer which may effectively increase the soil shear strength and clay stiffness ( $G$ ) at small strains is much higher than the values used in the above analyses.

6.2.3 The best estimate of  $N_{\Delta u}$  from the laboratory pore pressure data on the cone shoulder is  $8.25 \pm 1.0$  for normally consolidated clay. This parameter is not apparently altered by increasing the penetration rate from 20mm/s to 3.2m/s. The ratio of the cone face to the cone shoulder pore pressures is 1.2:1 for normally consolidated clay but the field tests indicate that this ratio increases with increasing OCR. The dynamic pore pressures decrease up the shaft of the penetrometer rather slowly.

6.2.4 Visual analysis of split samples around the axes of penetration reveal a thin layer (less than 1mm thick) immediately around the shaft and cone face which probably represents a shear surface in the soil. Outside this zone appreciable downward displacement of the soil is seen extending some 2 radii from the shaft wall, the greatest displacement lying adjacent to the shaft wall and shear zone.

6.2.5 The laboratory data demonstrates that the dissipation of pore pressure on cessation of penetration can be used to calculate values of  $c_h$  that are in agreement with independent evaluations.

The method of Baligh and Levadoux has been shown to be reliable for normally consolidated clays. This method includes a correction to account for the dissipation occurring under conditions of recompression rather than virgin consolidation which is not allowed for by other published methods. The data also demonstrates that the dissipation is most rapid on the cone face and becomes progressively slower at points further up the penetrometer shaft.

6.2.6 From the results of field tests no scale effect on the penetrometer data can be detected between  $5\text{cm}^2$  and  $10\text{cm}^2$  penetrometers. Although different  $q_c$  values were recorded values of  $q_t$  and pore pressures matched well between the two sizes.

The ratio of excess pore pressures on the cone shoulder and face from the field data was shown to be consistent with the laboratory value. In addition a potentially useful variation in this ratio with OCR was observed.

### 6.3 Practical Conclusions and Recommendations

- 6.3.1 Field tests using penetrometers saturated with glycerin and water gave identical results. Penetrometer saturation is maintained with glycerin for much longer periods on exposure to air or in partially <sup>saturated</sup> soil and thus its use is recommended for routine onshore PCPTs. It is recommended that porous elements and other cavities are dry before attempting to saturate with glycerin. Pre-assembled piezocone penetrometers are more difficult to saturate satisfactorily than designs which enable separate saturation of filters and cavities. This fact should be considered in the design of piezocone penetrometers.
- 6.3.2 Following from 6.2.3 it can be seen that the ratio of excess pore pressures on the cone face and shoulder is likely to be a useful indicator of OCR. It is therefore recommended that both measurements be made in routine PCPTs.
- 6.3.3 Although strain gauged load cells are probably the most convenient method for recording the forces acting on the cone tip and friction sleeve, poor quality data can be produced if certain precautions are not taken. The small

diameter cylindrical load cells of scaled down penetrometers may be subject to appreciable problems of zero shift due to temperature effects. These may be aggravated by poor dissipation of the heat generated from the strain gauges. It is recommended that the zero shift of penetrometer load cells should be examined both for conditions of external temperature change ( $0^{\circ}$  to  $30^{\circ}\text{C}$ ) and for changes in external thermal conductivity. The latter may be determined between air and water.

Care needs to be taken to avoid excessive noise to signal levels on the load cell output lines when measuring relatively low resistances in soft clays. This is a particular problem for penetrometers designed for field use which require high capacities to measure resistances in sands and prevent damage on stones.

6.3.4 Laboratory PCPTs in clay may be successfully conducted if:

- (a) The clay is consolidated one-dimensionally from a slurry (without radial drainage).
- (b) The consolidation stresses are not released prior to the PCPT.
- (c) Suitable boundary conditions are imposed.



Rigid bottom and radial boundaries combined with a flexible stress controlled top boundary was found to be suitable provided that the tank diameter was 40 to 50 times the probe diameter and radial stress measurements were made for the correction of measured pressures. The use of smaller diameter tanks is liable to generate excessive boundary effects unless the boundary conditions are modified.

#### 6.4 Recommendations for Further Analytical and Practical Work.

- 6.4.1 The work presented herein is intended to be of use as a data base against which the current numerical modelling of the CPT can be compared. The strain path analysis that is being developed for cone penetration in clay uses a simple elasto-plastic soil model. Due to the difficulties of obtaining stress equilibrium throughout the deformed region around the cone, this soil model is undoubtedly the most suitable for the analytical development. However, it is recommended that two additional aspects of soil behaviour be considered. These are the marked variation in soil stiffness with strain and the increase in undrained peak shear strength with strain rate. In order to gauge the significance

of these two aspects of clay behaviour it is recommended that they initially be studied with the simpler cylindrical cavity expansion technique before incorporation into a strain path formulation.

In order to obtain data for the variation of shear modulus with shear strain some careful laboratory testing is recommended with use of a small strain device such as a resonant column. Shear modulus should be determined down to a shear strain of about  $10^{-4}\%$ .

It may be possible to obtain data on variation of shear strength with rate from ring shear testing or special vane testing at high rates of shear. Although problems may exist in determining the thickness of the shear zone, and therefore the precise shear strain rate the trend at high rates of strain should be given from such tests.

- 6.4.2 It is recognised that only limited data was obtained at the higher penetration rates of which the equipment was capable. It is therefore recommended that one further cake of normally consolidated kaolin be tested at varying rates

between 20mm/s and 3m/s. Although such a test series was planned in the final sequence of the present work a laboratory accident damaged the cell and cake before the start of penetration testing.

- 6.4.3 As a continuation of the present series of tests on normally consolidated clays, it is recommended that the behaviour of overconsolidated clay be examined with the present apparatus. It is suggested that the majority of tests be carried out at the standard rate of 2cm/s to provide data directly comparable to routine PCPTs. However, the effect of faster rates of penetration would be of interest to provide data relevant to pile driving and other rapid penetration problems. Although kaolin is a convenient material for such testing due to its high permeability and short consolidation times, it is suggested that a few normally consolidated and overconsolidated tests be carried out using a clay of different mineralogy. This would enable the broader relevance of the results to be demonstrated.

## REFERENCES

A.S.T.M. (1977) "Standard method for deep, quasi-static, cone and friction-cone penetration tests of soil." American Society for Testing Materials, Standard D3441.

ACAR, Y.B., TUMAY, M.T. and CHAN, A. (1982) "Interpretation of the dissipation of penetration pore pressures." Proc. International Symposium on Numerical Models in Geomechanics.

ALMEIDA, M.S.S. and PARRY, R.H.G. (1985) "Small cone penetrometer tests and piezocone tests in laboratory consolidated clays." Geotech. Testing J., Vol.8, No.1.

BALIGH, M.M., AZZOUZ, A.S., WISSA, A.Z.E., MARTIN, R.T. and MORRISON, M.J. (1981) "The piezocone penetrometer." Cone Penetration Testing and Experience, A.S.C.E., St. Louis.

BALIGH, M.M. and LEVADOUX, J.N. (1980) "Pore pressure dissipation after cone penetration." Report R80-11, M.I.T. Dept of Civ. Eng.

BALIGH, M.M. and VIVATRAT, V. (1979) "In-situ measurements in a marine clay." BOSS '79.

BARENTSEN, P. (1936) "Short description of a field testing method with a cone shaped apparatus." 1st ICSM, Cambridge Mass. Vol.1.

BATTAGLIO, M., JAMIOLKOWSKI, M., LANCELLOTTA, R and MANISCALCO, R. (1981) "Piezometer probe test in cohesive deposits." Cone Penetration Testing and Experience, A.S.C.E., St. Louis.

## References/2

- BEGEMANN, H.K.S. (1953) "Improved method of determining resistance to adhesion by sounding through a loose sleeve placed behind the cone." 3rd ICSMFE, Zurich Vol.1.
- BEGEMANN, H.K.S. (1963) "The use of static soil penetrometers in Holland." New Zealand Engineering Vol.18, No.2.
- BEGEMANN, H.K.S. (1965) "The friction jacket as an aid in determining the soil profile." 6th ICSMFE, Montreal, Vol.1.
- BEMBEN, S.M. and MYERS, D.A. (1974) "The influence of rate of penetration on static resistance values in Connecticut River Valley varved clay." 1st European Symposium on Penetration Testing, Stockholm.
- BISHOP, A.W. and HENKEL, D.J. (1962a) "The measurement of soil properties in the triaxial test." 2nd Edition, pub. Edward Arnold, London p129.
- BISHOP, A.W. and HENKEL, D.J. (1962b) op.cit.p.175f.
- BISHOP, R.F., HILL, R. and MOTT, N.F. (1945) "The theory of indentation and hardness tests." Proc. Physical Soc., Vol.57, Part 3, No.321.
- BOONSTRA, G.C. (1936) "Pile loading test at Zwinjndrecht, Holland." 1st ICSM, Cambridge, Mass. Vol.1.
- BRINCH-HANSEN, J. (1961) "A general formula for bearing capacity." Bulletin No.11, Danish Geot. Inst., Copenhagen.
- BRUZZI, D and CESTARI, F. (1982) "An advanced static penetrometer." 2nd European Symposium on Penetration Testing, Amsterdam.

### References/3

BURD, H.J. and HOULSBY, G.T. (1985) "Finite element analyses of two cylindrical expansion problems involving near incompressible material behaviour." Report No. OUEL 1580/85, SM056/85 Univ. Oxford.

BUTTERFIELD, R. and BANNERJEE, P.K. (1980) "The effect of porewater pressures on the ultimate bearing capacity of driven piles." 2nd S.E. Asian Conference on Soil Engineering.

CAMPANELLA, R.G., GILLESPIE, D. and ROBERTSON, P.K. (1982) "Pore pressures during cone penetration testing." 2nd Europ. Symp. on Pen. Test., Amsterdam, Vol.2.

CAMPANELLA, R.G., ROBERTSON, P.K. and GILLESPIE, D.G. (1981) "In-situ testing in saturated silt (drained or undrained?)" 34th Can. Geot. Conf.

CAMPANELLA, R.G., ROBERTSON, P.K., GILLESPIE, D.G. and GRIEG, J. (1985) "Recent developments in in-situ testing of soils." 11th ICSMFE, San Francisco, Vol.2.

CARTER, J.P., RANDOLPH, M.F. and WROTH, C.P. (1979) "Stress and pore pressure changes in clay during and after the expansion of a cylindrical cavity." International Journal of Numerical and Analytical Methods in Geomechanics Vol.3 No.3.

CHANDLER, R.J. and MARTINS, J.P. (1982) "An experimental study of skin friction around piles in clay." Geotechnique Vol.32 No.2.

COX A.D. (1962) "Axially - symmetric plastic deformation in soils - II. Indentation of ponderable soils" Int. J. Mech. Sci. 4, pp 371-380.

DE BEER, E. (1977) "Static cone penetration testing in clay and loam." Sondeer Symposium, Utrecht.

#### References/4

DE BORST, R. (1982) "Calculation of collapse loads using higher order elements." I.U.T.A.M. Conf. on Deformation and Failure of Granular Materials, Delft.

DE BORST, R. and VERMEER, P.A. (1982) "Finite element analysis of static penetration tests." 2nd European Symposium on Penetration Testing, Amsterdam.

\*

FRANKLIN, A.G. and COOPER, S.S. (1981) "Tests in alluvial sand with the PQS probe." 10th ICSMFE, Stockholm.

GIBSON, R.E. (1950) "Discussion on Paper by Guthlac Wilson." J.Inst. of Civ. Eng. Vol.34 p382.

GIBSON, R.E. and ANDERSON, W.F. (1961) "In-situ measurement of soil properties with the pressuremeter." Civ.Eng. and Pub.Works Rev. Vol.56 No.658.

GODSKESEN, O. (1936) "Investigation of the bearing-power of the subsoil (especially moraine) with 25 x 25mm pointed drill without samples." 1st ICSM, Cambridge Mass. Vol.1.

GUE, S.S. (1984) "Ground heave around driven piles in clay." Doctoral thesis, University of Oxford.

HIGHT, D.W., GENS, A. and JARDINE, R.J. (1985) "Evaluation of geotechnical parameters from triaxial tests on offshore clay." Offshore Site Investigation '85, International Conf. Soc. Underwater. Tech., London.

\* DELFT (1936) "The predetermination of the required length and the prediction of the toe resistance of piles" 1st ICSM, Cambridge, Mass. Vol. 1.

## References/5

HOULSBY, G.T. (1982) "Theoretical analysis of the fall cone test." Geotechnique Vol.32 No.2 pp111-118.

\*

HUIZINGA, T.K. (1951) "Application of deep penetration tests to foundation piles." Building Research Congress, London, Div.1 Part III.

ISSMFE (1977) "Report of the sub committee on standardization of penetration testing in Europe." 9th ICSMFE, Tokyo.

JAMIOLKOWSKI, M., LANCELLOTTA, R., PASQUALINI, E. and MARCHETTI, S. (1979) "Design parameters for soft clays." Design Parameters in Geotechnical Engineering, 7th ECSMFE, Brighton.

JANBU, N. and SENNESET, K. (1974) "Effective stress interpretation of in-situ static penetration tests." 1st Europ.Symp. on Pen. Testing, Stockholm, Vol.2:2.

JONES, G.A. and RUST, E. (1982) "Piezometer penetration testing CUPT." 2nd Europ. Symp. on Pen. Test., Amsterdam. Vol.2.

JONES, G.A. and VAN ZYL, D.J.A. (1981) "The piezometer probe - a useful investigation tool." 10th ICSMFE, Stockholm.

KAY, J.N. and PARRY, R.H.G. (1982) "Screw plate tests in a stiff clay." Ground Engineering Vol.15. No.5.

KERISEL, J. (1967) "Scaling Laws in soil mechanics." 3rd Panam.Conf. on Soil Mechs. and Found. Eng., Caracas, Vol.3.

\*

HOUSLBY G.T. and WROTH C.P. (1982) "Determination of undrained strengths by cone penetration tests", ESOPT II, Amsterdam, Vol. 2.



## References/6

- KIRKPATRICK, W.M. and KHAN, A.J. (1984a) "The reaction of clays to sampling stress relief." *Geotechnique* Vol.34 No.1.
- KIRKPATRICK, W.M. and KHAN, A.J. (1984b) "The influence of stress relief on the vane strength of clays." *Geotechnique* Vol.34 No.3.
- KJEKSTAD, O., LUNNE, T. and CLAUSEN, C.J.F. (1978) "Comparison between in-situ cone resistance and laboratory strength for overconsolidated North Sea clays." *Marine Geotechnology* Vol.3., No.1.
- KOUMOTO, T. and KAKU, K. (1982) "Three dimensional analysis of static cone penetration into clay." 2nd Europ. Symp. on Pen. Test., Amsterdam, Vol.2.
- KRAFT, L.M. Jr. (1982) "Effective stress capacity model for piles in clay." *ASCE-JGED*, Vol.108, GT.11.
- LACASSE, S., JAMIOLKOWSKI, M., LANCELLOTTA, R. and LUNNE, T. (1982) "In-situ characteristics of two Norwegian clays." 10th ICSMFE, Stockholm.
- LACASSE, S. and LUNNE, T. (1982) "Penetration tests in two Norwegian clays." 2nd Europ.Symp. on Pen. Test., Amsterdam, Vol.2.
- LADANYI, B. (1963) "Expansion of a cavity in a saturated clay medium." *ASCE-JSMFD* Vol.89, SM4.
- LADANYI, B. and EDEN, W.J. (1969) "Use of the deep penetration test in sensitive clays." 7th ISCMFE, Mexico.
- LEVADOUX, J.N. and BALIGH, M.M. (1980) "Pore pressures during cone penetration in clays." Report R80-15, Dept.Civ.Eng., M.I.T.

## References/7

LUGER, H.J., LUBKING, P. and NIEUWENHUIS, J.P. (1982) "Aspects of penetrometer tests in clay." 2nd Europ. Symp. on Pen. Test., Amsterdam, Vol.2.

MARAYAMA, S. and SHIBATA, T. (1964) "Flow and stress relaxation of clays." Symp. on Rheol. Soil Mechs., Grenoble.

MARR, L.S. (1981) "Offshore application of the cone penetrometer." ASCE Conf. on Cone Pen. Test. and Experience., St. Louis.

MEYERHOF, G.G. (1951) "The ultimate bearing capacity of foundations." Geotechnique Vol.2.

MITCHELL, J.K. (1964) "Shearing resistance of soils as a rate process." ASCE-JGED Vol.90, SM1.

MUROMACHI, T., TSUCHIYA, H., SAKAI, Y. and SAKAI, K. (1982) "Development of multi-sensor cone penetrometers." 2nd Europ. Symp. on Pen. Test., Amsterdam, Vol.2.

NAGASWARAN, S. and HOUSLBY, G.T. (1984) "A study of consolidation with radial drainage." Report SM36, Dept.Eng.Sci., Univ.Oxford.

NASH, D.F.T. and DUFFIN, M.J. (1982) "Site investigation of glacial soils using cone penetration tests." 2nd Europ. Symp. on Pen. Test., Amsterdam, Vol.2.

NIEUWENHUIS, J.K. and SMITS, F.P. (1982) "The development of a nuclear density probe in a cone penetrometer." 2nd Europ. Symp. on Pen. Test., Amsterdam, Vol.2.

## References/8

- PEACOCK, J.D. (1980) "Scottish late-glacial marine deposits and their environmental significance." in "The Quaternary in Britain" Ed. Neale and Flenley, Pergamon Press.
- PRANDTL, L. (1920) "Uber die Harte plastischer Korper." Nachr. Kgl. Ges. Wiss. Gottingen, Math. Phys. Klasse: 74-85.
- RANDOLPH, M.F., CARTER, J.P. and WROTH, C.P. (1979) "Driven piles in clay; the effects of installation and subsequent consolidation." Geotechnique, Vol.29, No.4.
- RANDOLPH, M.F. and WROTH, C.P. (1978) "An analytical solution for the consolidation around a driven pile." Univ. Cambridge, Dept. of Engineering. Soils/TR50.
- RICHARDSON, A.M. and WHITMAN, R.V. (1963) "Effect of strain-rate upon undrained shear resistance of a saturated remoulded fat clay." Geotechnique, Vol. 13 No.4.
- ROCHA FILHO, P. (1982) "Influence of excess pore pressure on cone measurements." 2nd Europ. Symp. on Pen. Test., Amsterdam, Vol.2.
- ROY, M., BLANCHET, R., TAVENAS, F. and LA ROCHELLE, P. (1981) "Behaviour of a sensitive clay during pile driving." Can. Geot. J., Vol.18.
- ROY, M., TREMBLAY, M., TAVENAS, F. and LA ROCHELLE, P. (1982a) "Development of pore pressures in quasi-static penetration tests in sensitive clay." Can. Geot. J., Vol.19.
- ROY, M., TREMBLAY, M., TAVENAS, F. and LA ROCHELLE, P. (1982b) "Development of a quasi-static piezocone apparatus." Can. Geot. J., Vol.19.
- SCHAAP. L.H.J. and HOOGENDOORN, H.G. (1983) "A versatile measuring system for electric cone penetration testing." Symp. on Field Meas. in Geomechs., Zurich.

## References/9

- SCHMERTMANN, J.H. (1974a) "Penetration pore pressure effects on quasi-static cone bearing  $q_c$ ." 1st Europ. Symp. on Pen. Test., Stockholm.
- SCHMERTMANN, J.H. (1974b) "Pore pressures that produce non-conservative  $q_c$  data." Discussion, 1st Europ. Symp. on Pen. Test., Stockholm.
- SISSONS, J.B. (1967) "The evolution of Scotland's scenery." Pub. Oliver and Boyd.
- SKEMPTON, A.W. (1951) "The bearing capacity of clays." Building Research Congress, London. Vol.1.
- SLOAN, S.W. and RANDOLPH, M.F. (1982) "Numerical predictions of collapse loads using finite element methods." Int. J. Num. & An. Meth. in Geomec., Vol.6., No.1.
- SMITS, F.P. (1982) "Penetration pore pressure measured with piezometer cones." 2nd. Europ. Symp. on Pen. Test., Amsterdam, Vol.2.
- SODERBERG, L.O. (1962) "Consolidation theory applied to foundation pile-time effects." Geotechnique Vol.12, No.2.
- STEENFELT, J.S., RANDOLPH, M.F. and WROTH, C.P. (1981) "Instrumented model piles jacked into clay." 10th ICSMFE, Stockholm, Vol.2.
- SUGAWARA, N. and CHIKARAISHI, M. (1982) "On estimation of  $\theta'$  for normally consolidated mine tailings using the pore pressure cone penetrometers." 2nd Europ. Symp. on Pen. Test., Amsterdam, Vol.2.

## References/10

- TERZAGHI, K. (1943) "Theoretical soil mechanics." Pub. J. Wiley, New York.
- TERZAGHI, K. and PECK, R.B. (1967) "Soil mechanics in engineering practice." 2nd. Ed., Art.44, Pub. Wiley.
- THORBURN, S., LAIRD, C.L. and REID, W.M. (1981) "The importance of the stress history of cohesive soils and the cone penetration test." Structural Eng., Vol.59A, No.3.
- TOOLAN, F.E. and FOX, D.A. (1977) "Geotechnical planning of piled foundations for offshore platforms." I.C.E. Proc., Part 1, Paper 7996.
- TORSTENSSON, B.-A. (1975) "Pore pressure sounding instrument." ASCE Conf. In-situ Meas. Soil Prop., Raleigh.
- TORSTENSSON, B.-A. (1982) "A combined pore pressure and point resistance probe." 2nd Europ. Symp. on Pen. Test., Amsterdam, Vol.2.
- TUMAY, M.T., ACAR, Y.B., CEKIRGE, M.H. and RAMESH, N. (1985) "Flow field around cones in steady penetration." ASCE-JGE Vol.111, No.2.
- TUMAY, M.T., BOGGESS, R.L. and ACAR, Y. (1981) "Subsurface investigations with piezocone penetrometer." ASCE Conf. Cone Pen. Test. and Exp., St. Louis.
- UNIVERSITY OF STRATHCLYDE (1983) "Glacial and post-glacial features of Strathclyde." Field Notes for Geol. Soc. of London, Eng. Group.

## References/11

VERMEIDEN, J. (1948) "Improved sounding apparatus as developed in Holland since 1936." 2nd ICSMFE, Rotterdam.

VESIC, A.S. (1972) "Expansion of cavities in infinite soil mass." ASCE-JSMFD, Vol.98, SM3.

WISSA, A.E.Z., MARTIN, R.T. and GARLANGER, J.E. (1975) "The piezometer probe." A.S.C.E. Conf. In-situ Meas. Soil. Prop., Raleigh.

WROTH, C.P. (1984) "The interpretation of in situ soil tests." 24th Rankine Lecture, Geotechnique Vol.34, No.4.

ZUIDBERG, H.M., SCHAPP, L.H.J. and BERINGEN, F.L. (1982) "A penetrometer for simultaneously measuring of cone resistance, sleeve friction and dynamic pore pressure." 2nd Europ. Symp. on Pen. Test., Amsterdam, Vol.2.